OLLSCOIL LUIMNIGH
UNIVERSITY OF LIMERICK

Development of a 'Smart Glove' Monitoring System for Personal Protective Equipment Applications

A ***Major Qualifying Project*** Report

submitted to the Faculty

of the

WORCESTER POLYTECHNIC INSTITUTE
Worcester, Massachusetts, USA

in partial fulfilment of the requirements of the

Degree of Bachelor of Science

on this day of

Friday, October 17th, 2008

by

Erik B. DeVolder

Nikolas K. Ledoux

Olusope M. Otuyelu

Zachery R. Van Ness

Advisor _____
Prof. Alexander M. Wyglinski

Advisor _____
Prof. Richard F. Vaz

Abstract

A proof of concept prototype of a “smart glove” system, which could monitor the physiological stresses related to repetitive strain and vibration-induced injuries, was developed at the University of Limerick Enterprise Research Centre in Ireland. The device logged grip force, vibration and goniometry data and could alert the user if dangerous vibration levels were reached. This prototype will provide a basis for future developments of devices that would enable safety by providing more information about injury risk in the workplace.

Acknowledgments

The "smart glove" project team would like to extend our thanks and gratitude to some individuals and organizations who helped us in the process of completing our project, from assisting with the prototype design and building, editing and compiling the project report, as well as, making our stay in Limerick comfortable during the 10 week period. We would like to acknowledge the following individuals:

Enterprise Research Centre (ERC)

First, we would like to thank the entire staff of the Enterprise Research Centre (ERC) at the University of Limerick (UL) for their support and invaluable input to our project.

Special thanks go to Dr. Mark Southern, who was our primary MQP liaison for his enthusiasm and support during the process of completing the project.

Special thanks go to John Harris for providing us with all of his electrical engineering and technical knowledge, access to the necessary laboratory equipment we needed during the course of our project and helping us in the process of laying out and manufacturing the printed circuit boards (PCBs) for our prototype.

Special thanks go to Seamus Clifford for helping us in arranging brainstorming sessions and meetings with the group and our procuring the electrical parts needed to design and build our prototype.

Special thanks go to Dr. Leonard O'Sullivan for providing us with the end user requirements for the final product and insight into issues concerning vibration induced and repetitive strain injuries.

Worcester Polytechnic Institute (WPI)

First, we would like to thank the Interdisciplinary and Global Studies Division (IGSD) and Worcester Polytechnic Institute (WPI) for providing us with the opportunity of completing our Major Qualifying Project (MQP) abroad in an excellent environment.

We also would like to thank our Worcester Polytechnic Institute advisors, Professors Alexander Wyglinski and Richard Vaz, for their guidance, support and insight for the duration of our project. They provided us with both technical and non-technical help and ensured that we started up our project to a smooth start. Our weekly teleconference meetings helped to continually reiterate our project goals and make sure that we were able to effectively complete our project in the 10 week period.

We would also like to thank David Willens for assisting us with building the enclosure for the prototype's circuitry.

Ms. Charlotte Tuohy

Extra special thanks to Ms. Charlotte Tuohy, our Limerick liaison, for all her help in getting us settled in Limerick, providing us with the amenities we needed, and going out of her way repeatedly to ensure that we had a comfortable stay in Ireland.

Authorship Page

Erik DeVolder, Nikolas Ledoux, Olusope Otuyelu, and Zachery Van Ness all contributed to the writing and editing of the project report.

Table of Contents

List of Figures

List of Tables

Executive Summary

Many workers experience injury in their daily activities [1]. Often, poor work environments subject employees to physical stresses that can have lasting debilitating effects. Many important systems can be broken up into two categories: *repetitive strain injuries (RSI)* and vibration induced injuries, both of which may cause decreased productivity or even absenteeism. Repetitive strain injuries and vibration induced injuries such as episodic finger blanching are common industrial ailments, but since they occur gradually over time, it is difficult for workers or employers to detect, predict, and prevent injury. These problems can be addressed by implementing workspace auditing to verify that exposure limits have not been exceeded and ensuring the presence of safe working habits and proper protective equipment.

Three important factors related to occupational injury are: wrist movement and angle, grip force, and hand-transmitted vibration [5]. Excessive exposure to these factors can cause RSI or vibration-induced injury. Currently, there are devices that are available on the market to measure hand-transmitted vibration and grip force [4] [36]. These are just some of the factors contributing to occupation-related injury. Although these commercially available products can be modified to measure some of the other factors, there is no single product on the market that will measure all relevant factors as part of one lightweight, non-invasive unit. The equipment currently available is expensive and is too bulky to be practical for use in an industrial setting, so there is a need for portable technology that can be used to monitor the conditions that the upper limbs are exposed to within the workplace.

The benefits of having a device that is capable of tracking all of these relevant data during the work day, are that real time dangers experienced at work can be evaluated, solving the problem of the worker not knowing when a particular task poses a health risk. This data would also be useful for ergonomic researchers, for furthering their understanding of the causes of occupation-related injuries.

Our goal was to design a prototype “smart glove”, that measures and monitors the magnitude and direction of hand and arm vibration, the wrist angles corresponding to wrist flexion and extension, and impacts experienced by the hand. It should collect this data such that it can be exported to a computer for analysis and alert its user when the exposure limits have been exceeded.

We began our research with the following objectives:

- To select appropriate sensors based on size, sensitivity, range, power consumption and durability
- To select a microcontroller with an appropriate number of ports, data storage, USB interoperability, ADCs, and an LCD driver
- Designing the interface circuitry between the sensors and the microcontroller
- Designing the systems to alert user of dangerous exposure (auditory, somatic/tactile, visual)
- Designing the interface between microcontroller and PC (SD card)
- To write software that will store, write, and analyze data on the microcontroller

The prototype “smart glove” system, incorporated angle, pressure, and vibration sensing into a non-invasive, lightweight glove, to be used by a worker. Transducers were used to sense the severity of these factors, and then fed that information into a processing unit, which could evaluate the vibration exposure and store the sensor data on a memory card. With this memory card functionality, the user could potentially upload the data to a PC whenever the glove is not in use or when the information is needed. By analyzing incoming vibration data, the glove could alert the user when harmful vibration levels had been reached. This could help to prevent workers from injuring themselves from overexposure to vibration, while still allowing them to be productive. Also, the ability to measure vibration simultaneously with wrist angle and grip force will be useful in determining their relationship and how they contribute to the severity of vibration induced injuries such as episodic finger blanching.

The approach to designing the “smart glove” system began with a basic top-level design in which the key block components were identified. We conducted a careful examination of the user requirements, from which we were able to determine quantitative specifications, such as the range of vibration frequencies the glove will need to measure. Next we conducted research into transducer technologies that could achieve the user specifications. From this research we were able to perform value analysis to choose optimal sensors based on factors such as pricing, performance, and power consumption. Concurrent with this, we chose a microcontroller which met our design objectives. Finally, we designed interface circuitry between the microprocessor and inputs, an auditory and visual alert system and SD capability. Within each sub block in our top level scheme, we followed the design flow of design, test, re-design, re-test, as necessary until proper functionality was reached. In the end, we were able to take our final design build our subsystems on PCBs and assemble our proof of concept prototype.

1 Introduction

Workers in a variety of fields often experience injuries resulting from their daily occupations [1]. Poor design of hand-held tools, occupation sites, and work systems can expose employees to debilitating stresses. Many symptoms fall under the category of *repetitive strain injuries (RSI)*, which may cause decreased productivity or even absenteeism. In the USA, RSI injuries comprise about 60% of occupational ill health [1]. The exact causes of RSI are not well understood, so it can be difficult to quantitatively assess a work area for safety.

Vibration induced injuries are another problem for many manual laborers. According to estimates, 1.7% to 3.6% of workers in the USA and Europe are exposed to potentially harmful hand-transmitted vibration [2]. One example of a vibration-induced injury is *Raynaud's Phenomenon*, a disorder in which blood circulation to the fingers is halted in the presence of cold temperatures [3]. This causes fingers to turn white and lose both feeling and dexterity. Workers exposed to excessive stresses and vibrations are in danger of damaging the hands, wrists, and arms.

Since RSI and vibration induced injuries occur gradually over time, it is difficult for workers or employers to detect, predict, and prevent injury. Currently, devices such as the *VATS*™ (Vibration Analysis ToolSet) and the FSA Glove Pressure Mapping System (with its hand sensor array), as shown in Figures 1, 2 and 3 below, are available on the market to measure hand-transmitted vibration and grip force [4] [34].

Figure 1: FSA Glove Pressure Mapping System [12]

[Image used courtesy of NexGen Ergonomics, Inc.]

Figure 2: VATS (Vibration Analysis ToolSet) [4]

[Image used courtesy of NexGen Ergonomics, Inc.]

Vibration and grip force are just some of the factors contributing to occupation-related injury. Although the VATS system can be modified to include grip force sensing, there is no single product on the market that will measure all relevant factors as part of one lightweight, non-invasive unit. The ability to track all relevant data during the workday would allow for the evaluation of real time dangers, solving the problem of the worker not knowing when a particular task poses a health risk. This data would also be useful for ergonomic researchers, for furthering their understanding of the causes of occupation-related injuries.

Three important factors related to occupational injury are: wrist movement and angle, grip force, and hand-transmitted vibration [5]. Excessive exposure to these factors can cause RSI or

vibration-induced injury. Our goal is to use transducers to sense the severity of these factors, and then feed that information into a processing unit to evaluate health risks and store information electronically.

Specifically, this project aims at developing a prototype “smart glove” system, which will incorporate angle, pressure, and vibration sensing into a non-invasive, lightweight glove, to be used by a worker. The glove will have the capacity to store ergonomic data and upload it to a PC whenever the glove is not in use or when the information is needed. Furthermore, the processor will analyze incoming data, alerting the user when harmful vibration levels have been reached. This will help to prevent workers from injuring themselves from overexposure, while still allowing them to be productive. Using this safety device as an auditing tool will assist employers in optimizing the amount of time that a worker can safely spend on a task. Reducing the incidence of stress-related injuries through monitoring will decrease the amount of employee compensation that employers need to provide, therefore increasing their profitability. It will also provide data for ergonomists to assess the safety of a workplace. Particularly, the ability to measure vibration simultaneously with wrist strain and hand force will be useful since the relationship between these is not well understood.

The approach to designing the “smart glove” system began with a basic top-level design in which the key block components were identified. We conducted a careful examination of the user requirements, from which we were able to determine quantitative specifications, such as the range of vibration frequencies the glove will need to measure. Next we conducted research into transducer technologies that could achieve the user specifications. From this research we were able to perform value analysis to choose optimal sensors based on factors such as pricing, performance, and power consumption. Concurrent with this, we chose a microcontroller which would be able to receive and process all information, as well as transmit it to a PC via USB. Finally, we designed interface circuitry between the microprocessor and inputs, and the software to evaluate and transfer data to the PC. Within each sub block in our top level scheme, we followed the design flow of design, test, re-design, re-test,

as necessary until proper functionality was reached. In the end, we were able to take our final design and commit it to various circuit boards, in order to have a complete prototype.

1.1 Project Description

1.1.1 Problem Statement

Repetitive strain injuries and vibration-induced injuries such as episodic finger blanching are common industrial ailments, which could be prevented by safe working habits and proper protective equipment. These problems can be addressed by implementing workspace auditing to verify that exposure limits have not been exceeded.

There is a need for portable technology that can be used to monitor the conditions that hands and arms are exposed to within the workplace. The equipment currently available is expensive and is too bulky to be practical for use in an industrial setting.

1.1.2 Project Goal

Our goal is to design a prototype “smart glove”, that measures and monitors the magnitude and direction of hand and arm vibration, the wrist angles corresponding to wrist flexion and extension, and impacts experienced by the hand. When in use, the glove will collect this data such that it can be exported to a computer for analysis, or in the case of exceeding an exposure limit, the glove will alert its user of the danger.

1.1.3 Project Objectives

Our project objectives identify our deliverables over a 10 week duration and these are defined below:

- To select appropriate sensors based on size, sensitivity, range, power consumption and durability
- To select a microcontroller with an appropriate number of ports, data storage, USB interoperability, ADCs, and an LCD driver
- Designing the interface circuitry between the sensors and the microcontroller
- Designing the systems to alert user of dangerous exposure (auditory, somatic/tactile, visual)
- Designing the interface between microcontroller and PC (USB)
- To write software that will store, write, and analyze data on the microcontroller

1.1.4 Project Specifications

The project team was able to determine user requirements for the "smart glove" from the information obtained from discussions with our project sponsors and advisors, as well as carrying out preliminary background research on the project and issues surrounding it.

1.1.4.1 Explicit Requirements

Through conversations with ergonomics expert Dr. Leonard O'Sullivan, we were given several explicit user requirements for the smart glove system.

- **Measurement of Parameters**
    - **Pressure**: The prototype should be able to measure the forces experienced by the hand (i.e. fingers and palm) when the user of the glove grips equipment in the workplace.

    - **Goniometric measurements**: The glove should be able to measure the angle of deviation of the wrist, and this would be used to determine the amount of flexion and extension of the wrist.
    - **Vibration**: The glove should be able to measure the magnitude of the vibrations experienced by the hand, in order to the user's assess the user's exposure.
- **Alert System**: The glove should alert the user when the period of exposure to vibration becomes hazardous, and this can be done using multiple sensory mechanisms.
- **Visual Display**: The glove should have a clear visual display which indicates current exposure conditions and the allowable time for remaining in those conditions.
- **Data Storage**: The glove should be able to continuously track and upload the measurements taken and store the values until when they are downloaded to a computer. The memory size will be variable depending on the size of the SD card used to store the data.
- **USB Connectivity**: The glove should be able to download the collected data to a computer via a USB socket, which may also be used to charge the battery.
- **Power Consumption**: The glove should have a rechargeable battery and the components should have low power consumption.
- **Minimization of Design**: Since the type of application the circuitry will be used for is going to be worn by manual laborers, there is a need to make the system as small as possible so that when it is integrated in a glove, it does not impede or restrict the movement of the fingers and wrist. This will be done by making use of components that are smaller and lighter so they will not take up as much space.
- **Cost**: The components of the glove should be reasonably priced, such that they can be easily obtained, in order for the finished product to be affordable for the end user. There is no

explicitly stated price cap since our sponsors did not want to limit the technology used in developing the prototype.

- **Portability**: The finished product should be compact so that is easily transported and transferred from one employee to another so it can be implemented in industrial setting.

1.1.4.2 Implicit Requirements

We also brainstormed a set of implicit requirements for the system.

- **Hand movement**: The glove should not impede or restrict the user's movement, so it should be lightweight.
- **Ergonomics**: The glove should be ergonomically compatible with the hand of the user, i.e. it should be design specifically to fit a human hand comfortably.
- **User Interface**: The glove should be intuitive to use, since most of the users will be unskilled workers in industrial settings.
- **Durable**: Because of the environments where the glove will be used, it needs to be able to last for an extended period of time and withstand failures caused by factors in the surrounding area.

From the end user requirements, we were able to generate a block diagram that gave a basic overview of the components and sub-systems that will make up the “smart glove” device.

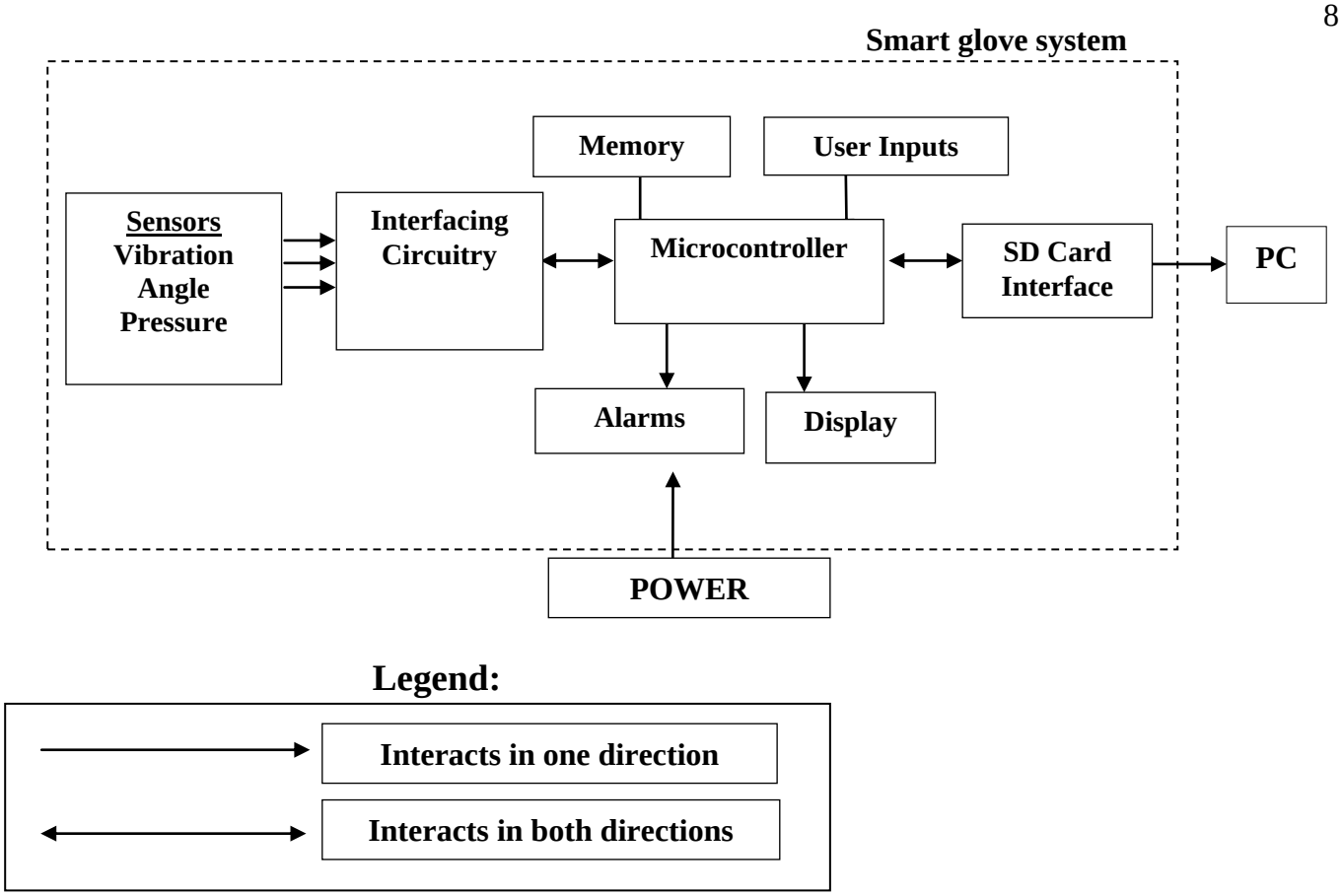

Figure 3: Preliminary Block Diagram of "Smart Glove" Prototype

The arrows shown in Figure 3 indicate the direction of data flow between each of the modules. The flow and collection of data begins with the sensors, continues through the microprocessor and ends when the transmission of the data has reached the SD card, display module, and in the event of exceeding the exposure limits, the alert systems.

2 Background

In this chapter, the potential causes and effects of repetitive strain and vibration induced injuries are discussed. We also review the prior art of ergonomic hand-wrist measurement devices in order to identify the limitations in existing technology such that we may improve upon them in our design.

2.1 Background Information on Vibration Induced Injuries

Vibration exposure can cause serious harm to workers [2]. Understanding the dangers of hand-transmitted vibration and how to measure and prevent them are crucial in order to mitigate vibration induced injuries. Depending on the magnitude, frequency, and duration of vibration exposure, several vascular, neurological, bone, and/or joint conditions may develop. Excessive vibration exposure can give rise to some physically debilitating conditions such as episodic finger blanching (white finger), neurological conditions, as well as other muscoloskeletal disorders. These conditions are discussed in the following sections.

2.1.1 Vibration Induced White Finger

Vibration induced white finger (VWF) is one type of secondary Raynaud's disease, in which the victim experiences "intermittent bilateral blanching of the fingers" [3]. Beginning with the whitening of fingertips in the presence of cold, continued exposure to vibration can increase the blanched area, spreading to other fingers, and affecting all phalanges down to the palm.

VWF attacks typically do not exceed 30 minutes, and the most painful moment of the attack is when blood returns to the digits and when dilation of the blood vessels occurs. One challenge of VWF is that while it is caused by vibration, the attacks are actually triggered by the cold. Since a worker may not experience an attack while in a warm work environment, prevention is crucial, because the symptoms do not occur immediately. One way to minimize symptoms is to reduce the pressure exerted on the

vibrating tool [7]. Therefore, a system that could measure both of these factors simultaneously would be a powerful auditing tool for assessing workplace dangers.

Studies have shown that often attacks do not occur until years have passed since first vibration exposure. 20% of caulkers and riveters working in a dockyard reported VWF after 6 years of vibration exposure, while 50% reported symptoms after 18 years [6].

In rare advanced cases, repeated attacks of severe finger blanching can lead to ulceration or gangrene in the fingertips [2]. If the attack takes place during a occupation, the worker might lose touch, sensation, and dexterity, increasing the risk of injury due to accidents.

The probability and severity of white-finger symptoms appear to be influenced by several factors, such as vibration frequency, magnitude, direction, and duration, as well as ergonomic factors such as grip force and arm posture [2]. Also, one's susceptibility to ailments, medical history or drug intake, can play a role in the severity of the symptoms. However, although the relationship between vibration exposure and symptom development is complex, studies have suggested that cumulative exposure before the appearance of white finger is approximately proportional to the inverse of the magnitude of that exposure. That is, if the magnitude of vibration is doubled, half the amount of years of exposure would produce the same effect. This shows that while the exact symptoms might be difficult to predict, the risk of injury is much higher in the presence of vibration exposure over time.

2.1.2 Neurological Disorders

Workers exposed to vibrations may experience neurological symptoms independent of other vibration-induced disorders [2]. Such symptoms include tingling and numbness in the fingers and hands, reduction in the sense of touch and temperature, as well as a loss of manual dexterity. Surveys show that about 80% of a group of vibration-exposed workers experienced peripheral neurological disorders, and that sensory loss is experienced by users of a wide range of tool types.

Another neurological disorder experienced by those exposed to vibrations is *carpal tunnel syndrome* (CTS) [3]. Between the bones of the wrist and the transverse carpal ligament is the carpal tunnel, through which the median nerve passes. If this nerve is injured, then numbness, loss of feeling, or loss of grip can result. It is important to consider other ergonomic risk factors when evaluating any occupation task, since disorders such as CTS may be caused from a variety of stresses, not necessarily vibration alone.

2.1.3 Musculoskeletal disorders

Investigations have shown a high occurrence of bone vacuoles and cysts in the hands and wrists of workers exposed to vibration [2]. Workers using pneumatic percussive tools, such as those found in mines, road construction, and metalworking occupations, have been found to experience excess occurrence of wrist and elbow osteoarthrosis [2]. The vibrations and shocks from these tools tend to be in frequencies lower than 50Hz, but with high acceleration magnitudes. In some countries, including France, Germany, and Italy, workers operating hand-held vibrating tools receive compensation if they experience bone and joint disorders, which are considered occupational diseases [2].

Workers with extended exposure to vibration might complain of muscular weakness, diminished muscle strength, and pain in the arms or hands [2]. It has also been found that vibration exposure is associated with a reduction in hand grip strength.

2.1.4 Measuring Hand Transmitted Vibration

The four main considerations known to contribute to hand-transmitted vibration symptoms are [2]:

- Frequency spectrum of mechanical vibration
- Magnitude of vibration
- Duration of exposure during the work day

- Cumulative exposure

The standards for measuring these are outlined by the *International Organization for Standardization* (ISO). Considerations of the vibration transducer will be left to section 3.2.3, in which the rationale for accelerometer selection is detailed.

2.2 Background Information on Repetitive Strain Injuries

A *repetitive strain injury* (RSI) is a term used to refer to a set of musculoskeletal symptoms, resulting from performing repetitive movements over a prolonged period of time [8]. It is also called a *work related upper limb disorder* (WRULD). It affects the muscles, tendons and nerves in the hands, wrists, arms, upper back, and other areas of the body depending on the work being performed. It occurs mostly when the muscles are kept tense for extended periods of time, as a result of bad posture, sustained force and repetitive movements, such as those commonly experienced by assembly line workers. Symptoms of RSI include recurring pain and discomfort in the affected areas, loss of grip, fatigue, sleeplessness, and numbness of the arms. Experiencing these can result in absenteeism and the inability of workers to function effectively, both at home and at work.

Excessive work pressures, such as physically and mentally demanding jobs, time pressures and a lack of control, can often act alongside physical risk factors such as force, posture and repetition to influence both the onset and duration of RSI [9]. RSI conditions are not generally visible to the public, so people are unaware of the gravity of its effects on those who are affected [10]. There is a lack of research and available educational material on the causes of RSI related conditions, their prevention, and their treatment methods. There are two different types of RSI and these are outlined below.

2.2.1 Type 1 RSI

Type 1 RSI is used to describe a specific range of musculoskeletal disorders that occur in the upper and lower limbs [10]. The causes of these disorders, which include repetitive movements, bad posture, stress, etc, are thought to be related. The symptoms common among these disorders are numbness, tingling, sharp pain, dull ache, weakness, loss of grip, and restricted movement of limbs. These symptoms can often make people incapable of carrying out simple tasks, both at home and at work. Some conditions that are under the Type 1 RSI umbrella are listed below [10]:

Adhesive capsulitis (frozen shoulder) [11]: This is a condition in which the connective tissue surrounding the shoulder joint becomes inflamed and stiff, growing together with abnormal bands of tissue, as is illustrated in Figure 4 below. This restricts the motion of the arm ('frozen shoulder') and causes pain.

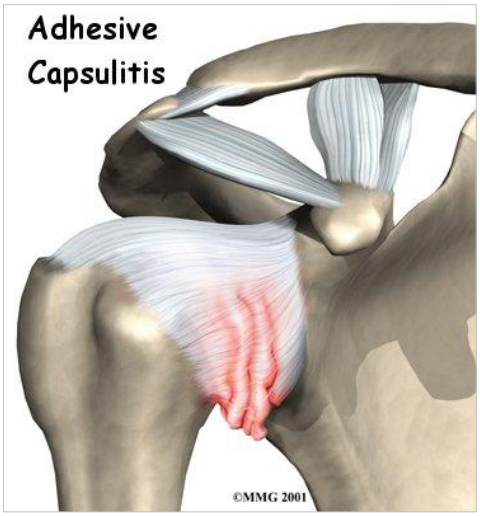

Figure 4: Adhesive Capsulitis [11]

[Image courtesy of Medical Multimedia Group LLC, www.eOrthopod.com]

Bursitis [12]: This occurs mostly in the elbows and knees and is caused by the inflammation of the sacs of synovial fluid (bursae) found in these areas, as a result of repetitive movement and excessive pressure. It can also cause other inflammatory conditions such as rheumatoid arthritis. Figures 5 and 6

illustrate the swelling of the bursae in the elbow, giving both internal and external views of the effects of bursitis on the human arm.

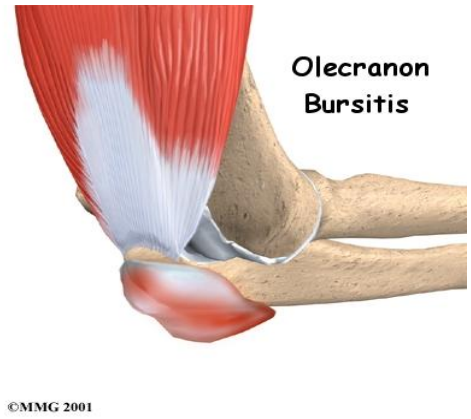

Figure 5: Olecranon (Elbow) Bursitis [12]

[Image courtesy of Medical Multimedia Group LLC, www.eOrthopod.com]

Figure 6: Person with Olecranon bursitis [13]

[Image released into the public domain by its author, NJC123]

Carpal tunnel syndrome [14]: The repeated flexion and extension of the wrist causes the inflammation of tendons, leading to pressure on the median nerve as it passes through the carpal tunnel, as is illustrated in Figure 7 below. This results in numbness, weakened grip, as well as burning and tingling in the hand and arm.

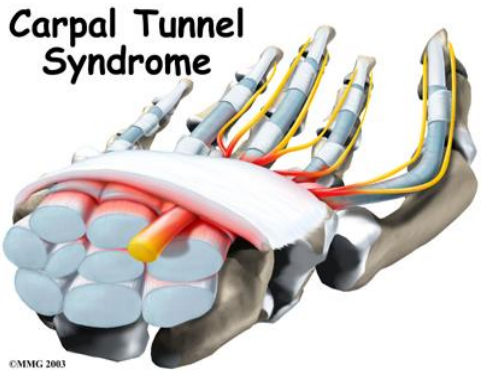

Figure 7: Carpal tunnel syndrome [14]

[Image courtesy of Medical Multimedia Group LLC, www.eOrthopod.com]

Cervical spondylosis [15]: This condition is caused by the narrowing or closure of the spinal canal, resulting in the compression of nerve roots, and causing severe pain and weakening of the muscles.

Cubital tunnel syndrome [16]: It occurs when the ulnar nerve is obstructed or compressed during its path along the inside edge of the elbow, as is shown in Figure 8 below. This compression can be caused by injury or any other physiological abnormalities and results in sensations similar to those that come from hitting the “funny bone.” During the later stages of the condition, when the ulnar nerve has been affected severely, the small and ring fingers may curl up to form an 'ulnar claw'.

Figure 8: Cubital Tunnel Syndrome [16]

[Image courtesy of Medical Multimedia Group LLC, www.eOrthopod.com]

De Quervain's syndrome [17]: This is an inflammatory condition where there is a thickening of the tendon tunnel, constricting the movement of the tendons and resulting in soreness of the forearm, wrist and thumb. This makes grasping objects between the hand and the thumb painful.

Dupuytren's contracture [18]: This is a disorder of the fingers where the fingers bend towards the palm and cannot be fully extended. This condition, which is shown in Figure 9, commonly affects the little and ring fingers, and is caused by the abnormal thickening of the connective tissues within one's hand due to carrying out repetitive motions with the fingers and hands positioned improperly.

Figure 9: Dupuytren's contracture of the fourth finger [19]

[Image by Frank C. Müeller, available under the Creative Commons Attribution-Share Alike]

Epicondylitis (tennis / golfer's elbow) [20] [21]: It is the muscle lesion or inflammation of tendons at the point where they attach to the bone on both the outside and inside of the elbow. This condition occurs when the collagen strands of the tendon become abnormally arranged as a result of wear and tear associated with carrying out repetitive motions that apply too much strain to the tendons. The collagen loses its strength and becomes more susceptible to injury. As this occurs, the body forms scar tissue over the tendon. Constant strain and overuse prevent the scar tissue from healing properly and the continuous build-up of scar tissue causes the tendon to thicken, causing pain when the elbow is moved.

Ganglion cyst [22]: It is a swelling that occurs around the joints and tendons in the hand or foot especially on the fingers and wrist. It is believed to be caused by the overuse of a joint, which causes the degeneration of the fibrous tissue, eventually developing into a cystic structure that could be painful and interfere with using the hand. Figure 10 gives an internal view of the effects of ganglion cysts on the human hand.

Figure 10: Ganglion Cyst [22]

[Image courtesy of Medical Multimedia Group LLC, www.eOrthopod.com]

_blank

Rotator cuff syndrome [23]: It is a condition that involves the tearing of tendons of the rotator cuff muscles. It is caused by the overuse of the shoulder, injuries and degeneration of the tendons as one ages. The condition can vary from the partial tearing and fraying of the tendons to the complete detachment of the tendons from the humeral head at the shoulder joint, as is shown in Figure 11. This results in loss of function and movement in the arm and shoulder and causes pain depending on the degree of damage at the rotator cuff.

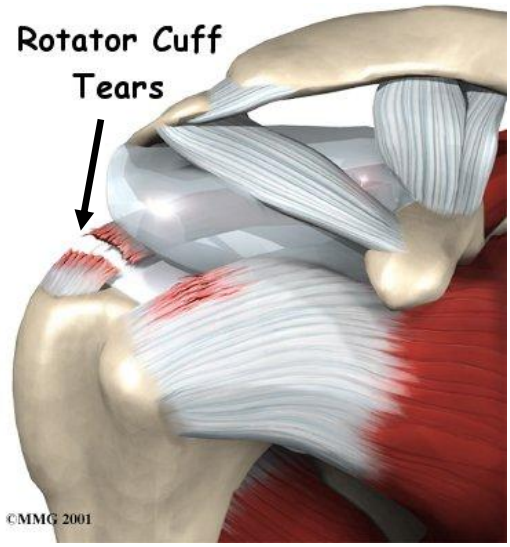

Figure 11: Rotator Cuff Tears [23]

[Image courtesy of Medical Multimedia Group LLC, www.eOrthopod.com]

Tendinitis [24]: Tendinitis, (or 'tendinopathy', as it is currently referred to), is an injury resulting in tears in the muscle fibers from overuse, causing an increase in tendon repair cells that may lead to reduced tensile strength, increased thickness of the tendon and restricted movement of the joints. In extreme cases, it may cause the weakened tendon to rupture with a sudden force or heavy lifting, which may necessitate surgery.

Trigger finger/thumb [25]: It is also referred to as 'stenosing tenosynovitis' and is a condition that is caused by the thickening in the tendon, forming a nodule, shown in Figure 12. This affects the movement of the tendons as flexion occurs (i.e. bending the fingers or thumb toward the palm of the hand). The formation of the nodule can be triggered by the use of pistol-gripped hand tools or steering wheels, as well as, rheumatoid arthritis. This causes pain when the finger or thumb is bent and a clicking sensation heard when the nodule moves through the ligaments in the finger. When the nodule gets too large, it may get stuck, and causes the finger to be locked in the 'flexed trigger' position, as is illustrated in Figure 13.

Figure 12: Trigger finger [25]

[Image courtesy of Medical Multimedia Group LLC, www.eOrthopod.com]

_blank

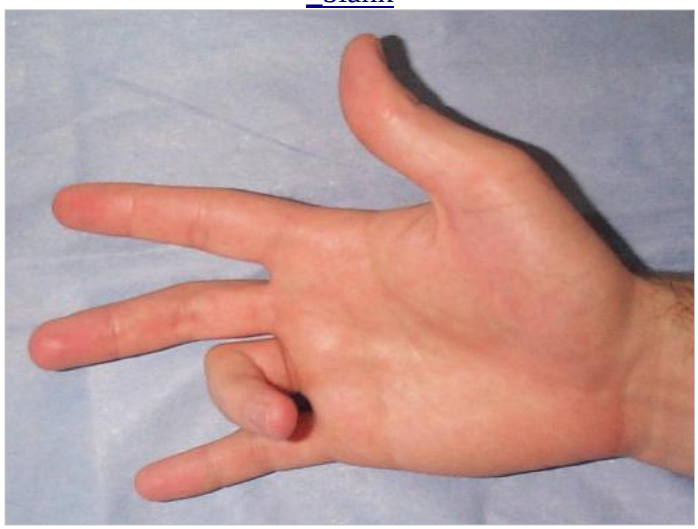

Figure 13: Finger joint displaying trigger finger [26]

[Image courtesy of Jeff Whiting]

Table 1 gives a summary of the symptoms of these Type 1 RSI conditions and their symptoms.

Table 1: Summary of some Type 1 RSI conditions and their symptoms

Conditions	Symptoms
Adhesive Capsulitis [11]	• The connective tissue surrounding the shoulder joint becomes inflamed and stiff, restricting the motion of the arm • The person experiences pain when moving the arm and shoulder
Bursitis [12]	• Inflammation of the sacs of synovial fluid (bursae) found in the elbows and/or knees
Carpal tunnel syndrome [14]	• Numbness in the wrist and arms • Weakened grip • Burning and tingling in the hand and arm.
Cervical spondylosis [15]	• Severe pain • Weakening of the muscles
Cubital tunnel syndrome [16]	• Experiencing sensations similar to those that come from hitting the "funny bone." • During the later stages of the condition, the small and ring fingers may curl up to form an 'ulnar claw
De Quervain's syndrome [17]	• Soreness of the forearm, wrist and thumb • Grasping objects between the hand and the thumb becomes painful
Dupuytren's contracture [18]	• It commonly affects the little and ring fingers • The fingers bend towards the palm and cannot be fully extended
Epicondylitis (tennis / golfer's elbow) [20][21]	• Inflammation of tendons at the point where they attach to the bone on both the outside and inside of the elbow • The tendon loses its strength and becomes more susceptible to injury. • As, a result, scar tissue is formed over the tendon, and the continuous build-up causes the tendon to thicken, causing pain when the elbow is moved

Table 1: Summary of some Type 1 RSI conditions and their symptoms (continued)

Conditions	Symptoms
Ganglion cyst [22]	• Swelling occurs around the joints and tendons in the hand or foot especially on the fingers and wrist. • It develops into a cystic structure that could be painful and interfere with using the hand.
Rotator cuff syndrome [23]	• The tearing of tendons of the rotator cuff muscles. • It can vary from the partial tearing and fraying of the tendons to the complete detachment of the tendons from the humeral head at the shoulder joint • Loss of function and movement in the arm and shoulder • Pain is experienced when moving the arm and shoulder
Tendinitis [24]	• There are tears in the muscle fibers that may lead to reduced tensile strength, • Increased thickness of the tendon and restricted movement of the joints • In extreme cases, it may cause the weakened tendon to rupture with a sudden force or heavy lifting, which may necessitate surgery.
Trigger finger/thumb [25]	• Experience problems moving bending the fingers or thumb toward the palm of the hand • It causes pain when the finger or thumb is bent and a clicking sensation heard • In extreme cases, it can cause the finger to be locked in the 'flexed trigger' position

2.2.2 Type 2 Repetitive Strain Injuries

Type 2 RSI is also referred to as non-specific pain syndrome (NSPS) or diffuse-RSI. Workers, especially those working in offices, have sometimes experienced pain in different parts of the body,

which were not directly associated with the areas experiencing strains and vibrations. This causes a problem for medical personnel trying to detect signs of injury and the nature of these ‘diffuse’ conditions, because they do not satisfy the diagnostic criteria for well-defined medical disorders [27]. For this reason, this condition, which is also known as neuropathic arm pain (NAP), is not recognized as an industrial disease, causing difficulties for workers trying to gain access to benefits for the treatment of their ailments.

One possible cause of non-specific pain syndrome may be nerve damage similar to a number of other painful neurological conditions [10]. RSI conditions occur in both upper and lower limbs and affect the spine in various areas, which in turn can cause referred pain into the limbs, making diagnosis difficult.

Research carried out at University College London indicated that RSI patients have a reduced sensitivity to vibration and more painful responses to test stimuli [28]. This is because during limb movement, there are mechanical strains exerted on peripheral nerves and this causes inflammation and injury of these minor nerves, resulting in changes in the functions of tissues and organs. This also caused some restrictions in the mobility of the median nerve, which supplies information back to the brain about sensations felt in the hand, resulting in the 'diffuse' pain felt by a person experiencing NSPS.

There are some factors that should be taken into consideration when changes are being made to the workplace in order to reduce the risk on further damage to the employees. These are [10]:

- the pace of the work carried out
- the number and duration of rest breaks that the laborers have
- the amount of repetition and force associated with movements
- posture
- the use of ergonomically designed tools and equipment

These factors vary with individual behaviors and workplace practices, and there needs to be integrated management approaches, which address both the organizational and the physical aspects of a worker's occupation and work environment [9]. According to Owen Tudor, who is the Health and Safety Commissioner (HSC) in the UK, this will include “identifying the signs of RSI early, in order to treat the individuals and remedy the causes, including stress and other psychosocial factors in the workplace, before the condition moves into its chronic phase".

2.3 Effects of RSI on Economy and Industry

Repetitive strain injuries (RSI) are a major occupational health problem in the workplace and a significant cause of lost production. The increase in the prevalence of work-related RSI is also affecting the economy.

Each year in the United States, it is reported that there are about a million people who take time off from work to treat and recover from musculoskeletal pain and loss of function due to repetitive and forceful motions experienced by the upper extremities [29]. The cost to industry is estimated to be $13 to $20 billion annually, and this is caused by workers' compensation costs associated with absenteeism of workers. There are other indirect costs to the employers that should be taken into consideration when determining the effect of RSI on the economy, which increase the estimates to as high as $45 to $54 billion annually. These costs are summarized in table 2 below [10]:

Table 2: Summary of indirect costs of RSI to businesses

Indirect costs of RSI to businesses and industry
Loss of productivity and businesses efficiency
Increased insurance premiums
Loss of revenue
Reduced worker morale
'Presenteeism'
Increased retirement costs for employees who are permanently unable to work
Increased injury benefits in industries
Increase in the recruitment and training costs
Bad publicity
Litigation costs and compensation payments to employees pursuing negligence claims

'Presenteeism' is when employees who are not able to function effectively as a result of illness or injury, still go into work because they are afraid of losing their jobs or experiencing other disciplinary action as a result of their absence from work [10]. This results in reduced productivity and may affect the quality of goods produced by the laborers.

Also, the loss of skilled workers results in an increase in the recruitment and training costs to replace the manpower. These costs become higher as more experienced workers need to be replaced. The business can also experience difficulties recruiting new laborers because of bad publicity from having their employees affected by RSI and other related conditions.

These estimates are based only on reported cases of work-related musculoskeletal disorders, and according to Praemer, Furner, and Rice [30], data collected in 1995 showed that the economic cost associated with both occupational and non-occupationally related disorders is as high as $215 billion.

From this information, it is such as to be more expensive for employers and their insurers to ignore RSI amongst their workers, because it would cost far more to pay the compensation and benefits packets than the costs to rectify the deficiencies in the design of products, workplaces and work systems that require high degrees of repetitiveness, insufficient rest time, and impose poor postures and excessive loads on the soft tissues of users.

Employers need to carry out risk assessments in order to identify what elements present can cause harm to their workers and determine whether the existing precautions in place are adequate to prevent these injuries or if there needs to be improvements made [31]. This will help to avoid accidents and ailments that can incur and increase the costs to their businesses, as well as efficiently manage the risk of RSI.

RSI also increases the cost of social security benefits that the government provides, especially to unemployed adults with families. In the statistical yearbook of Ireland [32], social welfare expenditure increased from 8.8% of the GNP in 2005 to 9.0% in 2006, and 18% of this cost incurred in 2006, was due to expenditures related to illness, disability and caring. Also, the number of recipients of illness, disability and caring payments rose by 43% between 1999 and 2006, and the net non-capital health expenditure rose by 155% from €4,573.9m in 1999 to €11,645.8m in 2006, and the chart below shows the proportion of recipients of weekly social welfare payments for 2006. The costs associated with illness, disability and care amounted for 24% of the social welfare payments in Ireland, which and this causes the suggestion that the increased prevalence of RSI among workers in factories and industries was a contributing factor.

There are no recently published statistics explicitly showing the effects of RSI on the economy and workforce of Ireland , partly due to the amount of time it takes to carry out a study, as well as, the small size of the population and economy. As a result, more prevalence is seen to be on treating workplace related back injuries rather than upper limb disorders. In order to estimate the effects of RSI on the Irish economy, we will use information from studies done in the United Kingdom as being representative of Ireland because of the similarity in their economy and industries.

In Great Britain, there were about 1.1 million people in 2001/2002, who were reported to have suffered from musculoskeletal disorders, which were caused and worsened by the type of work they did [31]. An estimated 12.3 million working days were lost due to work-related musculoskeletal

disorders, and the average number of days taken off between 2001 and 2002 was 19.4 days. These figures include upper limb disorders from which approximately 400,000 people suffered, resulting in a loss of around four million working days in the same period.

It is clear from these statistics that RSI affects a significant portion of workers. In order to reduce the occurrence of the harmful disorders associated with RSI, experts suggest preventative action [5]. Furthermore, there are no mathematical models for estimating the contributions of force, posture, repetition, rest/recovery time to experiencing RSI conditions. The "smart glove" system aims to monitor these parameters, so that this data can be used to assess and prevent the risks present in the workplace.

2.4 Prior Art and Research

2.4.1 Prior Art for Pressure sensing

Various products measure the pressure a hand exerts, including several commercially available pressure sensing glove designs. These are grip dynamometers, which are available from various vendors: the Pressure Profile Systems (PPS) FingerTPS, the Force Sensing Applications (FSA) Glove Pressure Mapping System (GPMS), the I-CubeX TouchGlove and the FSA Hand Sensor Array (HAS) [33], [34], [35], [36]. Dynamometers are gripped like pliers, while FingerTPS and GPMS are worn like gloves. The Hand Sensor Array, on the other hand, is draped over an object before it is grasped. Dynamometers only measure grip strength, while the other products are used to map pressure.

Grip dynamometers are instruments that measure the force the subject applies to the handle [33]. They cost around €200 ($300 USD), and can measure 890N (200 lbs) and greater. Dynamometers are used in studies, such as Mathiowetz *et al.*, as medical tools for measuring patients' grip strength, and in evaluations of pressure sensing glove designs [37], [33], [38]. Although dynamometers are useful for strength evaluation, they are inappropriate for measuring grip pressure in a work place, due

to the inability of the user to operate tools at the same time as the dynamometer. An example of a dynamometer is the Jamar Plus+ Digital Hand Dynamometer, which costs $349.95 USD, stores data from different trials, and computes their statistics [33]. It powered by two AAA batteries and has a simple, segmented display.

Several commercial products can be used to measure and map grip pressure. Examples are the PPS FingerTPS Wireless Tactile Force Measurement System, the FSA Glove Pressure Mapping System and the FSA Hand Sensor [35], [36]. The first two products are worn like gloves, while the HAS draped over the object being studied and then gripped. A picture of FingerTPS is shown in Figure 14 and the GPMS is shown in Figure 16. Refer to Figure 1 in Section 1 for a picture of GPMS.

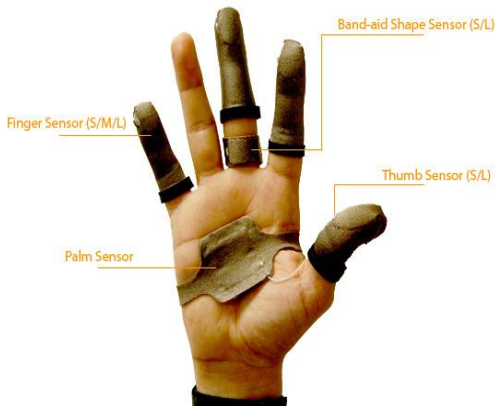

Figure 14: PPS FingerTPS [39]

[Used with permission from Pressure Profile Systems, Inc.]

The I-CubeX TouchGlove is a unique case, because the glove itself is a collection of sensors [36]. However, when they are connected to I-CubeX's Digitizer, the system outputs a MIDI signal corresponding to the pressure exerted on each sensor. It is marketed as more of a do-it-yourself "toy" than as an ergonomics tool. For example, its website showed an application where two of the gloves were used to create a virtual drum set. Touch Glove and the Digitizer are shown in Figure 15 below.

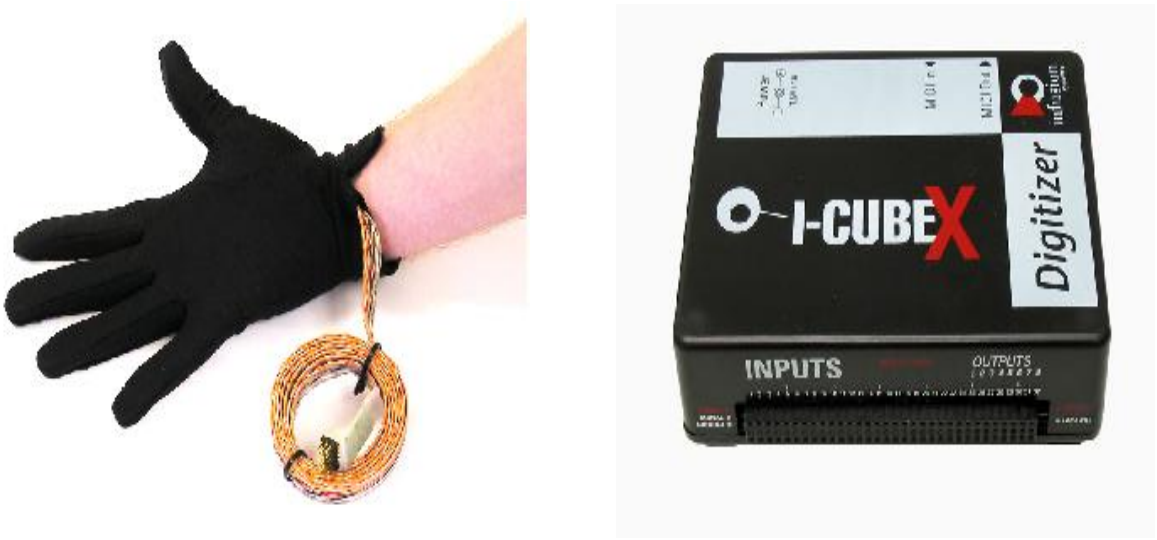

Figure 15: I-CubeX TouchGlove and Digitizer [36]

[Images courtesy of Infusion Systems Ltd.]

FingerTPS uses up to six capacitive pressure sensors (refer to Section 3.1for more detail) that are sampled at 100 Hz, come in four different varieties and are mounted as shown in Figure 14 [34], [39]. It sends data via Bluetooth to a computer from a transmitter worn on the back of a belt [34]. PPS's software displays the measurements in real-time and has a video playback feature. FingerTPS has a battery life of about four hours and recharges through USB. It senses up to 44.5 N (10 lbs), is accurate up to .44 N and comes with a straightforward calibration tool. The advantages of this system are its accuracy, comfortable design and wireless real-time display of the interpreted data. In addition, its use of rechargeable batteries through USB is convenient. Finger TPS has several disadvantages, especially in an industrial environment. It has a low sensing range compared to the 100N this project needs to measure (Appendix G-1), does not work over an industrial temperature range (only 0 to 50^{o} C), and does not have the battery life to make measurements throughout an 8+ hour work day [33], [34].

The FSA Glove Pressure Mapping System uses a glove that is covered with an array of 20 or 24 piezo-resistive pressure sensors (refer to Section 3.1 for more detail) [35]. This device is shown in Figure 16 below.

Figure 16: FSA Glove Pressure Mapping System (left) and Hand Sensor Array (right) [4]

[Images used courtesy of NexGen Ergonomics, Inc.]

The GPMS is calibrated to measure up to 690 kPa (100 Psi). Like the FingerTPS, this product comes with a sensor calibration device [34], [35]. Its sensors are sampled at over 100 Hz, and the data is stored on an optionally belt mounted computer [35]. This data can then be exported through a serial port on a computer, which displays the pressure measured by each sensor. With 20 sensors, GPMS can store roughly 5734 scans. There is an optional 4 MB memory expansion, various available glove sizes, and an optional kit for wireless communication with the serial port. Additionally, the scanning interval can be adjusted from tens of milliseconds to minutes through software. It can be used with either a 9V battery or an AC adapter supply power. Advantages of this system are its ability to store many scans, its comfortable, glove design, and its customizability (sensor placement, glove size and scanning rate). A disadvantage is its size and the long, awkward cables that it uses. Figure 16 shows the bulky enclosure that the user can wear on his belt, the long cables extending from the sensors, and the ribbon cable, which could potential interfere with the task the user is studying. Also, given the small sensing area of each sensor (0.635 cm (.25”) x 0.636 cm), the calibrated range is inadequate to measure the 100N that this project demands (Appendix G-1). It is prohibitively expensive, at €4400.58 ($6376.00 USD) for a 24-sensor glove or €3861.55 ($5595.00 USD) for a 20-sensor glove [40]. This price is for the sensor itself. An email from David Pinchefsky (Appendix G-2) a sales representative at NexGen Ergonomics explained that these systems require a Base System, which costs €4451.65 ($6450 USD)

or €4589.69 ($6650 USD), depending on the model. It would seem that the large array of sensors would be advantageous, but a study by Jung et al. of the GPMS found that its accuracy greatly decreased with an increasing number of sensors [38].

The FSA Hand Sensor Array is a soft, flexible array of 8 x 8 or 24 x 24 piezoresistive sensors. By covering an object with the array, the distribution of pressure can be displayed in real-time and exported to a spreadsheet [35]. Like the FingerTPS, this product can record a video of the real-time data and has a calibration kit [34], [35]. An interesting feature is that it can be configured in LabView to sound an alarm if a set pressure threshold is passed [35]. It can use the same optional wireless kit as the FSA GPMS. The combination of real-time display and exporting data to a spreadsheet is an advantage of this product, as is the alert feature and the resolution of the large sensor array. However, it is not calibrated to measure over 207 kPa (30 psi), and is not appropriate to use throughout a workday because of its handkerchief-like design. Finally, the HSA, though less expensive than the GPMS is still fairly expensive, at €931.74 ($1350.00 USD) for an 8 x 8 array and €2260.33 ($3275.00 USD) for a 24 x 24 array [40]. Additionally, it requires the previously mentioned Base System.

The I-CubeX TouchGlove uses six piezoresistive sensors, mounted on the fingertips and palm [36]. In conjunction with the Digitizer, it outputs MIDI signals, which can be used to control digital media. The glove itself is Nylon, made for either hand and only comes in a medium size. Another advantage is that the sensors have a wide range of range of over 98N (22 lbs). The sensors operate from -20C to 100C. Each sensor connects via twisted pair to a male header that plugs into the Digitizer. The Digitizer samples at up to 250 Hz with a 12 bit ADC. Its power is supplied via an AC adapter, and it can be used with or without a computer. This product is fairly costly, since the glove itself is €233.46 ($342.82 USD) and the Digitizer costs €407.93 ($599.00 USD).

Thus, several products, which sense the forces a hand exerts, are on the market. Dynamometers are used to evaluate one’s grip strength and are meant for more of a clinical environment [33]. The

FingerTPS and the GPMS are both pressure sensing glove designs with varying strengths and weaknesses [34], [35]. The Hand Sensor Array is a cloth-like device that could cover a tool, etc, and be used to collect pressure data [35]. Lastly, the I-CubeX TouchGlove was a pressure sensing glove design that is used in conjunction with a MIDI controller [36]. Although it is similar to the FingerTPS and GPMS, it is used in a very different application [34], [35], [36]. A "smart glove," immediately has an advantage over these devices in that it detects other stresses in addition to pressure. Tailoring the "smart glove" for an industrial setting, designing it with a sufficient pressure sensing range and battery life will also be advantageous. Concepts, such as the calibration tools, adjustable sampling rate, and memory expandability were things to consider in our design. Table 3 below summarizes the advantages and disadvantages of the discussed products.

Table 3: Comparison of Pressure Sensing Products Summary

Grip Pressure Sensing Product	Advantages	Disadvantages
Dynamometers [33], [33], [38]	• Large sensing range • Inexpensive	• Clinical devices not meant for industrial environment • Cannot be used simultaneously with tools
FingerTPS [34], [39]	• Customizable six-sensor glove design • High accuracy, wireless • Real-time graphical display • USB rechargeable batteries • Calibration tool	• Low sensing range, battery life • Not rated for industrial temperature range
GPMS [35], [37]	• Customizable glove design with up to 24 sensors • Adjustable scanning rate • Expandable built in data storage, exports data to computer • Optional wireless kit • Calibration tool	• Low sensing range • Expensive • Awkward cables • Potential accuracy issues
HAS [34], [35]	• Real time data, exports to spreadsheet • Conforms to various gripped objects • Can sound alarms in LabView • Optional wireless kit • Calibration tool	• Low sensing range, expensive • Awkward to use in workplace
TouchGlove [36]	• Six-sensor glove design • Adjustable sampling rate	• Low sensing range • Media controller not meant for industrial environment • Expensive

2.4.2 Prior Art for Goniometry

There is a broad range of goniometers available for the measurement of flexion and extension in the hand and arm. The measuring technology ranges from electro-optic or electromagnetic to purely mechanical.

Electro-optics have been used for biogoniometry, and are suited especially to joints which do not have a fixed axis of rotation, such as the knee [41]. These methods rely on photoelastic

birefringence induced by deforming an optical fiber [41]. Birefringence, or double refraction, is an optical effect which splits a single beam of light into two beams of light with orthogonal polarization [42]. One system utilities a photodiode to detect the polarized laser light beamed through a single-mode optical fiber [43]. When properly calibrated this system can relate changes in the angle of the optical fiber's bend with the changes in voltage caused by incident light on the photodiode [43]. Similar systems exist, with changes in the coherent light source [44], optical fiber [41], or polarization [44].

This technology was integrated into gloves as early as 1981 by Thomas Zimmerman at VPL Inc., who worked with NASA to design a data glove [45]. The glove was meant for virtual laboratories and workbenches [46]. The gloves contained optical fibers within the fingers, and it could measure finger flexion and extension using lasers and photodiodes [45]. However, this system was very expensive; the 1986 prototype cost over $9,000 [46].

Using the data glove as a starting point, AGE Inc. developed the power glove in 1989 [46]. In order to cut costs, the electro-optics were removed and replaced with conductive ink. The power glove houses two parallel pads of conductive ink for each finger [46]. The properties of the ink cause the conductance of the ink to change when the pads are bent. This allows the approximate flexion to be discerned with a resolution of 2 bits, recognizing 4 states [46]. The power glove was marketed to Nintendo as a controller peripheral to the original entertainment system and soon became a commercial success.

Air pressure has also been used to measure the flexion and extension of fingers [47]. Airtight PVC tubing is filled with air and fixed to the fingers [47]. Using pressure sensors, the flexion of fingers can be translated directly to a voltage [47]. By comparing these voltages to previously measured experimental values it is possible to determine an approximate hand configuration [47].

Electromagnetic goniometers also exist [48]. Permanent magnetics are implanted into one side

of a joint and a hall effect sensor is placed at the other [48]. As the joint rotates in the socket, the magnets bias a current upon the sensor. This can be translated into an estimation of the joint angle [48].

Several commercial products exist which measure the flexion and extension of joints in the arm and hand. An example of these products are the single and multiple axis goniometers sold by Biometrics Ltd [49]. These goniometers are attached to the body with medical tape, and are capable of measuring flexion and extension [49]. These sensors may incorporate strain gauges in order to make these measurements [49]. Unfortunately, this technology is proprietary.

Purely mechanical goniometers are also available. Baseline's series of goniometers attach to the hand to measure finger flexion [50]. Unfortunately, it can only measure movement in a single axis, and its accuracy is restricted.

Table 4 below summarizes the advantages and disadvantages of the discussed products.

Table 4: Comparison of Biogoniometric Measuring Solutions

Goniometric Sensing Product	Advantages	Disadvantages
Electro-Optic Goniometer [41], [43], [44], [45]	• Adequately accounts for rounded joints • Accurately measures join angle	• Power intensive • Complicated optics
Conductive Ink Goniometer [46]	• Low Power • Adequately accounts for rounded joints	• Low resolution • Limits to available technology • Initial prototypes are expensive
Air Pressure Goniometer [47]	• Adequately accounts for rounded joints • Can be created cheaply	• Poor resolution • Air tube can be bulky
Hall Effect Sensor [48]	• Adequately accounts for rounded joints • Accurately measure joint angle	• Invasive, must be surgically implanted • Sensor is vulnerable to common workplace interference • Expensive
Strain Gauge Goniometer [49], [50]	• Can be created cheaply • Low Power • Lightweight System	• Multiple gauges must be used to adequately measure rounded angles

3 Design Methodology

In this section, we will discuss the methods used to design the "smart glove" prototype. The project was divided into several subsystems, each of which was assigned to a specific team member. Using the implicit and explicit user requirements, as well as our background research, we were able to develop the components of each subsystem, as well as decide how they will interface with each other. In order to achieve functionality according to the project specifications, we conducted laboratory testing of each sub system. Our testing methods, as well as the rationale behind each test, are documented below.

3.1 Pressure sensor Selection

We used several criteria to select our pressure sensors. Since the design must not hinder the user's hand movement, the pressure sensors needed to be flexible and thin. Dr. O'Sullivan requested that the pressure sensors be accurate up to 100N (22.48 lbs) (Appendix G-1). Given the time and power constraints, it was important that the pressure sensor was low power and simple to implement. The cost of the sensors was also important, since the design requires six: one on each fingertip and the palm of the hand. Finally, the pressure sensor needed to be robust enough for an industrial environment.

We investigated several types of thin, flexible pressure sensors: capacitive, resistive and quantum tunneling composite (QTC). Capacitive sensors, which increase their capacitance as pressure is applied are considered the most sensitive and accurate type [51]. They require complex hardware, including their own microprocessor, which makes them impractical for our design [57]. Having a processor dedicated to one of our sensor subsystems would demand both time and decrease the battery life of our design. An example of a capacitive sensor that we looked at was a ConTacts C500 (Figure 17) by Pressure Profile Systems [52]. The C500 has built in hardware that outputs an analog signal

representing the pressure applied to the pad; however. It can measure forces up to ~138N. A major disadvantage is that the built in hardware is bulky, making this system inappropriate for a noninvasive design with multiple sensors, like ours.

Figure 17: **ConTacts C500 [41]**

[Image used with permission from Pressure Profile Systems, Inc.]

Piezoresistive pressure sensors, the second type of sensor we considered are simpler to implement than capacitive pressure sensors [51]. As pressure is applied, a piezoresistive sensor's resistance decreases. Unloaded, the sensor's resistance can be in the MΩ range and drop to tens of kΩ as pressure is applied [53]. There is a linear relationship between the sensor's conductance (1/R) and the applied force to the sensing area, making them simple to implement. Another advantage of a piezoresistive sensor is its resilience to noise. The disadvantages of piezoresistive sensors are hysteresis effects, their potential need for conditioning (ex. loading the sensor several times prior to use), and their relative inaccuracy compared to capacitive sensors [51], [53].

Two potential piezoresistive sensors for our "smart glove" were the Tekscan A201 and the Interlink 402. Table 5compares these components. We converted the units to SI as necessary. Neither of the sensors' literature expressed the accuracy the same way, except for their single part repeatability [54], [55], [56]. Figure 18 shows the Tekscan sensor and Figure 19 shows the Interlink sensor.

Figure 18: A Tekscan FlexiForce A201-100 from the 8-Pack Used in Prototyping

Figure 19: Interlink 402 (middle, top) [57]

[Image used with permission from Interlink Electronics Inc.]

The sensors are both flexible and similarly sized. The Interlink sensor had several major advantages. It cost less than half as much as the Tekscan sensor, worked over a wider temperature range, was rated to last ten times as long and did not require conditioning, according to a distributor's sales representative (Appendix G-3). However, Interlink's website and Gail Shaw, an Interlink sales manager emphasized that their sensors are not meant for qualitative measurements [57], (Appendix G-4). An advantage of the Tekscan part was that it was much more robust, being able to withstand up to 68.9 MPa (10000 psi) interfacing circuitry, it can respond to up to over 4000N [55]. In addition, it had slightly higher single part repeatability. Unfortunately, either sensor is weak against shear force, since they are laminated [53], [56]. Both sensors were relatively inexpensive though, and given Interlink's warnings about the making quantitative measurements with the sensors, and the greater robustness and repeatability of the A201, we determined that it was the best piezoresistive sensor for our project (Appendices E-3, E-4).

Table 5: Piezoresistive Pressure Sensor Comparison

Properties	**Tekscan Flexiforce A201** [55]	**Interlink FSR 402** [56]
Thickness	0.208mm	.20mm
Sensing Area (diameter)	9.53mm	12.7mm
Accuracy [54] Linearity (Error) Repeatability (single part) Repeatability (part to part) Hysteresis Drift	not specified <5% <2.5%** not specified <4.5% <5%	5% - 25% not specified 2.5 - 5% 15 - 25% not specified not specified
Response time	<5 us	not specified
Operating Temp.	-9 to 60 C	-30 to 70 C
Force Ranges	0-440 N and < 4448.2 N	< 1N to > 100 N
Max pressure	68.9 MPa	not specified
Lifetime	1 million	10 million
Other Notes:	Requires conditioning	Only recommended for qualitative measures
Price [53],[58]	75 € ($110 USD) / 8 sensors 9.375 € / sensor	43.11 € ($63.23 USD) / 10 sensors 4.31 € / sensor

*depends on measurement consistency
**requires conditioning

Another type of sensor we considered was QTC (Figure 20), which takes advantage of a quantum mechanics phenomenon to behave like a resistor that is sensitive to force [59]. These sensors are used in pressure sensitive cloth applications, so they seemed ideal for a "smart glove." The fact that they had resistive behavior meant that they would be simple to setup [60]. They also had high repeatability, were inexpensive and did not suffer from hysteresis or require conditioning. Unfortunately, the Peratech QSRC025130 and similar sensors are out of production and were available in limited quantities from one of Peratech's dealers (Appendix G-5). Sara Gott from Peratech said that they design sensors for customers instead now, but that this service was not free (Appendix G-6). The sensors had an appropriate range for our project, being rated for 0 – 100 N [60]. Unfortunately, we could not choose QTC sensors because non-custom sensors were not available. Since Peratech claims that they can serve as direct replacements for piezoresistive sensors, future work on this project should consider a setup that uses QTC sensors instead of resistive sensors.

Figure 20: QTC Sensors [61]

[Image used with permission from CUI Inc.]

Having compared several alternatives for pressure sensors, we determined that the Tekscan Flexiforce A201 was the best choice for the "smart glove" prototype. QTC sensors seemed like a promising option; however, they required having a custom sensor designed. Nevertheless, the A201 was thin, flexible, inexpensive, simple to implement and had the range of sensitivity needed for this project. Furthermore, it could withstand a tremendous amount of force, which would be advantageous in an industrial environment.

3.1.1 Preliminary Sensor Testing

Having chosen a sensor pressure sensor, our next step was to gather calibration data. The A201-100's conductance had a strong linear correlation to the force applied to its sensing area, according to Tekscan's documentation [62]. By taking multiple resistance measurements at known forces and performing a linear regression of this data, we could determine this relationship for each of the glove's six sensors. Since the part-to-part repeatability of the A201 was unknown, we labeled each sensor so we could determine the data set to which each one corresponded. Measurements were made using Dr. O'Sullivan's force gauge (Figure 21) (Rated for 0 – 2200 N x 1 N / 0-500 lb x 0.2 lb) and a digital multimeter. We adapted the contact point of the force gauge to the pressure sensors using a bolt as a puck. The bolt was an appropriate choice because it had a slightly smaller diameter than the

sensing area and was rigid enough to transmit the force. To prevent uneven loading, the bolt was filed until it was acceptably level. Figure 22 shows the sensors and the puck.

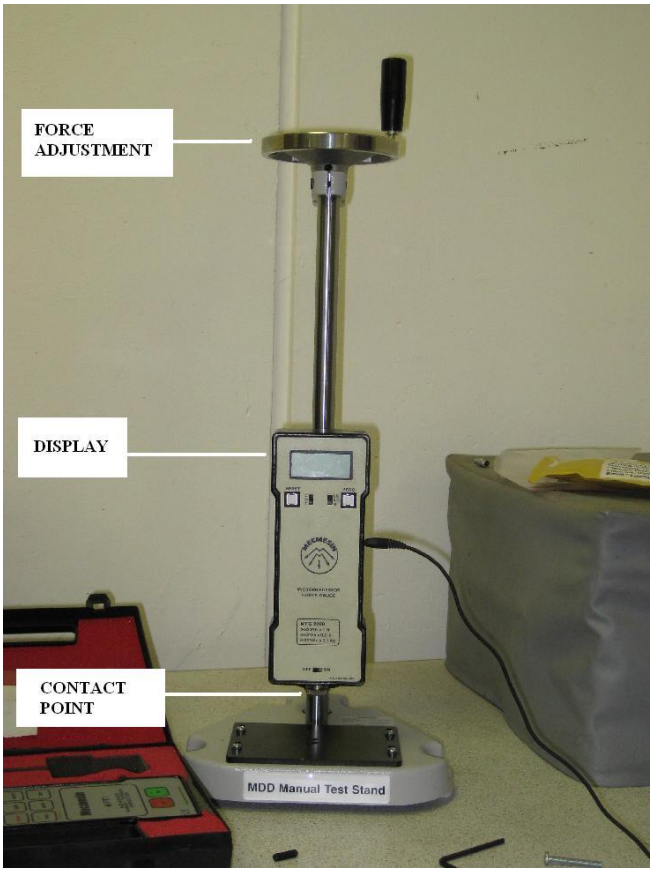

Figure 21: Dr. Leonard O'Sullivan's Force Gauge Used for Calibration at University of Limerick

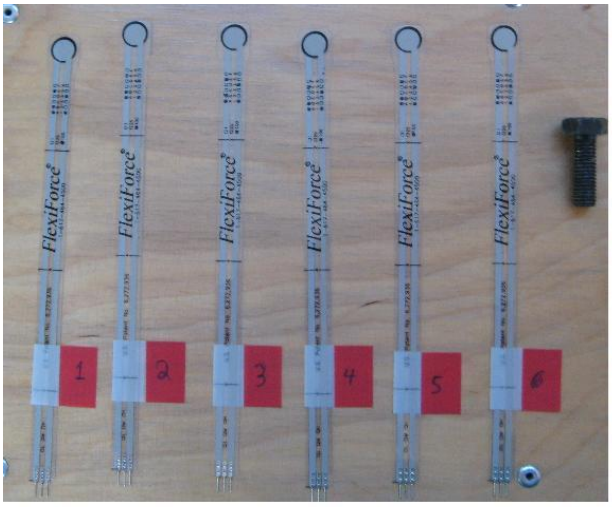

Figure 22: Tekscan A201-100 Sensors and Puck (Bolt)

We first conditioned each sensor in accordance with the FlexiForce User Manual. This involved applying 110% of the greatest force being measured five times, and allowing time for the sensor to stabilize between presses [62]. Conditioning each sensor ensured the repeatability of its conductance to force characteristic. In practice, this procedure would only need to be repeated if the glove was unused for several weeks. We conditioned Sensor 1 for 444.8 N (200 lbs) and sensors 2 – 7 for 890 N (100 lbs). We took a series of 12 resistance measurements with the DMM for each of the six sensors calibrated for 100 lbs [62]. These measurements were made at multiples of ~10 lbs (44.4 N) from 0 to 100 lbs and at multiples of ~25 lbs (111.2 N) from 0 to 100 lbs. The plot in the User Manual took measurements up to 100 lbs, so this setup was similar to Tekscan's. We used the first sensor to compare data from a sensor conditioned 200 lbs to a sensor conditioned for 100 lbs. We inserted the sensors into a breadboard to make it easier to connect the DMM's clips to its two leads. Figure 23 shows the setup for the calibration measurements. Their unloaded (no pressure applied) resistances were too large to measure accurately with the DMM, so the first point used in every plot corresponded to ~10 lbs. It was difficult to set the force gauge to exactly 10.0, 20.0, 25.0 lbs, etc, so we chose the closest force at which we could stabilize it (ex. 10.2, 19.8, 24.6 lbs, etc.). We took the inverse of the sensors' resistances to compute the conductance and plotted this against the force (converted to N). We plotted each sensor's conductance to force characteristic and generated linear regressions in Excel.

The conductances of the seven sensors all had strong linear correlations to the force applied to their sensing areas, since each one had an R^2 that was close to 1.0. In fact every line's R^2 was greater than or equal to 0.98. Table 6 summarizes the results for each sensor, listing their regression line and R^2. Appendix D shows the data for each sensor and its plot. Note the similarity of the regression lines. The slopes ranged from 6E-8 to 10E-8 S/N and the intercepts ranged from .7E-6 to 5E-6 S. The sensor conditioned for 200 lbs had a similar conductance-force characteristic to the six that were conditioned

for 100 lbs. The User Manual says that the "entire sensing area of the *FlexiForce* sensor is treated as a single contact point [62]." Therefore, we needed to divide by the sensing area ((π (0.00953/2)^2 = 71.3E-6 m^2) to make a pressure measurement based on these lines in software.

Table 6: Tekscan A201-100 Pressure Sensor Conductance to Force Linear Regression Lines

Sensor	Regression Line	R^2
1	G = 7E-8x + 5E-6	0.9986
2	G = 9E-8x + 3E-6	0.9891
3	G = 10E-8x + 2E-6	0.9893
4	G = 10E-8x + .7E-6	0.9893
5	G = 6E-8x + 5E-6	0.9893
6	G = 6E-8x + 5E-6	0.9893
7	G = 6E-8x + 2E-6	0.9893

G = Conductance in S, x = Applied force to the sensing area in N

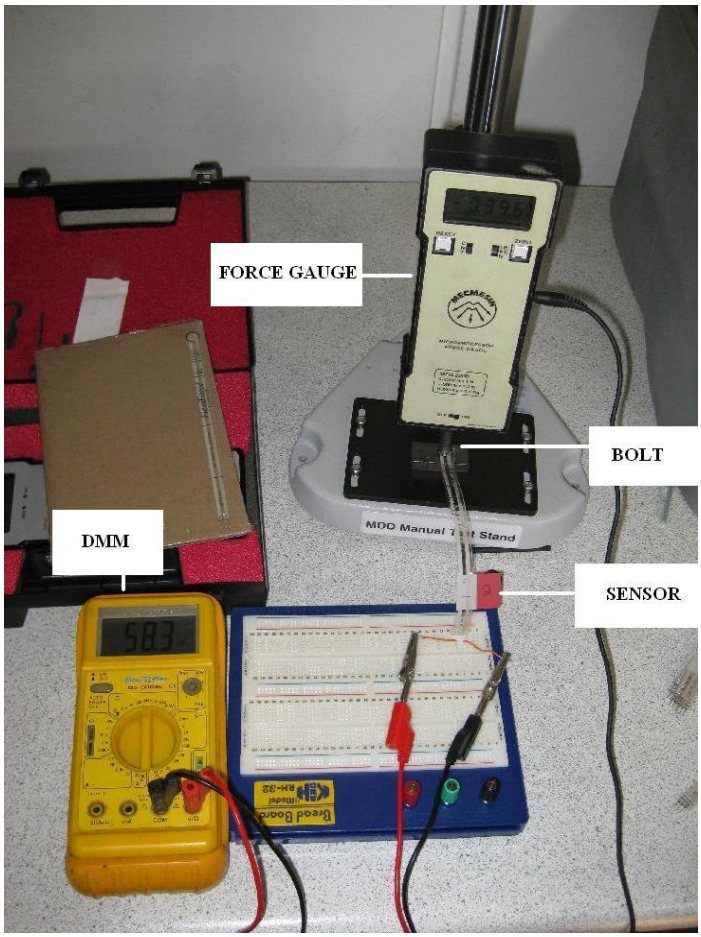

Figure 23: Tekscan A201-100 Sensor Calibration Setup Used in Dr. O'Sullivan's Lab at UL

3.1.2 Pressure Sensor Interfacing Circuitry Design

Since the applied force to our pressure sensors could be determined from the conductance, the interfacing circuitry for the pressure sensors needed to allow the microcontroller's software to quantify the sensor's conductance based on an ADC conversion (voltage). Essentially, the circuit needed to output a voltage that was directly proportional to a sensor's conductance. Tekscan recommended using a circuit (Figure 24), which was basically an op-amp in an inverting gain configuration with a fixed input voltage (V_D in Tekscan's circuit, V_{REF} in ours) and with the sensor controlling the gain [62]. Negative feedback forces the op-amp's inverting input to the same potential as the noninverting input, which is grounded. If V- is 0V (a "virtual ground"), by Ohm's Law, the current flowing through the sensor is V_D/R_{S1}. This current flows through R_F (the combination of R_f (fixed) and R_{f1} (potentiometer)) because of the op-amp's high input impedance, so $V_{OUT} = -(V_D/R_{S1})R_F = -V_D(R_F/R_{S1})$. The sensor's conductance, $1/R_{S1}$ is therefore $V_{OUT}/(-V_DR_F)$. We determined the relationship between the sensor's conductance and the applied force in section 3.3.1. Note that the reference voltage for the sensor had a negative potential so the output would have a positive relation to the sensor's conductance. The purpose of R_{f1}, which could be altered to change the gain was to make the resolution adjustable. For instance, if an ADC had an input range of 0-3.3V and the sensor would experience a range of forces from 0 to 100N, the 3.3V point should be set to correspond to when approximately 100N is applied to get the greatest resolution from the sensor.

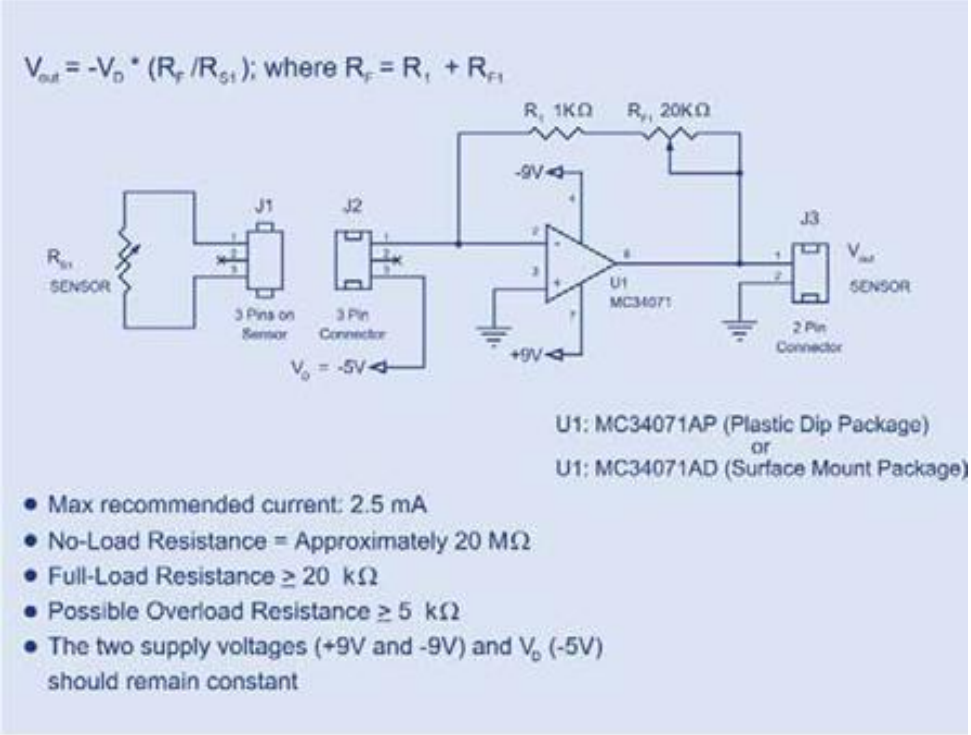

Figure 24: Tekscan A201 Example Circuit [62]

[Image used with permission from Tekscan Inc.]

Several changes needed to be made to Tekscan's circuit to tailor it to our application. Most of these changes pertained to the op-amp selection. A 3.3V single-supply op-amp, with a rail-to-rail output covered the input range of the MSP430's ADC12 [63]. It was also important that the op-amp had low power consumption, low DC errors, an industrial temperature range and low temperature susceptibility. Since the highest frequency power tools will cause the hands to experience approximately 1250 Hz, the gain-bandwidth product did not need to be substantial [2]. This also implied that a high slew rate was not necessary. Given a 1kHz sinusoid, which can swing from 0 – 3.3V, the slew rate needed to be at least the maximum of: $\frac{dV}{dt}(3.3\sin(2\pi 1250t)) = 0.0259$ V/µs.

Table 7: Comparison of Candidate Op-Amps Considered for the Pressure Sensor Signal Conditioning Circuitry

Name	OPA333/2333 [64]	OPA336/2336/4336 [65]	TLV341/2/2S/4 [66]	TLV2382 [67]	TLV2760/1/2/3/4/5 [68]
# Channels	1 or 2	1, 2 or 4	1, 2 or 4	1 or 2	1, 2 or 4
Bulk Price (Listed in $ USD) [69]	$1.2, $1.9	$0.4, $1.10, $1.75	$0.38, $0.45	$0.80	$.60 to $1.20, depending on package
Operating Range(C)	-40 to 150	-55 to 125	-40 to 125	-40 to 125	-40 to 85
V_{os} (Typ,Max)	2, 10 µV	60, 125 µV	0.3, 4 (4.5 T) mV	0.5, 4.5 (6.5 T) mV	550, 2500 (6800 T) µV
V_{os} vs. Temp (µV/C)	0.02, 0.05	1.5	1.9	1.1	9
I_b (Typ,Max, temp)	70, 200 (150 T) pA	1, 10 (60 T) pA	1, 100 pA (3000 T)	1, 60 (200 <70C, 1000 <125C) pA	3, 15 pA (200 T for xI package)
I_{os} ± Typ, Max	140, 400 pA	1, 10 pA	6.6 fA	1, 60 (100 <70, 1000 < 125C) pA	3, 15 pA (200 T for xI package)
A_0 Min, Typ	106, 130 dB	100 (90 for Quad package), 115	70 (60T), 110 dB at 20kΩ load or 65 (55T), 100 dB at 2kΩ load	80, 100 (77T) dB if V_s = 2.7V	93.1, 101.6 dB (91.4 T) converted from V/mV, if V_{DD} = 3.6V
GBW	350kHz	100 kHz	2.2 MHz	160 kHz	500kHz
Slew Rate V/µs	0.16	0.03	0.9	0.06 (0.05 - 0.08 T)	.11, .23 (0.09) Rising, 0.10, 0.22 (0.09) Falling
Vout range	30 -50 (70 T) mV from rail	3mV, (100 to 500 T) from rail	40 to 60 (85T) mV from low, 25 to 60 (85T) mV from high	200 (220), 160 mV (Vs = 2.7V, I_o = 100 µA)	50, 75 (100T) mV to 3.525, 3.55 (3.5T) V if I_o = 500 µA
I_{sc}	± 5mA	±5mA	6, 12 mA source, 10, 20 mA sink	400 µA	15 mV source, 19 mV sink at VDD = 2.4V
Supply Range	1.8 - 5.5V	2.3 - 5.5V	1.5 - 5.5 V	2.7-16V	1.8 to 3.6V (4V abs Max), ±0.8 - ±1.8 split
I_Q (per channel)	17 - 25 (28 T) µA	20, 32 (36 T) µA	70, 150 (200 T) µA	7, 10 (15 T) µA	20, 28 (30 T) µA powered, 10, 50 (400 nA) shut down

Table 7 compares several op-amps, which we considered for the pressure sensor conditioning circuitry. We chose the OPA2333 (dual OPA333) based on these criteria. It had a lowest input-offset voltage, which varied little with temperature [64]. It also had low input-bias current, low input-offset current, low quiescent current and an ample slew rate and gain-bandwidth product. Its major advantage over the other parts was its lower temperature susceptibility and extremely low $V_{OS.}$ Furthermore,

Texas Instruments recommended it for applications where it drives ADCs. Its disadvantage was that it was slightly more expensive than other parts, partially because it was only available in single or dual packages [69]. We weighed price less than the quality of the amplifier, since Dr. O'Sullivan emphasized accuracy more than cost, and since the components were relatively inexpensive (Appendix G-1).

Some of our other changes to the Tekscan circuit were the use of a lower reference voltage magnitude ($|V_{REF}|$) to reduce the power dissipated in each sensor ($P_{SENSE} = V_{REF}^2/R_S$, R_S = sensor's resistance) [62]. Some considerations were -500mV or -1V. A tradeoff was that decreasing V_{REF} required us to increase the gain and therefore use much larger resistances for the potentiometer. Additionally, it was difficult for us to find regulators that could supply an output less than 1.2V (another circuit could be used to invert the reference). Since other circuitry required a 1.5V reference, we chose -1.5V for V_{REF} to simplify the power section. Another advantage of -1.5V was that an alkaline battery could serve as the reference before the power section was prototyped.

Decreasing V_{REF} substantially necessitated increasing R_F so that there would be adequate gain to drive the output to the upper limit of the ADC's range once the maximum force we were measuring had been applied to the sensor. We chose a 200kΩ trimmer as R_{f1} because it allowed us to easily adjust the circuit during testing. Figure 25 shows the original schematic for the six identical pressure sensor circuits. Note that we routed the six outputs and three supplies to a connector. This is because we would not build the power circuitry on this board. Three OPA2333's provided the six op-amps needed. We bypassed each chip's supplies with 100nF caps, as their datasheets recommended [64].

The six trimmers enabled us to make sensitivity adjustments needed, so that each amplifier would clip slightly above the voltage corresponding to the maximum grip strength (discussed in Section 3.1). By substituting 100N into the regression lines in

Sensor	Estimated G_{100N} (S)	Estimated R_{100N} (Ω)	R_F (Ω)
1	12.0E-6	83.3E+3	177.8E+3
2	12.0E-6	83.3E+3	177.8E+3
3	12.0E-6	83.3E+3	177.8E+3
4	10.7E-6	93.5E+3	199.4E+3
5	11.0E-6	90.9E+3	193.9E+3
6	11.0E-6	90.9E+3	193.9E+3
7	8.0E-6	125.0E+3	266.7E+3

Table 8, we estimated the sensor's conductance at this point. Their resistances were the inverse of this quantity. The OPA2333's datasheet indicated that temperature could limit the output range to within 70mV of the rail [64]. When we calculated the trimmer setting, we used 3.2V as V_{REF} to ensure that the amplifier would not clip when 100N was applied. If $V_{OUT} = -V_{REF}(R_F/R_S)$, substituting 3.2V for V_{OUT}, -1.5V for V_{REF} and $R_{100N.}$ for R_S, the equation became: $3.3V = 1.5V(R_F/R_{100N.})$, where R_F is the series combination of the fixed resistor R_f and R_{f1}. The potentiometers' adjusted resistances were therefore: $R_{100N.}(3.3/1.5)$. Table 8 lists the sensors and their R_F calculations.

Table 8: R_F Settings for Sensitivity Adjustment

Sensor	Estimated G_{100N} (S)	Estimated R_{100N} (Ω)	R_F (Ω)
1	12.0E-6	83.3E+3	177.8E+3
2	12.0E-6	83.3E+3	177.8E+3
3	12.0E-6	83.3E+3	177.8E+3
4	10.7E-6	93.5E+3	199.4E+3
5	11.0E-6	90.9E+3	193.9E+3
6	11.0E-6	90.9E+3	193.9E+3
7	8.0E-6	125.0E+3	266.7E+3

Considering the size of these resistances, we needed to increase R_F from its original 1kΩ value or choose a larger potentiometer. We chose 100kΩ as the new value of the fixed resistor, R_f because it was readily available.

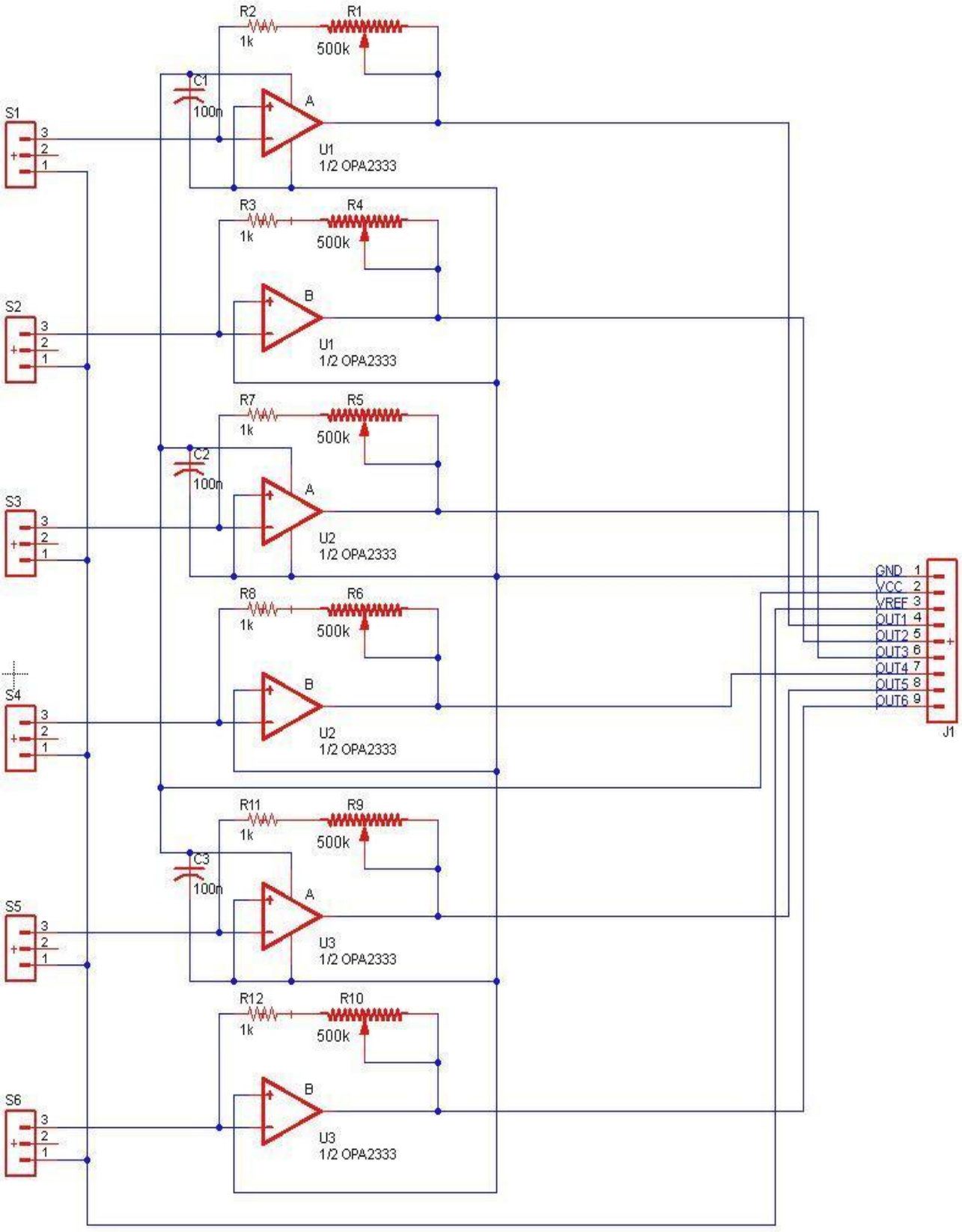

Figure 25: Original Pressure Sensor Conditioning Schematic: Amplifier Outputs Connected Directly to Microcontroller

3.1.3 Pressure Sensor Interfacing Circuitry Testing

Having determined the values for all of the passives components in the pressure sensor circuit and having ordered op-amps, we began our initial testing of this subsystem. Given the limited availability of power supplies, we used an AA battery as V_{REF}. It measured 1.6V on the DMM. Limited quantities of headers were available at the time, so we assembled two circuits (corresponding to sensors 2 and 3). Figure 26 shows the layout of the original prototype. Note the custom 8-SOIC breakout board.

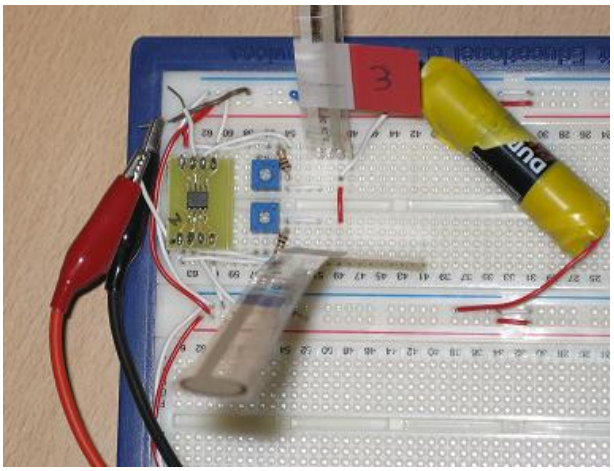

Figure 26: Initial Prototype of Pressure Sensor Circuitry – 2 Amplifiers on Breadboard with AA Battery as -1.5V

Immediately, we noticed a problem with noise, which was more apparent when the sensor was unloaded. To get a better understanding of the source of the noise, we set the oscilloscope to trigger on the edge of the noise and turned infinite persistence on. Figure 27 shows the output of the original circuit. We caused the large pulse by pressing the sensor firmly for roughly one second. Note the large amounts of noise when the sensor is unloaded (no pressure applied, $V_{OUT} \approx 0V$). Both circuits picked up high frequency noise (10's of kHz) and 50 Hz noise from the AC lines. Figure 28 and Figure 2929 show the high frequency noise and AC noise on the sensor 2 circuit respectively and Figure 30 and Figure 31 show the high frequency noise and AC noise on the sensor 3 circuit respectively. We

moved the sensors near the ground clip from the power supply to make the 50 Hz noise more noticeable.

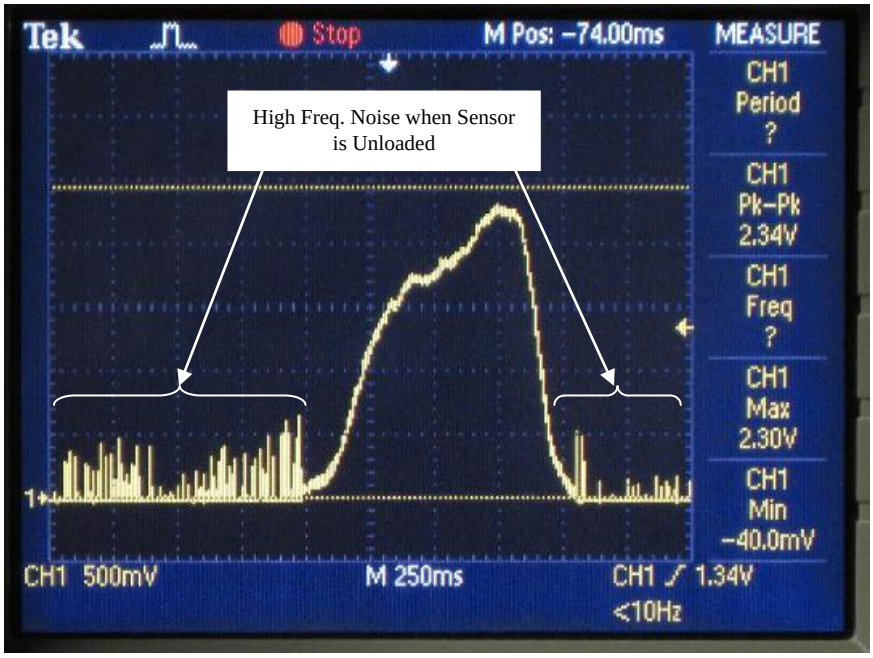

Figure 27: Output of Original Pressure Sensor Prototype

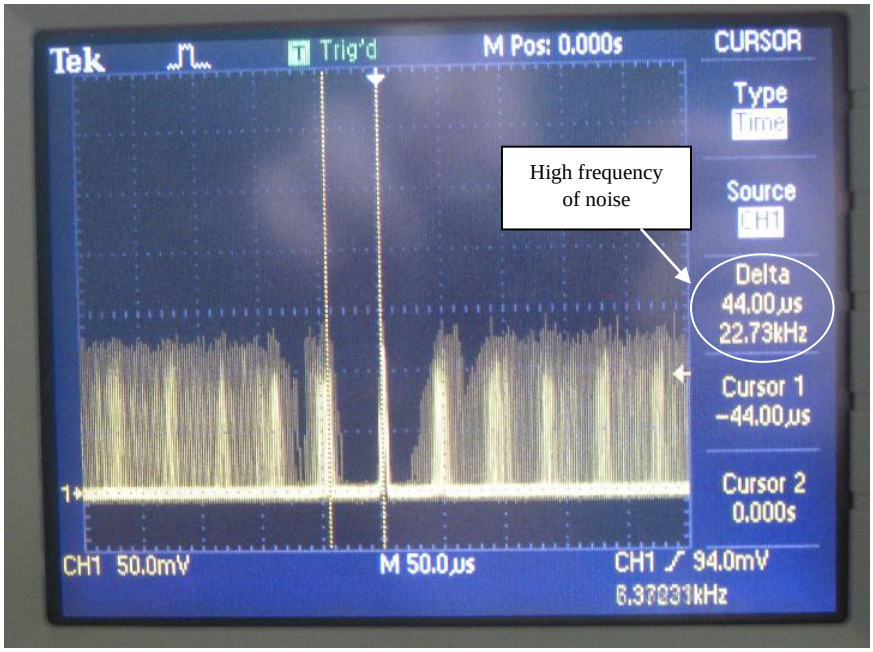

Figure 28: High Frequency Noise on Sensor 2 Circuit With Infinite Persistance

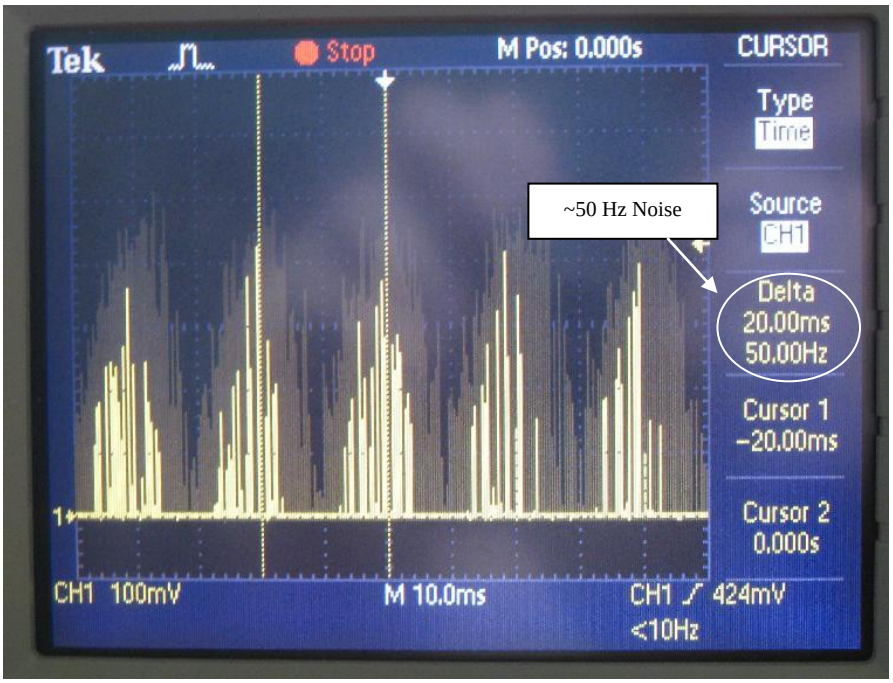

Figure 29: 50Hz noise on Sensor 2 Circuit

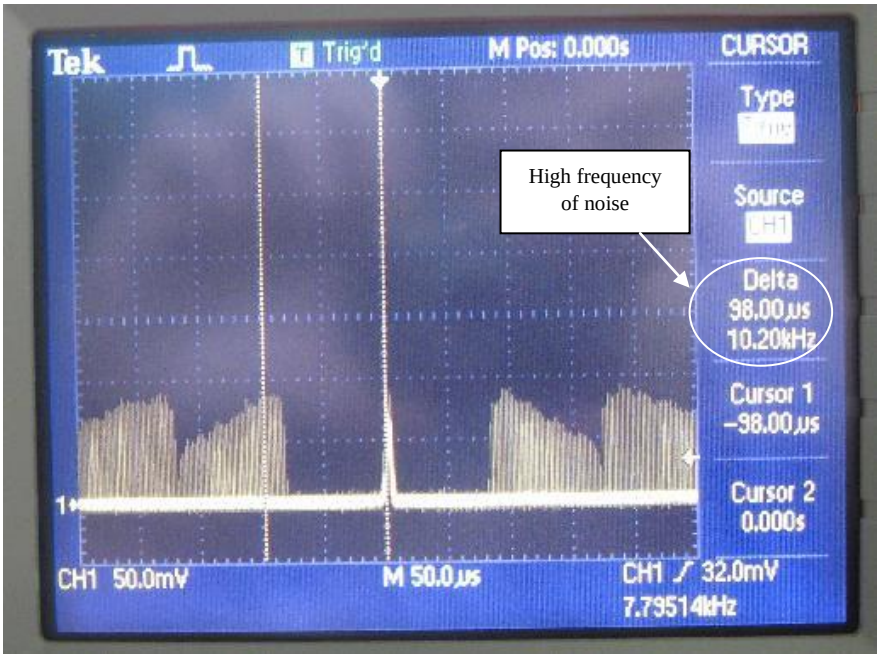

Figure 30: High Frequency Noise on Sensor 3 Circuit

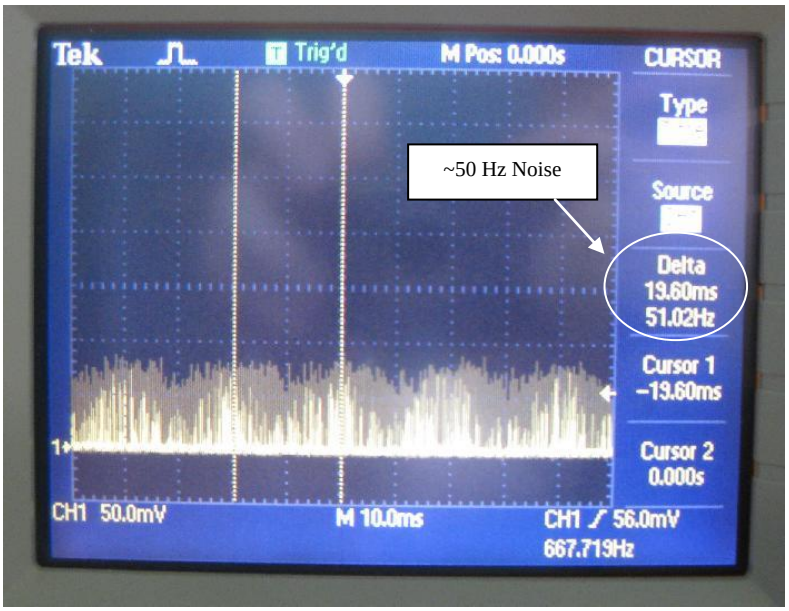

Figure 31: 50Hz Noise on Sensor 3 Circuit

The high frequency noise was the simplest problem to fix because it was above the range of frequencies that industrial equipment creates [2]. We added RC low-pass filters to each channel to attenuate the high-frequency noise. Figure 32 shows this simple circuit. The output is the node where the resistor and capacitor connect. It is a voltage divider with the resistor and capacitor's impedances (R and 1/sC respectively). $$V_{OUT} = \frac{Z_C}{R + Z_C} = \frac{1}{\left(\frac{R}{Z_C}\right) + 1} = \frac{1}{1 + sRC}$$. Thus, this circuit has a single left-hand pole at $\omega = 1/RC$, so frequencies above $f = 1/(2\pi RC)$ are attenuated.

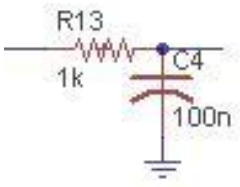

Figure 32: RC Low-pass Filter.

Given the limited amount of time remaining to complete our prototype at this point we chose1kΩ and 100nF for R and C since they were available in both through-hole and surface-mount packages. With this combination f_{3dB} was $1/(2\pi(1k\Omega)(100nF)) = 1.59$ kHz. This both preserved the frequency content that we were interested in and attenuated the higher frequency noise on our signal. Figure 33 and Figure 35 show the outputs of the two pressure sensor circuits and Figure 34 and Figure 36 show the noise (without persistence) after the low-pass filter was added. The signal was much cleaner, compared to the unfiltered output, as seen in Figure 26. Nevertheless, the 50 Hz noise was still noticeable (Figure 34 and Figure 36).

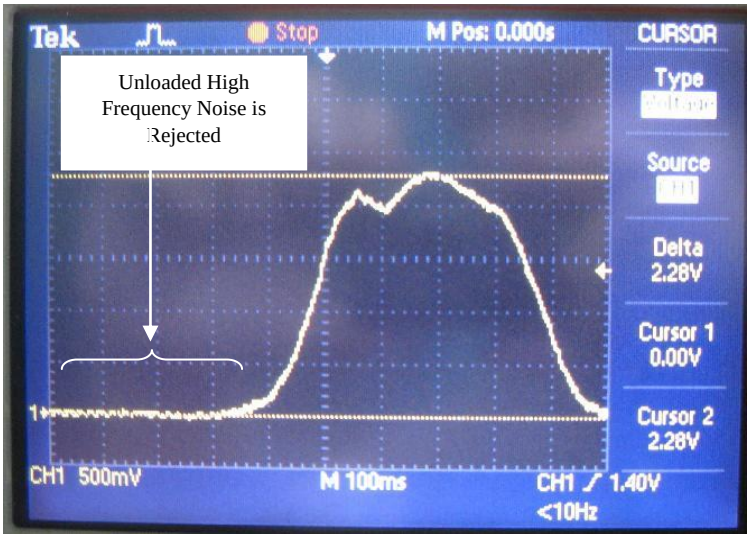

Figure 33: Sensor 2 Circuit Output with 1.59kHz LPF – High Frequency Noise Rejected

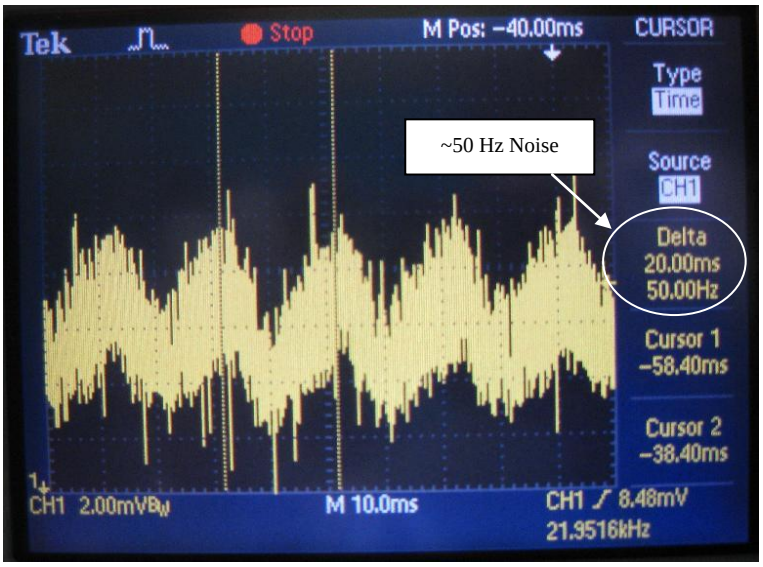

Figure 34: Sensor 2 Circuit Noise with 1.59 kHz LPF - Power Noise Still Visible

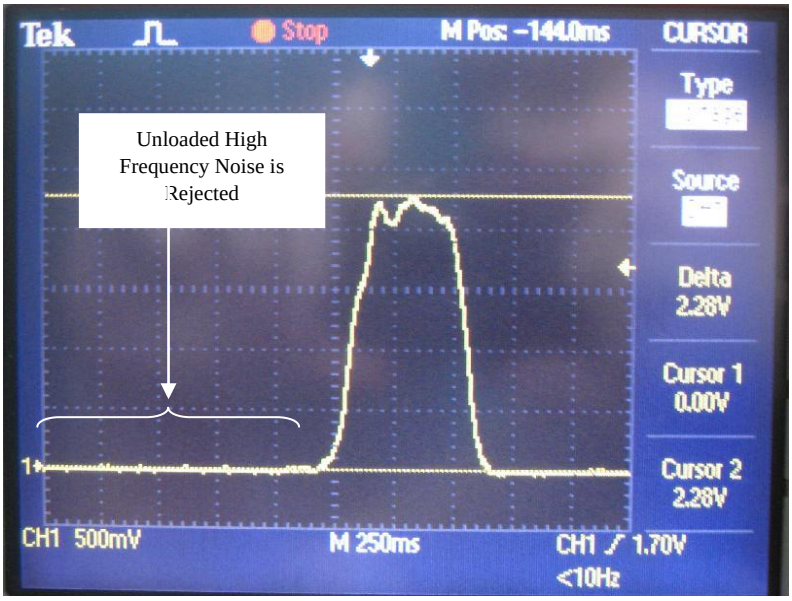

Figure 35: Sensor 3 Circuit Output with 1.59kHz LPF - High Frequency Noise Rejected

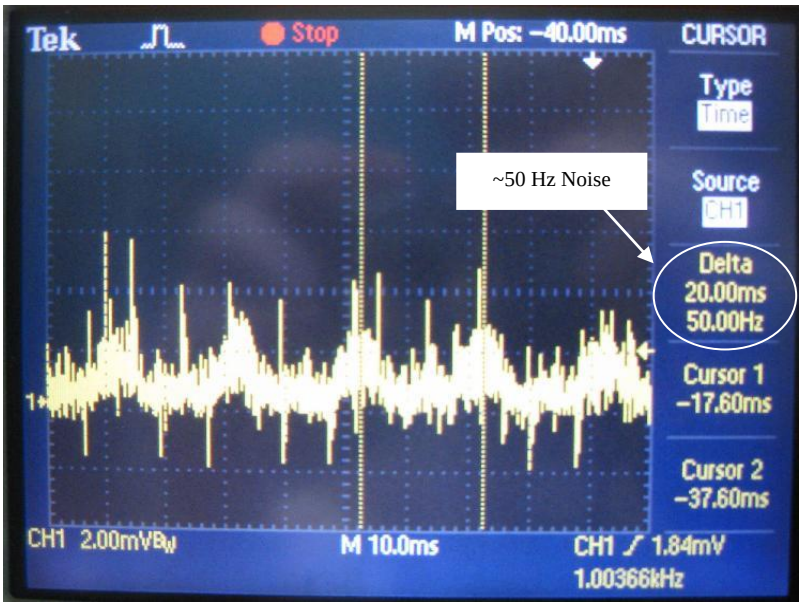

Figure 36: Sensor 3 Circuit Noise with 1.59kHz LPF – Power Noise Still Visible

To verify that the sensors themselves were picking up the noise, we substituted a 100kΩ resistor for each of the them, AC coupled the channels and measured the output of each op-amp. As the clean signals in Figure 37 and Figure **38**38 show, the noise was indeed being picked up by the sensors. Furthermore, measurements of V_{DD} (3.3V) and the reference voltage, V_{REF} (-1.6V) did not show any of the noise. We added a 100nF in parallel with V_D and it did not cause any noticeable improvement.

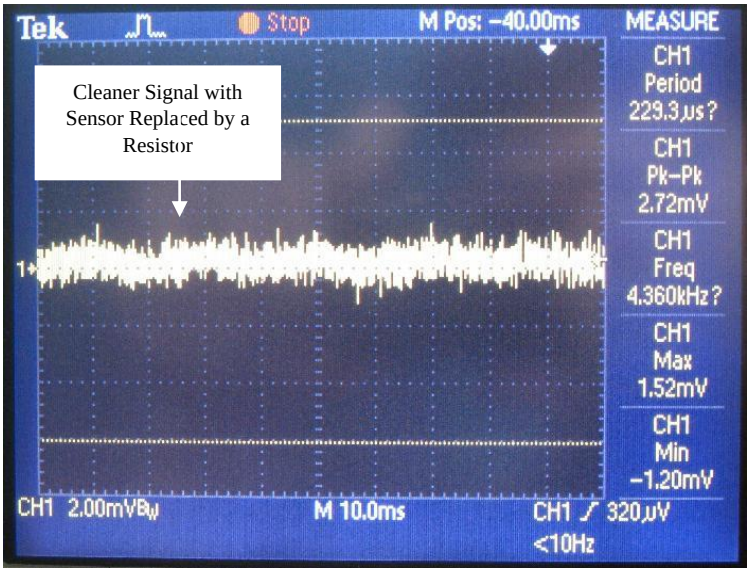

Figure 37: Sensor 2 Circuit Noise with 100kΩ as Sensor 2 – Minimal Visible Power Noise

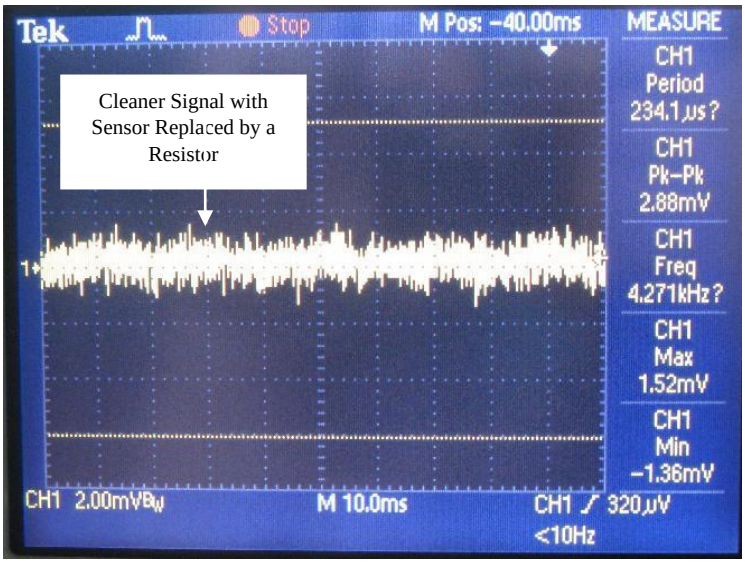

Figure 38: Sensor 3 Circuit Noise with 100kΩ as Sensor 3 – Minimal Visible Power Noise

Since the pressure sensors were picking up the power noise, we needed to add a notch-filter centered at 50 Hz (60 Hz if we were in a different region) to the circuit in addition to the low-pass filter. This circuit would be mounted on the back of the hand with the vibration sensing circuitry, so it was important to find a solution that required minimal components. Active filters would take up much board space, so we decided to look into notch filters made of passives. Time was another constraint at this point too, since we were into the ninth week of our project. We saw a potential solution in *The Art of Electronics*, by P. Horowitz and W. Hill [70]. A passive twin-T notch filter (Figure **39**39) adds the input signal to itself with a 180º phase shift at the cutoff frequency, f_c thereby causing theoretically infinite attenuation.

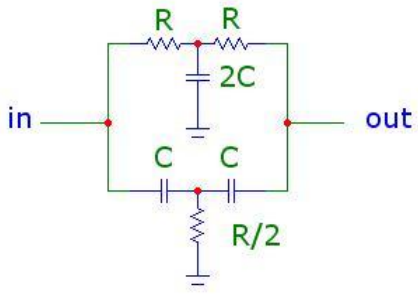

Figure 39: Passive Twin-T Notch Filter [70]

The cutoff frequency is: $f_c = \frac{1}{2\pi RC}$. Horowitz and Hill noted that this simple RC circuit could be used to reject power line interference, but warned that it required well-matched components and that its frequency response had a smooth drop-out about f_c. While this could be improved with an active version of the filter, this would require adding multiple op-amps to each circuit and cost board space and power. We chose components for this circuit based on what we had available. With C = 100nF, R needed to be approximately 31.8kΩ. We had 100nF, 30kΩ, 1kΩ and 600Ω through hole components on hand, so we made R with a series combination of 30kΩ, 1kΩ and a 600Ω (nominally 31.6kΩ) and R/2 with two of these in parallel (nominally 15.8kΩ). For C, we used the 100nF and for 2C, we placed two 100nF in parallel (nominally 200nF). Figure 40 shows a MULTISIM bode plot of this filter. Note that the pole is at approximately 50 Hz and the smooth response that Horowitz and Hill warned about.

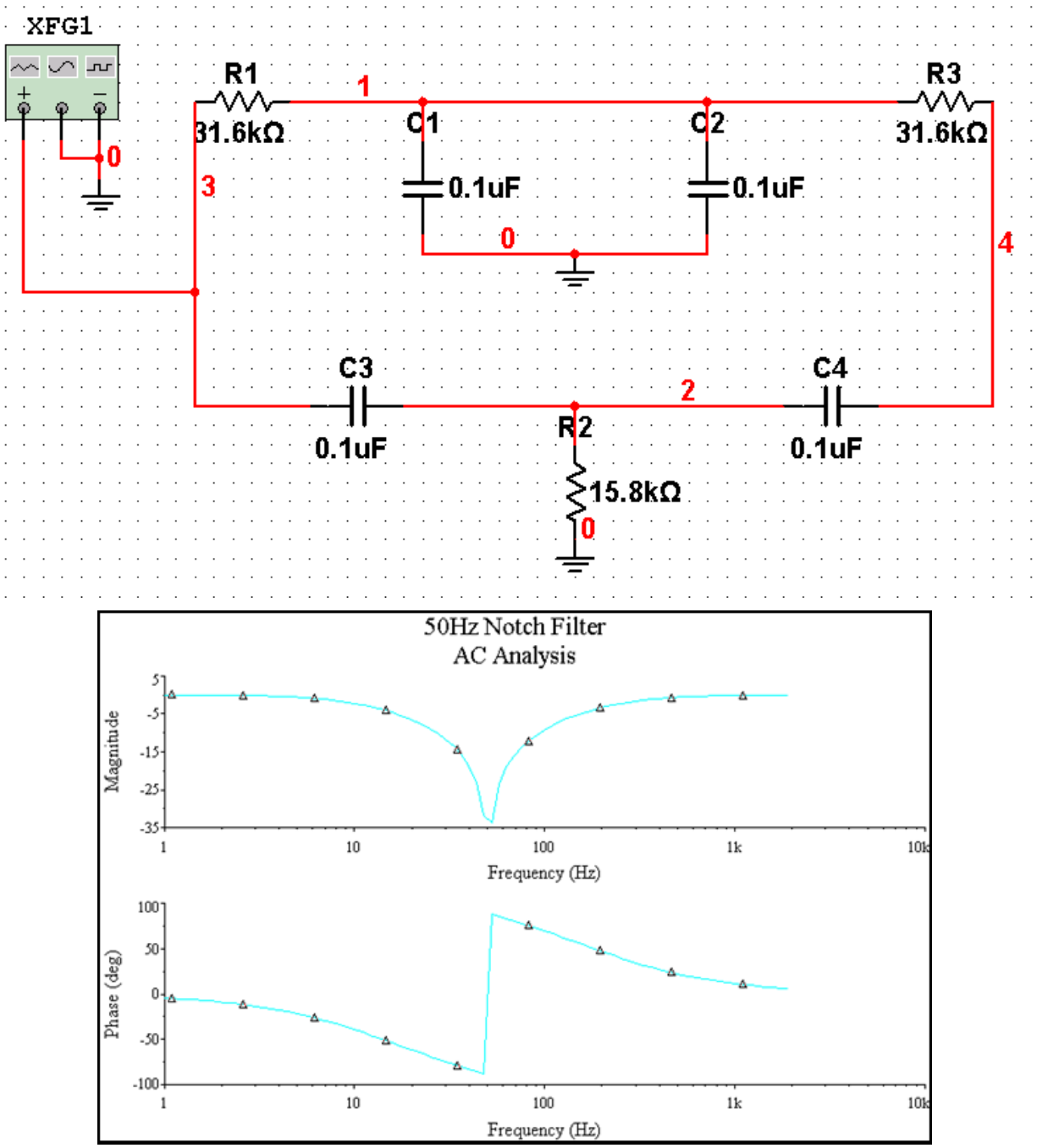

Figure 40: MULTISIM Simulation of Passive 50Hz Twin-T Notch Filter

The cutoff frequency for this filter is 50.37Hz. Ideally, we would want to reject 50Hz and 60Hz to account for regional power differences. 31.5kΩ and 100nF were chosen, since they were both available online [71]. A combination of 26.7kΩ and 100nF in this filter would have a cutoff frequency

of approximately 60Hz (59.61Hz) [70]. Only 13.3kΩ were available online for R/2, so we could use either two 26.7kΩ in parallel or accept the error [71]. An advantage of the single resistor for R/2 is that the two filters would be footprint compatible (though we could two surface-mount resistors directly on top of each other). For our prototype board we decided to only include a 50Hz notch filter, given the limited testing time we had remaining and our board space constraints. Dr. O'Sullivan told us that it would be acceptable to just have the prototype with a suitably clean output (Appendix G-1), therefore the 50Hz filter was fine. Figure 41 shows the original prototype of the filtered pressure sensor circuit.

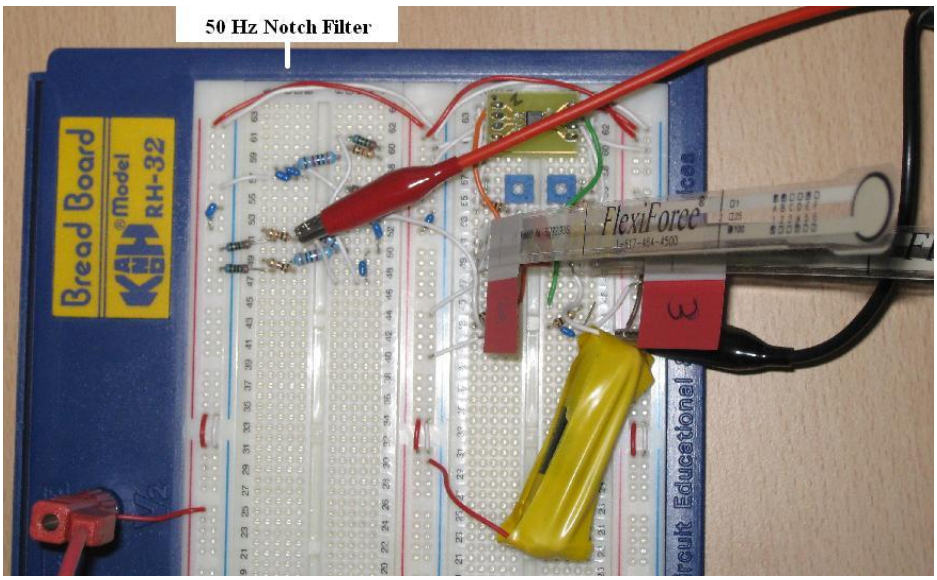

Figure 41: Initial Pressure Sensor Circuitry Prototype with 1.59kHz LPF and 50Hz Notch Filter

To compare the noise on the circuit with and without the notch filter, we connected one of the circuits to the oscilloscope, set the horizontal scale to 10ms/div (adequate to view 50Hz noise, which has a 20ms period) and AC coupled the channel. We then turned on infinite persistence and moved the sensor around to as many positions as possible to get an envelope for the noise. We repeated this with the sensing area pinched, thereby loading the sensor. Figure 42 and Figure 43 show the noise on the signal loaded and unloaded respectively. Note that the noise has a much greater swing when the sensor is loaded because the amplifier's gain was substantially higher. Only sensor 2 was tested with the filter

because it tended to pick up more noise than the sensor 3 circuit (possibly because of the breadboard layout).

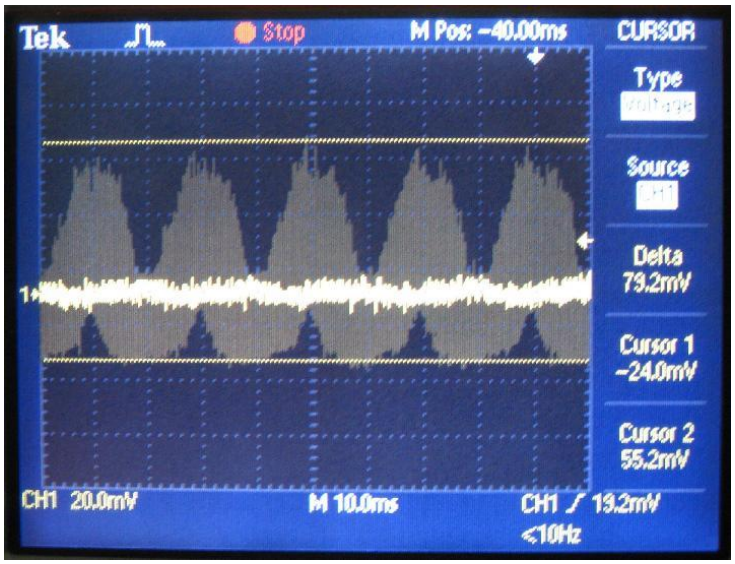

Figure 42: Sensor 2 Circuit 50Hz Noise Envelope with Sensor Unloaded

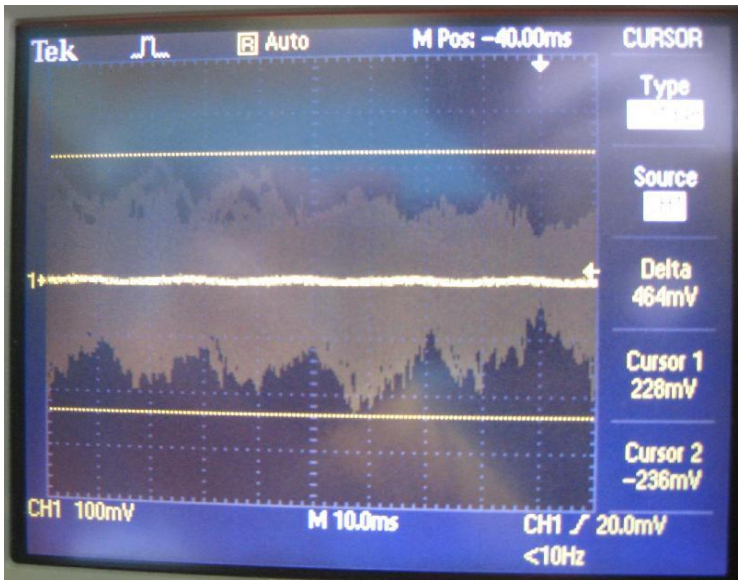

Figure 43: Sensor 2 Circuit 50Hz Noise Envelope with Sensor Loaded

We then measured the signal at the output of the notch filter for comparison. Figure 44 shows the output of the filter with the sensor unloaded. Note how much cleaner it is than the unfiltered signal in Figure 42. Likewise, the output of the filter with the loaded sensor, shown in Figure 45 is substantially cleaner than the unfiltered signal in Figure 43. It is important to take into account the fact

that this filter was built on breadboard with most of the components as parallel or series combinations (all 1% except for the 1kΩ, which was 5% and the 100nF, which was 20%). A more compact printed circuit board version of this circuit with more precise parts would be more accurate with the location of the filter's cutoff frequency, and like the rest of the circuit, be less susceptible to electromagnetic noise. Figure 46 shows the output of the pressure sensor circuit after the combination of low-pass and notch filtering.

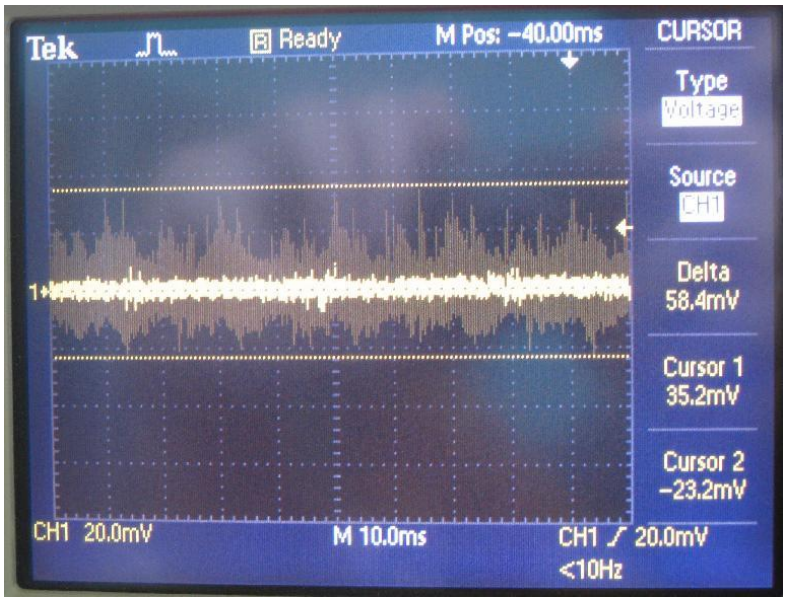

Figure 44: Sensor 2 Circuit Noise Envelope with Sensor Unloaded at Notch Filter Output

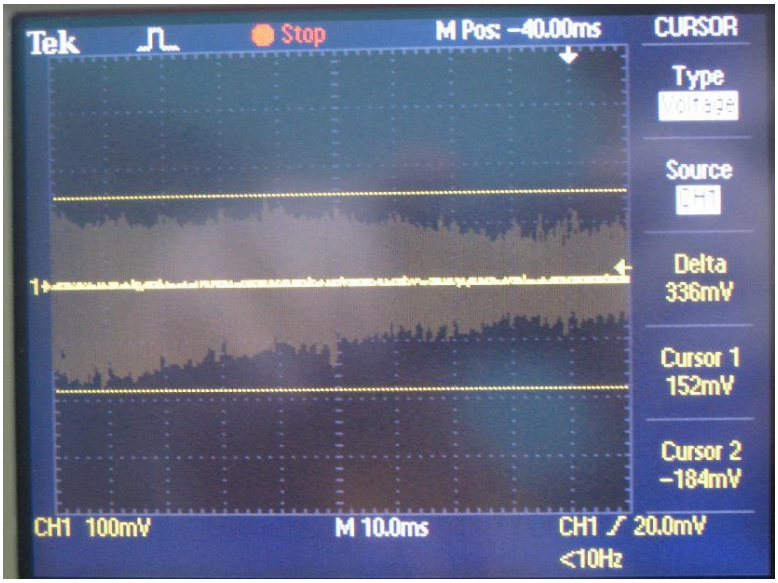

Figure 45: Sensor 2 Circuit Noise Envelope with Sensor Loaded at Notch Filter Output

Compared to the circuit without the 50Hz notch filter (Figure 33) and the output without either filter (Figure 27), this signal was much cleaner and would therefore yield more accurate ADC conversions.

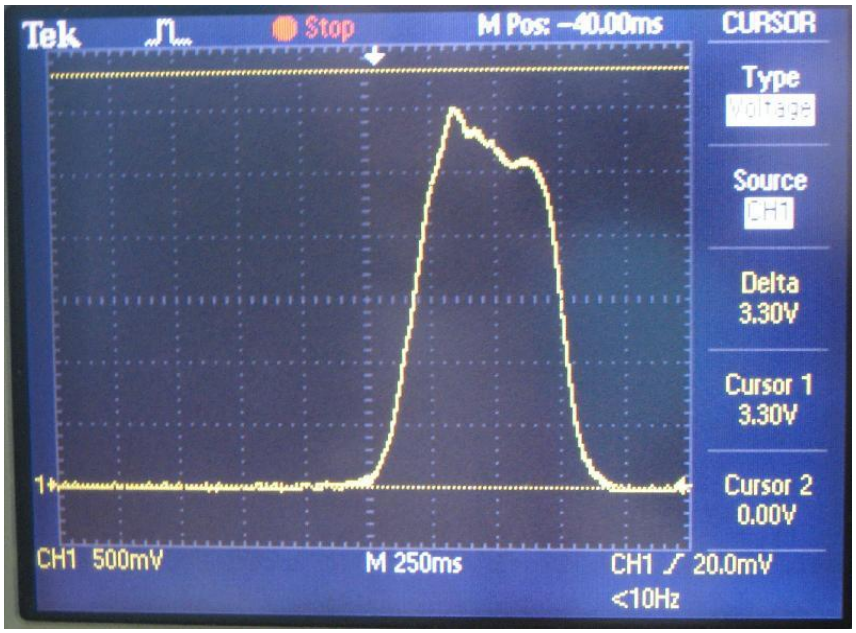

Figure 46: Low-pass and Notch Filtered Pressure Sensor Circuit Output

A final consideration was the circuit equivalent of the MSP430's ADC (7).

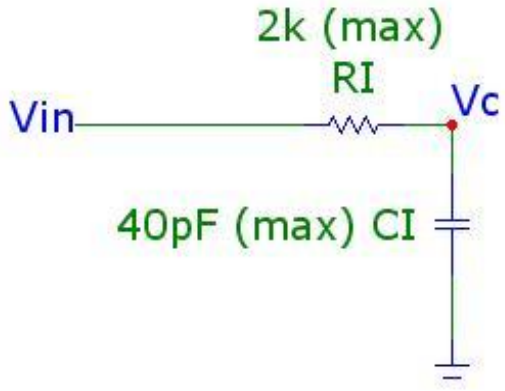

Figure 47: MSP430x4xx ADC Equivalent Circuit [72]

According to the MSP430x4xx User's Guide, V_C needed to charge to within ½ an LSB of Vin for an accurate conversion [72]. This circuit was essentially a low-pass filter with an f_{3dB} of

approximately $1/(2\pi(40pF)(2k\Omega)) \approx 2MHz$. The filtered signal from the pressure sensor conditioning circuit should pass without attenuation to the ADC, since its frequency content is well below this frequency.

Thus, we greatly improved the integrity of the pressure sensor prototype's output by adding 1.59kHz low-pass filters and 50Hz notch filters to each circuit. Though more accurate active filters could be used, the passive filtering both reduced power consumption and the footprint of each circuit [70]. This was especially important because the board would have six copies of each filter. Figure 48 shows the final schematic of the pressure sensor subsystem with the added passive filters. The three pin headers, S1 through S6 represent the sensors, which had three pin connectors (middle pin inactive). The accelerometer is mounted on the back of the hand as well, so it is in the upper right of the schematic. The six-pin header is where it connects to this board, and the four-pin header is the accelerometer's four outputs. Figure 49 shows the layout of the board that is mounted on the back of the hand.

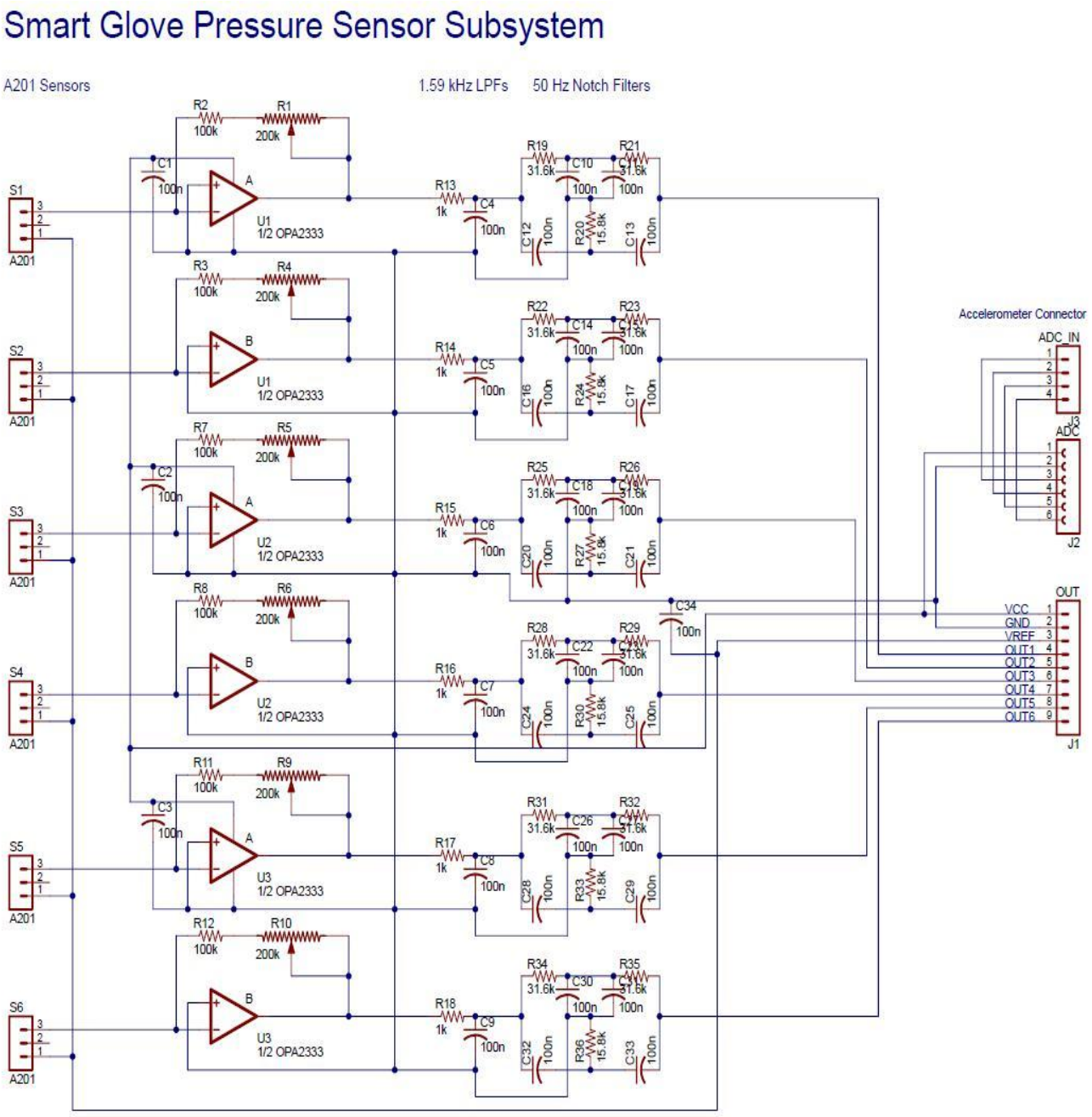

Figure 48: Pressure Sensor Signal Conditioning Schematic

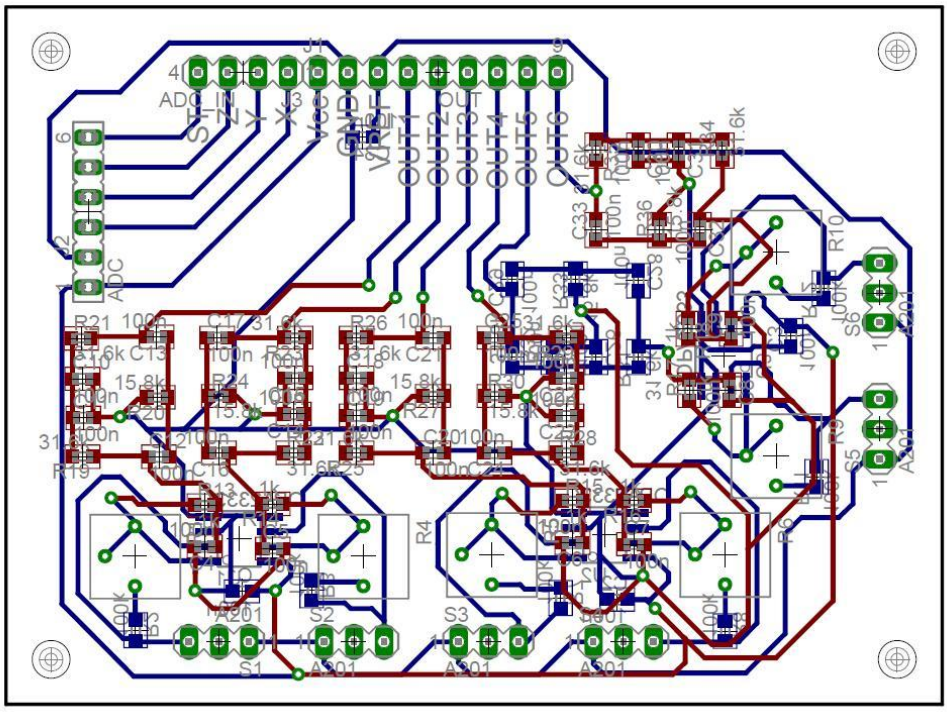

Figure 49: Pressure Sensor and Accelerometer PCB Layout

(Red = Top, Blue = Bottom, Green = Vias and Through Hole Pins, Gray = Silkscreen)

3.2 Accelerometer Selection

3.2.1 Measuring Hand Transmitted Vibration

The four main considerations known to contribute to hand-transmitted vibration symptoms are [2]:

- Frequency spectrum of mechanical vibration
- Magnitude of vibration
- Duration of exposure during the work day
- Cumulative exposure

The standards for measuring these are outlined by the *International Organization for Standardization* (ISO). The smart glove is designed to measure frequency, magnitude, and duration of work day vibration exposure.

3.2.2 Quantities to be measured

The ISO 5349-1 standard [2] establishes a weighted, RMS, vector sum value to represent the contribution of harm due to frequency, magnitude, and duration. This number, denoted by A(8), needs to be measured and calculated using the smart glove sensors and microprocessor in order to detect harmful vibration levels. Table 9 outlines the quantities that need to be measured and calculated in order to arrive at the A(8) measurement.

Table 9: Quantities needed to calculate A(8) measurement

Quantity	Description	Formula
$a_{h_x}(t)$, $a_{h_y}(t)$ $a_{h_z}(t)$	Instantaneous, single axis acceleration value (m/s^2)	
$H_w(s)$, $H_B(s)$	Frequency-weighting and band limiting filters	
$h(t)$, $H(s)$	Frequency-weighting, band limiting filter	$H(s)=H_w(s)H_B(s)$
$a_{hw_x}(t)$, $a_{hw_y}(t)$ $a_{hw_z}(t)$	Instantaneous, single axis, frequency weighted acceleration value	$a_{hw_x}(t) = a_{h_x}(t)*h(t)$
a_{hw_x}, a_{hw_y}, a_{hw_z}	Single axis, frequency weighted, RMS acceleration value	$a_{hw_x}=(< a_{hw_x}^2(t)>)^{1/2}$
a_{hv}	Vibration total value	$a_{hv}=(a_{hw_x}^2 + a_{hw_y}^2 + a_{hw_z}^2)^{1/2}$
T	Duration of exposure during workday	
T_0	Reference time of 8 hours	
A(8)	Daily vibration exposure (m/s^2)	$A(8)= a_{hv}(T/T_0)^{1/2}$

Figure 50 below shows a block diagram outlining the steps needed to convert three accelerometer measurements to A(8). The following discussion outlines the design and decision making processes for each major stage in that block diagram.

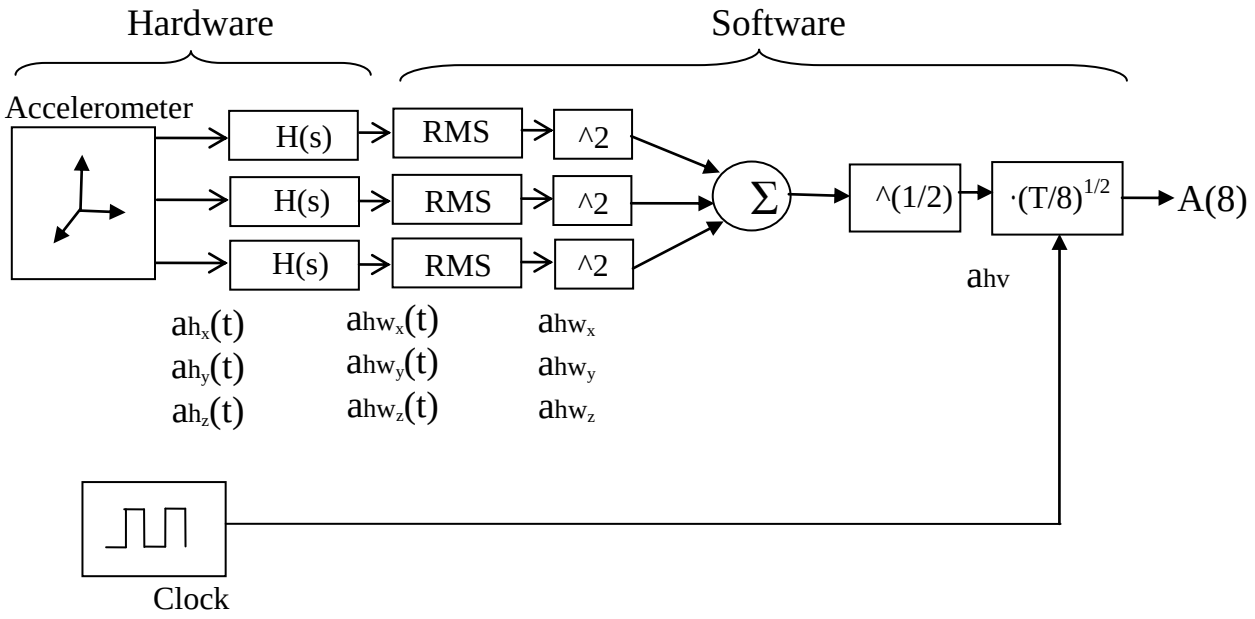

Figure 50: Conversion Process of accelerometer measurements to A(8), the ISO 5349 vibration standard measurement. Accelerometer signals are first individually filtered and frequency weighted, then the RMS of each is determined. The vector sum of the three outputs is then taken. Finally, the A(8) vibration total value may be calculated using the shown formula.

3.2.3 Accelerometer Background

Important factors to consider when choosing an accelerometer for vibration measurements include: accelerometer technology, magnitude range, frequency range, mass, and power consumption.

3.2.3.1 Technology

Three major types of accelerometers include piezoresistive, piezoelectric, and integrated circuit piezoelectric (ICP) [3]. Piezoresistive accelerometers use strain gauges to sense a force. Used in a wheatstone bridge, the piezoresistive accelerometer then provides a voltage signal proportional to acceleration. Piezoresistive sensors sense continuous as well as static accelerations, such as the acceleration due to gravity.

Piezoelectric accelerometers use crystals that possess the property of changing their charge when compressed or extended [3]. A small mass presses against the crystal, generating a charge output proportional to acceleration. Unlike piezoresistive sensors, these do not measure very low or

continuous frequencies. ICP are small silicon chips and can be mounted easily on a circuit board. The big advantages of ICP are their low cost and ease of signal conditioning.

3.2.3.2 Frequency Range

According to the ISO 5349-1:2001(E) standard on the evaluation of mechanical vibration, different frequencies contribute different levels of damage to the human body [2].
According to the ISP standard, frequencies of interest include those from 6Hz to 1250Hz. Therefore, any accelerometer chosen should be able to operate at those frequencies.

3.2.3.3 Magnitude Range

Part 2 of the ISO standard outlines how to practically measure vibrations in the workplace. It is suggested that the accelerometer be capable of measuring up to 50,000 m/s^2 [2]. However, many hand held power tools operate at far lower vibration magnitudes. A full table is shown in Appendix F. The tool with the highest vibration magnitude in this sample is the Makita Rotary Hammer Drill 10KG, with a vibration of $20.4m/s^2$. For prototype purposes, it is sufficient to measure the verage vibration magnitudes for common tools such as these. However, ideal measurement would be able to measure these less common, high magnitude spikes.

3.2.3.4 Power consumption and Mass

In order to keep the glove as light as possible, so as not to hinder the worker, a light, low power battery must be chosen. This requires that all system components consume as little power as possible. Hence, the accelerometer must have low power consumption as well as a low mass, so as not to load down the worker's hand.

3.2.4 Accelerometer selection

We investigated several tri-axial accelerometers, weighing the above constraints, along with price, to determine the most appropriate sensor for this prototype. A summary of the triaxial accelerometers that were investigated is shown in Table 10 below.

Table 10: Triaxial accelerometer options

	Magnitude Range	Sensitivity	Bandwidth (x,y,z) (Hz)	Power (mW)	Price
ADXL330	+/- 3g	300mv/g (typ)	1600, 1600, 550	0.324 (typ.)	€11.70 (Farnell)
DE-ACCM3D	+/- 3g	360mv/g (typ at 3.6V)	500Hz	1.8 (min)	$35.00
LIS302DL	+/- 2g , +/- 8g	~8mg/digits	100Hz, 400Hz	<1	$13.63
FAR-S2AB		~1000mV/g		9 (min)	
2440-025	+/- 25g	200mV/g	0-1500	330mW	$1,660
KS943B.10	+/- 600	10 ± 5 % mV/g	0.2 - 22000	24mW (min)	€ 880.00
KS943B.100	+/- 60	100 ± 5 % mV/g	0.5 - 22000	24mW (min)	€ 880.00
KS943L	+/- 240	14 ± 20 % mV/g	0.3 - 19000	0.4(min)	€ 1,080.00

Based on these considerations, we chose the ADXL330 as a cheap, high sensitivity, reasonable bandwidth, low power triaxial accelerometer.

3.2.5 ADXL330 – Analog Devices Triaxial +/- 3g IMEMS Accelerometer

In order to get the full functionality out of the ADXL330 accelerometer, we examined its parameters in detail.

3.2.5.1 Technology

The ADXL330 uses one mechanical sensor to sense acceleration in three directions. A micro-machined structure is suspended by springs over the surface of a silicon wafer. Plates are attached both to the moving mass as well as on fixed surfaces around the mass. The deflection of the structure is

measured using the capacitance between fixed and moving plates. This will sense dynamic acceleration resulting from vibration and shock as well as the static acceleration of gravity.

3.2.5.2 Frequency Range

At first, the 550Hz bandwidth of the z-axis on this accelerometer appears to be a problem. However, according to the ADXL330 data sheet, this bandwidth depends on an external capacitor, so this can be adjusted. With an output resistance of 32kΩ, the external capacitor creates a single pole low pass filter at the output. We simply need to use a sufficiently low capacitor at the output to create a pole at a very high frequency, so that this filter will not interfere with the frequency-weighting filter.

3.2.5.3 Magnitude Range

The ADXL330 can measure up to 3g (29.43m/s^2). With the accelerometer mounted with the z axis facing upwards, it should measure 9.81 m/s^2. This means that the lowest magnitude we can measure in the Z direction is 19.62 m/s^2, which is higher than the majority of power tools found in the chart in Appendix F. Therefore, using this accelerometer, we will be able to measure the vibration of the majority of hand held power tools, which will be sufficient to demonstrate this product as a proof of concept.

3.2.5.4 Power Consumption

The ADXL330 typically consumes 0.324mW of power [73]. Drawing 180uA at a typical supply voltage of 1.8v, the accelerometer will consume 1.8mA-hours during a 10 hour shift. Using a battery with at least 700mA-hours of storage, this accelerometer will represent less than 0.26% of our power budget.

3.2.5.5 Package and Size

The ADXL330 comes in a 4mm x 4mm x 1.45mm package [73]. This size is sufficiently small so that the accelerometer will not load down the hand. However, this small package is difficult to work with, so we purchased a breakout board from sparkfun.com, as pictured below in Figure 51 [74]. This board includes output 0.1 uF capacitors to ground for each of the accelerometer outputs. The breakout board allowed us to solder pins and use this accelerometer on a solderless breadboard for testing.

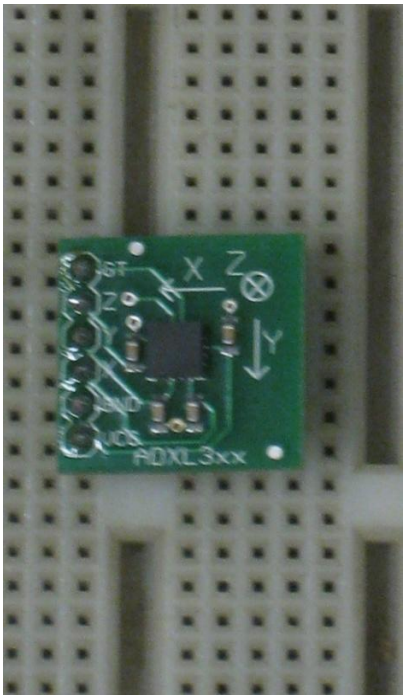

Figure 51: ADXL330 Breakout Board

3.2.6 Accelerometer Signal Processing

The ISP 5349-1 guide to the measurement of hand-transmitted vibration establishes a frequency -weighting filter that will attenuate different frequencies depending on the harm they contribute. This is given by the following transfer function:

$$H_w(s) = \frac{(s + 2\pi f_3)2\pi K f_4^{\,2}}{(s^2 + {2\pi f_4 s}/{Q_2} + 4\pi^2 f_4^{\,2}) f_3} \qquad \textbf{(1)}$$

The standard also defines a bandpass filter with the following transfer function:

$$H_b(s) = \frac{s^2 4\pi^2 f_2{}^2}{(s^2 + {2\pi f_1 s}/{Q_1} + 4\pi^2 f_1{}^2)(s^2 + {2\pi f_2 s}/{Q_1} + 4\pi^2 f_2{}^2)} \quad \textbf{(2)}$$

The value s represents 2πf, where f is frequency. The parameters f_1, f_2, …f_n represent resonant frequencies where the transfer function has a certain behavior. For example, in the bandpass filter, f_1 represents the lowest frequency that will be attenuated less than or equal to 3dB. Q is the selectivity value of a filter and effects how steep or slight the transfer function is at a cut off or resonant frequency. The values for resonant frequencies (f), selectivity values (Q), and the DC gain (K) are given in the Table 11 below:

Table 11: Values for resonant frequencies (f), selectivity values (Q), and the DC gain (K)

Band Pass Filter			**Frequency-weighting Filter**			
f1	**f2**	**Q1**	**f3**	**f4**	**Q2**	**K**
6.31 Hz	1258.9 Hz	0.71	15.915 Hz	15.915 Hz	0.64	1

Together, these filters select only the interesting range of frequencies (6Hz – 1250Hz) and establish the contributions of harm due to different frequencies. The combined filters make a single band-limiting frequency-weighting transfer function, the magnitude of which is depicted in Figure 52 below.

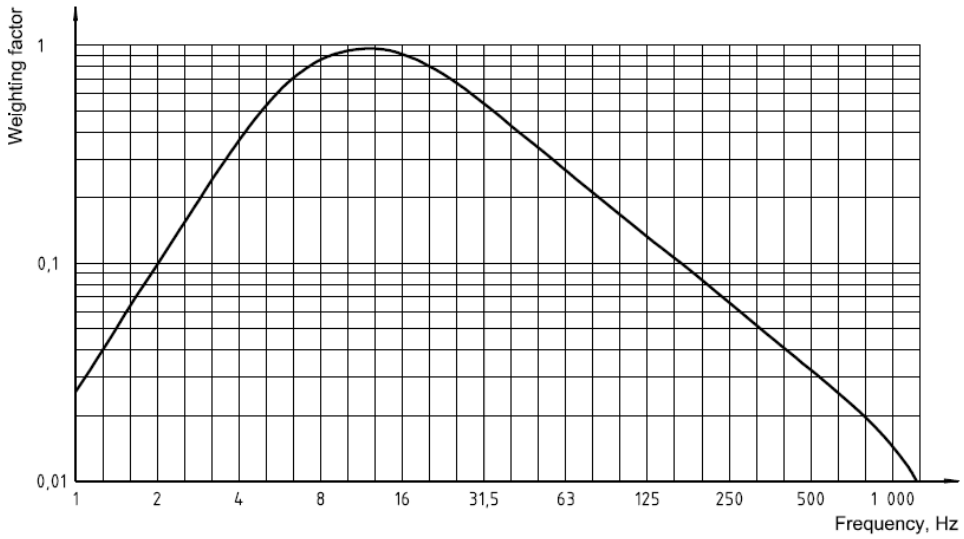

Figure 52: Frequency-weighting curve for hand-transmitted vibration, band-limiting included [ISO 5349-1:2001(E)]

In order to realize these filters, we used several active filter configurations: Sallen and Key lowpass, Sallen and Key highpass, as well as a single-zero filter. The block diagram for the total filtering block H(s) is shown in Figure 53 below.

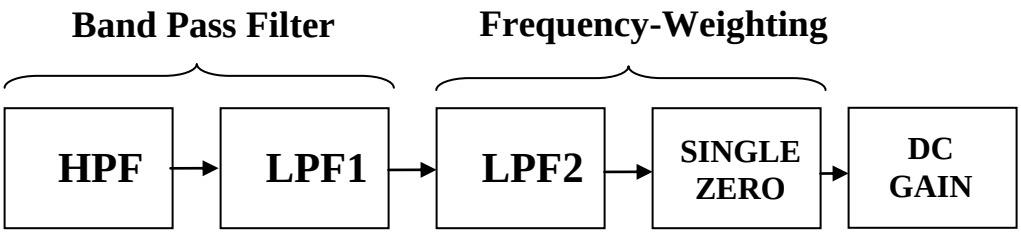

Figure 53: Block Diagram for filtering block H(s)

3.2.6.1 Band Pass Filter

The band pass filter, (H_b), is realized using a lowpass filter in series with a highpass filter. The Sallen and Key highpass filter has the following transfer function:

$$H_{HP}(s) = \frac{s^2}{(s^2 + {2\pi F_C s}/{Q} + 4\pi^2 {F_C}^2)} \qquad (3)$$

where

$$F_C = \frac{1}{2\pi\sqrt{R_1 R_2 C_1 C_2}} \qquad \textbf{(4)}$$

and

$$Q = \frac{\sqrt{R_1 R_2 C_1 C_2}}{R_2 (C_1 + C_2)} \qquad \textbf{(5)}$$

F_C is the cutoff frequency and Q is the quality factor. The circuit realization for this filter is pictured below in Figure 54 with the components labeled to be consistent with Equations 4 and 5 above.

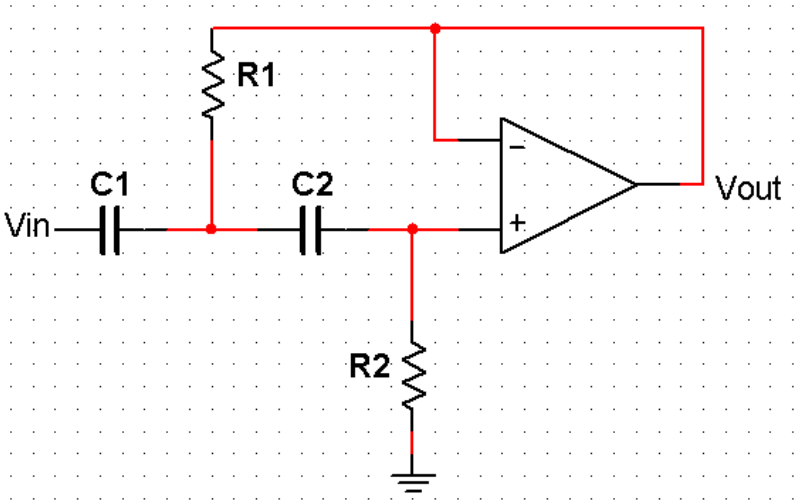

Figure 54: Sallen and Key Highpass Filter

The operation of this circuit can be seen by applying basic circuit analysis. At low frequencies, C_1 and C_2 behave like open circuits, so V_{in} is not passed to the output, and there is no positive feedback path [75]. The noninverting input is at 0v since no current flows through R_2. Negative feedback forces the inverting input, and hence the output, to also be 0v. At high frequencies, the capacitors behave like short circuits, passing the signal through a unity gain buffer. At $f=F_c$, the transfer function reduces to Q_j, and the signal is attenuated by the Q factor. When f is near F_c, positive feedback provides enhancement for the Q value, allowing for Q values higher than 0.5, which was previously unattainable by two-pole passive filters [75].

The Sallen and Key lowpass filter has the following transfer function:

$$H_{LP}(s) = \frac{4\pi^2 F_C{}^2}{(s^2 + 2\pi F_C s / Q + 4\pi^2 F_C{}^2)} \qquad \textbf{(6)}$$

where

$$F_C = \frac{1}{2\pi\sqrt{R_3 R_4 C_3 C_4}} \qquad \textbf{(7)}$$

and

$$Q = \frac{\sqrt{R_3 R_4 C_3 C_4}}{C_4 (R_3 + R_4)}. \qquad \textbf{(8)}$$

Figure 55 below shows the circuit realization for the Sallen and Key lowpass filter with the components labeled to be consistent with equations 8 and 9.

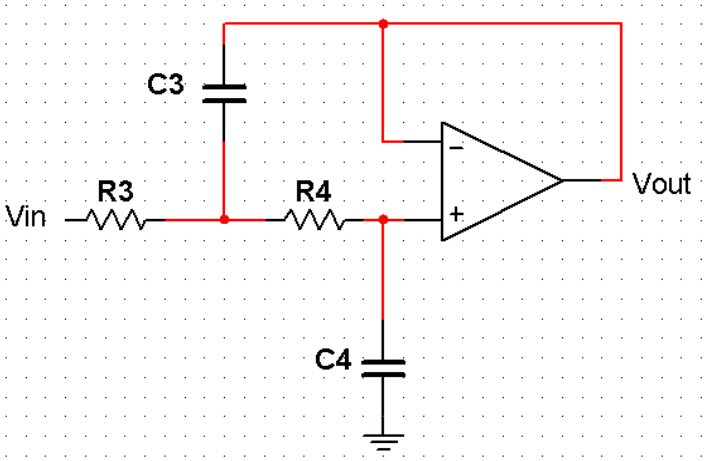

Figure 55: Sallen and Key Lowpass Filter

At low frequencies, the capacitors behave like open circuits and there is no positive feedback path. The circuit then behaves like a unity gain buffer, passing the input to the output unattenuated. At high frequencies, the capacitors behave like short circuits, and the voltage at the positive input is effectively shunted to ground. Positive feedback is not present since the output cannot affect the

voltage at the noninverting input. Negative feedback, however, is present and forces the operational amplifier inputs to be equal, forcing the output to be 0v. At f=F_c, the transfer function simplifies to –jQ, and the input signal is attenuated by the Q factor [75].

By cascading the highpass and lowpass filters, the transfer functions will multiply to produce the band pass filter shown in Equation 3. We were able to choose resistor and capacitor values to achieve values of F_C and Q that would match the bandpass transfer function given in the ISO 5349-1 standard.

3.2.6.2 Frequency-weighting Filter

The frequency-weighting filter, (H_w), is realized using a lowpass filter in series with a single zero filter. The lowpass filter is the same as that depicted above in Figure 56. The single zero filter is shown below in Figure 56. This circuit was designed my modifying a single zero, single pole circuit which was similar to this one except the capacitor was placed in parallel with the R_8 resistor [76].

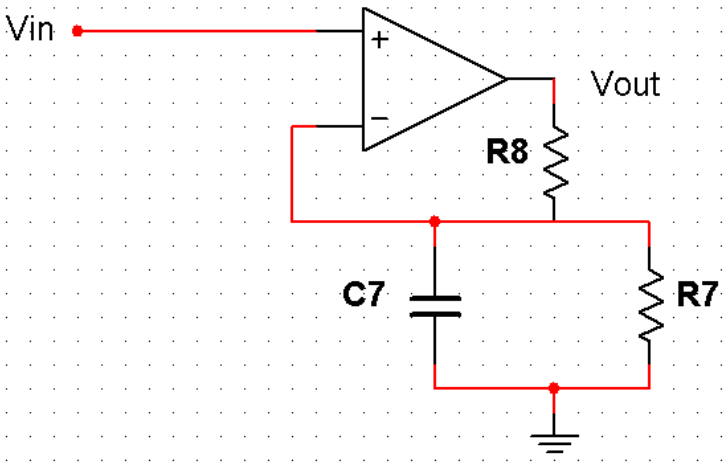

Figure 56: Single Zero Circuit

The single zero circuit has the following transfer function:

$$H_{SZ}(s) = \left(1 + \frac{R_8}{R_7}\right)\left[1 + s(R_7 \parallel R_8)C_7\right] \qquad \textbf{(9)}$$

A single-zero transfer function produces an increasing gain as frequency increases. We can see this functionality qualitatively in the circuit by noticing that at high frequencies, C_7 behaves like a short circuit, and the circuit looks like a noninverting amplifier with infinite gain. At low frequencies, the capacitor behaves like an open circuit and the gain is determined by the resistor values. The transfer function also shows that larger values of $s=2\pi f$ will increase the gain of the circuit.

By choosing appropriate passive component values, we were able to produce the frequency-weighting transfer function of Equation 9 above by cascading the single zero and lowpass filter circuits. The DC gain of the designed filter is not the same as that of the standard, but this will be corrected in software. The component values chosen to make the correct cutoff frequencies and Q values are shown in Table 12 below.

Table 12: Values for resonant frequencies (f), selectivity values (Q), and the DC gain (K)

HPF		**LPF1**		**LPF2**		**Single Zero**	
R1	140.6kΩ	R3	780.6Ω	R5	1.55MΩ	R7	20MΩ
R2	31kΩ	R4	1kΩ	R6	10kΩ	R8	20MΩ
C1	0.146uF	C3	0.2047uF	C5	0.644uF	C7	10uF
C2	1uF	C4	0.1uF	C6	0.1uF		

Because of the high number of components, we decided that it would be more practical to demonstrate vibration measurement in one axis rather than all three. Producing 3 PCBs with 15 passive components each, would have proved challenging in terms of fitting everything in a compact glove system. By proving the filters work in one axis, future development of this prototype will easily be able to implement it in all three axes using our design.

3.2.7 DC Add Circuit

In order to measure only changes in acceleration and not the effects of gravity, we capacitively couple the acceleration signal at the input. This removes the DC measurement of gravity, which we are not interested in for vibration measurements. This requires that the operational amplifiers of our filters

operate on dual supplies (-1.5v to +1.5v). However, the analog to digital converter of the microcontroller requires inputs from 0v-3.3v. This necessitates that we include a stage that adds 1.5v DC at our output. Using a simple adder circuit, shown below in Figure 57, we were able to accomplish this.

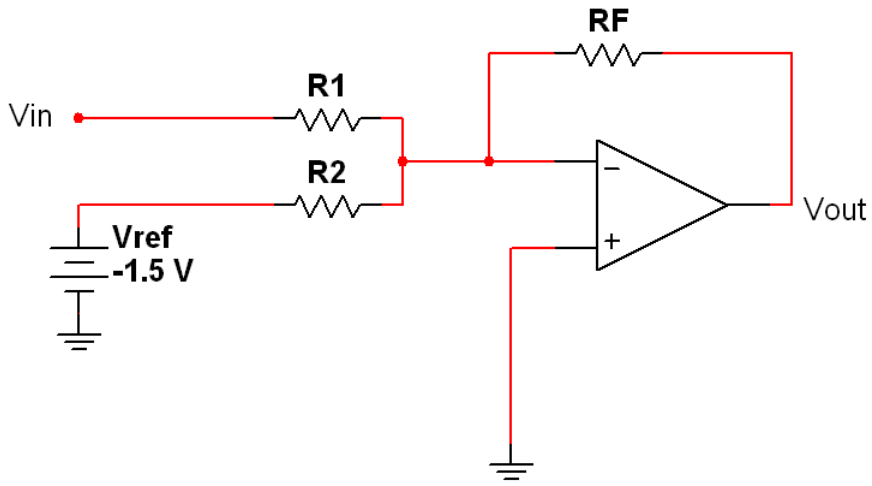

Figure 57: DC Add Circuit. This circuit adds a +1.5v DC bias to an input signal. The operational amplifier must be powered with VEE=0v and VCC= 3.3v.

Negative feedback forces the noninverting input of this circuit to be equal to the inverting input, which is connected to ground. Using Kirchoff's current law, we can write Vin/R1 + -1.5v/R2 = -Vout/Rf. Choosing Rf=R1=R2 gives: Vout=Vin + 1.5v, which gives us the required functionality.

3.2.8 Matlab Simulation

We used MS Excel to calculate resistor and capacitor values to produce the correct F_c and Q values. Next, we used MATLAB to verify that our designed filter would produce the transfer function of figure above. Below, in Figure 58, is the magnitude and phase of the transfer function of our design. The code used to produce these plots can be found in Appendix E.

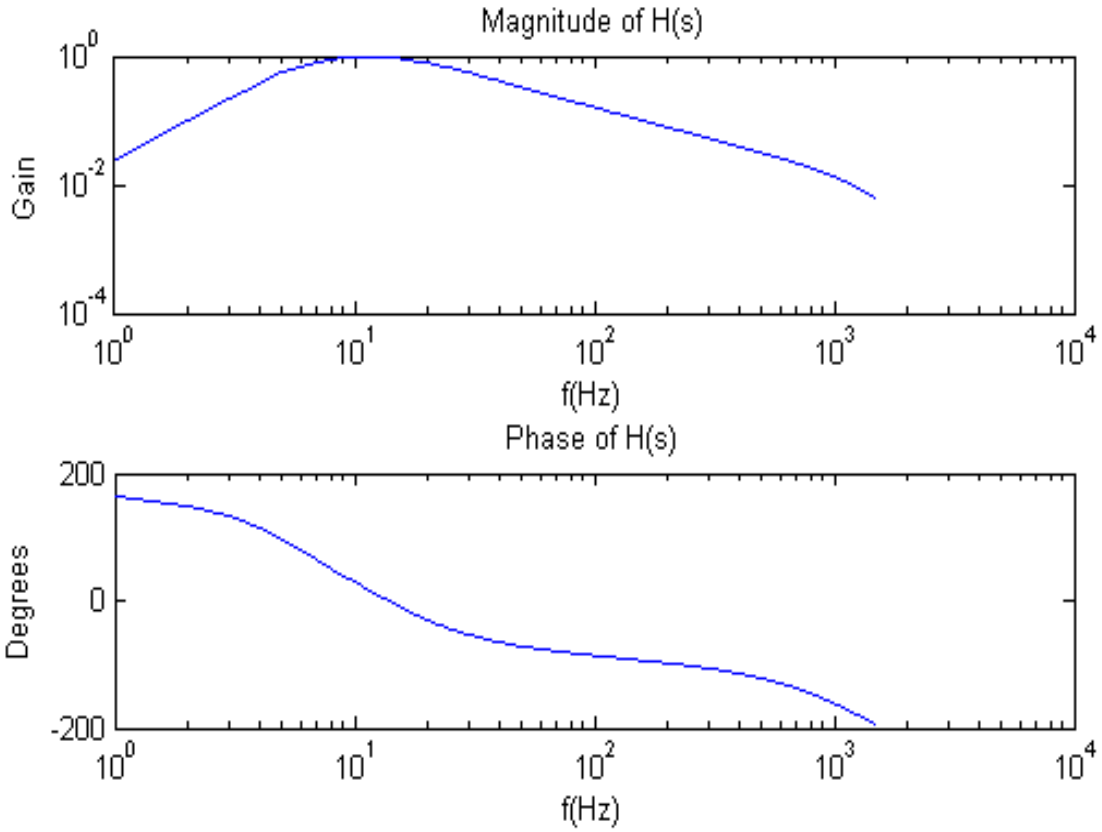

Figure 58: Magnitude(top) and Phase(bottom) of the designed transfer function with exact component values. Note the similarity of the magnitude plot to Figure 52, which shows the ISO standard transfer function for the measurement of hand transmitted vibration.

We can see from figure that the magnitude response looks like the one depicted in the ISO 5349-1 standard (Figure 52). We can also see that the system is stable, since the phase at unity gain is not close to -180^{o}.

3.2.8.1 Matlab Error Analysis

Because component values are not exact, there will be some error in the Fc and Q values. Using MATLAB, we conducted some tests to determine the errors of the A(8) acceleration total value as well as the result of the remaining time calculation. Figure 59 below outlines our method for simulating the process.

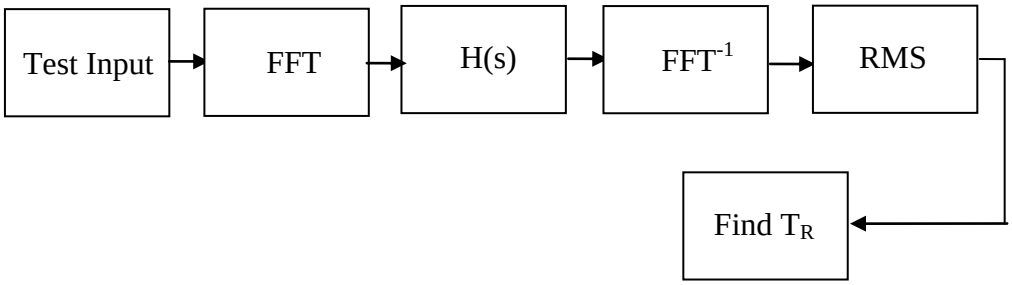

Figure 59: MATLAB simulation flow for error analysis

We simulated the band limiting and frequency weighting filters using the equations for each filter. We calculated the F_C and Q values using our resistor and capacitor values. We also calculated worst case values based on maximum and minimum resistor and capacitor tolerance errors.

Once we had the filters, we simulated an input by creating a sine wave. In order to pass this test input through the filter, we converted it to the frequency domain, multiplied it with the filter transfer functions, and brought it back to time domain. We then calculated the root mean square of this weighted signal and used that to calculate the time it would take to reach dangerous vibration exposure levels.

We ran tests for several different test frequencies of an input sinusoid of amplitude $20 m/s^2$, which is the highest acceleration impact value we expect from a power tool in the z direction. These are represented below in Table 13.

Table 13: Error of Remaining Time Measurement for Different Frequency Values

Amplitude m/s^2	Frequency (HZ)	T_{REM} (Hours)	T_{BAD} (Hours)	T_{error}	T_{est} (Hours)	T_{est} error	Improvement
20	5	7.0115	5.2663	-0.24891	5.27	-0.24838	0.000527704
20	6	4.3561	3.6568	-0.16053	3.67	-0.1575	0.003030233
20	7	3.2283	2.9934	-0.07276	3.07	-0.04904	0.023727659
20	8	2.6916	2.7105	0.007022	2.7	0.003121	0.003901025
20	9	2.4214	2.6119	0.078673	2.6	0.073759	0.004914512
20	10	2.2888	2.6206	0.144967	2.63	0.149074	-0.004106956
20	11	2.2377	2.7034	0.208115	2.7	0.206596	0.001519417
20	12	2.2413	2.8455	0.269576	2.83	0.26266	0.006915629
20	25	4.9284	8.956	0.817223	8.97	0.820063	-0.002840679
20	40	12.4433	24.7608	0.98989	24.77	0.990629	-0.000739354

T_{REM} was calculated by running the test input through the ideal frequency weighting transfer function, while T_{BAD} was calculated with the erroneous transfer function. We used the equation for daily vibration exposure A(8):

$$A(8) = A_h \sqrt{\frac{T}{8 \text{ hours}}} \qquad \textbf{(10)}$$

To test for the time that dangerous levels have been reached, we set A(8) to the exposure action value ($2.5 m/s^2$) and solved for T.

$$T_{ALARM} = 8\left(\frac{2.5}{A_h}\right)^2 \qquad \textbf{(11)}$$

To simulate how this would be calculated on the microprocessor, we created a time vector to represent the time elapsing while a vibrating tool is being used. This then allows us to calculate the remaining time T_{REM} that one has to use the tool. This is simply the difference between the alarm time and the current time, T_{CL} which we will eventually get from the microcontroller clock.

$$T_{REM} = T_{ALARM} - T_{CL} = 8\left(\frac{2.5}{A_h}\right)^2 - T_{CL} \qquad \textbf{(12)}$$

As we can see by the above equation, any error in A_h, the total vibration value, will be squared, resulting in even larger error. In an effort to reduce error, we will try to use a linear approximation, which will avoid taking the square of Ah. To do this, we first calculate the instantaneous A(8) value, then we calculate it's slope:

$$\frac{d(A(8))}{dt} = \frac{A_h}{2\sqrt{2}} \frac{2}{\sqrt{T_{CL}}} \qquad \textbf{(13)}$$

We can then use this to predict remaining time T_{EST} by solving:

$$\frac{d(A(8))}{dt} = \frac{\Delta A(8)}{\Delta t} = \frac{2.5 - A(8)}{T_{ALARM} - T_{CL}} \qquad \textbf{(14)}$$

The results of these calculations are shown above in Table 5. Unfortunately, while this does improve the time prediction for some values, it is not a significant improvement and does not solve our error problem.

3.3 Goniometric sensor Selection

Strain gages are passive components in which a correlation exists between the changes in physical dimensions and the changes in resistance [77]. They can be constructed out of a variety of materials, and come in different shapes and sizes [77]. The most common form for strain gages are simple foil gages. The foil strain gage consists of a wire shaped into a pattern [77]. When the pattern is expanded or contracted, the resistance between the two ending terminals of the wire changes [77]. A liquid mercury strain gage is often used in biomedical applications, such as measuring blood pressure

[77]. For our application, we use a foil strain gage, as a liquid filled strain gage would be vulnerable to vibration.

To accurately measure the deformation in the strain gage, a measurement circuit must be used. Two solutions were easily available; the Wheatstone bridge, and the Anderson Loop. The Anderson loop was selected, because of simple circuit topology, a smaller error signal, and easy calibration [78].

The Anderson loop was invented by Karl Anderson for NASA in 1992 [79]. The loop was patented soon after, but has since been released into the public domain [79]. The basic circuit consists of a constant current source, a sensor, modeled as impedance, and a reference impedance [80]. It can be easily expanded into multiple sensors, all in the same loop, all sensing independently of each other [81]. It works by placing the impedance in series with a constant current source. Figure 60 shows the Anderson loop. In our circuit, the strain gages can be treated as a variable resistor, and the reference resistor has a constant resistance.

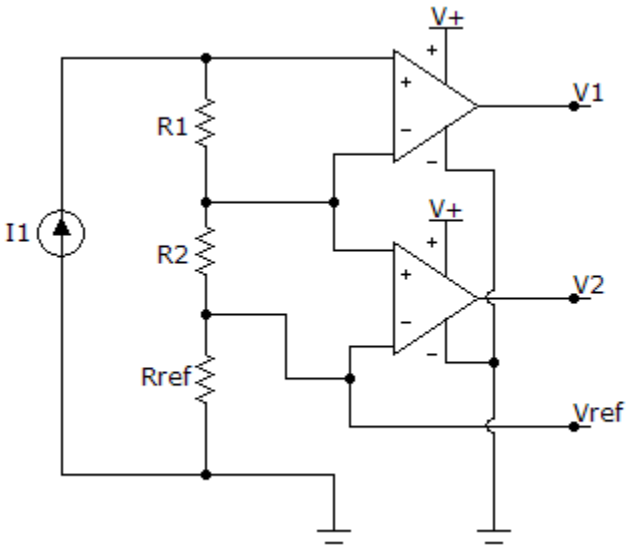

Figure 60: Multiple Sensor Anderson Loop

Equation 15 shows the voltage at the highest potential terminal of the first strain gage, V_{R1}. It is equal to the sum of the voltages across both the strain gages and the reference resistor.

$$V_{r_1} = R_1 I_1 + R_2 I_2 + R_{ref} I_1 \qquad (15)$$

Equation 16 shows the voltage at the highest potential terminal of the second strain gage, V_{R2}. It is equal to the sum of the voltages across the second strain gage and the reference resistor.

$$V_{R_2} = R_2 I_1 + R_{ref} I_1 \qquad (16)$$

The operational amplifiers work to subtract the voltages at across the resistors. The voltage V_1 is the difference between V_{R1} and V_{R2}. This is the voltage across the first strain gage. The voltage V2 is the difference between V_{R2} and V_{ref}, it is the voltage across the second strain gage.

One obvious requirement for a successful Anderson loop is a current source. For this application, we chose the LM334, a variable current source, which can be tuned with a resistor to values up to 1mA. However, at higher currents the LM334 is very temperature dependent. To avoid a severe temperature dependence, the LM334 should only be used to generate a current below 100 μA [82].

The current generated by the LM334 can be tuned using a resistor. The circuit shown in Figure 59 is the configuration used, with the LM334 sitting below the positive voltage terminal. The tuning resistor's resistance is 47 kΩ, and it provides a pathway for current to flow from the V_r terminal to V-. The relationship between IR, R and V_+ is shown in Equation 17 [82].

$$I_{SET} = \frac{V_r}{R_{SET}} * 1.059 \qquad (17)$$

This equation shows us that using the 3.3V microcontroller power supply, a 47 kΩ resistor, we will have a current of around 70 μA, which is well below the suggested 100 μA, and should give us a thermal independence. Figure 61 shows the Anderson loop with the LM334 working as a constant current source.

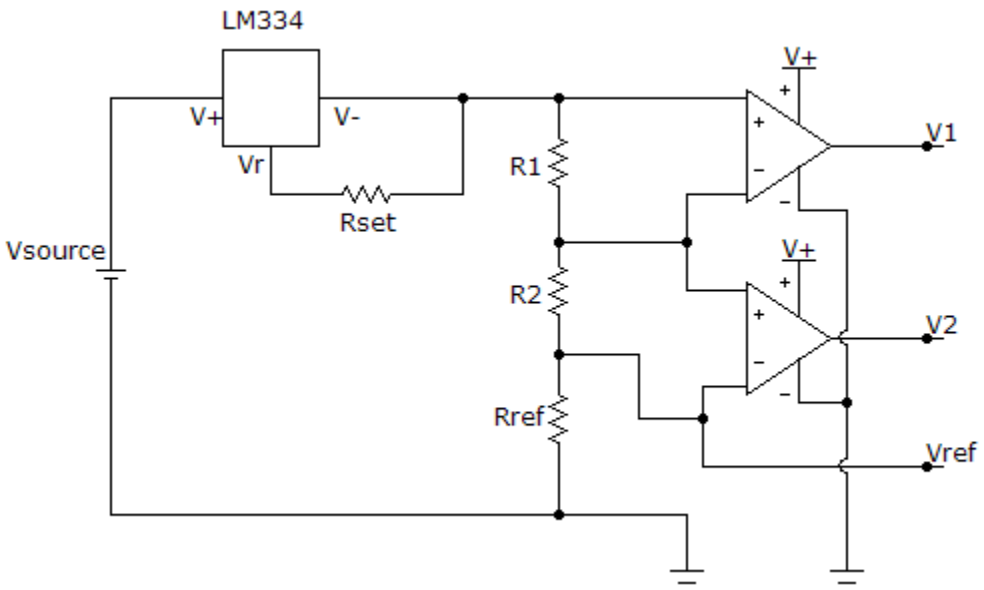

Figure 61: Multiple Sensor Anderson Loop with LM334 used as a current Source

The output voltages of the Anderson loop must be conditioned before being applied to the ADC terminals on the microcontroller. This is done through an additional amplification stage, bringing the voltages to the proper levels for digital conversion.

3.3.1 Re-Design of Goniometric Sensing system

Due to the failure of the strain gauges to withstand the rigor of an industrial setting, we decided to redesign the angle sensing system using a potentiometer instead. The potentiometer feature a shaft that, when rotated, will change the resistance of the device. By fixing two of these devices to the glove, and operating them within their linear range, we will be able to change the resistance of the potentiometer proportional to the angles of the wrist.

We chose a 47kΩ potentiometer which was available at Maplin Electronics in Limerick. This device was chosen because of its small size, smooth adjustability, and linearity. A picture of this potentiometer is shown below in Figure 62.

Figure 62: 47 kΩ potentiometer

A simple way to measure wrist angle is to use the potentiometer in the feedback loop of an inverting amplifier configuration, the gain of which would be proportional to the angle of the potentiometer. This configuration is shown below in Figure 63.

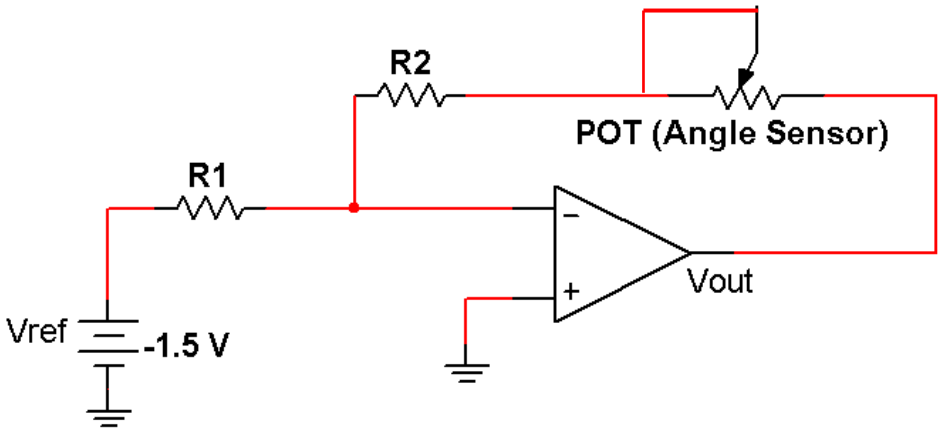

Figure 63: Angle Measuring Circuit Schematic

Negative feedback in this circuit forces the inverting input to be the same as the noninverting input. This means that the voltage across R_1 with current going towards the feedback loop will be -1.5V, and the current through it, by Ohm's law, will be $-1.5/R_1$. Since no current goes into the op amp inputs, all this current goes into the feedback loop. The current through the feedback, going towards the output is:

$$I_F = \frac{-1.5}{R_1} \quad (18)$$

Using Ohm's law, the voltage difference from the noninverting input to Vout can be written as:

$$0V - V_{OUT} = I_F(R_2 + R_{POT}) = \frac{-1.5}{R_1}(R_2 + R_{POT}) \quad (19)$$

This implies:

$$\Rightarrow V_{OUT} = \frac{1.5}{R_1}(R_2 + R_{POT}) \quad (20)$$

By choosing an R_2/R_1 ratio less than 1 we are able to get an output that will range from near 0v to approximately 3.3v, which is the range of inputs for the microcontroller analog to digital converter.

3.4 Microcontroller Selection

When we considered what kind of microcontroller to use for controling all of our peripherals and sensors, we had to first consider where it would be used, by whom and what it needed to be used for. We knew that we would have three major sensing systems; an accelerometer, measuring acceleration in three axes, a goniometer, measuring angles and repetition of wrist movement, and force sensors, measuring the forces felt at the palm and finger tips. We estimated that we would have a total of eleven signals that would need to be digitized for storage by the microcontroller. We also knew that we would have some kind of external data storage device, a display, a user input, and a method to communicate to a computer.

Since the person who would be operating the glove would not necessarily understand how it works internally, we need the microcontroller to be easily maintained and programmed. This would allow new software revisions or features to be added to the glove at a later date. This also makes prototyping easier, as we should be able to program our microcontroller multiple times.

The microcontroller must also be able to survive in an industrial environment. It should be able to withstand heavy vibration, as the glove's purpose is to measure vibration, and if the microcontroller was to fail without the operator knowing, it could have dangerous consequences. The microcontroller should also be able to withstand industrial temperatures.

There were a number of additional criteria that effected our selection of a microcontroller. Familiarity, ease of use, documentation, power consumption, size and cost were the primary factors that guided our selection of the MSP430FG4618. We searched for a microcontroller that met all of our specifications. Overall, we needed a microcontroller that could perform well in industrial environments, and still control all of our peripherals.

We were immediately drawn to Texas Instrument's line of lower power microcontrollers, the MSP430. This was a microcontroller that we had used in our coursework, and had programmed before using development kits for a variety of applications. There is a wealth of application notes and code examples, in both C and assembly, and there are freely available from the manufacturer. Depending on the type of memory, most of the MSP430 line could be easily reprogrammed multiple times. The MSP430 can be easily programmed or reprogrammed through a JTAG connection. TI also provides a free development environment, the IAR Kickstart.

After we chose the line of microcontrollers, we had to decide on the specific device. We knew from our design specifications that we would need an analogue to digital converter with at least 11 external channels. It also would need a serial interface to communicate with both the data storage and display peripherals. With these constraints, we gravitated towards the MSP430FG4618 device. It

contained an ADC with 12 external input channels, multiplexed with 4 internal channels. It contained 2 serial interfaces. It also contained the wealth of supporting application notes, datasheets, and sample code which was typical for any of the MSP430 devices.

3.5 Alert System Selection

The alert system of the device is an essential element of the user interface, because it will indicate when the vibration exposure limits have been reached and/or exceeded by the wearer of the glove. The components of this subsystem are geared towards alerting the user by targeting different senses at the same time. For example, a person working in an industrial setting can be alerted via visual and auditory mechanisms simultaneously. The combination of sensory mechanisms will help to gain the wearer's attention, quicker and more effectively than just using one mechanism.

Our considerations when selecting the components of the alert system were:

- **Ability of user to recognize the alert signal**: Some of the end users of the glove will be working in factory and industrial settings, where there are heavy equipment that generate indicators that could prevent the user from distinguishing the alerts when working in the factory.
- **Conveyance of gravity of situation**: As the exposure limits are exceeded, the alert system should be able to increase the intensity of the signals it is sending, so as to get the user's attention and in effect, prevent them from further hurting themselves.
- **Low power consumption**: The subsystem should run on low power because of the nature of work the users are doing, they may not have time to repeatedly recharge the power supply for the device.
- **Size**: The alert system should be small enough that it can be installed in a glove without it restricting or impeding normal movement of the fingers and wrist.

These elements will help in determining the characteristics of the system and may cause limitations in the number of options that can be investigated in the design process.

The senses that the alert system will focus on will be auditory (through the ears), visual (through the eyes) and maybe even tactile/somatic (through the skin).

It will not be practical to use the senses of taste and smell, because they are not directly related to the glove or the area where the vibration enters into the body. They also involve the use of more components that would not work well with the goal of minimizing the system design.

The transducers may not come with internal drive circuitry so the signal from the microcontroller may have to pass through a driver circuit. We had to consider the available 3.3V supply from the microcontroller when choosing the electrical components for the circuit because picking parts that require a voltage greater than 3.3V, will make us need to add some more control circuitry in the driver circuit.

3.5.1 Auditory Sensory Mechanisms

An effective method of alerting the user when they have been exposed to excessive vibration conditions, would be by using auditory means.

3.5.1.1 Audio Transducer Selection

Audio transducers are electronic devices that convert changes in electrical voltage into acoustic form [83]. They can either be electromagnetic or piezoelectric in nature. Electromagnetic audio transducers are transducers in which changes in the magnetic fields induce electric fields and vice versa [83]. They generate either a single continuous sound or intermittent tones and are available with either self-contained or external drive circuitry.

Piezoelectric audio transducers generate electric potential in response to applied mechanical stresses [83]. They have a metal plate that vibrates with the expansion or contraction of a piezoceramic element.

The option that would be more appropriate for our application will be the electromagnetic audio transducer, because the glove will be exposed to vibration and that could induce more mechanical stresses on the piezoceramic plate in the transducer if that option is used.

There are some factors that need to be taken into consideration when picking an audio transducer for this system, and they are:

- **Frequency**: This is the number of cycles that occur per unit time, usually one second, in Hertz. The audible frequency range for humans is between 20Hz – 20kHz, so the rated frequency of the audio transducer should be within this frequency range.
- **Sound pressure level (SPL)**: This is a logarithmic measure of the sound pressure relative to the lowest sound pressure possible for humans to hear, which is $2*10^{-5}$Pa, and is measured in decibels. Therefore,

$$Sound\ Pressure\ Level, SPL = 10\log\left(\frac{p^2}{{p_{ref}}^2}\right)$$

$$= 10\log(\frac{p}{p_{ref}})^2$$

$$= 20\log(\frac{p}{p_{ref}})$$

where p = sound pressure (Pa)

p_{ref} = reference sound pressure ($2*10^{-5}$Pa)

So, if the pressure is doubled, the SPL is increased with 6dB (i.e. 20log(2)).

The SPL for the transducer needs to be high enough to get the user's attention, but not to the point of causing unnecessary damage to them. The human threshold of pain is about 130dB and a short amount of exposure can cause damage to the ear. So, the SPL should be around 80 to 120 dB.

- **Size & weight**: As a result of the application of the circuitry, the transducer needs to be small enough so that it does not restrict the movement of the user.
- **Power consumption**: The transducer should consume a low amount of power, so that the system can work for extended periods of time without requiring continuous recharging. Low power consumption can be achieved by taking the following parameters into consideration:
    - Operating voltage rating
    - Maximum operating current
- **Cost**: The cost of the transducer is a factor making this decision, but since this project is a proof-of-concept, and we will only be purchasing a few samples for testing and prototyping, the cost will not be a main consideration.

We also took the operating temperature of the transducer into consideration, because the final device will be used in industrial settings where the temperatures may be higher or lower than normal room temperature.

The options for audio transducers that we looked at were buzzers and speakers. Table 14 shows the ideal rating requirements that will be used in choosing the audio transducers.

Table 14: Ideal Rating Requirements for Audio Transducers

Data sheet Properties	Ideal Values
Frequency	20Hz - 20kHz
Operating Temperature	-10 ~ 50ºC
Operating Voltage Range	0 - 3.6V
Rated Current	< 50mA
Resistance (Coil)	~ 20Ω
Sound Pressure Level	≥ 80dB
Weight	1-3g

Table 15 below shows the different audio transducer options under consideration and their power requirements.

Table 15: Audio Transducer Options [84], [85], [86]

Transducer Options	Size/Weight	Operating Voltage Range	Rated Voltage	Max. Rated Current	Coil Resistance
CQR SECURITY 41.T70P015H-LF	12mm x 8.5mm / 2g	1.0V ~ 5.0V	1.5V	30mA	16.0Ω ± 4.5
PRO SIGNAL ABT-410-RC	12mm x 8.5mm / 2g	1.0V ~ 3.0V	1.5V	15mA	42.0Ω ± 6
STAR MICRO. TMB-05	12mm x 9.5mm / 2g	4.0V ~ 6.5V	5.0V	30mA	Value not available

The next factors we took into consideration were the frequency ratings and the sound levels of the transducers. Table 16 below demonstrates the different frequency and sound level ratings of the transducer options.

Table 16: Comparison of frequency and sound levels of the audio transducer options [84, [85], [86]

Transducer Options	Resonant Frequency	Min. Sound Output at 10cm
41.T70P015H-LF	2048Hz	85 dBA
ABT-410-RC	2048Hz	80 dB
TMB-05	2300Hz ± 300	85 dB

After reviewing the transducer options and comparing them to the requirements listed in Tables 14 and 15, the transducer option that fulfilled most of these requirements is the CQR Security 41.T70P015H-LF magnetic transducer, which is shown in Figure 64 below.

Figure 64: CQR Security 41.T70P015H-LF magnetic transducer

The audio transducer did not have an internal driver circuit and the choice of our external driver is dependent on the type of audio signals that we require for our application, and the technical and power requirements of our chosen transducer. There would be no need for extra control circuitry in a situation where since the chosen audio transducer did not require a supply voltage above the available input voltage.

We decided on driving the transducer by using an astable multivibrator because it produces a continuous pulse that is capable of driving a wide range of devices like audio transducers.

An astable multivibrator is an electronic circuit that has no stable states i.e. it cannot exist indefinitely in one state, but continuously oscillates between two quasi-stable states, and it remains in each state for predetermined time intervals [84]. This can be implemented using a 555 IC timer.

A 555 timer is an integrated circuit timer which can operate as an oscillator, and the functional block diagram is shown below in Figure 65.

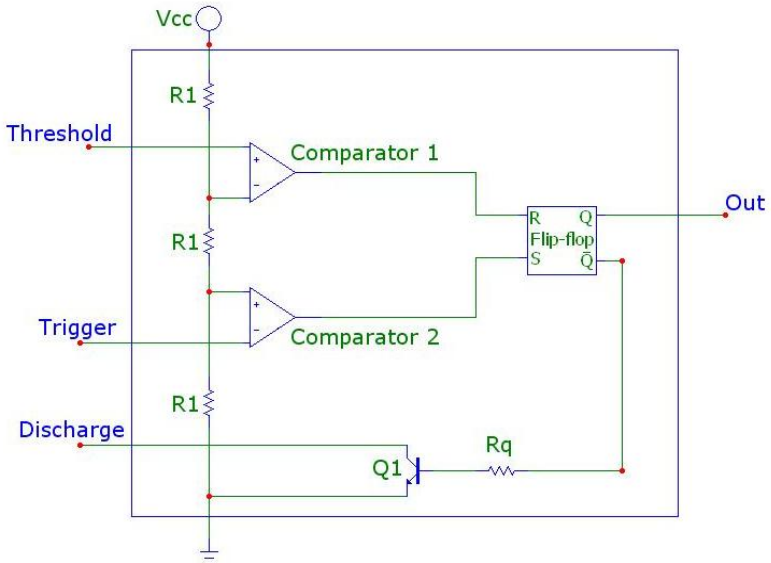

Figure 65: Functional Block Diagram of 555 timer

The timer circuit consists of two comparators, an SR flip-flop, and a transistor, Q_1, which operates as a switch [81]. There is also a voltage divider made up of three resistors of equal value, which are connected across V_{CC} and create the threshold voltages for the 2 comparators, V_{TH} and V_{TL} respectively, where

$$V_{TH} = \frac{2}{3}V_{CC} \qquad (21)$$

and

$$V_{TL} = \frac{1}{3}V_{CC} \qquad (22)$$

In astable mode, the 555 timer is connected as is shown in Figure 66 below.

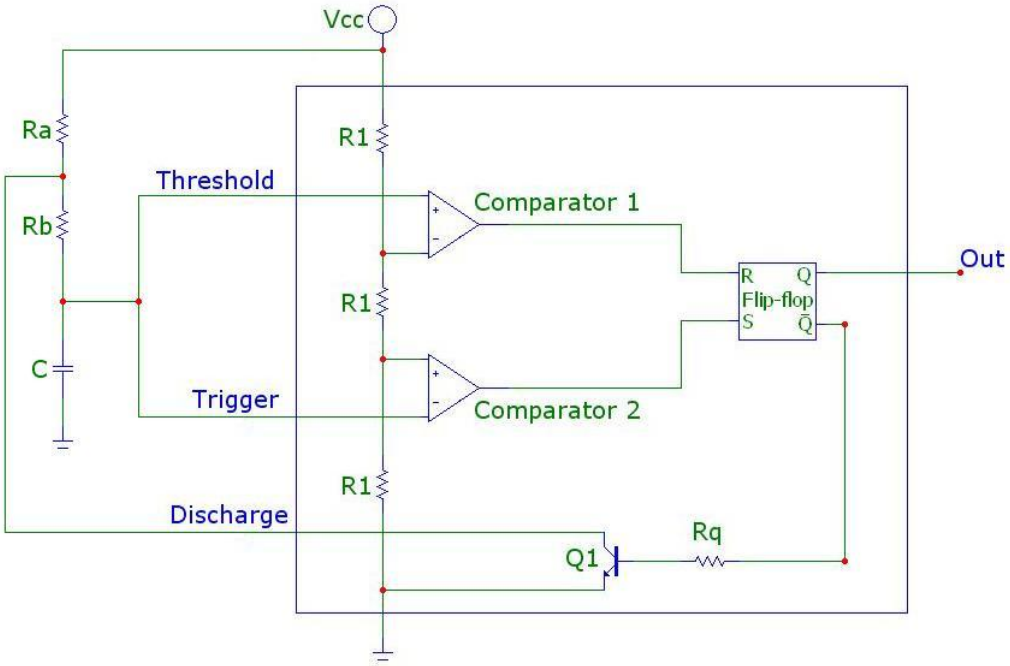

Figure 66: 555 timer connected as an astable multivibrator

There are two resistors, R_A and R_B, arranged in such a way that both of them are in the capacitor charging path and only one of them, R_B, is in the capacitor discharge path. R_A must have a resistance value greater than zero to prevent the discharge transistor from directly shorting V_{CC} to ground.

Assuming that the capacitor is initially discharged and the flip-flop is set such that Q1 is off and the V_O is high, when power is initially applied, the capacitor, C_T, charges up exponentially to V_{CC} through the series combination of the two resistors, and the duration of the charging time is

$$\boldsymbol{ln(2)(R_A + R_B) * C_T} \qquad \textbf{(23)}$$

As the capacitor voltage crosses V_{TH}, the output of the first comparator goes high and resets the flip-flop. This causes V_O to go low and the discharge pin is enabled, becoming grounded. Then the capacitor begins to discharge towards ground through R_B and the collector of Q_1, and as the capacitor voltage crossed V_{TL}, the output of the second comparator goes high and sets the flip-flop. This causes V_O to go high and the discharge pin is disabled. The duration of the discharging time is

$$\boldsymbol{ln(2)(R_B) * C_T} \qquad \textbf{(24)}$$

Therefore, the total period of the pulse is

$$\boldsymbol{T = T_H + T_L = ln(2)(R_A + 2R_B) * C_T} \qquad \textbf{(25)}$$

and the output frequency is the inverse of the period,

$$\boldsymbol{f = \frac{1}{T} = \frac{1}{ln(2)(R_A+2R_B)*C_T}} \qquad \textbf{(26)}$$

The capacitor voltage controls the trigger and threshold inputs, and this causes the timer to trigger itself repeatedly. The period and frequency of the pulses are dependent on the resistor and capacitor values and independent of V_{CC}. This is because the same voltage is used as the capacitor charging voltage and the reference voltage for the comparators inside the 555 IC.

The duty cycle of the output square waveform is

$$\boldsymbol{d = \frac{T_H}{T} = \frac{R_A+R_B}{R_A+2R_B}} \qquad \textbf{(27)}$$

In order to get a duty cycle of 50%, a diode can be placed across R_B. When this happens, this changes the charging and discharging paths of the capacitor. The capacitor now charges through only R_A and discharges only through R_B. The output frequency now becomes

$$\boldsymbol{f = \frac{1}{T} = \frac{1}{ln(2)(R_A+R_B)*C_T}} \qquad \textbf{(28)}$$

3.5.1.2 Application of Astable Multivibrator in Audio Circuit

We can also use the astable multivibrator to generate sound similar to the police siren. This circuit is made up of two 555 timers in astable mode and the unique sound is achieved by connecting the output of one 555 IC to the control voltage pin of the second timer, i.e. the frequency of the second

timer is controlled and modulated by the first timer. The reset pin of the timer is controlled by the output signal from the microcontroller, and this is used to turn the circuit on/off when the exposure limits are exceeded. The circuit diagram is shown in Figure 67 below.

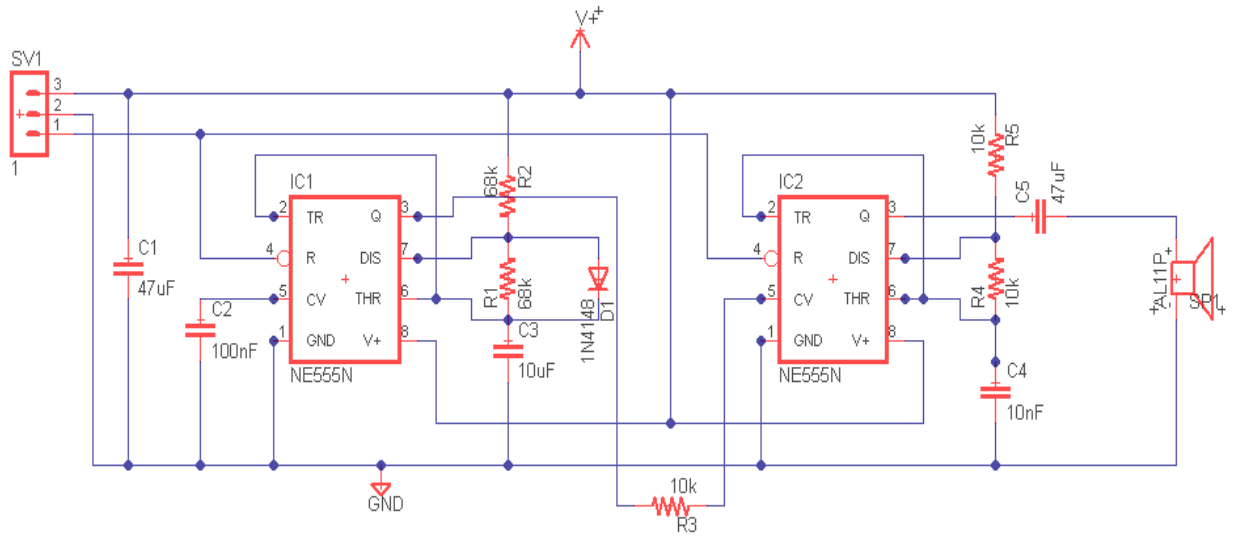

Figure 67: Circuit diagram of Siren generating circuit

The factors we took into consideration when choosing the 555 timer to implement this circuit were:

- It should have very low power consumption
- It should be capable of operating in astable mode
- It should have a high output current capability in order to be able to drive the transducer

We looked at the Texas Instruments line of 555 timers and the only timer that satisfied these requirements is the TLC555 LinCMOS Timer [89]. It has a very low power consumption of 1mW at V_{DD} of 5V. It can source or sink 100mA of output current, and is capable of driving the audio transducer.

To choose the values for R_A, R_B and C_T, we determined the values of the duty cycles and frequencies needed for each multivibrator. For the first circuit, we wanted a duty cycle of 50% and

needed the frequency of the output pulse to be low, with the minimum value being 1Hz. We also chose the capacitor value to be 10µF, which will allow us to be able to choose the resistor values.

By substituting these values in the equation for the output frequency, we find that $R_A + R_B = 144k\Omega$, and since the duty cycle is 50%, the value of R_A is equal to that of R_B. Therefore, 72kΩ is the maximum value of the resistors.

For the modulated circuit, we wanted a duty cycle of 33.33% and needed the frequency of the output pulse to be equal to or higher than the resonant frequency of the audio transducer, which is 2.048 kHz. We also chose the capacitor value to be 10nF.

By substituting these values in the equation for the output frequency, we find that $R_A + 2R_B = 70.444\ k\Omega$, and since the duty cycle is 33.33%, the value of R_A is equal to that of R_B. Therefore, 23.5kΩ is the maximum value of the resistors.

We will be able to choose the exact values that will be used in the circuits when the circuits are being tested, in order to obtain the results we need.

3.5.1.3 Audio Circuitry Testing

We built the finalized circuit on a breadboard and Figure 68 below shows a picture of the test setup for the circuit.

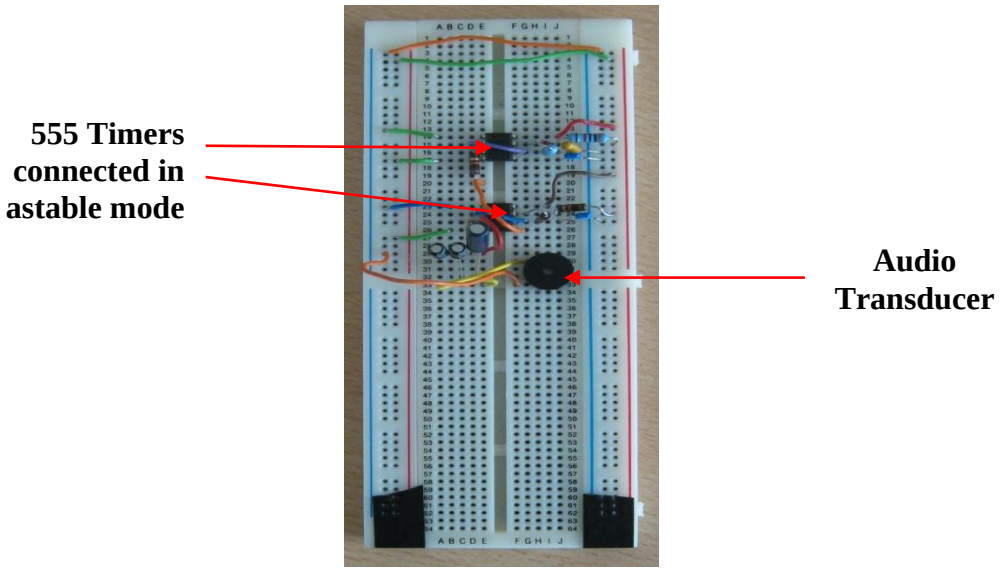

Figure 68: Audio test circuit for prototype alert system using two 555 timers and an audio transducer

When it was turned on, the transducer emitted a two-tone noise similar to that of a police siren, the noise seemed loud enough to alert a person working in an industrial setting.

We then designed a PCB for the circuit using EAGLE software, and Figure 69 below shows the board layout.

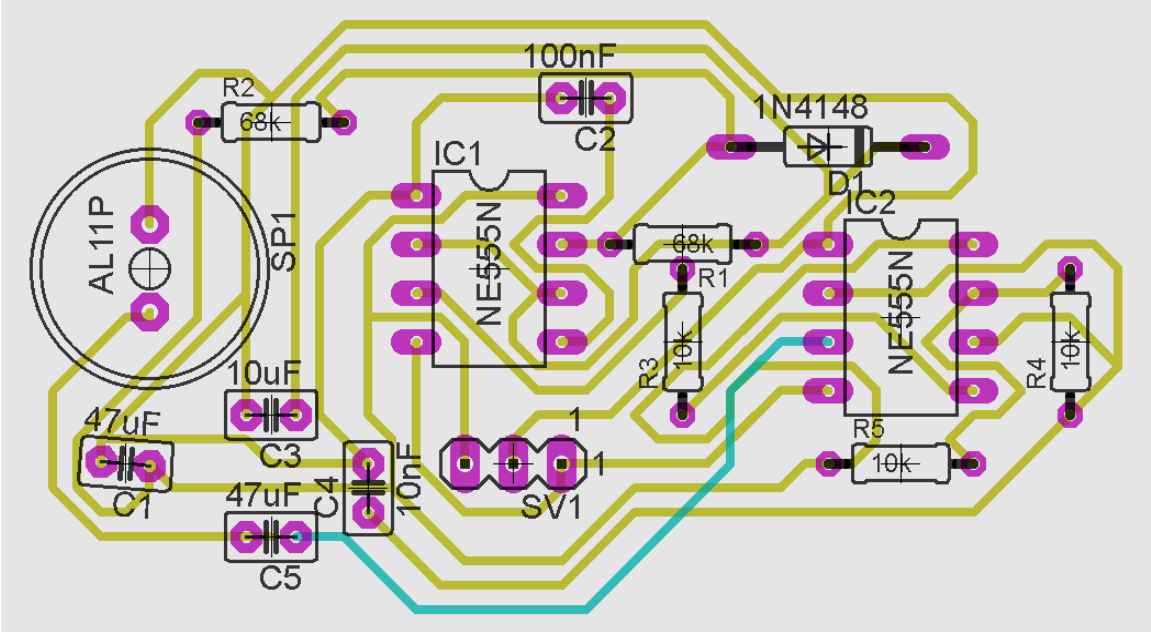

Figure 69: Printed circuit board layout for audio siren alert circuit

Figure 70 below shows the board after it was fabricated and assembled.

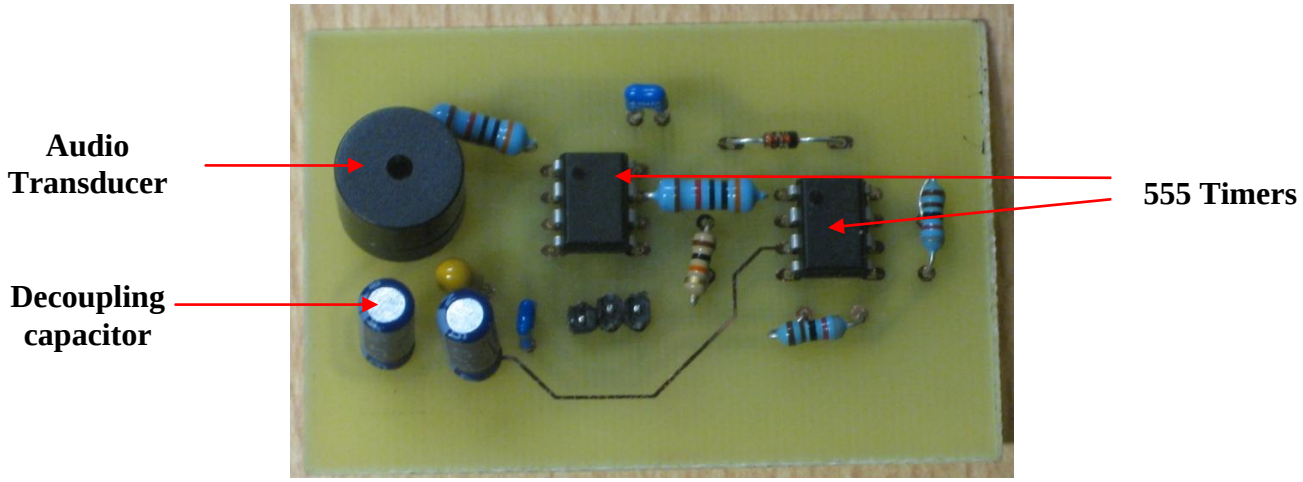

Figure 70: Assembled printed circuit board for the audio siren alert circuit

3.5.2 Visual Sensory Mechanism

Another method of alerting the user when they have exceeded the vibration exposure limits is via visual alerts.

3.5.2.1 Choosing Photo-electronic Transducers

Photo-electronic transducers are electronic devices that convert electrical energy into various forms of visible and non-visible light and vice versa. For the sake of making a working prototype, the ideal transducer that can be used to alert the glove user are light-emitting diodes (LEDs). LEDs convert forward current into visible light, and this makes it useful in display and indicator applications [90].

3.5.2.2 Application of Astable Multivibrator in Blinking LED Circuit

We can also use the astable multivibrator to generate a circuit that causes LEDs to flash back and forth. This would be able to draw the glove user's attention more quickly than a standard LED circuit. The reset pin of the timer is controlled by the output signal from the microcontroller, and this is used to turn the circuit on/off when the exposure limits are exceeded. The circuit is made up of one 555 timer and the circuit diagram is shown in Figure 71 below.

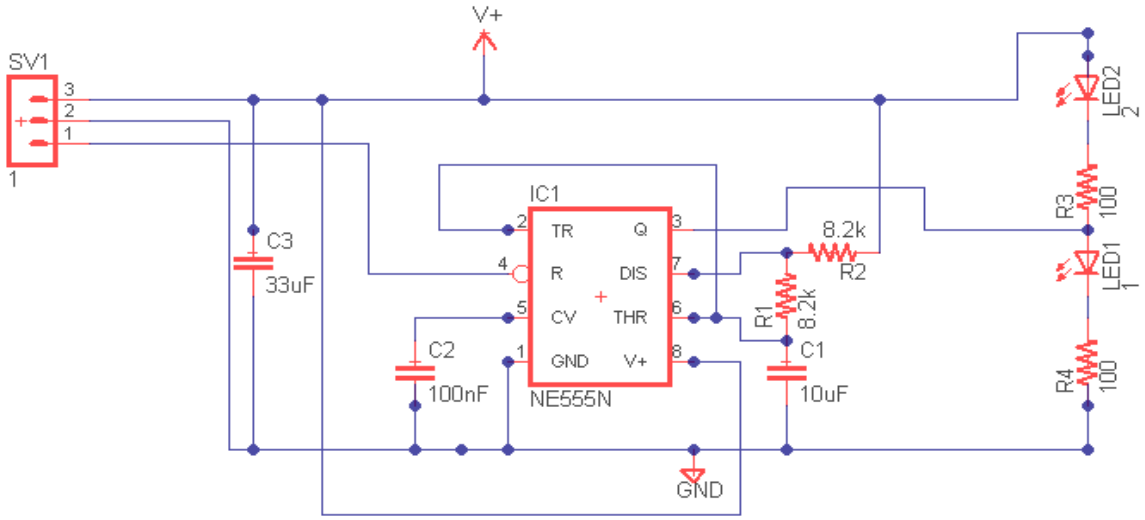

Figure 71: Circuit Diagram for Flashing LED circuit

3.5.2.3 LED Circuitry Testing

We built the finalized circuit on a breadboard and Figure 72 below shows a picture of the test setup for the circuit.

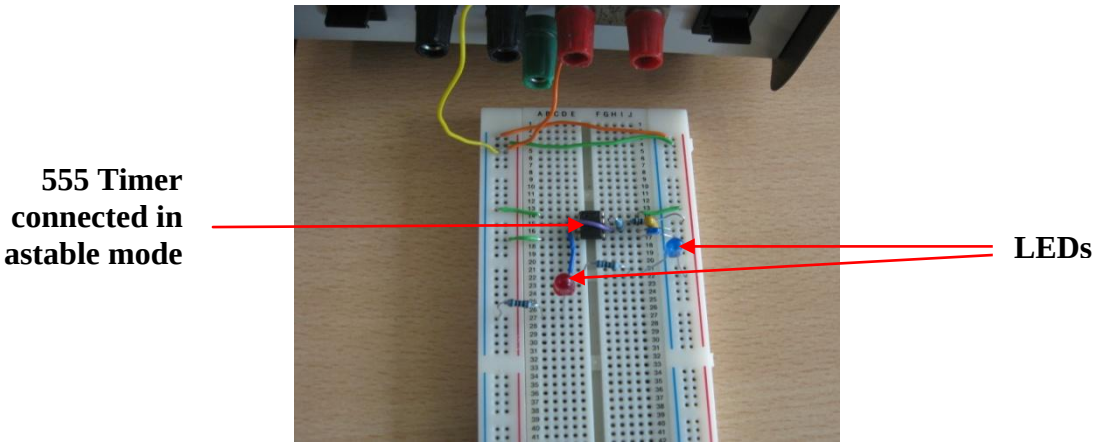

Figure 72: Breadboard test circuit for LED user alert system. This circuit is part of the entire alert system that notifies the user during dangerous vibration exposure conditions.

When the circuit was turned on, the LEDs flashed back and forth at a frequency of 5.9Hz, so that the user is able to notice the lights and stop using the equipment.

We then designed a PCB for the circuit using EAGLE software, and Figure 73 below shows the board layout.

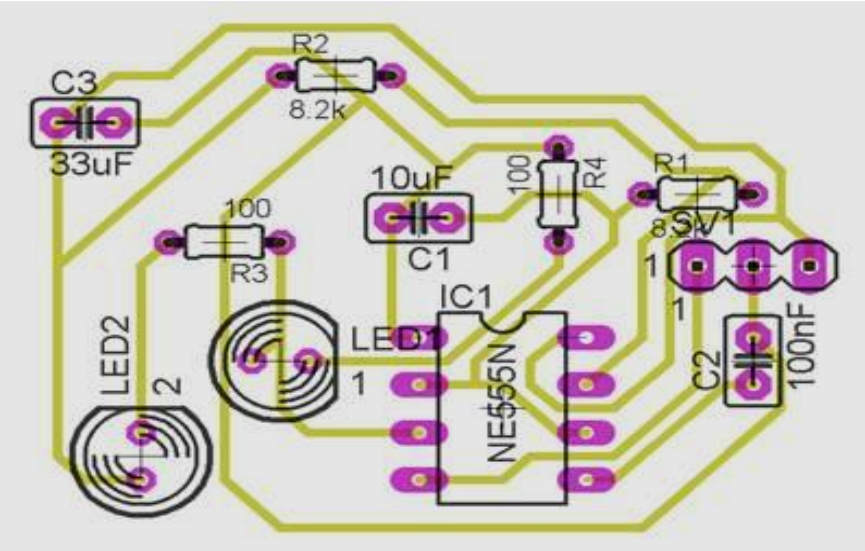

Figure 73: Printed circuit board layout for LED flashing user alert circuit

Figure 74 below shows the board after it was fabricated and assembled.

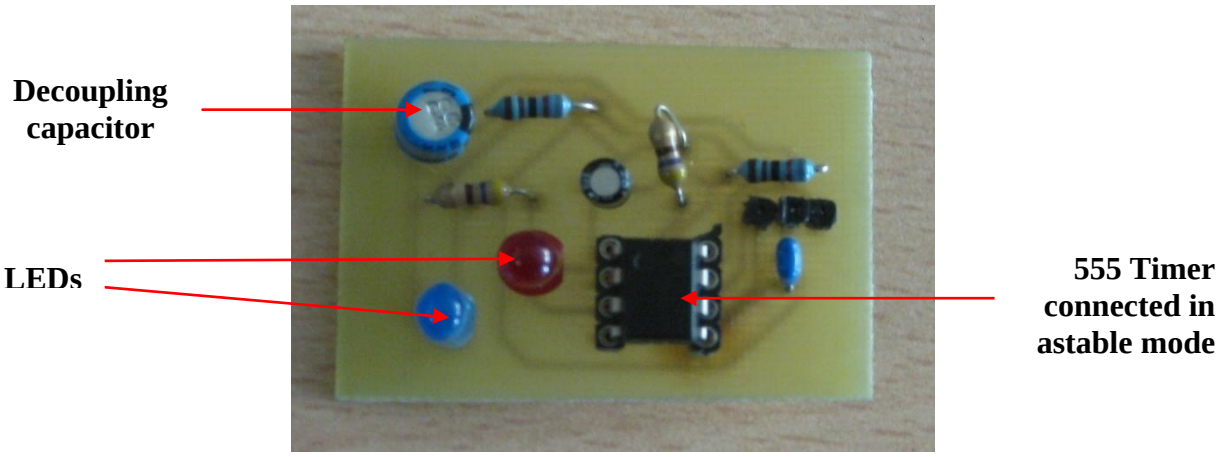

Figure 74: Assembled printed circuit board for the flashing LED user alert system

3.6 Data Storage

Memory storage is an important part of the smartglove design. It was imperative that the memory be something which would be able to stand up to industrial temperatures and conditions. We needed something which was lightweight, low power, and with ample storage space. It also had to be something that could communicate with both an external computer and the embedded microcontroller in the glove. For these reasons, we selected the SD card, as our memory storage.

The secure digital (SD) card is a memory device, which uses flash memory to store information. It is commonly seen in digital cameras or other small electronic devices. The SD Card was a joint effort between the Matsushita Electric Company, the Toshiba Corporation and the SanDisk Corporation[91]. The companies altered the MultiMediaCard to add additional features for improved security, error correction, and power consumption. For example, SD cards manufactured by SanDisk boast a sleep feature. A SanDisk SD card automatically goes into a low power sleep mode after five milliseconds have passed without a command. Sending any command to the SD card will awaken it from its slumber [92].

SD cards may contain as much as four gigabytes of available memory. There are related devices which are smaller, like the microSD, or have more available memory, like the SDIO. We choose the SD card because of the wealth of support in data sheets, application notes, and code provided by Texas Instruments[93].

There are two communication protocols that can be used to communicate with an SD card. Regardless of the method of communication, the SD card is sent commands. The specific device library depends on the manufacturer and features of each individual card. The available commands are divided into classes. These classes correspond to functions, such as reading data, writing data, locking the card, or erasing data [91].

The SD bus mode uses four data lines, along with a clock. However, the methods are proprietary. We decided not to pursue this method of communication because of the lack of available support, and the prohibitive cost of becoming a member of the Secure Digital Association.

The SD card specifications also permit communication through a SPI interface. This consists of two data lines, a clock signal, and a chip select signal. The data lines, SIMO and SOMI, allow for full duplex communication between the SD card and another device. The SD card acts as a slave device. Commands must be sent via the SPI protocol[93]. In the smart glove, the MSP430FG4618 uses the universal synchronous/asynchronous receiver/transmitter provides the appropriate input[91].

To communicate with the SD card through a SPI bus, the SD card must first be placed into SPI mode. This is done by driving the CS to ground, and transmitting the reset command. If this initialization is successful, the SD card will respond in SPI mode to the master. SD commands are six bytes long, and transmitted with the most significant bit of data first. To communicate with any SD card, it is important to limit the command library to the basic commands that every card contains. Otherwise, there would be a possibility of an unrecognized command. When initializing the SD Card, the SPI clock, which in the “smart glove” was sourced by the internal digitally controlled oscillator, must have a frequency below 400 kHz. After SPI communication has been initiated, the clock's frequency can be raised until it reaches the maximum allowable frequency of the SD card.

Information must be written to the SD card in blocks of 512 bytes. However, data can be read from the SD card in a block as small as a single bit. Whenever a command is sent to the SD card in SPI mode, a response is transmitted back to the master. The response is a byte long, and it corresponds to a status code, signifying an error or the state of the SD card [91].

3.7 Power Subsystem

The microcontroller, sensor and alert subsystems required various supplies and reference voltages, which demanded multiple DC-DC conversions. We planned to use a 3.7V Lithium-Ion

battery because of they were rechargeable, are available in small sizes and had high capacities [94]. We needed to generate +3.3V, +9V and ±1.5V from such a battery. The circuit, which accomplishes these conversions is in Figure 75. Each supply was connected to six-pin headers so that cabling from other boards could be soldered to it.

The OLED display required +9V. To step +3.7V to +9V, we used a MAX761 Adjustable Step-Up DC-DC Converter [95]. The MAX761 was an ideal choice, since it was a low-current, high-efficiency device according to its datasheet. The circuit we chose to use the MAX761 in is based on Figure 5 in its datasheet. The capacitors and the 18µH inductor chosen based on their specifications. The datasheet for the MAX761 specifies that for input voltages up to 5V, an 18µH with over 1A peak current and a DC resistance less than 100mΩ is appropriate. The Panasonic ELC09D180F inductor has an equivalent series resistance of 0.038Ω and a maximum current of 2A [96]. This circuit is indicated on the prototype's power schematic (Figure 75).

Each of the signal conditioning circuits requires -1.5V. This conversion is made in two stages. A negative voltage is first generated, then it is regulated to approximately -1.5V. The first stage is based on a circuit idea found online that John Harris suggested as an alternative to a voltage inverter [97]. A 555 timer set up for a frequency of approximately 118kHz [98] (see the calculation below based on the datasheet: R_B = 5kΩ, R_A = 2.2kΩ, C = 1nF) passed a square wave to two cascaded voltage doubler circuits, resulting in a negative DC voltage [84]. Note that R_B was two 10kΩ resistors in parallel, so their combined resistance is 5kΩ (no 5kΩ resistors were available).

$$\boldsymbol{f_{555}} = \left(\frac{\mathbf{1.44}}{\mathbf{1}\boldsymbol{nF}(\mathbf{2.2}\boldsymbol{k}\Omega+\mathbf{5}\boldsymbol{k}\Omega)}\right) = \mathbf{118.03}\boldsymbol{kHz} \quad \textbf{(29)}$$

This circuit outputs a negative voltage with a magnitude great enough for the LM337 adjustable negative regulator [99]. The output voltage of this circuit varies, depending on its load to a potential of -4V or more negative. Without the additional voltage doubler, the output was not negative enough for the LM337 to operate properly once the regulator loaded it. Using Schottky diodes rather than ordinary

diodes made the magnitude of the output greater, since Schottky diodes have lower forward voltage drops. There were not enough 1N5817s available, so we used a combination of them and BAT42s. Originally, the capacitors were 330µF, but we increased this to 1000µF, so the circuit's output magnitude would decrease less as the regulator drew current from the capacitors. Increasing the frequency of the timer from its original setting of 59kHz also improved this circuit by charging the capacitors double the frequency.

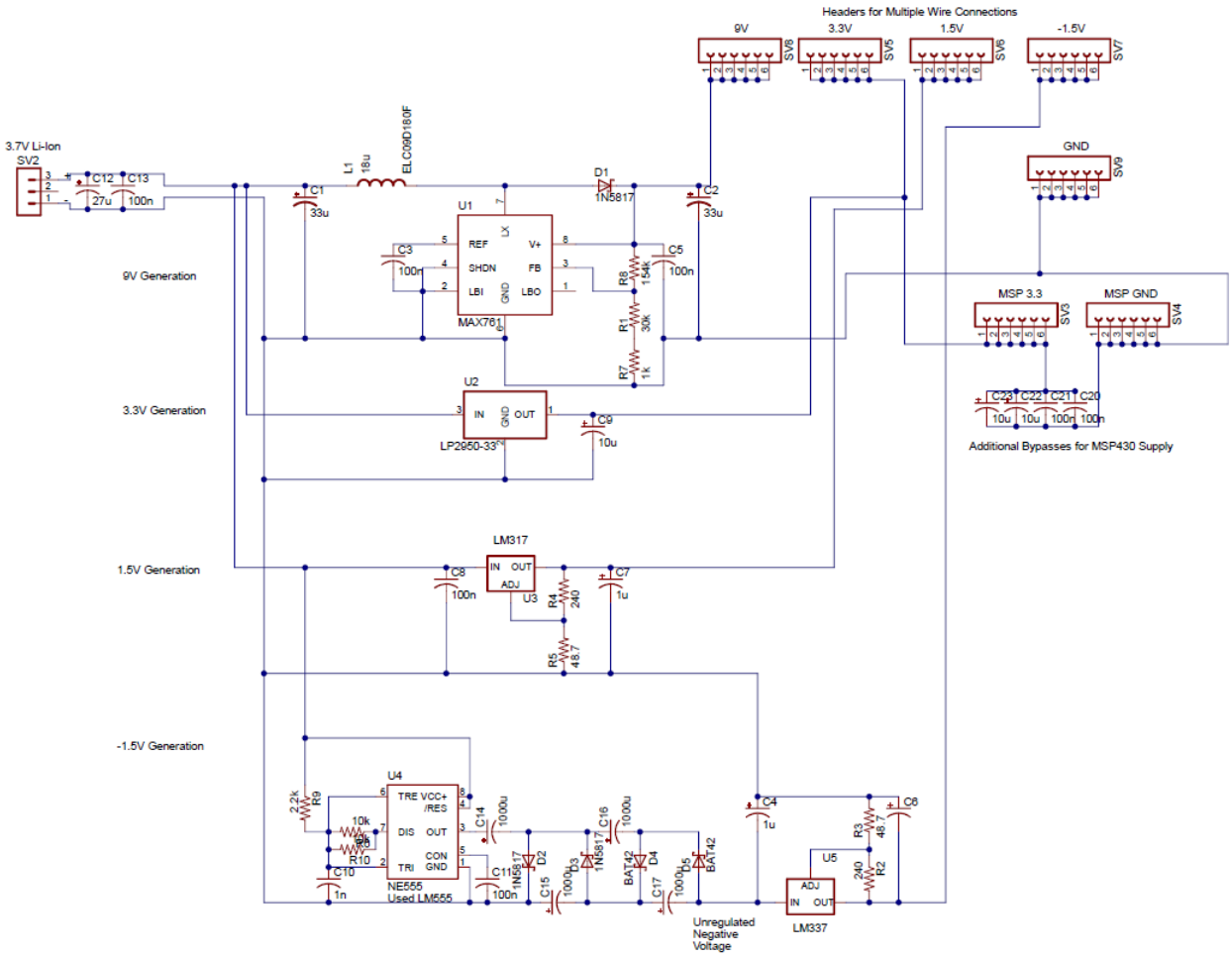

Figure 75: Prototype DC-DC Conversion [95],[97],[99],[108],[101]

A LM337 converts the output from the 555 voltage inverter-multiplier to a regulated -1.5V level. For an LM337 configured as shown in Figure 75, the resistances have the following relation to the output voltage [99].

$$R_3 = R_2\left(\frac{-V_o}{-1.25} - 1\right) \quad \textbf{(30)}$$

For R_2 = 240Ω, R_3 needed to be approximately 48Ω. A 48.7Ω was the closest available value. $-V_O$ is approximately -1.5V with these resistors.

Converting 3.7V to 1.5V was necessary for the vibration sensing subsystem. We used an LM317 adjustable regulator because it available. The LM317 is a similar device to the LM337, regulating a positive voltage instead of a negative voltage [100]. In its setup in our circuit (Figure 75) has an output that can be determined by the equation below.

$$V_{OUT} = 1.25\left(1 + \frac{R_5}{R_4}\right) + I_{ADJ(R_2)} \quad \textbf{(31)}$$

Since I_{ADJ} is at most 100μA, we assumed this term would be approximately 0V. Removing this term, setting R_4 to 240Ω (as suggested),V_{OUT} to 1.5V and solving for R_5, we determined that R_5 should be approximately 48Ω. We used 48.7Ω, as we did with the LM337. This circuit output a regulated 1.5V.

The last voltage that we needed to convert 3.7V to was 3.3V, which every subsystem required. An LP2950-33 fixed 3.3V regulator accomplished this for us with a minimal footprint [101]. We simply needed to connect our battery to its input and bypass the output properly. This is a "micropower" regulator, which makes it ideal for generating the 3.3V supply in a production version of the "smart glove." The minimal amount of external components that it requires also is an advantage. This circuit is shown in **Error! Reference source not found.**. A PCB layout for this circuit is shown n **Error! Reference source not found.** and the bread-boarded prototype is shown in Figure 77. Unloaded, the DC to DC conversion circuit consumed approximately 20mA with a 3.7V input.

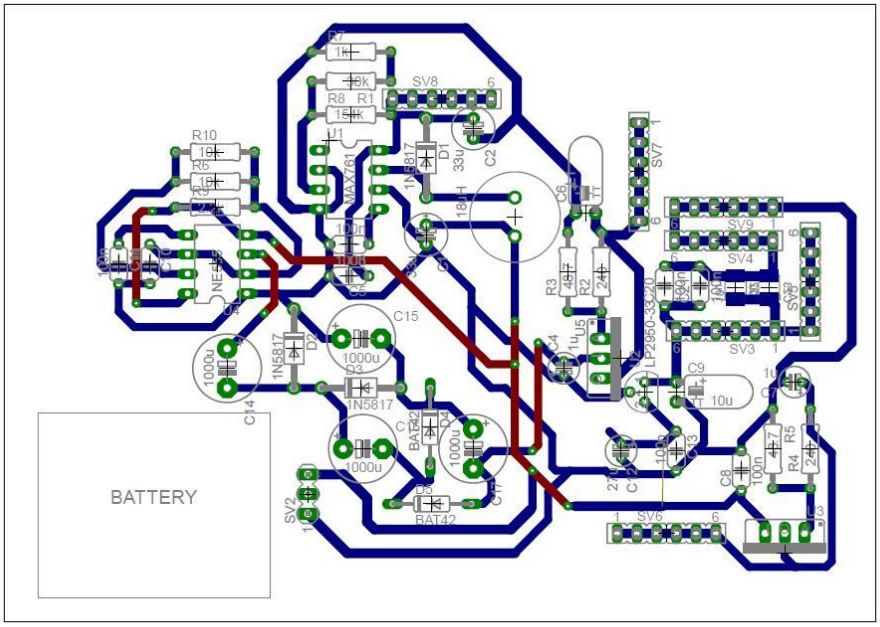

Figure 76: Initial Prototype Power Circuit PCB Layout

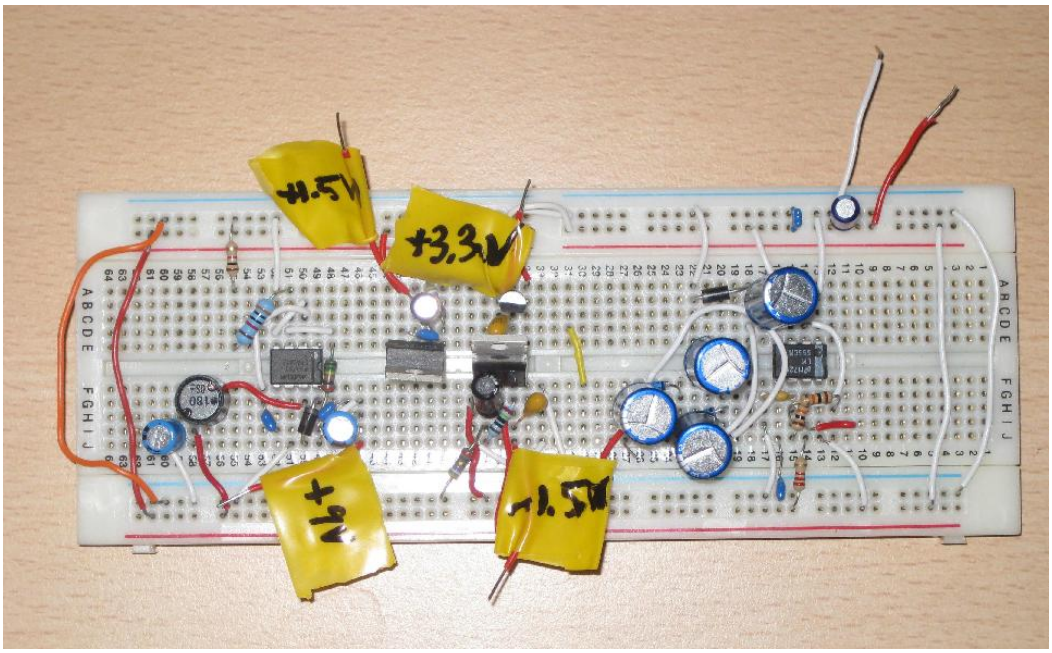

Figure 77: Initial Prototype Power Circuit – Outputs Electrical Tape Indicates Voltages

4 System Specifications

In this chapter, we will discuss each sub system of our proof of concept prototype. We will explain the individual functions of each sub system, and then present the entire integrated system. We also included technical information on all major electrical components and software used in this project.

4.1 System Overview

The main purpose of the overall system is to prevent the onset of repetitive strain injury (RSI) by monitoring and measuring the parameters that contribute to it, so that it limits exposure the user's exposure in terms of duration and severity [5]. The “smart glove” proof-of-concept prototype is divided into the following main subsystems:

- Sensing Circuitry: This is made up of the sensors that measure and monitor the magnitude and direction of hand and arm vibration, the wrist angles corresponding to wrist flexion and extension, and impacts experienced by the hand.
- Microcontroller: This is made up of the MSP430FG4618 microcontroller circuitry and the data storage system.
- Alert System: This is made up of audio and visual sensory mechanisms that alert the user when the period of exposure to vibration becomes hazardous
- Power System: This system converts the voltage from a rechargeable lithium ion battery to various supplies and references that the other systems require.

Figure 78 gives a basic overview of the components and sub-systems that will make up the “smart glove” device.

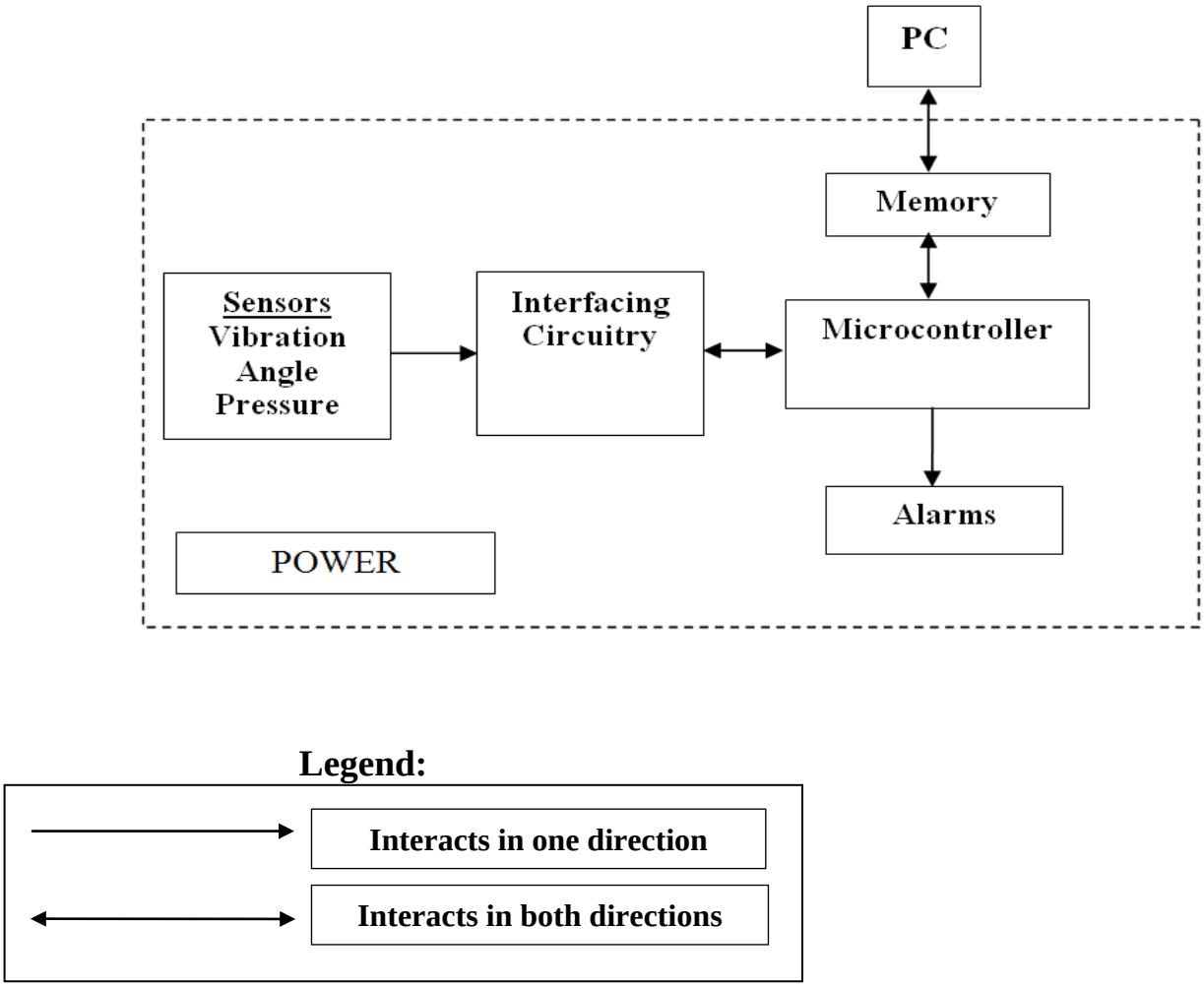

Figure 78: Block Diagram of "Smart Glove" Prototype

The arrows shown in Figure 78 indicate the direction of data flow between each of the modules. The flow and collection of data begins with the sensors, continues through the microprocessor and ends when the transmission of the data has reached the SD card, display module, and in the event of exceeding the exposure limits, the alert systems.

The MSP430FG4618 microcontroller is the centre module of the proof-of-concept device and it is used to process the sensor interface signals received from the sensing circuitry in the course of the workday. It analyzes the incoming data of the magnitude and direction of hand and arm vibration and compares it to the vibration exposure limit determined by ISO. When the harmful vibration levels have

been reached and exceeded, the microprocessor triggers the alert system, in order to warn the glove user. It also writes the raw data from its ADC to the SD card

4.2 Sensing Circuitry

4.2.1 Pressure Sensor Module

The pressure sensor subsystem outputs six voltages, which are directly proportional to the pressure applied to each of the flexible Tekscan A201 sensors. This is possible since the sensors are variable resistors with conductances that have strong linear correlations (determined empirically) to the force applied to their sensing areas. Each of the six virtually identical circuits interfaces with the microcontroller's analog to digital converter. A negative reference voltage causes current to flow through the sensor. Op-amp circuitry converts this current to a voltage. Passive low-pass filters and notch filters attenuate the noise that the sensors tend to pick up. A trim potentiometer on each circuit enables individual sensitivity adjustments. The trimmers are adjusted so that each circuit's output saturates (approx. 3.3V) when a force slightly above 100N is applied to each sensor. Figure 79 shows the pressure sensor module, its components and their functions.

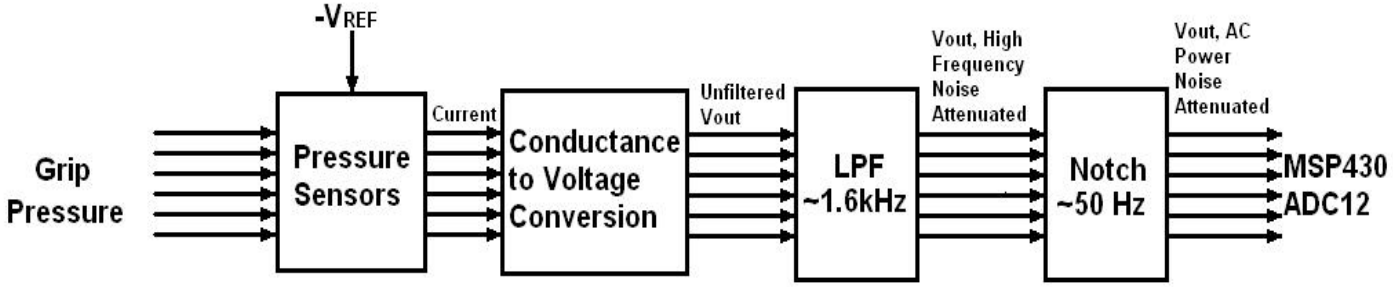

Figure 79: Pressure Sensor Module Block Diagram

4.2.2 Accelerometer Module

The vibration sensing system is composed of the accelerometer module, signal conditioning, and software methods to convert the signal into the standard form as outlined in the standard for hand transmitted vibration measurement [1]. A block diagram of these components is shown below in Figure 80, and each block is discussed in more detail in the following sections.

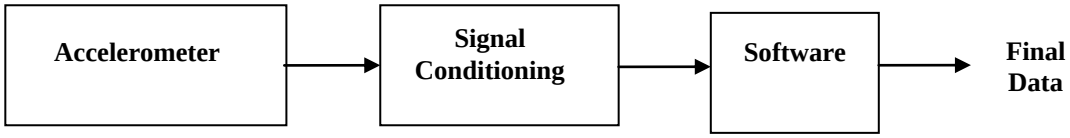

Figure 80: The accelerometer module consists of the physical accelerometer transducer, which sends a raw signal to conditioning circuitry before it is finally ready to be interpreted in software on the microcontroller. The final data at the output conforms to the ISO standards for hand transmitted vibration measurement and can then be used to calculate exposure time limits.

4.2.2.1 Accelerometer Module

The accelerometer selected to sense the vibration was the ADXL330. With three axes and the ability to measure +/3g, this was a cheap device capable of measuring the vibration transmitted by many power tools. This device comes in a lead frame chip scale package (LFSCP), but it is available in a breakout board from sparkfun.com [74].

For the sake of creating the prototype, we will only be measuring the vibration in the z axis to prove that the subsystem actually works. Also, the single prototype filter circuit board used was bulky and took up a lot of space.

4.2.2.2 Signal Conditioning

In order to comply with the standard for hand transmitted vibration measurements, we constructed analog filters to perform frequency weighting functions on the vibration signal. The filters consisted of two Sallen-Key lowpass filters, a single zero filter, and a DC gain stage. This allowed us

to pass only the most important signals through to the accelerometer, where the data could be read from an ADC and interpreted.

Passive components were chosen with minimized tolerances. The TLV2764 Quad Low Power Op-Amp was chosen for use in the amplifiers and active filters because of its low current draw and adequate gain bandwidth product.

4.2.2.3 Software Interpretation of Accelerometer Data

The root mean square of each accelerometer axis signal is calculated in real time on the microprocessor. These are then vector summed to find the acceleration total value due to all three axes. With this value, we can calculate the daily vibration exposure A(8) as a worker uses a tool throughout the work day [1]. We can also calculate the remaining time one has to safely use a tool by using the A(8) formula [1].

4.2.3 Goniometric Sensor Module

The goniometry sensor subsystem outputs three voltages, two of which directly relate to voltages across strain gages and the other is a reference voltage. Each of these signals serves as an external input to the microcontroller's ADC and is tied to an appropriate pin. The valid range for input to the ADC is from the microcontroller's power source's potential of 3.3V to 0V. Figure 81 shows a block diagram of these systems.

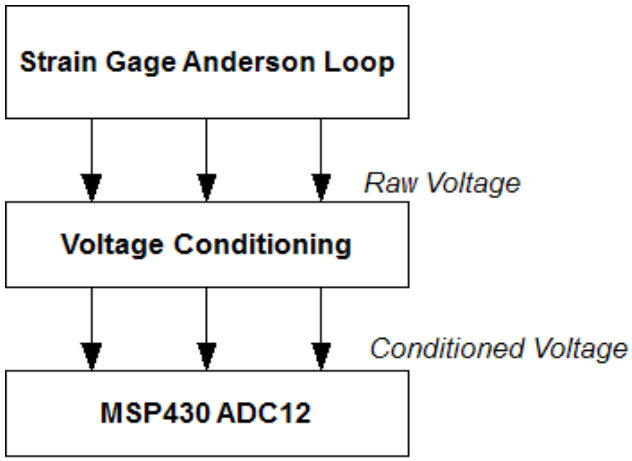

Figure 81: Functional Block Diagram of Goniometry Subsystem

4.3 Alert System

The alert system is made up of the audio and visual sensory mechanisms. These circuits are controlled by the microcontroller to turn on when the vibration exposure limits are exceeded.

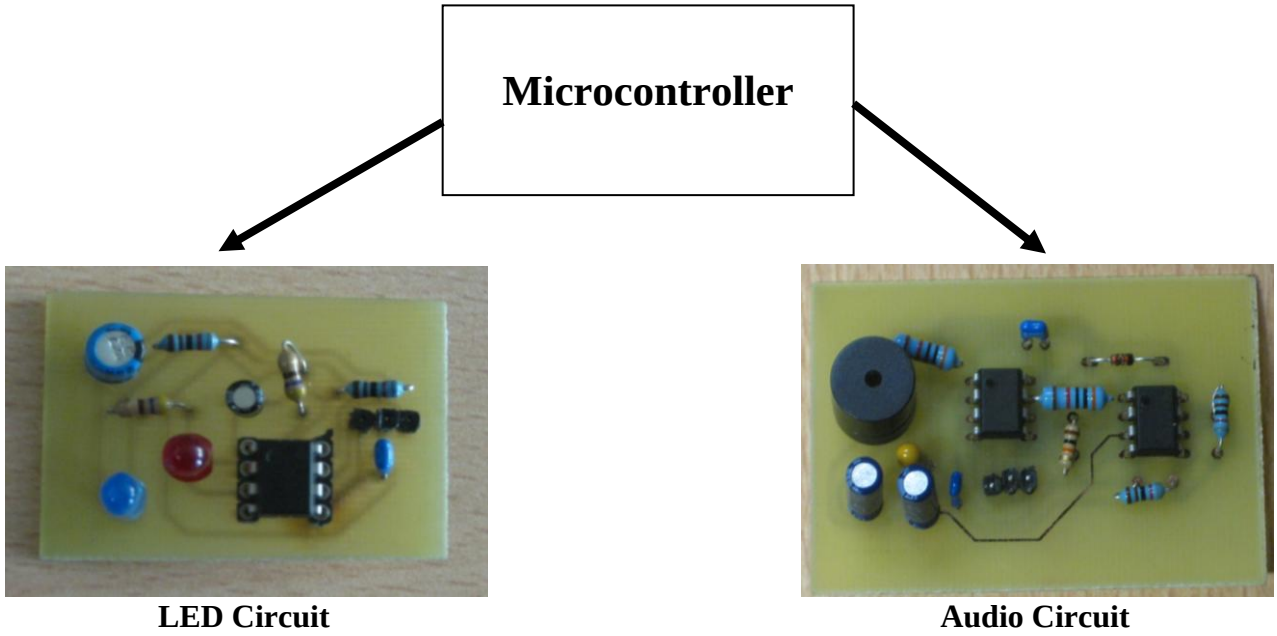

Figure 82: User alert system consisting of a visual flashing LED and a loud siren. These alerts are controlled by the microcontroller

They are connected to pins #, whuch are two of the I/O ports of the MSP430FG4618. These pins are set as outputs, because the data flow occurs from the microcontroller to the alert circuitry when the interrupt service routine (ISR) is enabled.

4.5 Power System

The power system made four different DC to DC conversions from a +3.7V supply (like a lithium-ion battery). We used a MAX761 step-up converter to boost +3.7V to +9V for the OLED's supply. An LP2950-33 fixed linear regulator converted +3.7V to +3.3V, which the alert system, the sensor systems and the microcontroller all needed. An LM317 linear regulator converted +3.7V to +1.5V. The accelerometer system required +1.5V as an op-amp supply. All of the sensor systems required -1.5V. The pressure sensor and goniometry systems required this voltage as a reference and the accelerometer system used it as an op-amp supply. We accomplished this conversion in two steps. A voltage inverter and multiplier circuit generated a negative voltage with a great enough magnitude to supply an LM337 negative linear regulator. The LM337 converted this voltage to -1.5V. This circuit was only for our prototype and we chose parts based on their availability, rather than their power consumption. Therefore we did not attempt to determine how long it could run on a lithium-ion battery with all of the systems consuming the "worst case" amount of power. Figure 83 shows a block diagram of the power system.

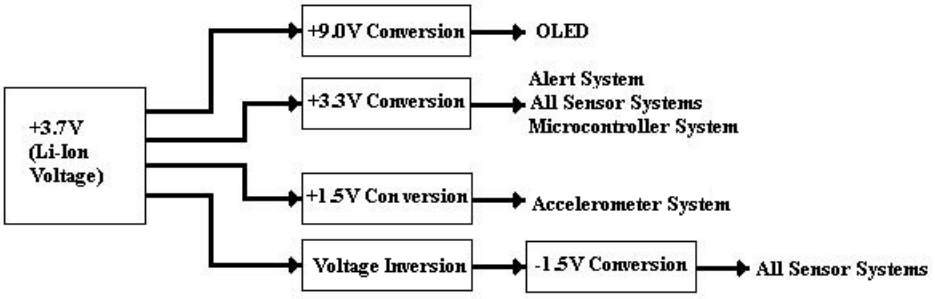

Figure 83: Power system block diagram. The system takes +3.7v as input and provides four different output voltage levels for different systems in the "smart glove" design.

5 Implementation and Integration

In this chapter, we present the results of the system integration and implementation processes. From these results, we were able to identify flaws, which we could then correct by redesigning and making changes to the subsystems, which we also documented in this section.

Since the "smart glove" had many different systems that needed to function together for the prototype to function, we needed a methodical approach to its integration. Our strategy was as follows:

1. Once satisfied with each block's performance on a breadboard in the context of our proof-of-concept prototype, rebuild that block on a custom PCB.
2. Debug the custom PCBs as necessary.
3. Prepare the glove and enclosure for assembly (ex. drill holes, find standoffs, etc.)
4. Begin assembling the enclosure and glove, verifying the separate functionality of each board in the enclosure or on the glove at each assembly step.
5. Assemble the prototype and debug the entire system's software and hardware as necessary.

As the prototype block diagram in Figure 78 shows, a key step in integrating this system was getting the microcontroller block functional. Since we stacked many of the block's boards in an enclosure, it was necessary for us to be sure that each system worked with the power board before adding other layers. If one board on a low layer of the enclosure suffered a problem, we would not be able to reach it with oscilloscope or DMM probes.

As an initial proof of concept before pursuing the remainder of the project in the United States, we combined our working prototypes of the power system and the pressure sensor system with the microcontroller board. The power breadboard supplied a single pressure sensor circuit with +3.3V and its -1.5V reference, while the MSP430 made an analog to digital conversion. We applied pressure to the sensor and verified that the conversion succeeded. Figure 84 below shows the subsystems connected for Analog to Digital conversion.

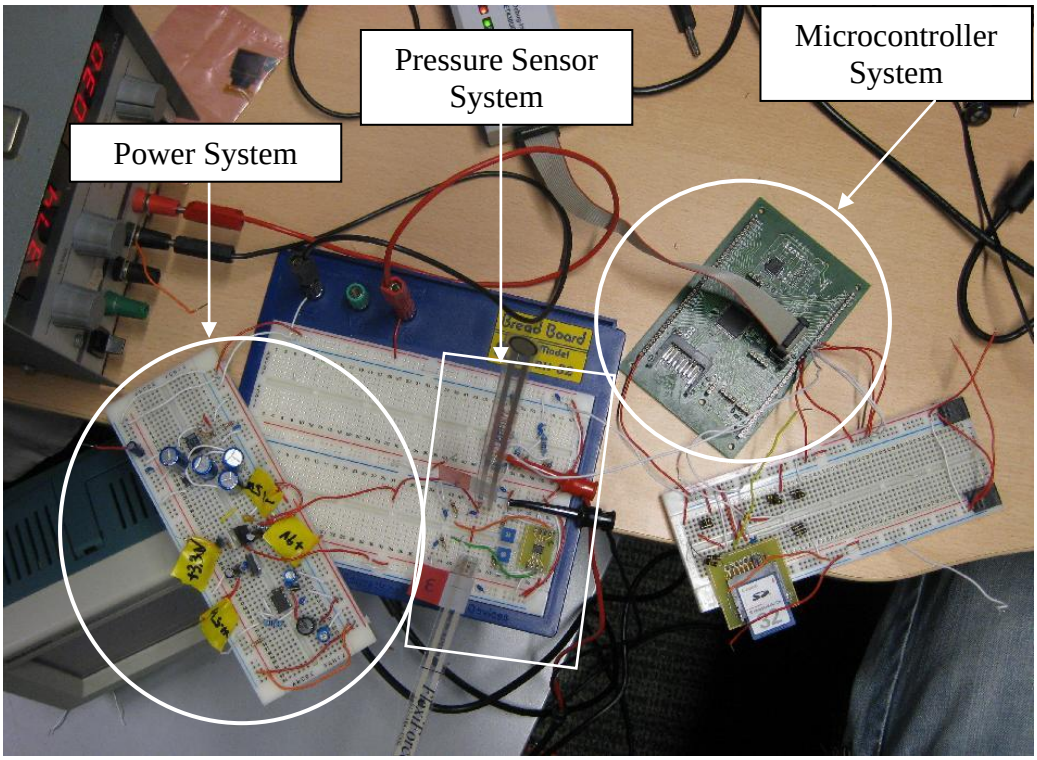

Figure 84: Initial Prototype of Power System, Pressure Sensor System and Microcontroller System Set Up for an Analog to Digital Conversion

The new DC-DC conversion circuit enabled us to eliminate the need for multiple voltage sources to provide +3.3V (which is representative of a Li-ion battery) and the -1.5V reference voltage required by the pressure sensor circuitry. The 3.3V battery would have supplied the MSP430 with power, but we used the JTAG to power the microcontroller for convenience. The power supply provides +3.7V. An NB-4L battery was available, but connectors were not available and we had not yet built a custom one.

5.1 Frequency weighting filter implementation

In order to implement the band limiting frequency weighting function for the signal coming out of the accelerometer, we tested each component filter individually and then put them together and tested the performance of the entire system.

5.1.1 Low Pass Filter 1

To test the first low pass filter we used a function generator to input a sinusoid of amplitude 1.54V. By measuring the amplitude and time delay of the output signal, we were able to calculate the gain and phase of the transfer function over a range of frequencies. By plotting on logarithmic axes, we were able to verify the magnitude transfer function of this filter. This is depicted in Figure 85 below, using the collected data.

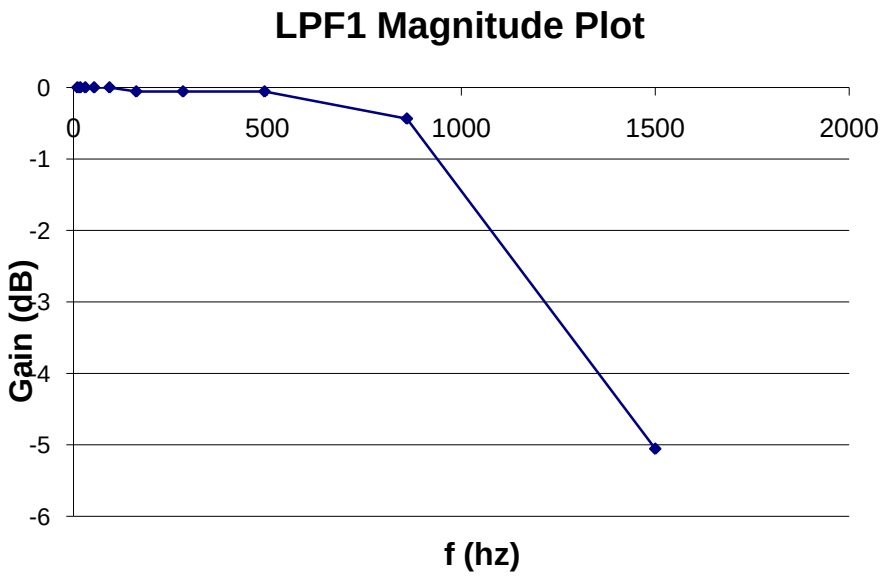

Figure 85: Magnitude transfer function of the first stage low pass filter. This data was collected by comparing input output magnitudes of test sinusoid waveforms. Here we notice the -3dB gain frequency is near 1200Hz, as expected

To verify the cutoff frequency, we found the frequency at which the input signal was attenuated by Q=0.71, since the transfer function magnitude is equal to this value at $f=F_C$. The input and output signals at this frequency are shown below in Figure 86. We determined the cutoff frequency to be 1450 Hz, which is higher than the expected 1250Hz, due to the tolerance of the passive component values.

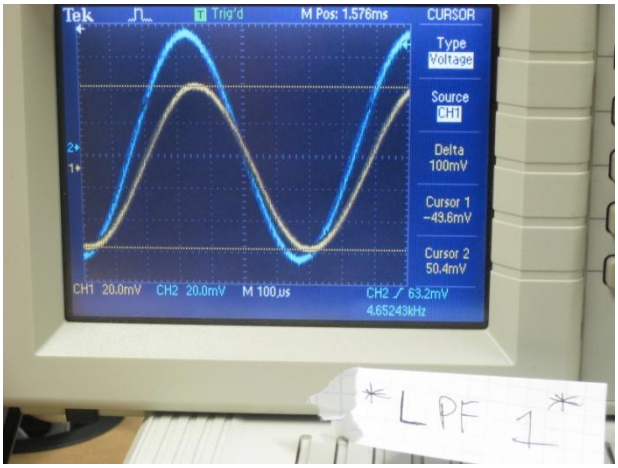

Figure 86: Input and output signals for the first stage low pass filter at the cutoff frequency. At this frequency, the output signal is attenuated by the Q factor, 0.71.

5.1.2 Low Pass Filter 2

We conducted the same tests for the second lowpass filter, which is shown below in Figure 87. We determined the cutoff frequency of this filter to be 14Hz, which is slightly lower than the expected 15.9Hz, due to the tolerance of passive component values.

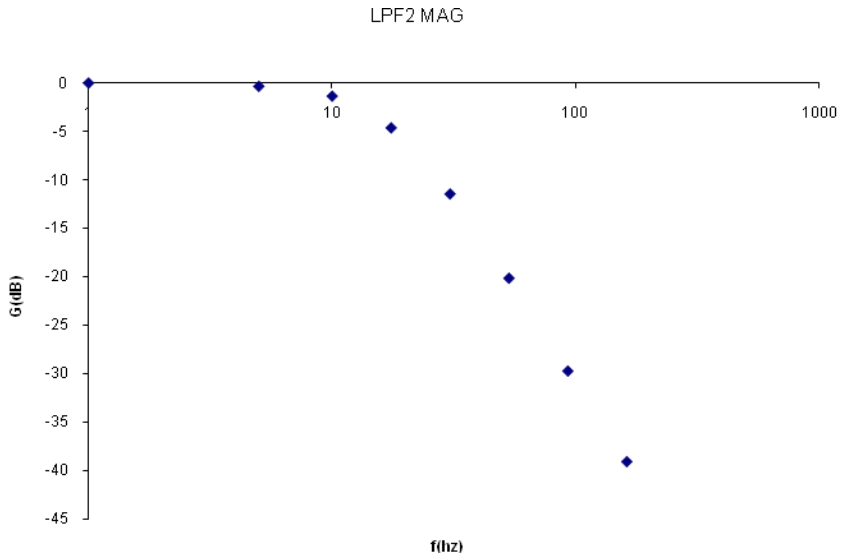

Figure 87: Magnitude transfer function for second stage low pass filter. The 3-dB frequency is close to the 15.9Hz, as expected.

5.1.3 Frequency Weighting Circuit

We could not test the single zero circuit on its own since the gain of that circuit rises rapidly, and would result in clipping at the output. Instead, we cascaded the second lowpass filter with this filter to produce the frequency weighting circuit. The magnitude transfer function resulting from these tests is shown below in Figure 88.

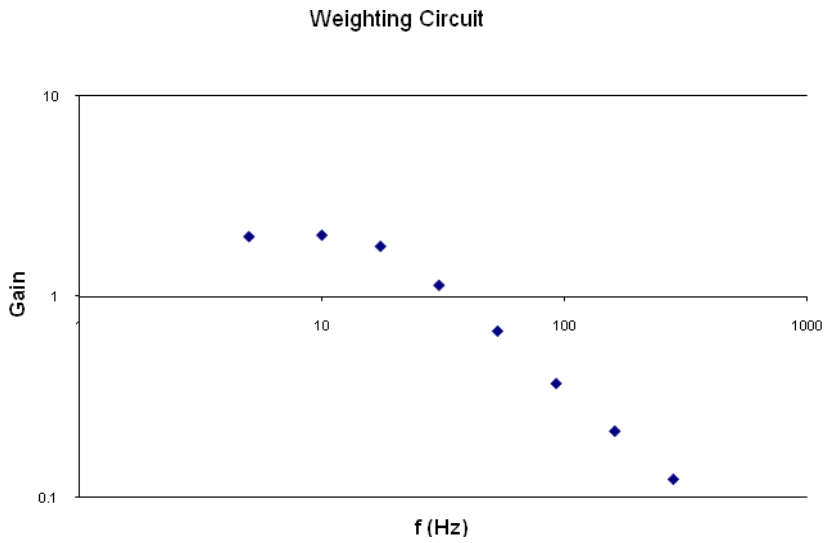

Figure 88: Frequency weighting magnitude transfer function (=Single Zero filter cascaded with Low Pass Filter 2)

We verified this transfer function by using MATLAB to plot the ideal frequency weighting transfer function. This is shown below in Figure 89. As we can see this follows our data closely.

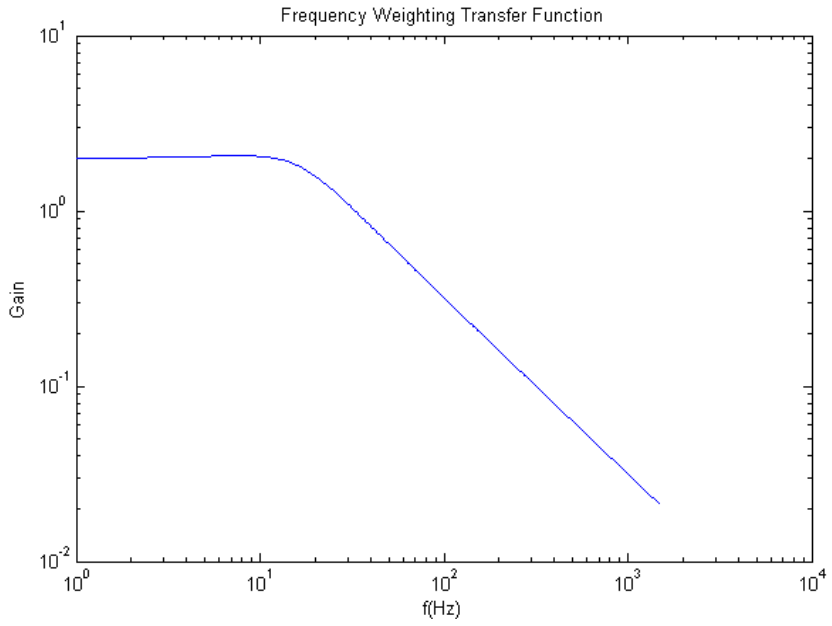

Figure 89: Matlab plot of ideal Frequency Weighting Magnitude Transfer Function (=Single Zero transfer function * Low Pass Filter 2)

5.2.4 High Pass Filter Implementation

When we tested the high pass filter, we found that the circuit attenuated signals of frequencies up to about 50Hz, when it was supposed to only attenuate signals of frequencies below 6 Hz. Because our prototype will demonstrate acceleration measurement in the z-axis only, and we do not expect acceleration at these low frequencies in this axis, we decided to omit the high pass filter from our design in order to focus on more important hardware concerns.

5.2.5 Frequency Weighting Printed Circuit Board Testing

Using Eagle LS circuit layout software, we designed the schematic for or frequency weighting band limiting filter. This schematic is shown below in Figure 90.

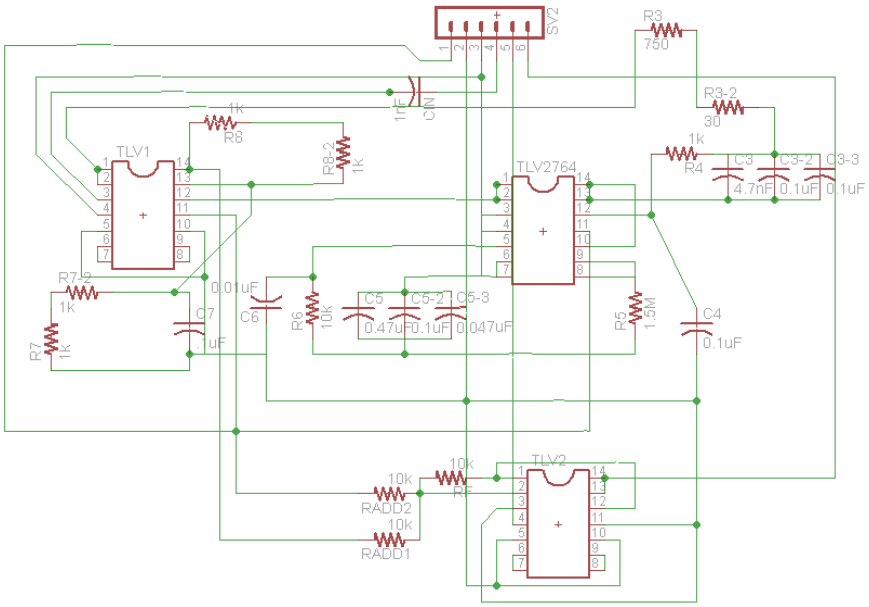

Figure 90: Schematic for Frequency Weighting Band Limiting Circuit

We also designed the layout for this circuit, which is shown in Figure 91 below.

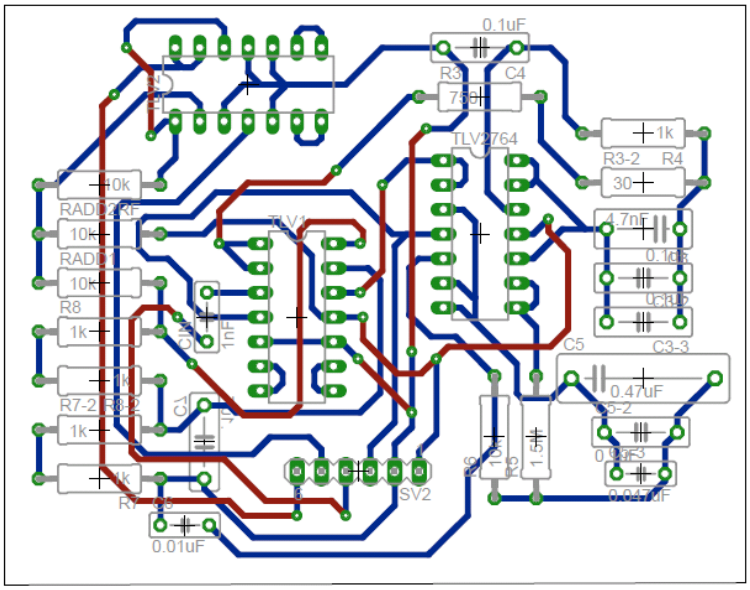

Figure 91: Layout for Frequency Weighting Band Limiting Circuit

Once the boards were assembled, we could test their functionality. First we tested the signal coming out of the first low pass filter. Using a 10Hz sinusoidal input, we found a gain of unity. This is shown below in Figure 92. This low pass filter has a cutoff frequency at about 1200Hz.

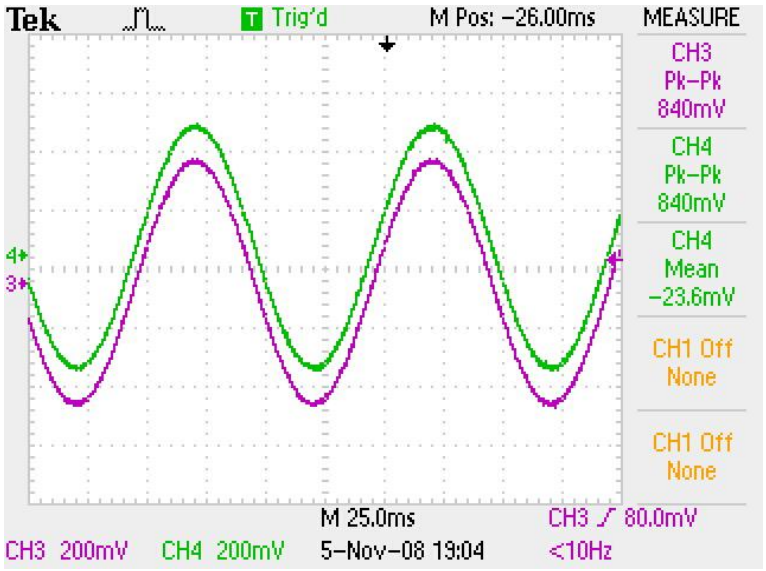

Figure 92: Input and output signals for the first stage lowpass filter (designed for 1200 Hz cutoff). The test input is a 10hz sinusoid. The output signal is unattenuated and shows very small phase delay, as expected.

In order to test the second low pass filter, which has a much more crucial effect on our signal, we input sinusoids of varying frequencies until we found the cutoff frequency. We found this to be

14.2Hz, which is lower than the expected 15.9Hz due to component tolerance error. The input and output waveforms at this frequency are shown below in Figure 93.

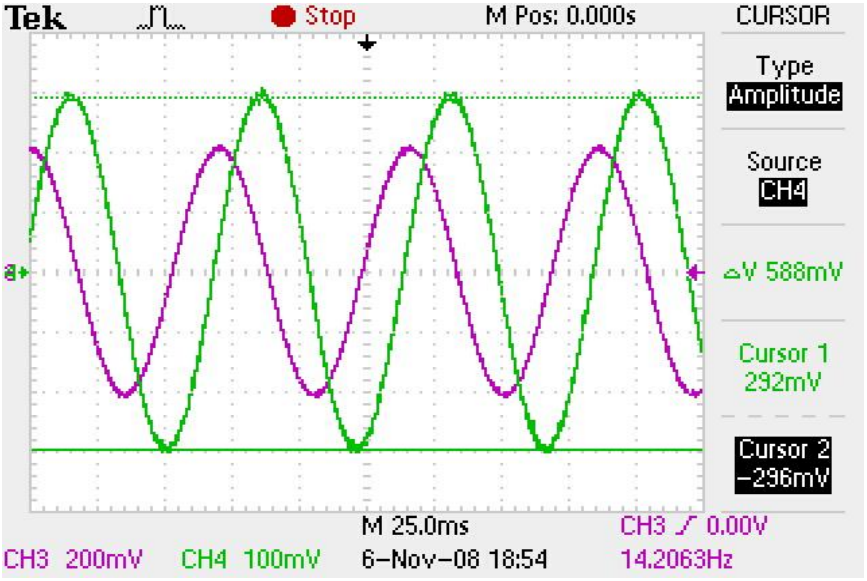

Figure 93: Input and output waveforms for the second stage lowpass filter (designed for 15.9Hz cutoff). The test input is a 14.2 Hz sinusoid. The output signal is attenuated by the Q factor at 14.2Hz, identifying this frequency as the cutoff for this filter.

Finally, we tested the Single Zero circuit. At 10Hz, we expect a gain of 2 from the input to output. The measured gain, however, is 1.44V/0.832V=1.73. This is lower than expected because the cutoff frequency of the second low pass filter is also lower than expected, resulting in attenuation at 10Hz. The input and output waveforms at 10Hz are shown below in Figure 94.

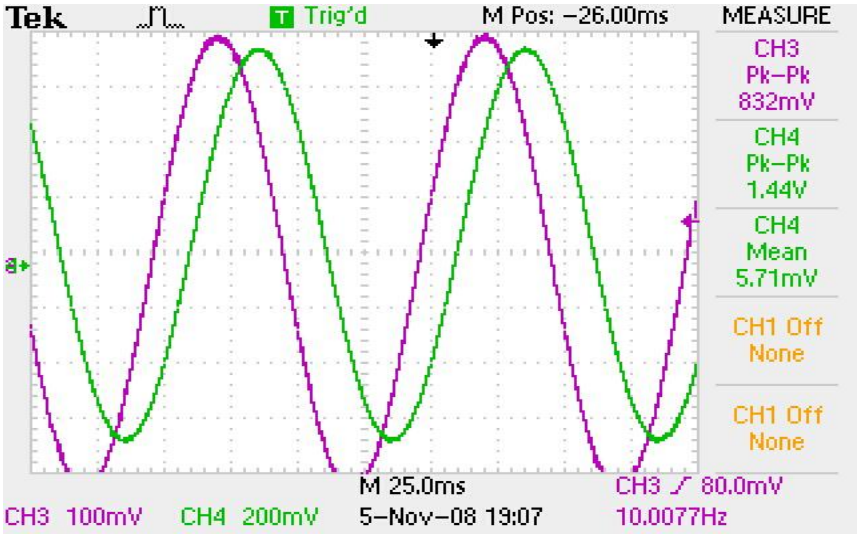

Figure 94: Input and output waveforms for the single zero filter. The input test signal is a sinusoid at 10 Hz. We notice a gain at the output that is 1.73, which is close to our design value of 2.

We also tested the Single Zero circuit at 20 Hz, where we measured a gain of 1.04V. The input output waveforms at this frequency are shown below in Figure 95.

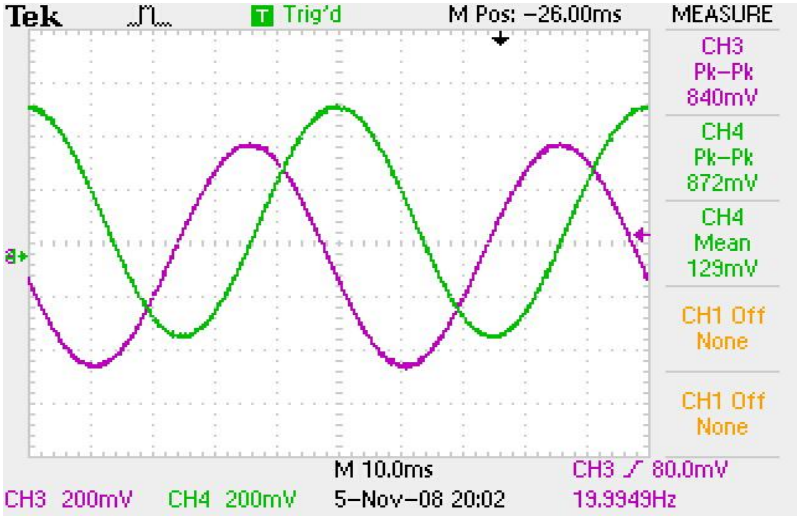

Figure 95: Input and output waveforms for the single zero filter with an input sinusoidal test signal at 20 Hz. We notice a gain at the output of 1.04, showing the filter's decreasing gain as frequency increases.

Finally, we tested the summing circuit at the output to verify that the signal sent to the analog to digital converter would be centered at 1.5v. As expected, our output signal uses the full range from 0v-3.3v and is ready to be sent to the microcontroller. This output is shown below in Figure 96. A 10Hz sinusoidal input was used.

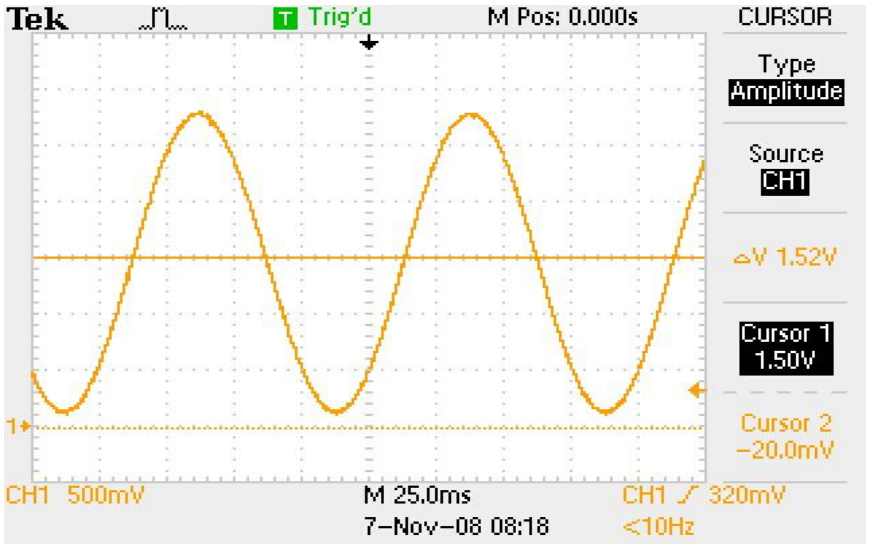

Figure 96: Output of frequency weighting band limiting circuit (with DC summing). This is the output of the entire signal conditioning circuitry for the vibration signal. The input test signal was a sinusoid at 10 Hz which was centered at 0v. The output is cen

5.2 Goniometric Sensor Implementation

When the original implementation of the strain gauges as goniometric sensors failed because of material difficulties, we defaulted to our secondary plan of the implantation of potentiometers as goniometric sensing devices. We are not the first to use potentiometers as indicators of goniometric position [102]. In order to achieve a voltage output proportional to the angle of the potentiometer, we needed to find the resistance of the potentiometer for a range of angles. Because we need to measure wrist angle in two axes, we used two potentiometers and collected data for each. These are shown below in Figures 97 and 98.

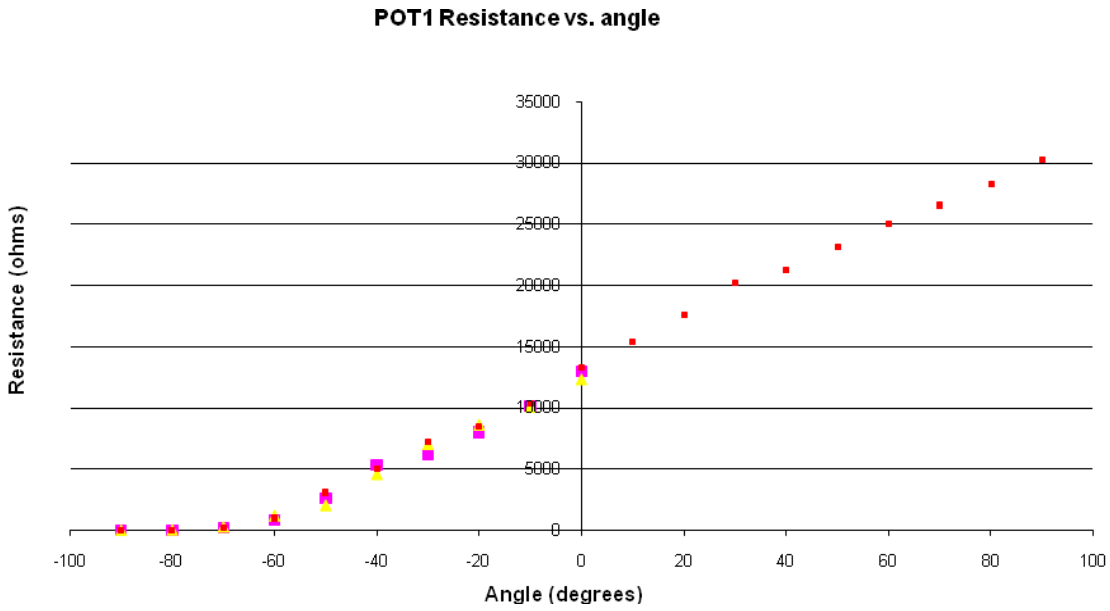

Figure 97: Potentiometer 1 Resistance vs. Angle. Below -60^{o} we notice that there is a nonlinear relationship between angle and resistance. Beyond -60o, however, we see linear behavior. If we use this potentiometer in its linear region, resistance will be propo

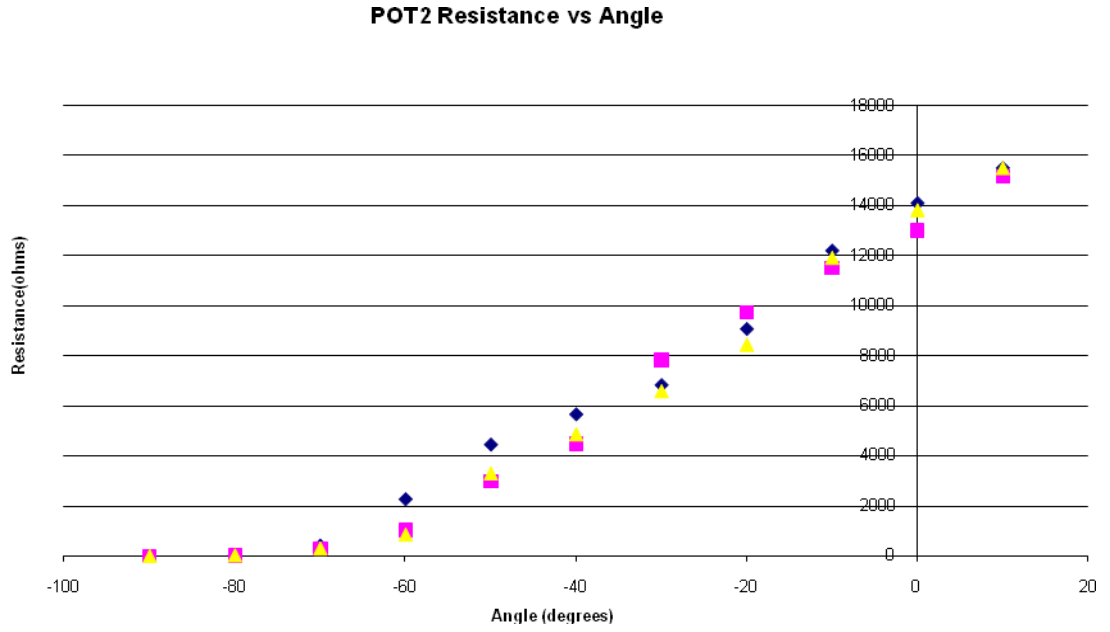

Figure 98: Potentiometer 2 Resistance vs. Angle. As with potentiometer 1, we took measurements to find the linear region of operation in order to be able to extract angle data.

The potentiometers were adjusted to the smallest resistance, which we decided would be mounted to represent -90^{o} of vertical wrist extension/flexion measurement. The second potentiometer,

which measures horizontal wrist angle, will not measure from -90^{o} to +90^{o}. Therefore less data was needed for the second potentiometer since it will be used in a smaller range of angles. Several trials of data were taken in an effort to average out the data and reduce error.

We can see from the data in Figures 1 and 2 that the potentiometers show linear behavior starting at about -60^{o}. By offsetting the potentiometers, we can use them in their linear range to get resistance proportional to angle. Omitting data before -60^{o}, we were able to find regression lines for the average of each set of data. These are shown below in Figures 99 and 100.

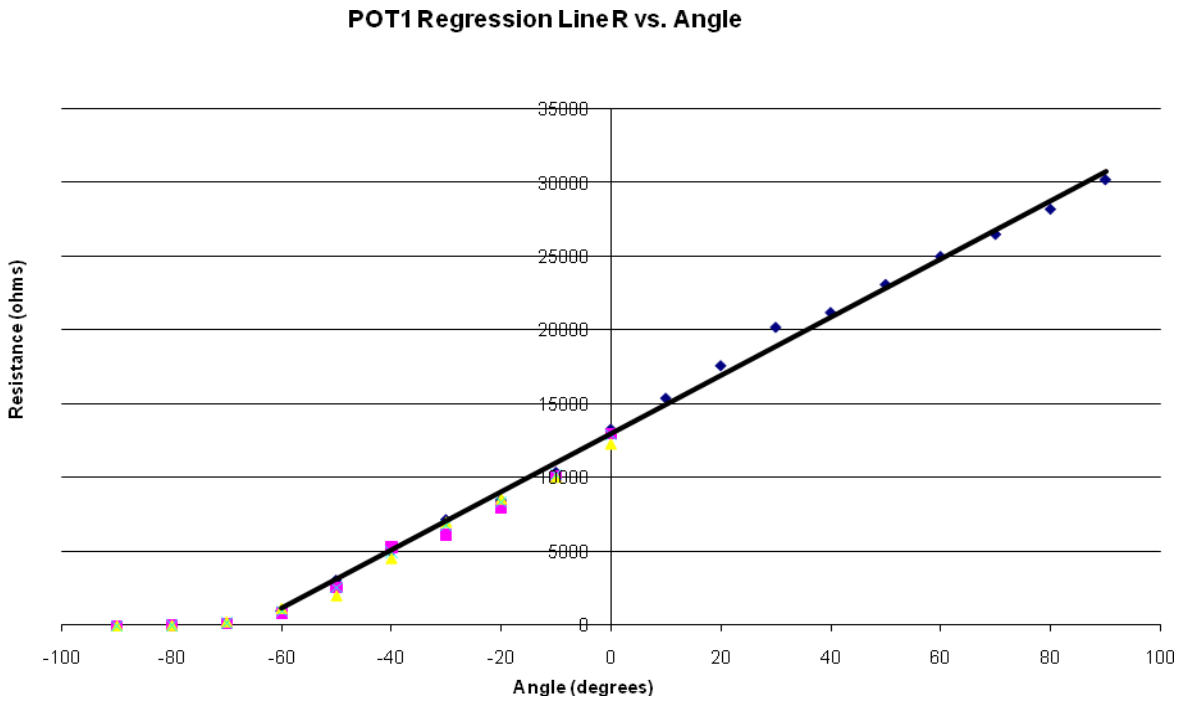

Figure 99: Potentiometer resistance vs. angle plot (for multiple trials of data) with regression line. Because we have a linear relationship between resistance and angle, we will be able to relate angle to voltage using a linear amplifier. The equation for this

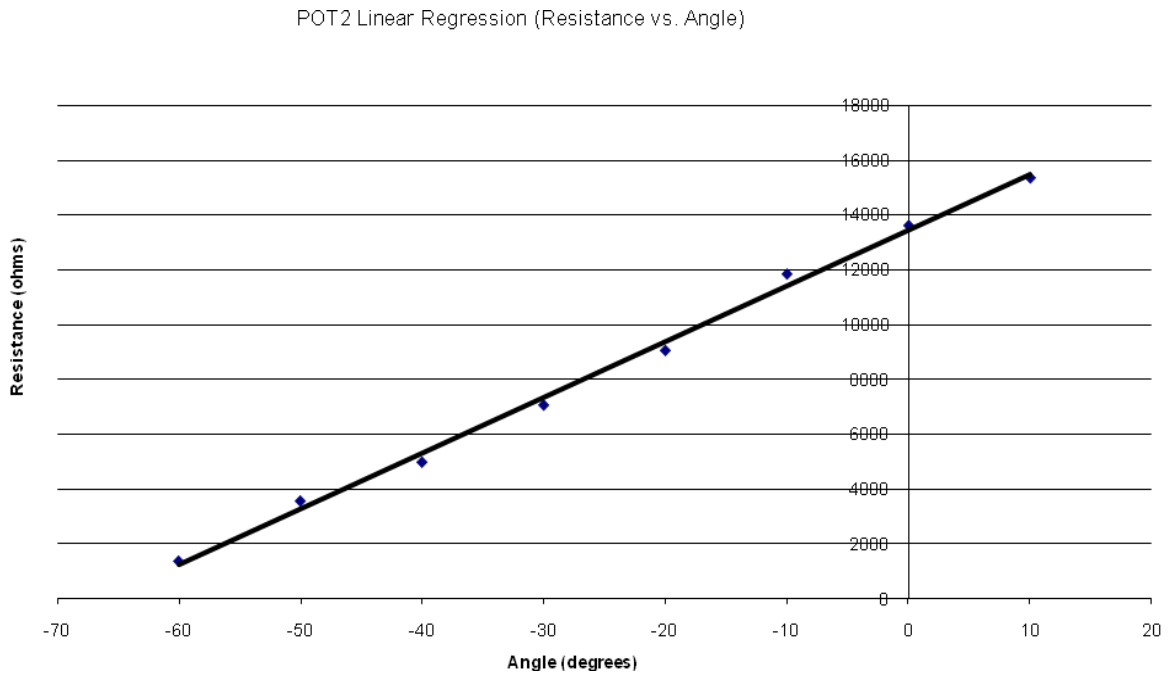

Figure 100: Potentiometer 2 Regression vs. Angle. In order to account for any differences in the potentiometers, we found the regression line for potentiometer 2 just as we did for potentiometer 1.

The equation for the regression line of the first potentiometer is:

$$y = 197.18x + 13032$$

Using this equation, we were able to relate the resistance of the potentiometer, R_{POT}, to the angle of the potentiometer. Using -60^o of potentiometer angle as our new starting point to represent -90^o of wrist angle, we were able to derive an equation relating the resistance of the potentiometer to wrist angle, θ_w.

$$R_{POT} = 197.18(\theta_w + 30^o) + 13032$$

By plugging this equation into the above equation for Vout of the angle sensing circuit, we get:

$$V_{OUT} = \frac{1.5}{R_1}\left(R_2 + 197.18(\theta_w + 30^o) + 13032\right)$$

which relates the output of the circuit to the angle of the wrist. We then set Vout to 3.0v θ_w to $+90^o$ to represent the most extreme positive wrist angle, and we found an equation relating R_1 and R_2. Choosing a convenient value for R_2, we arrived at R_1=1kΩ and R_2=22kΩ. This gives us a range of 0.15V to 2.57V of the output corresponding to the range of -90^o to $+90^o$ of wrist angle.

We implemented this circuit on a solderless breadboard and took output measurements for different potentiometer angles. A graph showing the line representing the expected output vs the collected data points is shown below in Figure 101.

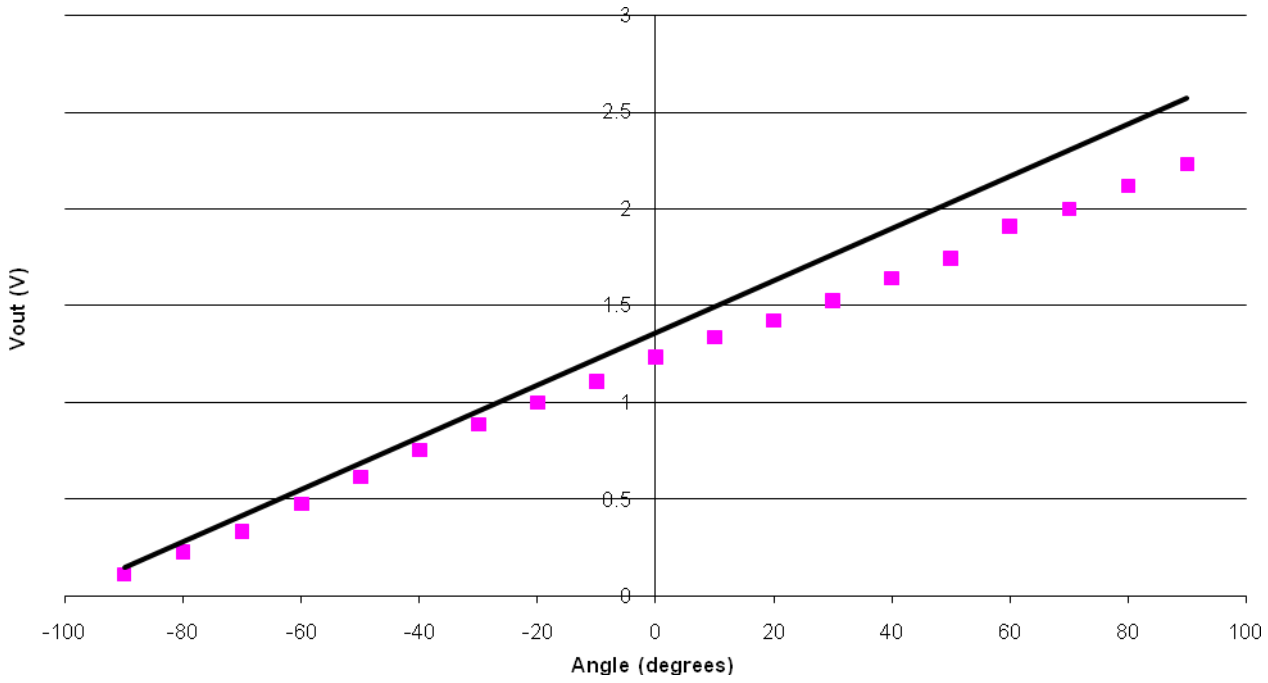

Figure 101: Expected and Measured Output vs. Angle (Potentiometer 1). The line comes from equation 4 which relates voltage output of the amplifier to expected angle measurement. Here we can see that the data closely follows the expected behavior.

We observe that the data follows the expected output very well for negative angles, but appears to deviate more for positive angles. This is most likely due to error in angle measurement with a protractor, which is compounded with each successive angle measurement. Our previous data, as well as the linearity of the amplifier transfer function, has convinced us that the output is linear with respect to wrist angle and it will follow this characteristic.

The same linear regression approach was applied to the second potentiometer. The same amplifier circuit was used, and the output of this with respect to horizontal wrist angle is shown below in Figure 102.

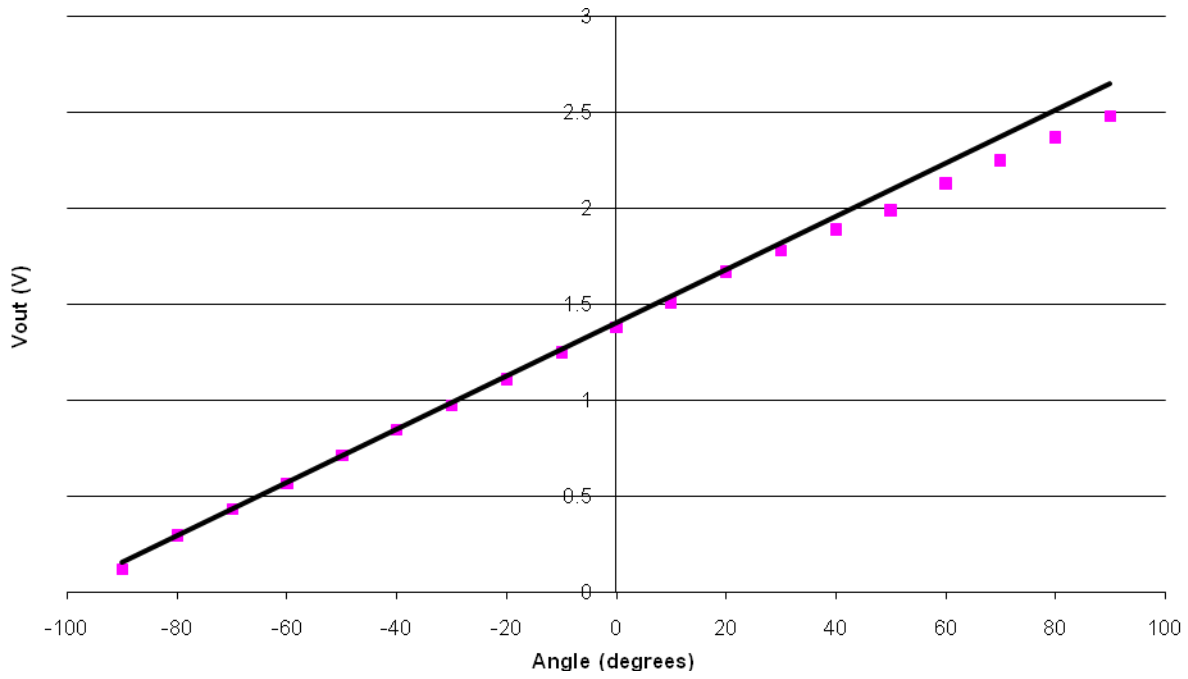

Figure 102: Expected and Measured Output vs. Angle (Potentiometer 2). We evaluated the sensing circuit for potentiometer 2 just as we did with potentiometer 1.

The testing of the goniometry board was straightforward. A laboratory power supply provided +3.3V and the -1.5V reference. Using a, oscilloscope, a DMM and a protractor, we verified that the circuit functioned like the original one that we built on a breadboard. We attached a cardboard cutout to each potentiometer to mark the 0^o point, and used a coffee stirrer to indicate the wiper bolt's angle. We then compared the output voltage measured on the DMM to our previous measurements. Figure 103 shows the testing setup. We used the breadboard to connect wires to the pins of each potentiometer. **Error! Reference source not found.** shows the coffee stirrer and cardboard ttachments that we used in conjunction with a protractor to set the angle.

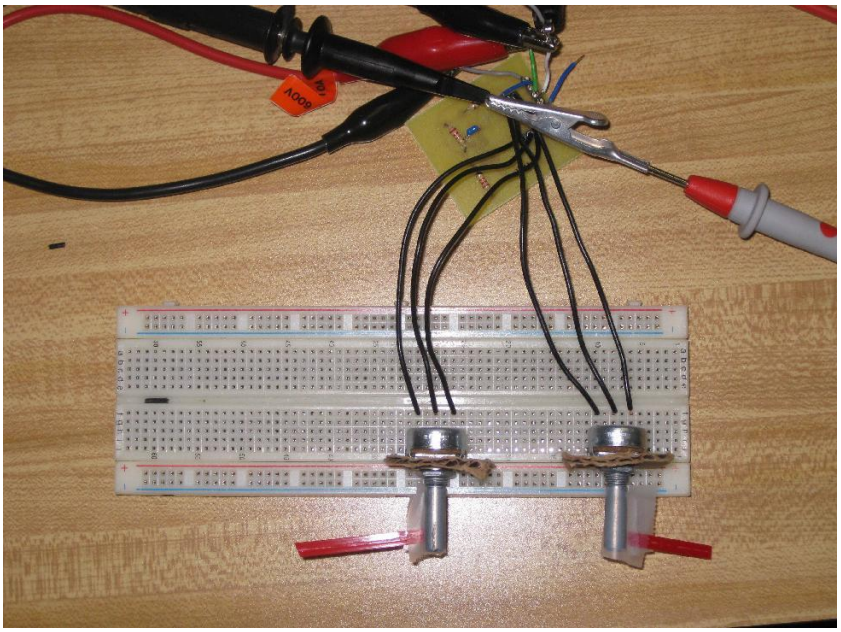

Figure 103: Goniometry Board Testing

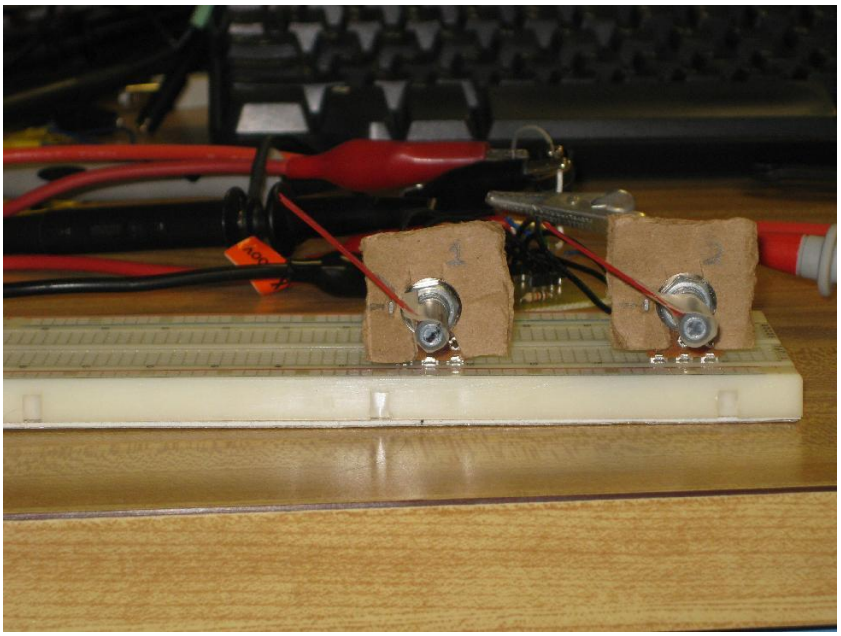

Figure 104: Goniometry Board Testing Angle Adjustment

5.3 Pressure Sensor Implementation

As was the case with the goniometry circuitry, testing the pressure sensor board proved straightforward. Being one of the two boards that we mounted on the glove itself, it was a critical part of our system for us to test. Therefore it was the first board that we tested when we returned to WPI. Figure 105 shows this board set up with six A201 sensors. The right side of the board in the image corresponds to the bottom of layout in Figure 49.

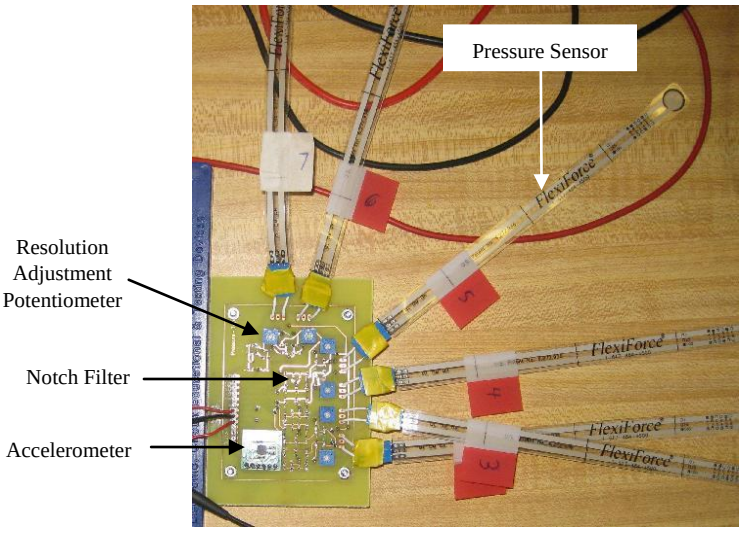

Figure 105: Pressure Sensor Board Testing

Note that the visible side of the board corresponds to the red layer in Figure 49. We soldered wires in the female berg connectors (connectors for flexible PCB, like the pressure sensor's material) that we ordered for the pressure sensors. We did not want to risk damaging the sensors by soldering them into the board or by cutting them and properly connecting the berg connectors. Also note the accelerometer breakout board in the bottom left of the pressure sensor board.

We powered the board using a two-channel power supply and checked the output of each of the six pressure sensor channels with an oscilloscope. Each output behaved similarly to the original bread-boarded prototype that we tested at the ERC. Since we were in the United States, the 50Hz notch filter would not reject AC power noise. It did not appear to have a significant effect on the signal at the bench where we tested the board though. Figure 106 through Figure 111 show the six outputs. Note how waveforms 1 through 6 in these figures are virtually identical, because the six circuits are identical. We pressed each sensor firmly against the lab bench and triggered the oscilloscope on the sensors' rising edges to create these waveforms. Note their similarity to Figure 46, which shows the output of the original bread-boarded prototype. Multiple kHz noise was still slightly noticeable on the signals, despite the RC low pass filter. We decided that this noise was tolerable for our prototype though.

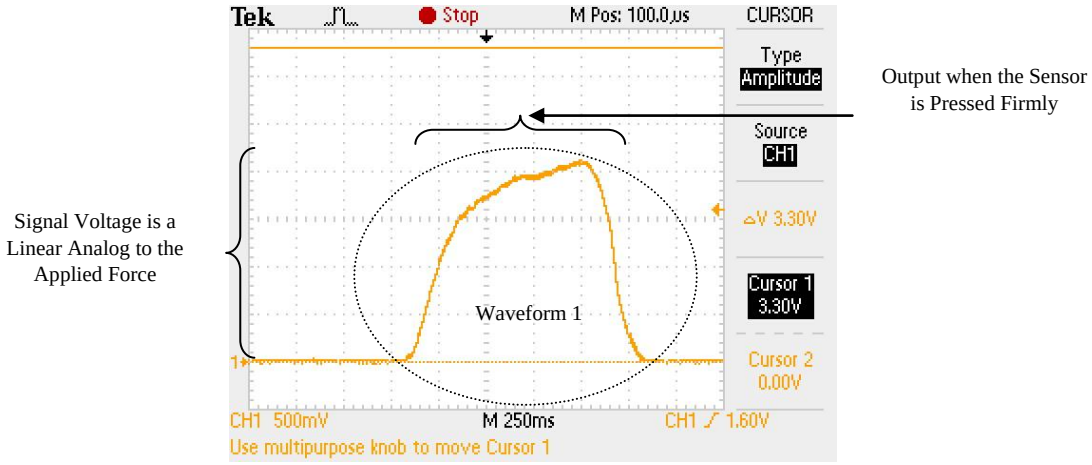

Figure 106: Pressure Sensor PCB Channel 1 (Sensor #2) Output – One of Six Identical Circuits

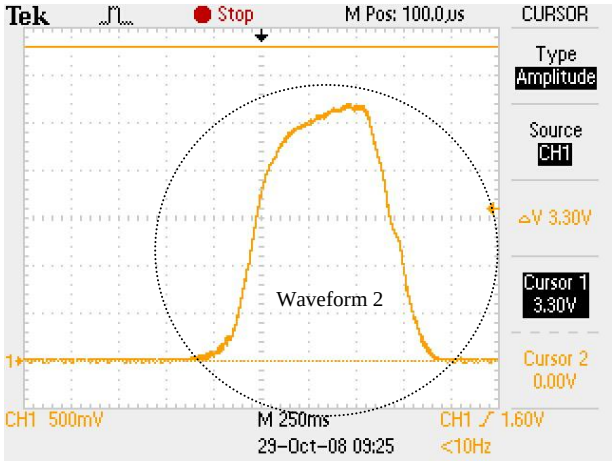

Figure 107: Pressure Sensor PCB Channel 2 (Sensor #3) Output – One of Six Identical Circuits

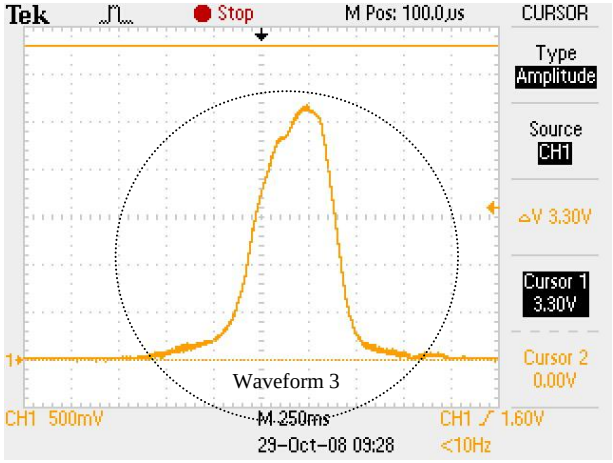

Figure 108: Pressure Sensor PCB Channel 3 (Sensor #4) Output – One of Six Identical Circuits

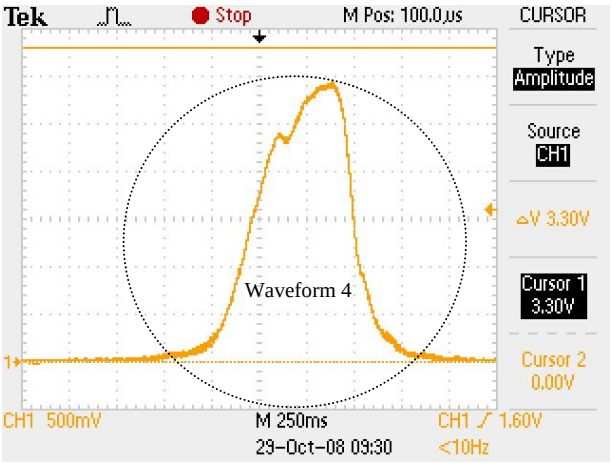

Figure 109: Pressure Sensor PCB Channel 4 (Sensor #5) Output – One of Six Identical Circuits

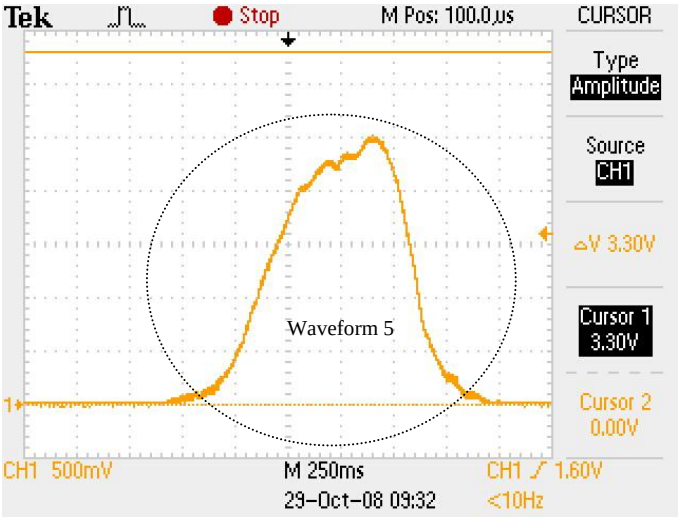

Figure 110: Pressure Sensor PCB Channel 5 (Sensor #6) Output – One of Six Identical Circuits

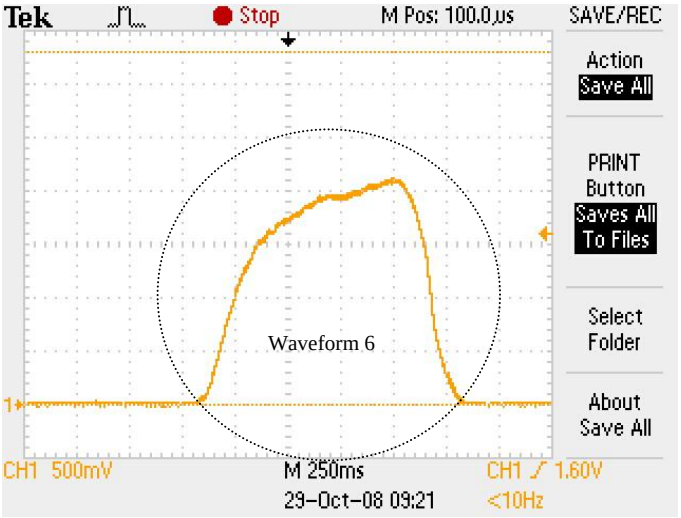

Figure 111: Pressure Sensor PCB Channel 6 (Sensor #7) Output – One of Six Identical Circuits

5.4 Power System Implementation

Testing the power circuitry was more challenging than the pressure sensor circuitry. We connected the assembled board to +3.7 from a lab power supply and discovered that only the +1.5V and +9V circuitry functioned. By comparing the schematic to the LP2950's datasheet, we determined that although he schematic was correct, we needed to switch the input and output pins of the package [101]. Since the middle pin was ground, this was a simple matter of reversing the package.

Having the +3.3V circuit working, we began debugging the -1.5V circuit. We first checked the timer circuit and noticed that there was no signal at its output. Although the layout shows vias and bottom layer connections before pins three and four of the LM555, these traces were entirely on the top layer of our board. Since the solder joints were on bottom of the board, we did not have the power pin or output pins connected. We fixed this problem by soldering the chip on the top layer.

The 555 circuit was still not functioning correctly. Checking the schematic, we found that we had drawn the timer's resistor divider circuit incorrectly (Figure 75). This made the layout incorrect as well. The corrected schematic is in Figure 112.

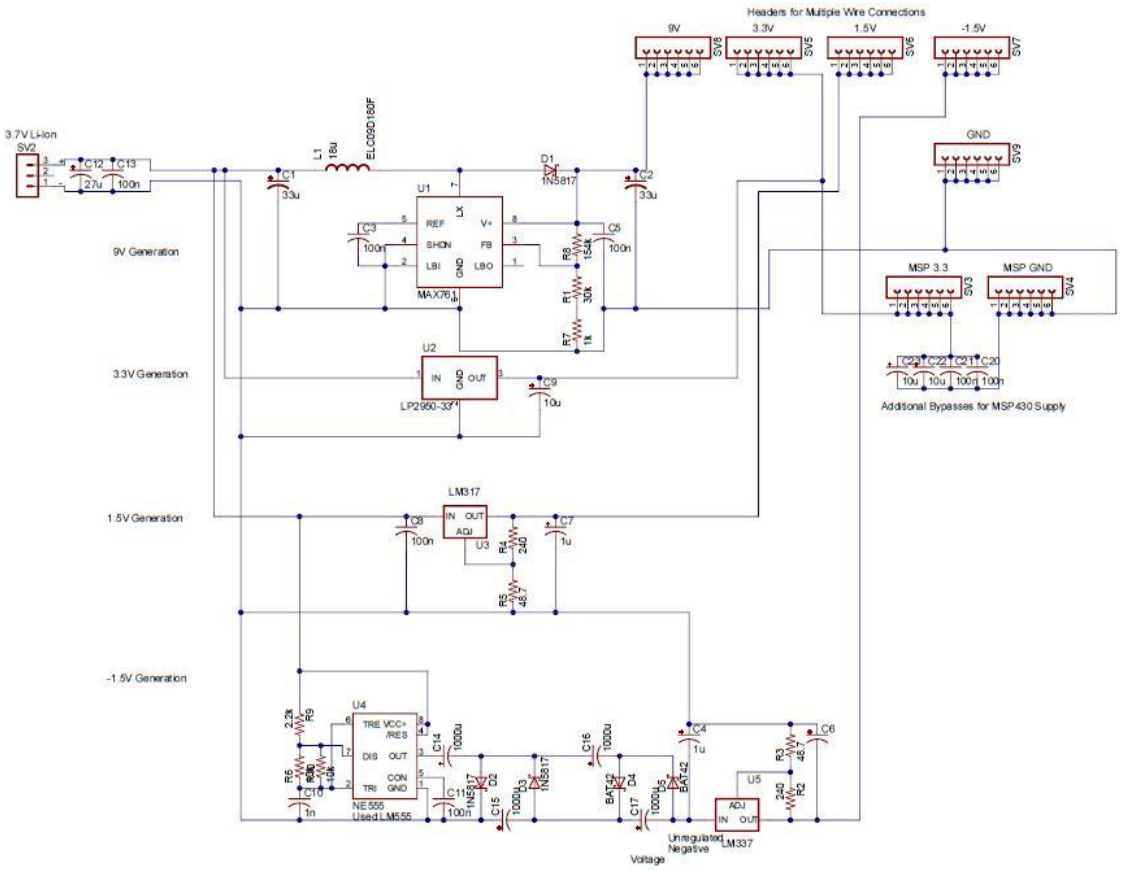

Figure 112: Corrected DC to DC Converter Circuit

The rework to fix this mistake is in Figure 113. The red X symbol indicates a place where we cut the trace, and the green lines indicate where we soldered wires.

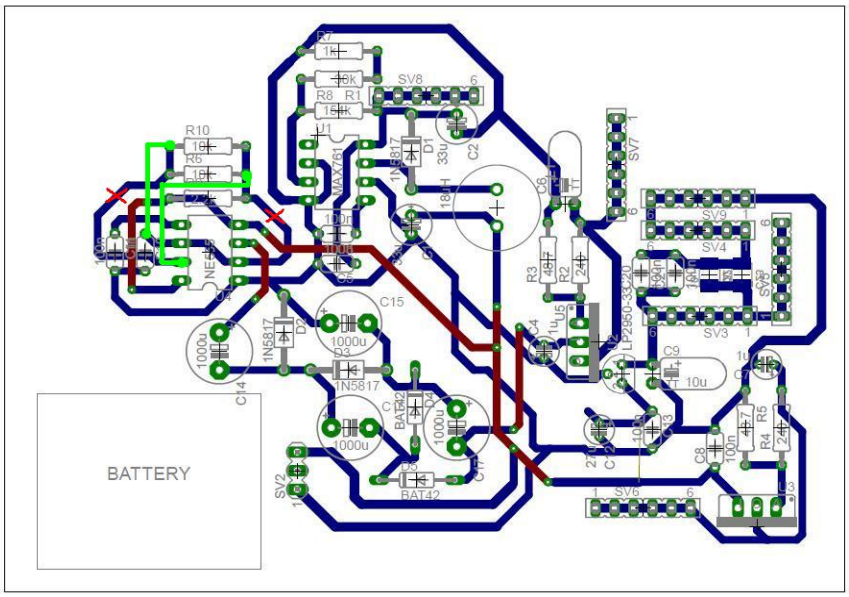

Figure 113: DC to DC Converter Circuit Rework

Once we made these corrections to the 555 circuit, the -1.5V circuit functioned correctly. Having all four of the DC to DC converter blocks functioning, we completed its debugging. A revised layout is in Figure 114. Figure 115 shows the assembled and reworked board.

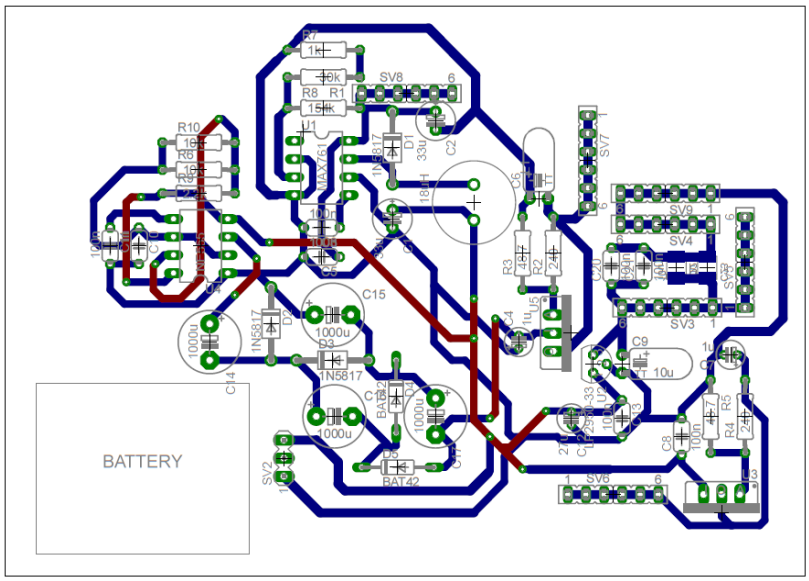

Figure 114: Revised DC to DC Converter Layout

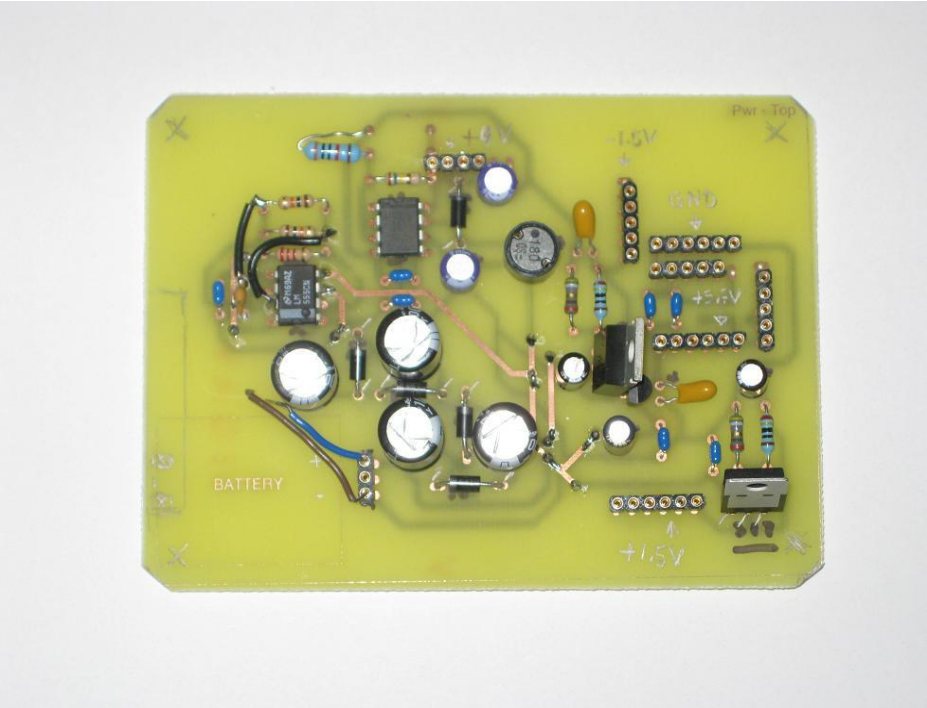

Figure 115: Power Board with Rework

5.5 Prototype Assembly

The "smart glove's" variety of subsystems made it impractical for us to attach all of the circuitry directly to a glove. We mounted all of the sensors, the pressure sensor signal conditioning board and the goniometry signal conditioning board on the glove. We connected the battery, power board, accelerometer filter board and the alert and microcontroller subsystems in the enclosure. The functioning, assembled prototype is in Figure 116. The glove connects via bundled wires to the enclosure, which an adjustable Velcro strap holds to the arm.

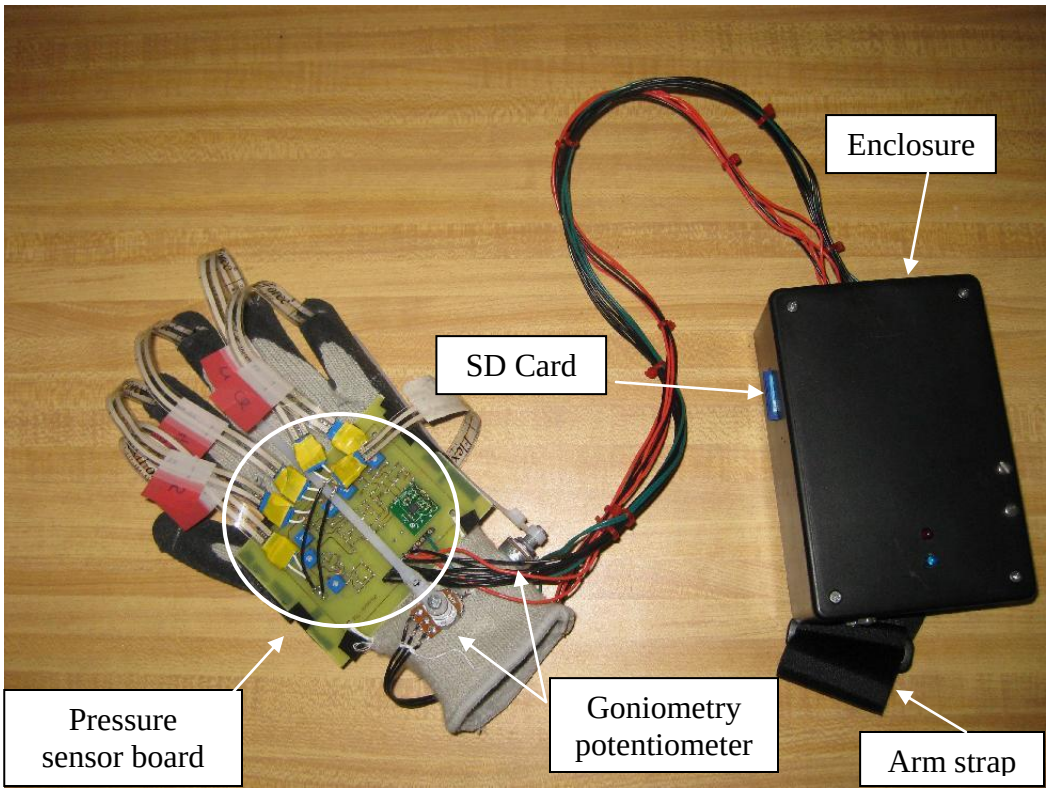

Figure 116: Complete "smart glove" prototype showing glove, sensors, and enclosure.

5.5.1 Glove Assembly

As Figure 117 shows, we attached pressure sensor board on the back of the hand behind the knuckles, and the goniometry board on the bottom of the wrist. The way that we soldered the accelerometer onto the pressure sensor board, the +x, +y and +z directions correspond to downward, right and into the page respectively in Figure 119. Electrical tape covers the bottom of each board to protect their components from getting caught on the material and to prevent short circuits. We stitched the boards to the gloves through holes drilled in their corners.

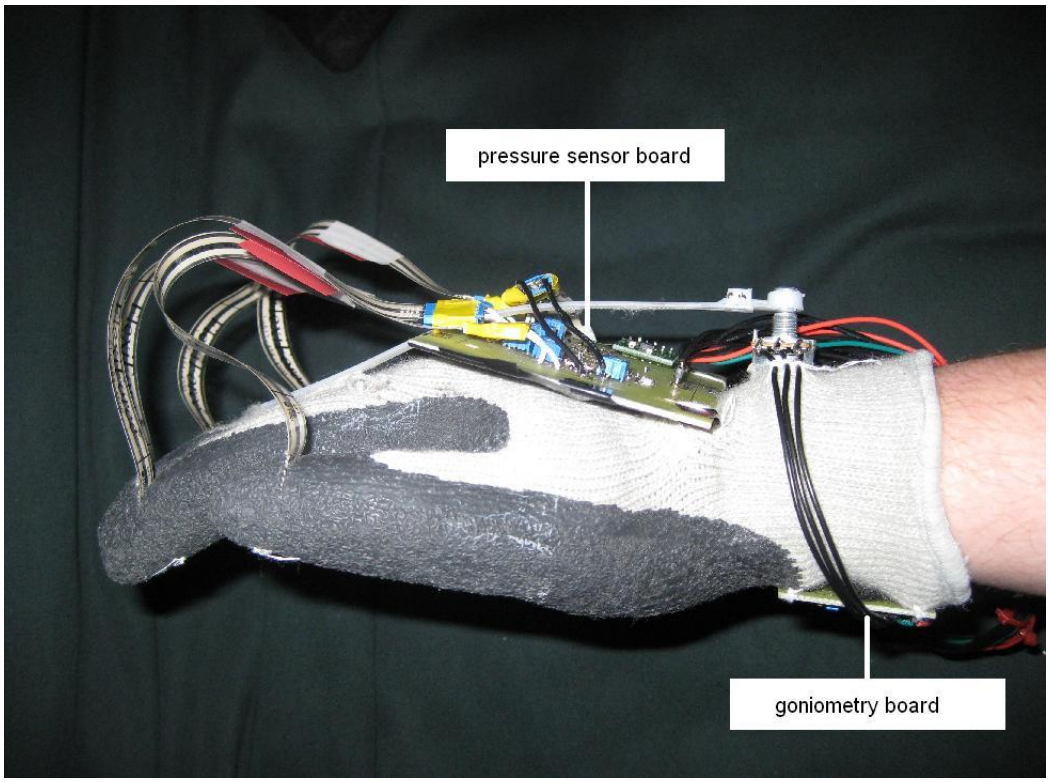

Figure 117: Pressure Sensor and Goniometry Boards Mounted on the Glove

We stitched the seven pressure sensors to their appropriate spots on inside of the glove to avoid the risks associated with an uneven surface of glue [53]. This involved inserting each sensor through a slit in the glove's material and stitching them to the glove, taking care to avoid the conductors and sensing area, as illustrated in Figure 118.

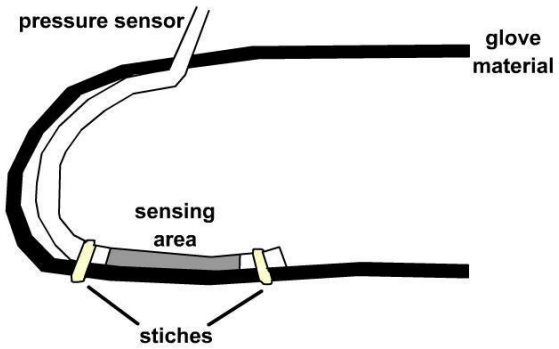

Figure 118: Pressure Sensor Fingertip Mounting Cut-Away

The labels remain on the sensors so that they can still be associated with the data sets from our initial testing. We also needed to lengthen the wires connecting the palm sensor's socket to the pressure sensor board.

A combination of stitching and glue holds the two potentiometers to the glove. Additionally, we soldered a wire loop to the potentiometer on the top of the wrist to reduce its tendency to move. We used 8-inch wire mounting ties to fix the potentiometers' wiper adjustment bolt to the glove. On the potentiometer side, loops in the ties fit snugly onto the bolts; on the glove side, we fastened the tie with glue.

The glove connects to the power, microcontroller and accelerometer boards via approximately 2' of bundled 22 AWG wire. We bound the supply, reference and ground lines together and the signal lines together with tie wraps. We soldered these wires into their sockets on the glove boards to prevent them from falling out, as some tended to do when we were testing the accelerometer. Figure 119 shows the assembled glove. We verified that the pressure sensor and goniometry circuits worked with their mounted sensors, once we assembled the glove. Figure 120 shows us testing the pressure sensors while powering the glove with the enclosure's power board. The incomplete enclosure is in the right of the image.

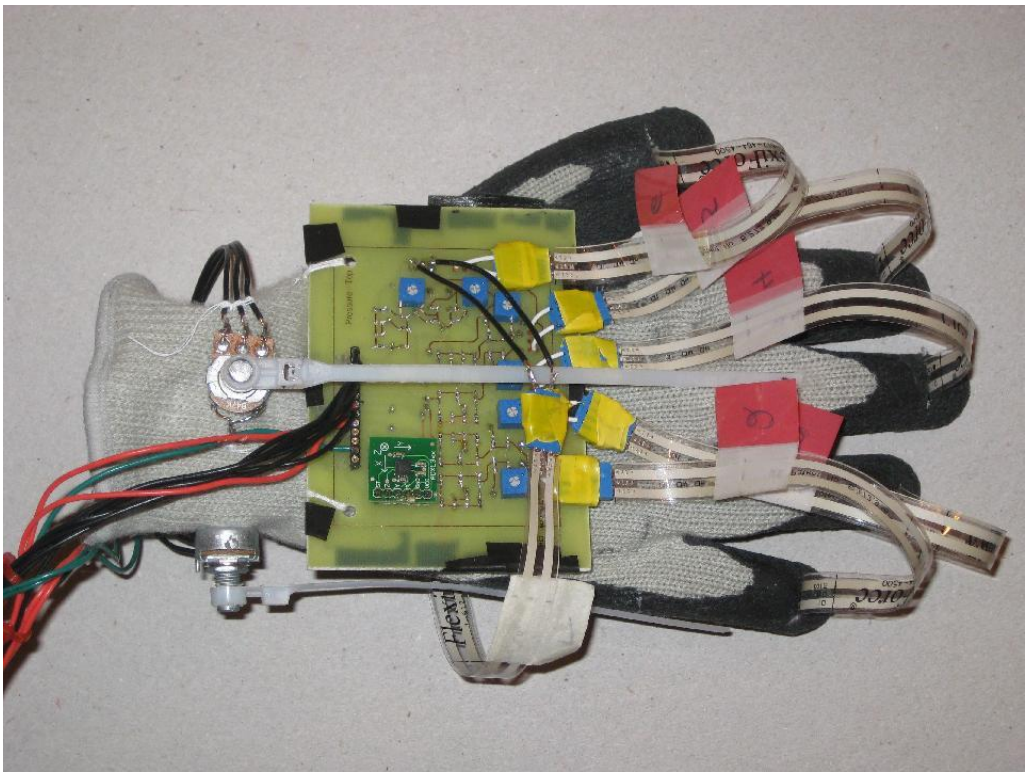

Figure 119: Glove Top View

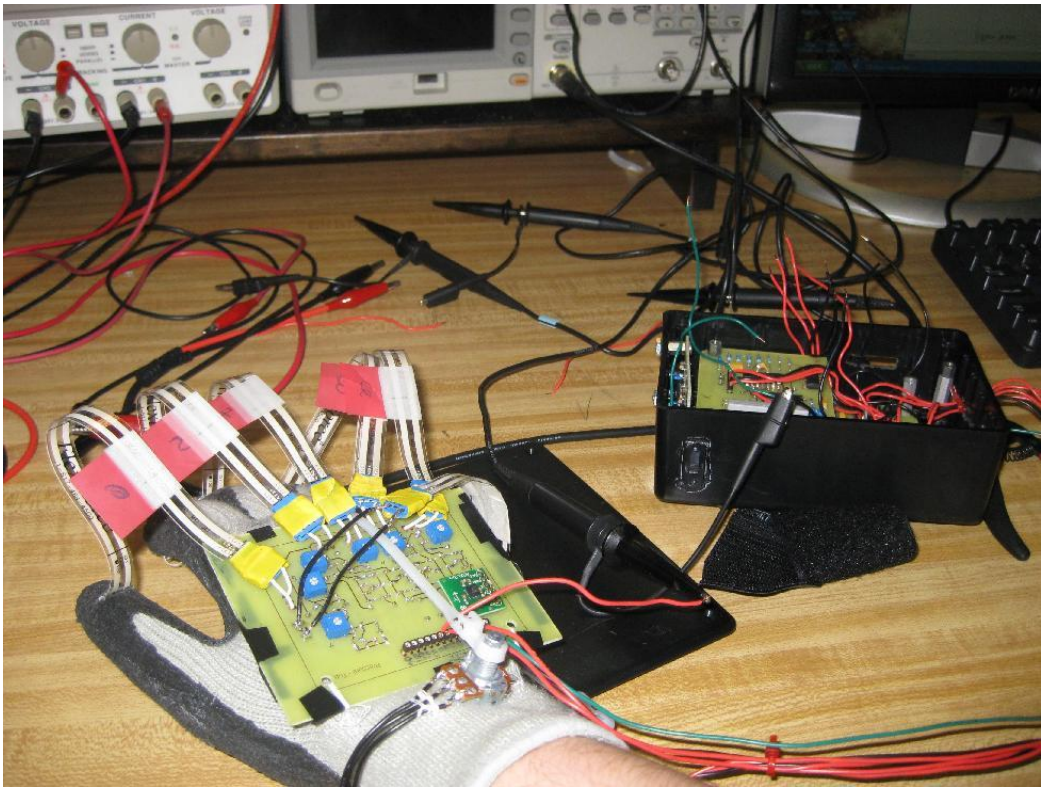

Figure 120: Glove Pressure Sensor Testing

5.5.2 Enclosure Assembly and Testing

The enclosure contains the power, microcontroller and alert subsystems as well as the filter for the accelerometer's z-axis. The boards are stacked with spacers as Figure 121 shows. The power board, on the lowest layer connects to the battery via nuts with springs soldered to the threads. We wired the battery's positive terminal to a single-pole, single-throw switch, which connects to the power board's battery input.

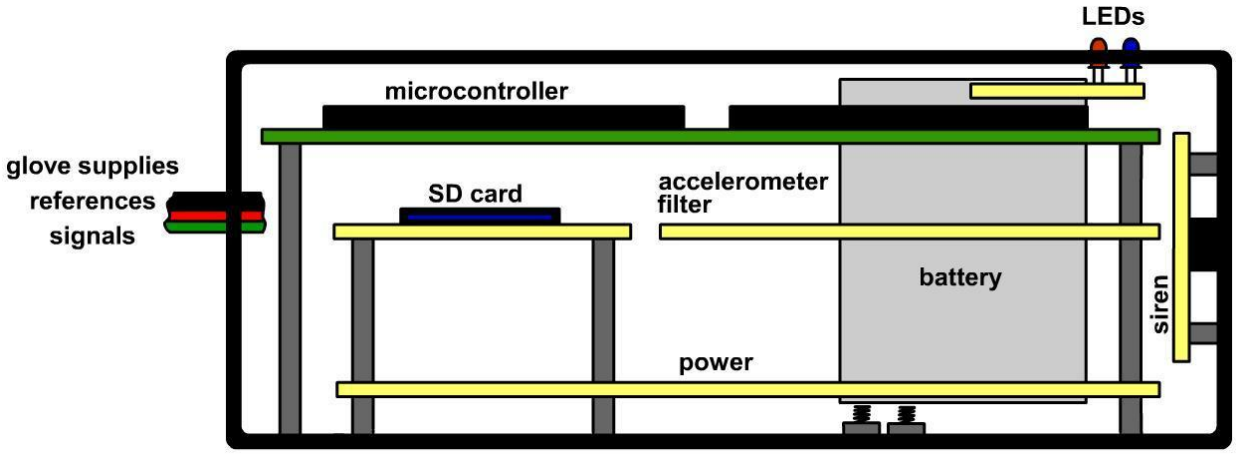

Figure 121: Enclosure Cut-Away

Figure 122 shows the power and siren boards in the enclosure as we began assembling it. In this image, the right of the enclosure corresponds to the right of the illustration in Figure 121. When we made rectangular openings in the enclosure, we first drilled several holes, then used files to cut out the remaining plastic. Excepting the data lines from the glove and the potentiometer connections, green wires denote data lines, black wires denote grounds and red wires denote supplies or references. The siren board was the first board that we fastened to the enclosure. We drilled a hole in the side of the enclosure directly above the buzzer to make it more audible. The spring-loaded battery connectors are at the top of the enclosure. The battery rests between the two standoffs that are against the enclosure's side. Later, we added another ¼" standoff next to the battery springs to support the other side of the battery. Note that inserting the battery in backwards will not harm any circuitry, since it

will not contact the springs. The top of the enclosure holds the battery against the springs with foam. We verified that all of the supplies on the power board worked with the NB-4L battery, then verified that the siren board functioned by connecting its control line to +3.3V.

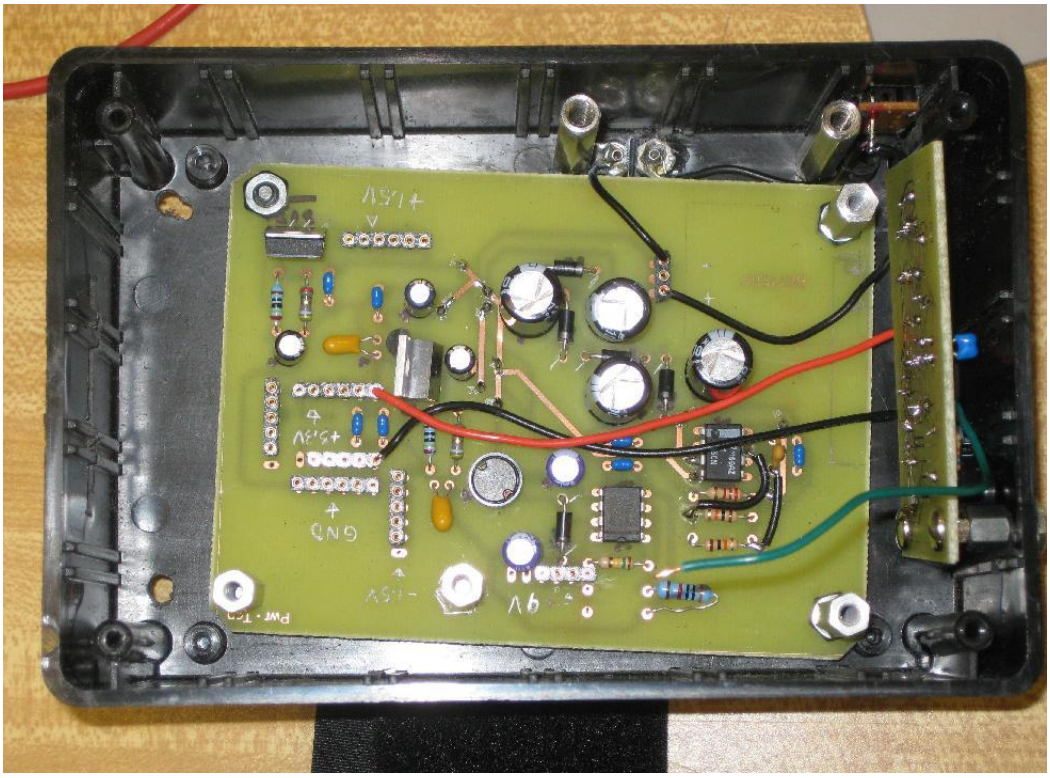

Figure 122: Enclosure - Power and Siren Boards

With the power and siren boards functioning in the enclosure, we added the accelerometer filter and made sure that it was functioning as it did before the power board supplied it. Figure 123 shows the enclosure with the accelerometer filter and the battery. Figure 124 shows the enclosure and glove while we verified that the filter behaved as it did previously. We connected the SD breakout board directly to the right of the filter board. We directly soldered it to pins on the microcontroller board, so we could not take a photo of it in the enclosure. This image also shows the goniometry board's location on the glove and roughly where we attached the pressure sensors (below the areas that the white thread encloses). Once we determined that the sensor, power and siren circuits were working, we assembled the new SD card breakout board and connected it to the microcontroller board.

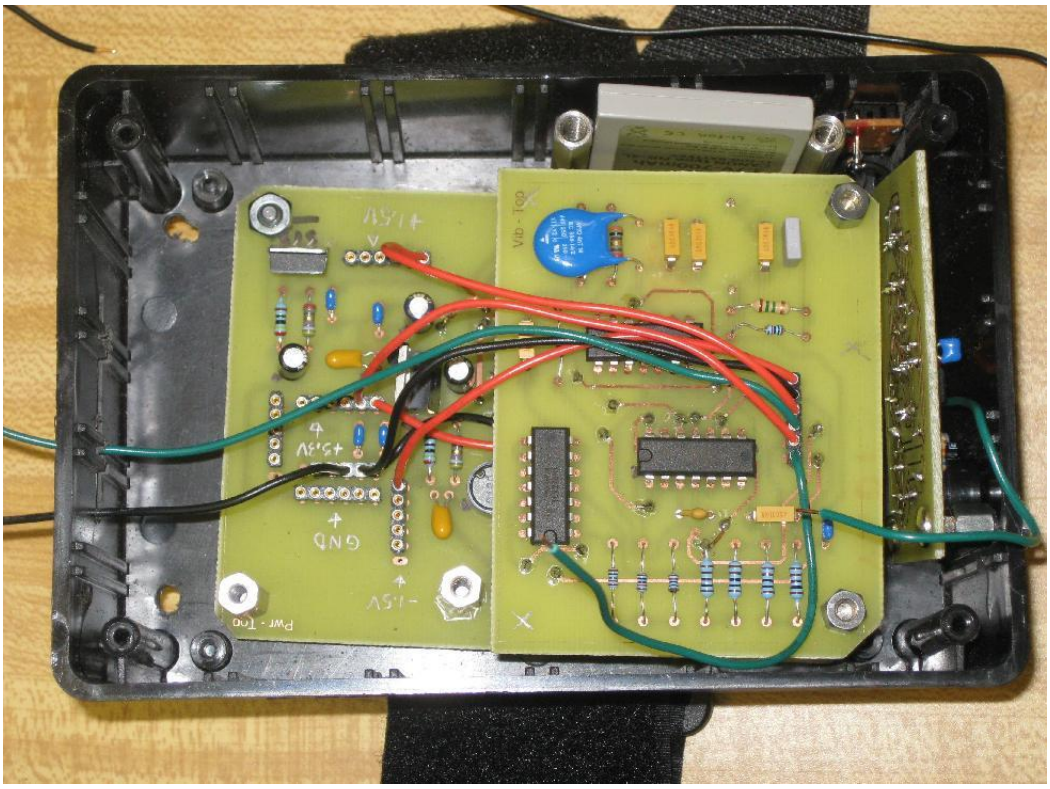

Figure 123: Enclosure - Accelerometer Filter and Battery

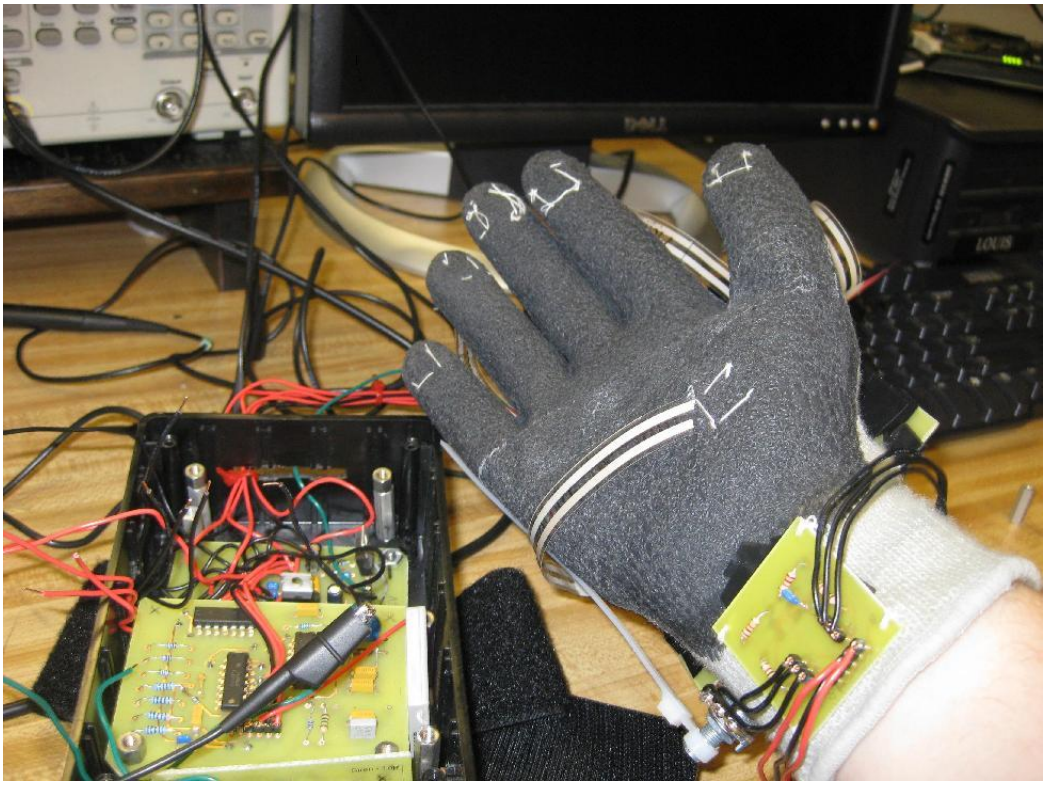

Figure 124: Enclosure - Accelerometer Filter Testing

We later determined that there were incorrect connections on the SD card board, so we had to disconnect it and the microcontroller board for rework. Once we fixed these errors and assembled the enclosure, the remaining hurdles we faced were software related. Figure 125 shows the microcontroller board in the enclosure. The easiest way to connect the SD card breakout board to the original socket was by soldering wires directly to its pins. We made all of the other connections within the enclosure by wiring the boards' sockets together. The LED board rests on the microcontroller board above the unused USB bridge chip. The holes on the top of the enclosure hold it in place. We covered the bottom of the LED board with electrical tape as we did to the pressure sensor and goniometry boards to prevents short circuits. Although we could have fastened the LED board to the top of the enclosure, we decided that it was easier to remove the battery or program the microcontroller this way.

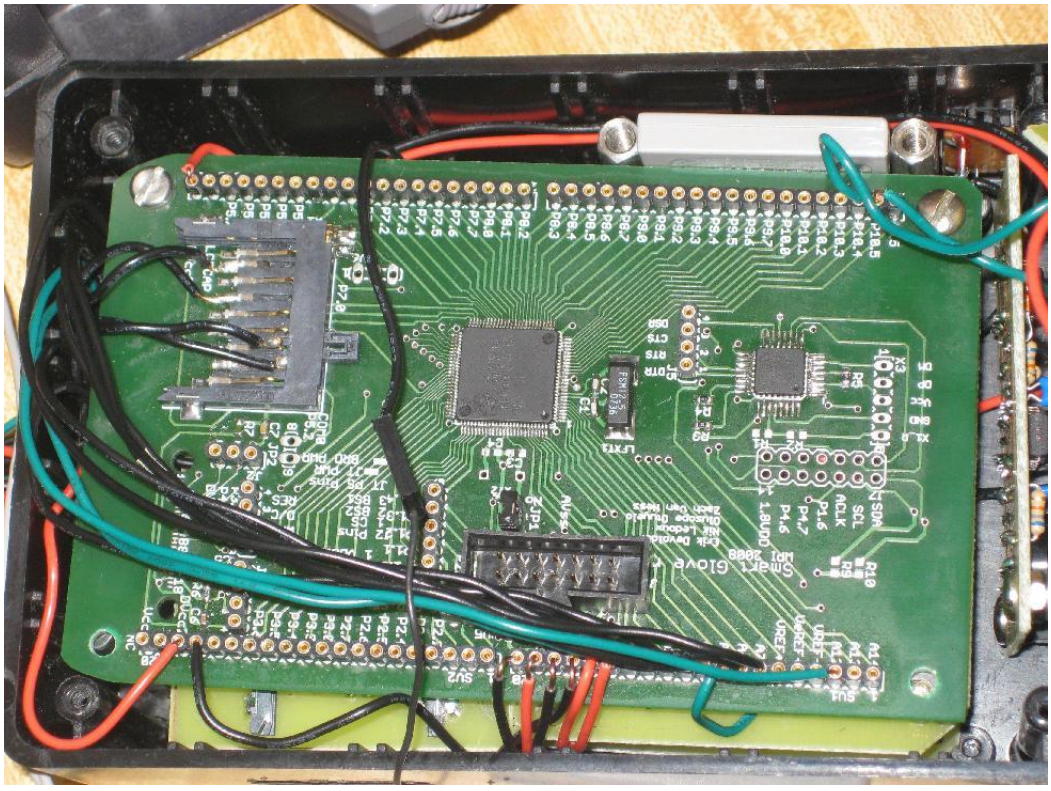

Figure 125: Enclosure - Microcontroller and SD Boards

5.6 Glove Functionality Testing

Once the glove was assembled, we tested each sensor, and verified measurement operation using an oscilloscope to look at the outputs.

5.6.1 Pressure Sensing

The outputs of the pressure sensing interface circuitry for each sensor mounted in the glove are shown below in **Error! Reference source not found.**126 through **Error! Reference source not und.**131. Note how waveforms 7 through 12, in these images are virtually identical because their six circuits are identical. It is clear that an increase in force translates into an increase in voltage for every single sensing pad. These waveforms show that the pressure sensing pads work when embedded into the fabric of the glove.

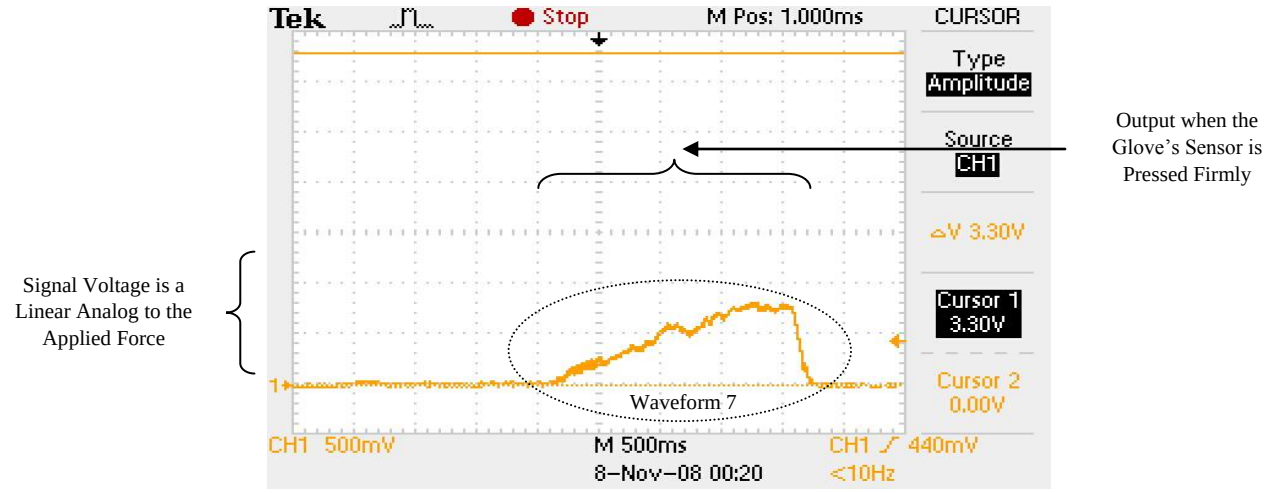

Figure 126: Sensor 2 - Little finger - One of six identical circuits

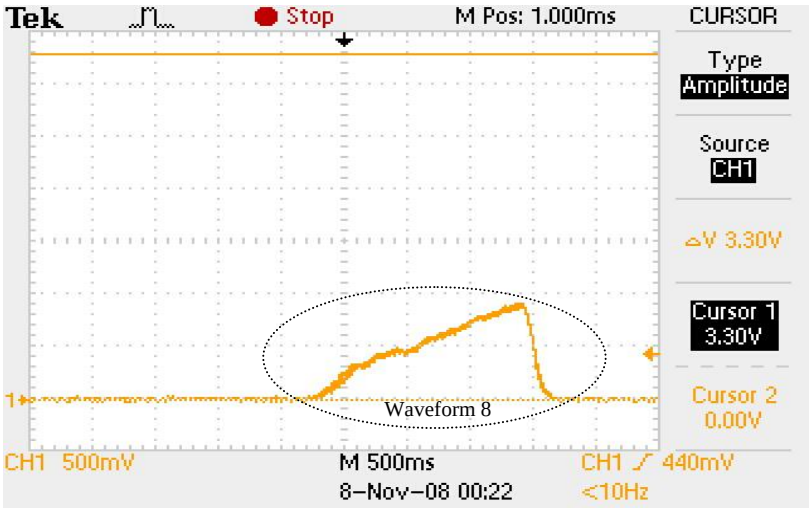

Figure 127: Sensor 3 - Ring finger - One of six identical circuits

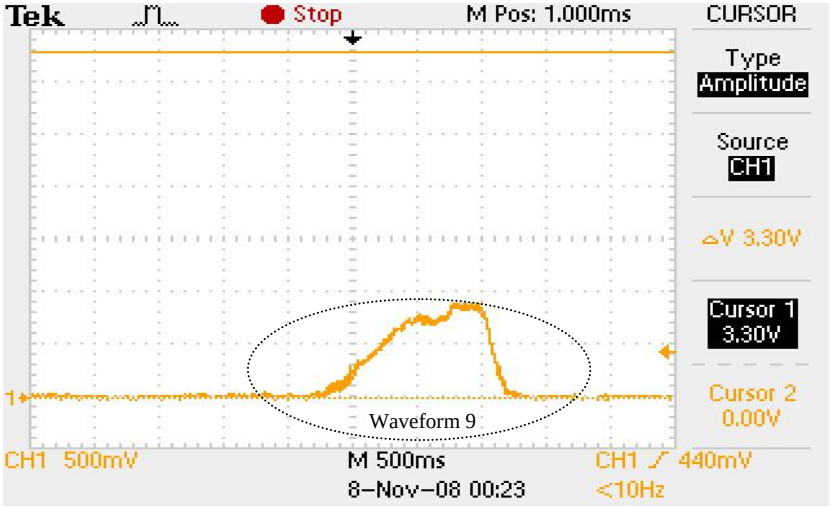

Figure 128: Sensor 4 - Middle finger - One of six identical circuits

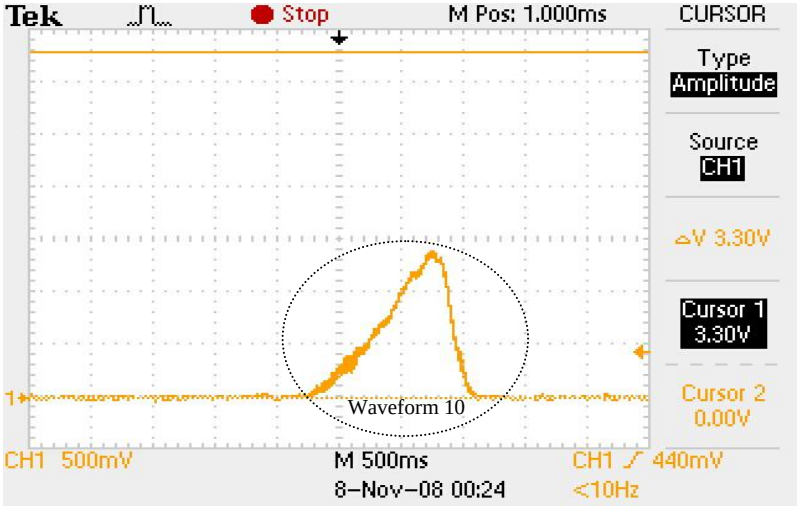

Figure 129: Sensor 5 - Index finger - One of six identical circuits

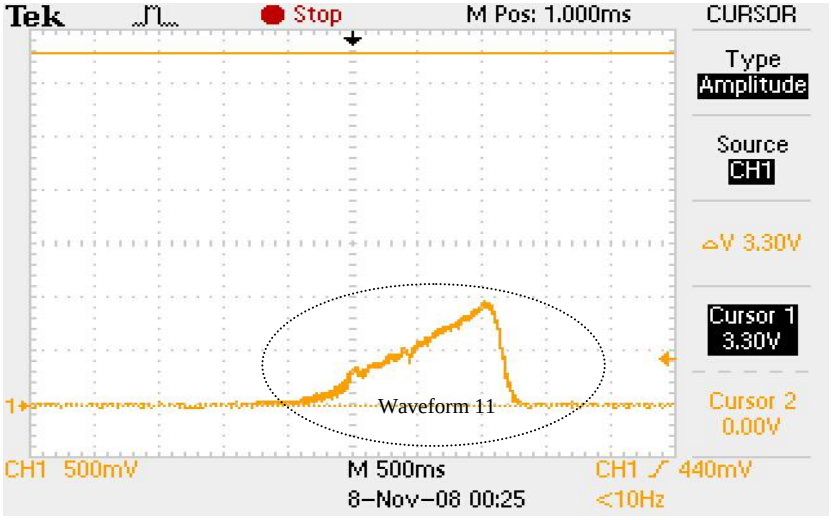

Figure 130: Sensor 5 - Thumb - One of six identical circuits

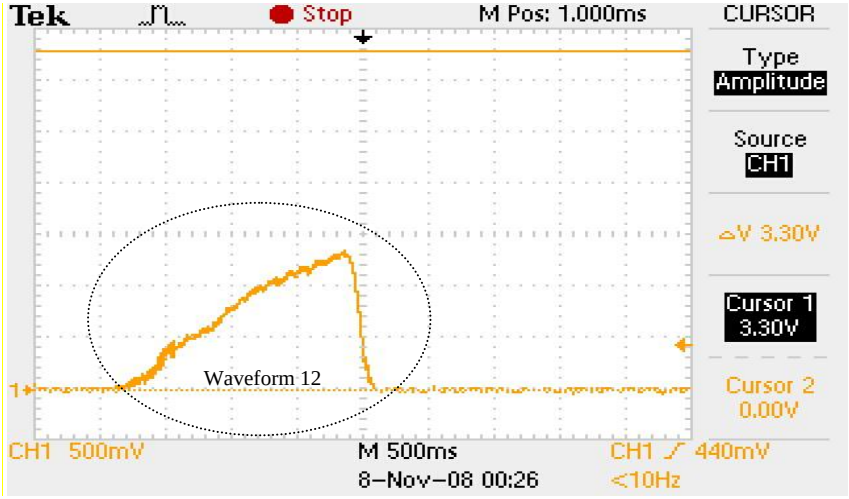

Figure 131: Sensor 5 - Palm - One of six identical circuits

When configured on the glove, it proved more difficult to get outputs at high range of the circuit's output. The rubber coating on the work glove that we used may have dampened the force that each sensor experienced. Also, given the locations of the sensing areas on the finger tips, it was not as easy to press them as firmly as when the sensors were not mounted. We needed to take care to press the sensing area and not its border; otherwise, the output would be much lower and noisier.

5.6.2 Angle Sensing

We tested the angle sensors mounted on the side and top of the glove by flexing and extending the wrist and viewing the resulting output signals. These are shown below in Figure 132 and Figure 133.

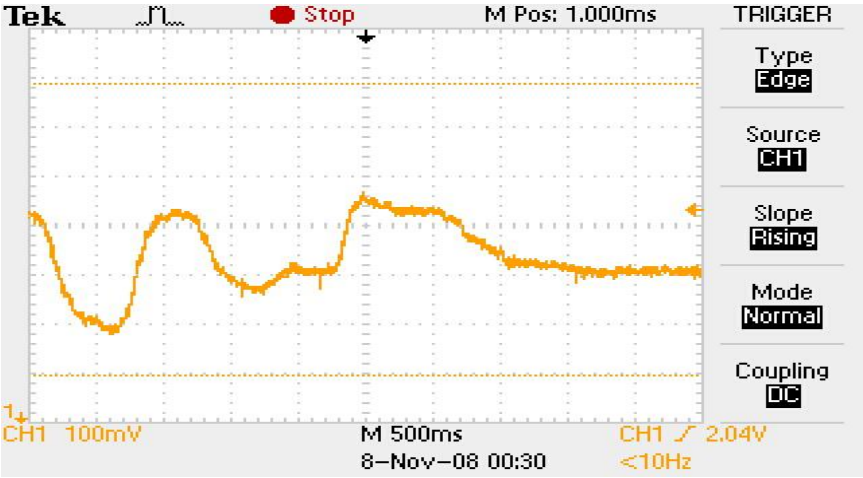

Figure 132: Side angle sensor output

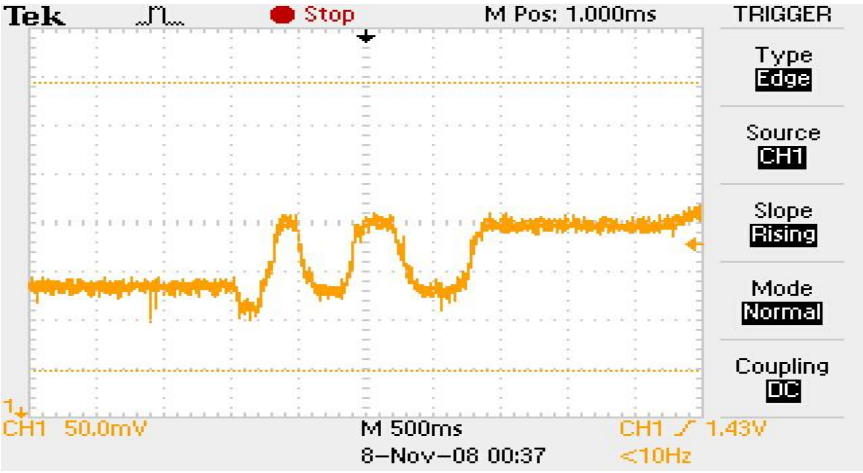

Figure 133: Top angle sensor output

As we can see from the above figures, we do get an amplified output from the angle sensors proportional to wrist angle. Unfortunately, we do not get the full range of outputs we expect. This is due to the mounting of the potentiometers on the wrist. The base orientation of the potentiometer moves too much with the wrist, changing the axis of wrist measurement, resulting in a measurement which is smaller than expected.

5.6.3 Vibration Sensing

We tested the vibration sensor by moving the hand wearing the glove and measuring the output on the oscilloscope. This is shown below in Figure 134.

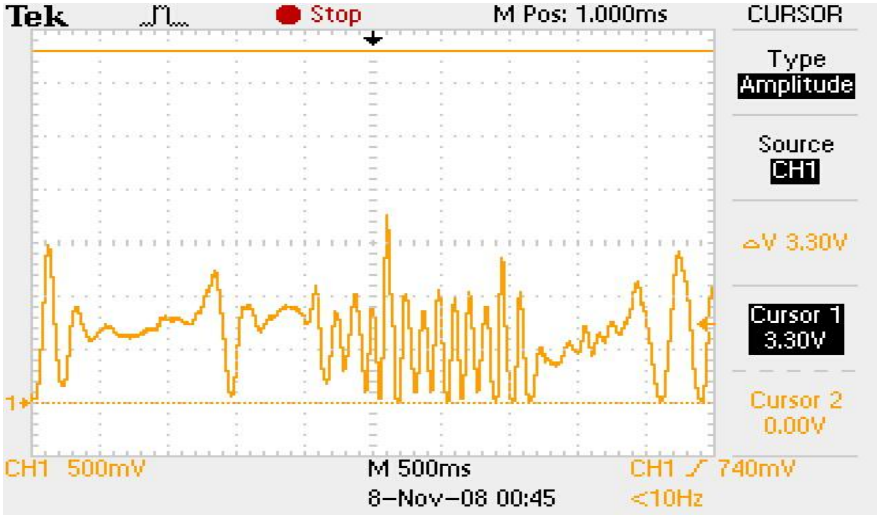

Figure 134: Vibration sensing output

We observed a curious effect at the output of our analog filter with the accelerometer used as the input. The DC level of the output is dependent on the orientation of the accelerometer with respect to gravity. This was a very unexpected result since we used a coupling capacitor at the input of the analog filter stage to remove any DC inputs. Indeed, placing a scope probe on the signal just after it passes through the capacitor shows no DC voltage component.

The consequence of this problem is that large magnitude acceleration peaks will cause clipping at the output when the hand is oriented parallel to the ground. If the accelerometer is flipped upside down, the output is centered at 1.8V, and will operate as desired, measuring the full range of acceleration as expected.

5.7 Microcontroller Implementation

The Breakout board, made in Eagle, is shown in Appendix H. It shows all the data lines from the MSP430 brought out to pins, so that every pin was available for input/output and debugging. Once

the boards were ordered and assembled, the msp430 was able to be programmed through a j-tag interface. At first, this was unsuccessful. This was because all of the power and ground lines must be connected for successful programming. After this hurdle was passed, the MSP430FG4618 was successfully programmed with some basic code.

The code was developed in stages. First, the ADC code was implemented. This code initializes the twelve external analog to digital conversion registers for input, and sets the ADC module for multiple channel, sequence of conversion. This samples the voltages at the ADC input pins, and stores a result into an ADC conversion register. The data stored in this register, which, in an interrupt service routine is moved into an array which holds eight of these results, before an operation must occur which will prepare the data for storage.

This code operated successfully, the voltage present on the ADC input pins could be verified that they were present on the microcontroller through the j-tag interface. With the important part of the code working correctly, the next important stage of development was implementing the SD card for data storage.

There were numerous hurdles in correctly interfacing the SD card to the MSP430FG4618. The first was the incorrect placement of pull up resistors and the short of wires on the development. The SD-MSP430 interface, shown in Figure 135, shows the incorrect SD card implementation.

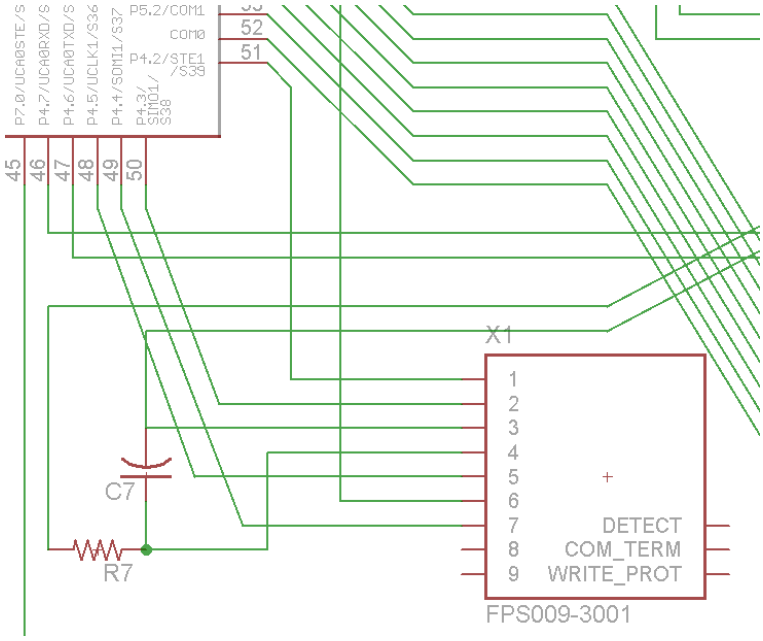

Figure 135: Incorrect SD card layout schematic, from the final Eagle layout. Note the different pin connections between this and Figure 136 below.

This was fixed by creating a separate board, with the schematic shown in Figure 136.

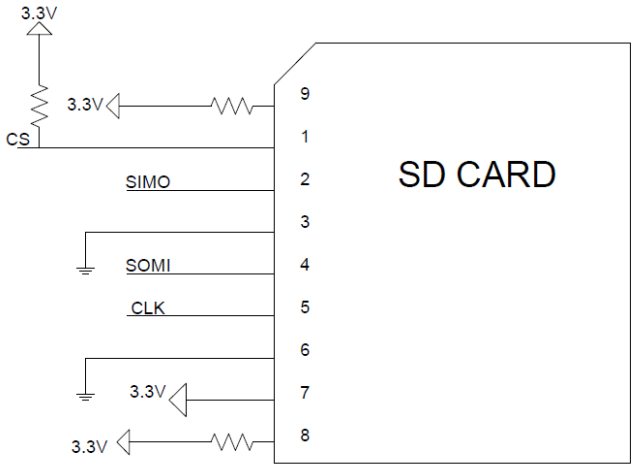

Figure 136: Correct SD card layout

The SD card and the MSP430 communicate through SPI. This is done by initializing the SPI controller and connecting the master and slave input and output to the correct SD card pins, as shown in Figure 136. However, when the data to initialize the SD Card into SPI mode was sent, no response was received by the MSP430, or sent by the SD Card. This was because the SD Card was not backwards

compatible with the MMC protocols. When an SD card was procured which was compatible with these protocols, the SD card could be easily written to, and read from.

In order for the data to be stored into the SD card, it must be within a certain format. The SD card must receive data in 512 byte blocks. This means that 512 characters or integers must be sent at a time. The eight elements of the array which is filled in an interrupt routine with data from the ADC results register is stored into the 512 element array called a data buffer. This buffer is then written to the SD card.

The elements in this buffer array are sorted by the sensor. All the conversion results obtained from the analog input A0, are located next to each other in the array, and thus in the SD card memory. This makes it easy for extraction using a hex viewer, as the data for each sensor is grouped together within the block.

6 Recommendations/Future Work

Our project goal was to develop a proof-of-concept prototype of the "smart glove". Through rigorous testing of our end product, we have identified several areas that need to be developed further, in order for to further develop on future generations of the prototype and make this product marketable.

In the process of completing our project, we were able to accomplish most of the objectives that were initially identified at the beginning of the 10 week period. In order for our device to effectively fulfill all the stipulations given, the following modifications need to be made to each of the subsystems and the entire system as a whole.

6.1 Pressure Sensing

Several improvements could be made to the pressure sensor subsystem of "smart glove." The accuracy of the data from the "smart glove's" pressure sensor data conversions should be analyzed by comparing the microcontroller's measurements against the readings on a force gauge. A calibration tool for conditioning the sensors could be developed. As Tekscan's documentation notes, the sensors need to be conditioned if they are unused for several weeks [62]. A fixture for the glove that applies pressure to each sensor if the glove is not being used could be used to keep the sensors conditioned. Another option is a device that can be easily used to apply 110N to each sensor.

The sensing areas of the A201 sensors were appropriate for our prototype, but could be improved in a custom Flexiforce sensor [53]. Tekscan can provide custom Flexiforce sensors in virtually any shape, so sensors shaped for each fingertip, and the palm of the hand can be designed. The Flexiforce manual warns that loading the edge of the sensing area causes errors in the measurements, so a sensing area that is large enough to accommodate many hand sizes for each of the six locations will provide a

more accurate reading than the A201 sensors.

Another possibility is using textile-like QTC sensors (discussed in Section 3.1) [59]. Peratech no longer manufactures generic sensors, so custom parts would need to be designed. Since they are similar to textiles, they could be a natural choice for "smart" clothing such as this. Choosing a different sensor would involve changing the interfacing circuitry and software because the material has a different force to resistance characteristic (logarithmic in this case) [60]. It would also necessitate a study of the sensor itself. A detailed integration guide is available from Peratech.

Possible improvements for the pressure sensor signal conditioning circuitry mainly involve the selection of passive components. Since this was a prototype, we used potentiometers to adjust the gain of each circuit individually. A fixed resistor on the order of 300kΩ could replace the sensitivity adjustment trimmers. This would sacrifice the circuit's resolution for durability. This resistance is high enough to ensure that all of the circuits will not saturate at 100N, based on our estimations when we set the potentiometers. Vibration could damage a trimmer or change its setting. The software that interprets the pressure sensor data would also be simpler because it would not need to keep track of each of the six sensors' trimmer values. Furthermore, it will make manufacturing more complicated if six trimmers needed to be adjusted for each product.

Using tighter tolerance capacitors, like 5% in the notch filters will improve their effectiveness [70]. The parts that 60Hz versions of the filters needed were unavailable when we built our prototype, so we did not include them in the schematic. Adding a 60Hz notch filter to each circuit will prevent regional power differences from affecting the sensors' accuracy, but it will cost board space. Another possibility is changing the notch filter from 50Hz to 60Hz, depending on where "smart glove" is being sold. In the prototype's case, the two filters were footprint compatible. Notch filters with flatter responses could be investigated as well, at the risk of increasing each pressure sensor circuit's footprint. Another possible filtering consideration is improving the low-pass filter on each circuit to

improve its rejection of multiple kHz frequencies. Perhaps a higher-order filter or capacitors with better dielectrics could be used.

6.2 Accelerometer

In order to improve upon the vibration measurement capabilities of this prototype, we have several recommendations having to do with the acceleration transducer as well as the frequency weighting methods.

6.2.1 Accelerometer Technology

The ADXL330 triple axis accelerometer we used to measure vibration is small, low cost, and can measure vibration in three axes. However, it is limited in both its magnitude range of measurement as well as bandwidth in the z direction. While we can demonstrate basic operation as a proof of concept with this device, an accelerometer with better capabilities should be found for future industrial applications in order to achieve more accurate measurement.

The 2440-025 model accelerometer from Silicon Designs can measure up to 200g of acceleration and has a bandwidth greater than 2kHz [103]. However, this device costs $1660 US and so may not be practical for mass production and implementation [103]. Investigation into a cheaper accelerometer which will meet the necessary bandwidth and magnitude range is needed for further design.

Some accelerometers that measure high magnitudes have lower sensitivity. One option that should be investigated is the use of two accelerometers in a design, one which will measure lower magnitude vibration and one that will measure the high impact spikes.

Another possible method of measuring both high and low magnitude acceleration spikes effectively is to use only a low magnitude accelerometer but estimate the high peak values by

calculating the slope of the function near clipping. This method, suggested by John Harris, is illustrated in Figure 137 below.

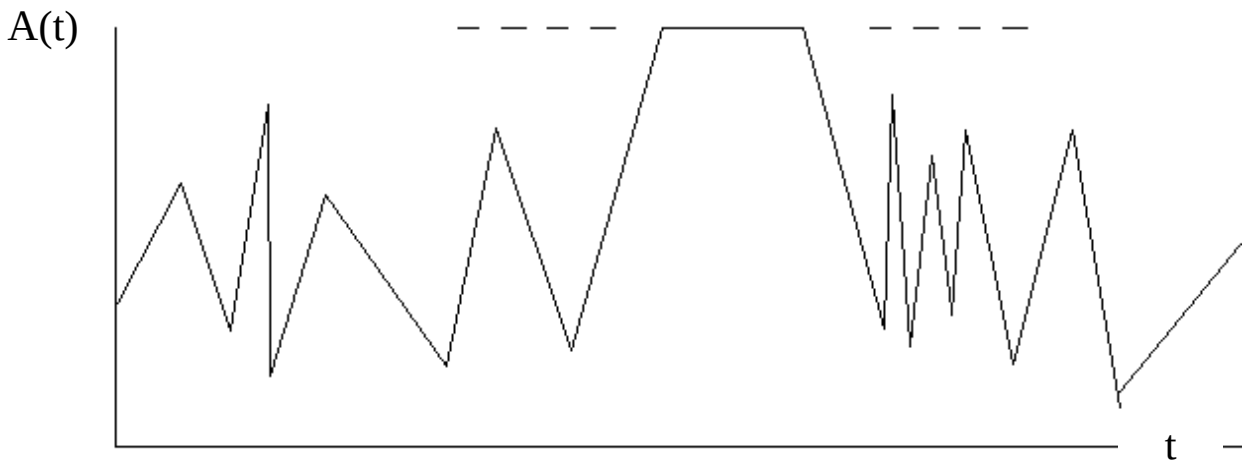

Figure 137: Technique for estimating a high amplitude peak

If an acceleration signal has an occasional spike that causes the output voltage to swing and hit the positive supply rail, the signal will be clipped. However, it may be possible to estimate the magnitude of the peak voltage by investigating the slope of the signal near the clipped portion.

6.2.2 Filter Techniques

We used analog filters to perform the band limiting and frequency weighting of the accelerometer signal. One advantage to this method is that no signal processing will needed to be done in software, which allows us to use a cheaper, low power, low cost microcontroller.

A major disadvantage of analog filtering is the error introduced by passive components with high tolerance values. Because the formula needed to compute remaining time amplifies the error in the acceleration total value, even small errors in passive component values can result in highly erroneous remaining time calculations. Because of budget and time constraints, we needed to prototype and test these filters using through hole components, which are not all available in the low

tolerances we need for accuracy. Future development of analog filters should investigate surface mount passive components with low tolerance values (1% or less).

It may also be worthwhile to avoid analog filters in favor of digital signal processing. This would reduce the amount of components needed, and possibly reduce error in measurement.

The ISO standard for hand transmitted vibration measurement suggests one-third-octave band analysis as an alternative to using a single frequency weighting, band limiting transfer function [1]. This method involves discrete weighting values for specific frequency ranges. Investigations into how to realize this type of analysis could be useful.

6.3 Goniometric Sensing

The goniometry sensing capability can be greatly increased. If the power concerns can be addressed, an optoelectronic solution could easily replace the current potentiometers. If the potential goniometry solutions analyzed in the sensor selection are revisited, it makes sense to use the laser/photodiode solution. This is a method which allows a greater resolution of data, allowing the angle of wrist to be determined with greater accuracy and precision.

6.4 Microcontroller

The microcontroller board's size can be greatly reduced. Originally, we had planned to include the USB bridge chip and OLED on that board. We also routed most of the MSP430's pins to female headers so that it would be easy to test. With the unused pins properly dealt with, and the USB bridge and OLED circuitry removed, the microcontroller board can probably be reduced to a third of its size. This space could be used for power, interfacing or alert circuitry. The board that we built for this project was essentially a breakout board for the MSP430FG4618. Its layout and design is an area for major improvement.

6.5 Display

Adding a display to the glove would greatly increase its value. The power sources and microcontroller ports are available for the implementation, however, the room in the housing is not available, nor was the time for the implementation. It would be simple to add an LCD display, without a backlight, which could act as a watch, or a sensing display.

6.6 Alert System

The size of the alert system board can be further reduced by implementing 555 timers on the Schmitt trigger inputs of the MSP430. Also, the alert system can be developed to stimulate the user's sense of touch. This can be achieved using some form of piezo material, which will contract as the magnitude of the vibration increases. Also, when the user exceeds the vibration exposure limits, the material should restrict any further movements of the hands, and in effect, the use of the tools and machinery.

6.7 Power

The circuits that convert 3.7V to ±1.5V can be improved in terms of their physical footprint and power efficiency. An alternative to the 555 inverter-multiplier circuit is a component MAX860 charge-pump voltage converter [104]. This can be setup with minimal external components as a circuit that inverts the input voltage. Connecting a MAX860 as show in Figure 138 will invert the battery's voltage. A negative regulator could be then be used to output a regulated -1.5V.

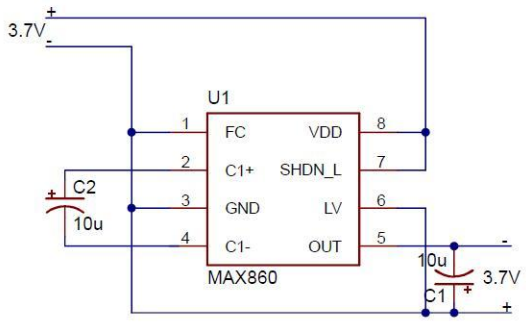

Figure 138: MAX860 Voltage Inverter Circuit [104]

Lower power, low-dropout regulators than the LM317 and LM337 could be substituted as well. We chose these regulators because they were readily available. These, combined with the +9V and +3.3V circuits should be a sufficiently low-power DC-DC conversion subsystem for the "smart glove" to be used throughout a workday. Once a more practical power circuit is assembled, an analysis of the "smart glove's" battery life should be carried out.

A low-battery indicator should be added to the device, as well as the capability for the microcontroller to power down the device before the battery discharges to the point where "smart glove" malfunctions. This could be easily implemented, since the MAX761 has built in low-battery detection capabilities [95]. Regulators like the MAX667, which is a possible substitute for the LM317 do as well [105].

Batteries should be investigated and compared to choose a suitable, low-profile, high capacity rechargeable battery. We intended to use a replacement NB-4L lithium-ion battery because we had a charger from one of our cameras. This battery was suitably thin and had over 700mAh [94]. Once the USB functionality is realized, the battery could be charged via USB, which would reduce the cost associated with buying a separate battery charger. Maxim, for example has an application notes covering this and offers ICs for charging lithium-ion batteries over USB [106].

6.8 Wireless Capabilities

The product should include a software -based central RF transceiver, which will make use of the USB connection to PC to communicate with multiple gloves. This PC-based software application should be able to configure multiple “smart gloves” via USB, monitor the readings from gloves at regular intervals, and sending alert messages to one or all gloves simultaneously.

6.9 Physical Layout of Prototype

The boards we designed can all be improved in terms of their size and layout. Except for the microcontroller board, all of our boards were built at the University of Limerick with Cadsoft Eagle 5.2.0 Light Edition [107]. We assembled these boards ourselves, so the parts were spread out more than necessary to make the soldering easier. Vias could not be plated at the University, so we tried to minimize the amount we used in each design. The Lite edition would not allow us to build boards greater than 100 mm x 80 mm, which forced us to design a series of small boards when a larger one would be more practical. It also limited us to two signal layers (top and bottom). This prevented us from adding noise-reducing measures, like power and ground planes. Using more than two signal layers and surface mount components (where possible) will allow for a more compact layout.

We recommend that the sensing circuitry be built on flexible PCBs which would conform to the hand and allow for maximum movement of the hand and wrist. These boards should be embedded in a stable material, so that none of the forces and vibrations are absorbed by the material, in order to obtain more accurate readings from the sensor circuitry. Further redesign and minimization of the microcontroller circuitry and its peripheral subsystems will reduce the size of the plastic enclosure. An ideal size for this enclosure would be the size of a Personal Digital Assistant
(PDA) so that it can be worn comfortably on the upper arm, without restricting the movement of the upper limbs. and allow it to be may allow for them to be installed on the glove

7 Conclusion

The final proof-of-concept device presented to the ERC team accomplished the main objectives that were identified at the beginning of the 10 week period. Our project aimed at developing a proof of concept “smart glove” system, which incorporates angle, pressure, and vibration sensing into a non-invasive, lightweight glove, capable of real-time data logging in an industrial environment and storing the ergonomic data for future statistical analysis and research.

We fulfilled our project objectives by:

Delivering a stand alone, battery powered device capable of measuring four risk factors for hand injury during manual labor.

Our design proves the ability to incorporate three sensor systems, their interfacing circuitry, a power supply system, as well as a user alert system into a lightweight glove and arm band.

Designing a device capable of storing the real-time data for future analysis

The microcontroller is capable of reading in data from the sensors and then writing this information to the SD card. A PC can use a hex editor to extract the data from the SD card.

In fulfilling these objectives we have demonstrated the viability of an on site industrial safety auditing tool, which is capable of measuring the multiple risk factors that contribute to the onset and development of RSI and vibration induced conditions. Previously, devices used to assess industrial safety were incapable of measuring a combination of the risk factors, and in many cases were bulky, expensive, and therefore more suited for use in a lab than in the work environment.

With further development and refinement, our proof-of-concept system could be used for the following applications:

RSI research: This device will provide an opportunity for real-time data collected in an industrial setting to be used to research and analysis of the factors and determining how they contribute to the occurrence and severity of these injuries.

Reduction of incidence of RSI and vibration induced injuries: Alerting the users to when they have exceeded the ISO exposure limits will help in preventing workers from injuring themselves in the future. Determining the appropriate operating time for industrial equipment will allow employers to improve the safety of their work environments and practices.

We hope that the ERC team finds the entirety of the work done on this project including the report and proof-of-concept device useful, and sees this as a starting point in the further development of the product.

References

[1] Gallwey, T., & University of Limerick, "RSI research at UL, 2002". [Online]. Available: http://www.irishscientist.ie/2002/contents.asp?contentxml=02p236.xml&contentxsl=is02pages.xsl. [Accessed: August 12, 2008]

[2] International Organization for Standardization, "Mechanical vibration: measurement and evaluation of human exposure to hand transmitted vibration – parts 1 & 2: general guidelines", ISP 5349-1. Geneva: International Organization for Standardization, 2001a.

[3] Mansfield, N. J., "Human Response to Vibration", London: CRC Press, 2005.

[4] NexGen Ergonomics, "VATS™ (Vibration Analysis ToolSet)", NexGen Ergonomics, 2007. [Online]. Available: http://www.nexgenergo.com/safety/vats.html. [Accessed: Aug. 27, 2008].

[5] O'Sullivan, L.W., 2008.

[6] Nelson, C.M., "Investigation of the relationship between latent period for vibration-induced white finger and vibration exposure". Proceedings of the U.K. and French joint meeting on Human Response to Vibration, INRS, Vandoeuvre, France, September 26-28, 1988.

[7] Hire Station, "Hand Arm Vibration Policy Minimize, Manage & Monitor," Hire Station, 2007. [Online]. Available:http://www.hirestation.co.uk/images/fckimages

[8] World Health Organization, "Occupational Hazards", Anthology on women, health and the environment,WHO/EHG/94.11, 1994, pp. 111-144. [Online]. Available: http://whqlibdoc.who.int/hq/1994/WHO_EHG_94.11.pdf. [Accessed: August 12, 2008]

[9] Health and Safety Executive, "New guidance on using computers and preventing RSI", 2003a. [Online]. Available:

http://www.hse.gov.uk/press/2003/e03030.htm. [Accessed: August 27, 2008]

[10] RSI Awareness, "Upper Limbs Disorder: An Overview". [Online]. Available: http://www.rsi.org.uk/pdf/ULDs_Overview.pdf. [Accessed: August 12, 2008]

[11] "Adhesive Capsulitis", 2002. [Online]. Available: http://www.eorthopod.com/public/patient_education/6526/adhesive_capsulitis.html. [Accessed: August 25, 2008]

[12] "Bursitis", 2002. [Online]. Available: http://www.eorthopod.com/public/patient_education/6474/olecranon_bursitis.html. [Accessed: August 25, 2008]

[13] "Bursitis", 2002. [Online]. Available:

en:Image:Bursitis_Elbow_WC.JPG. [Accessed: August 25, 2008]

[14] "Carpal Tunnel Syndrome", 2002. [Online]. Available: http://www.eorthopod.com/public/patient_education/6564/carpal_tunnel_syndrome.html. [Accessed: August 25, 2008]

[15] "Neck Pain", 2002. [Online]. Available: http://www.eorthopod.com/public/patient_education/6452/neck_pain.html. [Accessed: August 25, 2008]

[16] "Cubital Tunnel Syndrome", 2002. [Online]. Available:

http://www.eorthopod.com/public/patient_education/6469/cubital_tunnel_syndrome.html. [Accessed: August 25, 2008]

[17] "de Quervain's tenosynovitis", 2002. [Online]. Available: http://www.eorthopod.com/public/patient_education/6454/de_quervains_tenosynovitis.html. [Accessed: August 25, 2008]

[18] "Dupuytren's contracture", 2002. [Online]. Available: http://www.eorthopod.com/public/patient_education/6557/dupuytrens_contracture.html. [Accessed: August 25, 2008]

[19] "Dupuytren's contracture", 2006. [Online]. Available:

http://upload.wikimedia.org/wikipedia/commons/9/94/Morbus_dupuytren_fcm.jpg.

[Accessed: August 25, 2008]

[20] "Lateral Epicondylitis", 2002. [Online]. Available: http://www.eorthopod.com/public/patient_education/6472/lateral_epicondylitis_tennis_elbow.html. [Accessed: August 25, 2008]

[21] "Medial Epicondylitis", 2002. [Online]. Available: http://www.eorthopod.com/public/patient_education/6473/medial_epicondylitis_golfers_elbow.html. [Accessed: August 25, 2008]

[22] "Ganglions of the wrist", 2002. [Online]. Available: http://www.eorthopod.com/public/patient_education/6456/ganglions_of_the_wrist.html. [Accessed: August 25, 2008]

[23] "Rotator Cuff Tears", 2002. [Online]. Available:

http://www.eorthopod.com/public/patient_education/6532/rotator_cuff_tears.html. [Accessed: August 25, 2008]

[24] "What type of injuries can happen to a tendon?", 2008. [Online]. Available: http://www.eorthopod.com/public/patient_education/9371/what_types_of_injuries_can_happen_to_a_tendon.html. [Accessed: August 25, 2008]

[25] "Trigger finger and Trigger thumb", 2002. [Online]. Available:

http://www.eorthopod.com/public/patient_education/6552/trigger_finger_and_trigger_thumb.html. [Accessed: August 25, 2008]

[26] "Trigger finger/thumb", 2006. [Online]. Available: http://www.med.und.nodak.edu/users/jwhiting/trigger.JPG. [Accessed: August 25, 2008]

[27] National Research Council and Institute of Medicine, "Musculosketal Disorders and the Workplace: Low Back and Extremities", Panel on Musculoskeletal Disorders and the Workplace. Commission on Behavioral and Social Sciences and Education, Washington, DC: National Academy Press, 2001.

[28] Greening, J., Lynn, B., & Leary, R., "Sensory and autonomic function in the hands of patients with non-specific arm pain (NSAP) and asymptomatic office workers", Pain, 104(ISSN 0304-3959), 2003, p. 275-281. [Online]. Available :

http://cat.inist.fr/?aModele=afficheN&cpsidt=14939633. [Accessed: September 1, 2008]

[29] Bureau of Labor Statistics, "Survey of Occupational Injuries and Illnesses", Washington, DC: U.S. Department of Labor, 1999.

[30] Praemer, A., Furner, S., Rice, D. P., "Musculoskeletal Conditions in the United States", Rosemont, IL: American Academy of Orthopaedic Surgeons, 1999.

[31] Health & Safety Executive, "Aching arms (or RSI) in small businesses: Is ill health due to upper limb disorders a problem in your workplace?", 2003b [Online]. Available: http://www.hse.gov.uk/pubns/indg171.pdf. [Accessed: September 1, 2008].

[32] Central Statistics Office, "Health and Social Conditions", Statistical Yearbook of Ireland 2007 Edition, p. 1649-1408, 2007.[Online]. Available:

http://www.cso.ie/releasespublications/documents/statisticalyearbook/2007/Statistical%20Yearbook%202007%20web%20version.pdf. [Accesed: August 27, 2008].

[33] "Sammons Preston", Sept. 4, 2008. [Online]. Available: http://www.sammonspreston.com/app.aspx?cmd=go_home. [Accessed: Aug. 26 – 28, 2008].

[34] "fingerTPS_specsheet_final-1-1.pdf," Sept. 4, 2008. [Online]. Available: http://www.pressureprofile.com/UserFiles/File/fingerTPS_specsheet_final-1-1.pdf. [Accessed: Aug. 26, 2008].

[35] "NexGen Ergonomics – Welcome", Jul. 4, 2008. [Online]. Available: http://www.nexgenergo.com/index.html. [Accessed: Aug. 26, 2008].

[36] "I-CubeX Online Store : Motion Sensors for Digital Media Control", Sept. 4, 2008. [Online]. Available: http://infusionsystems.com/catalog/index.php?osCsid=ea0abbdf8460c5448d05c6ed23af1a9c. [Accessed: Aug. 26, 2008].

[37] V. Mathiowetz, N. Kashman, G.Volland, K.Weber, M. Dowe and S. Rogers , "Grip and Pinch Strength: Normative Data for Adults, Archives of physical medicine and rehabilitation", Archives of Physical Medicine and Rehabilitation, vol 66, no. 2, p. 69-74, Feb. 1985. [Online]. Available: http://www.bleng.com/pdf/grip1.pdf. [Accessed: Aug. 13, 2008].

[38] K. Jung, Y. Heecheon and K. Ochae, "Evaluation of the FSA Hand Force Measurement System", Human Factors and Ergonomics Society: 50th Annual Meeting, 2006. October 16-20, 2006, San Francisco. [Online]. Available: http://141.223.62.152/03_publication/IC/06_HFES_FSA_Evaluation.pdf. [Accessed Aug. 26, 2008].

[39] "Home – Pressure Profile Systems", Sept. 4, 2004. [Online]. Available: http://www.pressureprofile.com/. [Accessed: Aug. 26, 2008].

[40] FSA Force Measurement Systems & Products U.S. Retail Price List (Effective June 1, 2008), NexGen Ergonomics Inc. Montreal., Canada.

[41] M. Patil and O. Prohaska, "Fiber Optic Sensor for Joint Angle Measurement", in IEEE Engineering in Medicine & Biology Society 10th Annual Conference, 1988, p. 803-804.

[42] G. Chartier , "Introduction to Optics", Springer, 2005, p. 179.

[43] M. Dono et all, "A Flexible Optical Fiber Goniometer for Dynamic Angular Measurements", in Instrumetation and Measurement Technology Conference, 2007.

[44] J. Jenson, J. Li and G. Sigel, "A Fiber Optic Angular Sensor for Biomedical Application", in IEEE Engineering in Medicine & Biology Society 11th Annual International Conference, 1989, p. 1118-1119.

[45] D. Gardner, "The Power Glove", Design News, 1989, p. 63-68.

[46] O. Grau and G. Custance, "*Virtual Art: From Illusion to Immersion*", MIT Press, 2003, p. 166-168.

[47] N. Karlsson, B. Karlsson and P. Wide, "A Glove Equipped with Finger Flexion Sensors as a Command Generator used in a Fuzzy Control System", IEEE Transactions on Instrumentation and Measurement, Vol. 47, No. 5, 1998, p. 1330-1334.

[48] P. Troyk et all, "Design and Implementation of an Implantable Goniometer", IEEE Transactions on Biomedical Engineering, Vol. BME-33, No. 2, 1986, p. 215-222.

[49] *Biometrics Ltd Research - Goniometers and Torsiometers*, 2006. [Online] Available: http://www.biometricsltd.com/y%20gonio.htm. [Accessed: Aug. 24 2008].

[50] G. Legnani et All, "A Model of Electro-Goniometer and its calibration for biomechanical applications", Medical Engineering & Physics, 2000, p. 711-722.

[51] C. Ashruf, "Thin flexible pressure sensors," *Sensor Review*, vol. 22, no. 4, pp. 322-327, 2002. [Online]. Available: Emerald, http://www.emeraldinsight.com/Insight/ViewContentServlet?Filename=Published/EmeraldFullTextArticle/Articles/0870220406.html. [Accessed: Aug. 26, 2008].

[52] Pressure Profile Systems, Inc., *ConTacts C500*, Pressure Profile Systems, Inc.

[53] Tekscan Inc., "Tekscan: Tactile Pressure Measurement, Pressure Mapping Systems, and Force Sensors and Measurement Systems," Sept. 25, 2008. [Online]. Available: http://www.tekscan.com/ [Accessed: Aug. 12, 2008].

[54] SensorsONE Ltd, "Interpreting specifications of pressure sensor accuracy," Sept. 29, 2008. [Online]. Available: http://www.sensorsone.co.uk/news/54/Interpreting-specifications-of-pressure-sensor-accuracy.html [Accessed: Aug. 19, 2008].

[55] Tekscan Inc., *FlexiForce The Leader in Standard & Custom OEM Force Sensing Solutions*, Tekscan Inc.

[56] *FSR Force Sensing Resistor Integration Guide and Evaluation Parts Catalog*, Interlink Electronics, Inc., Camarillo, CA.

[57] Interlink Electronics, Inc., "Electronic Signatures – Force Sensors," Sept. 22, 2008. [Online]. Available: http://www.interlinkelectronics.com/ [Accessed: Aug. 13, 2008].

[58] Pub No. 90-78721 *Force Sensing Resistor (FSR) Evaluation Parts Price List and Order Form*, Interlink Electronics, Inc., Camarillo, CA.

[59] Peratech Ltd., "Welcome to Peratech," July 31, 2008. [Online]. Available: http://www.peratech.com/ [Accessed: Aug. 13, 2008].

[60] Peratech Ltd., *QTC Sensor Series QTC Force Sensors*, Peratech Ltd, Jan. 2004.

[61] CUI Inc., "A Solutions Provider of Electro-Mechanical Components For OEM Manufacturing," Sept. 29, 2008. [Online]. Available: http://www.cui.com/ [Accessed: Aug. 13, 2008].

[62] Tekscan Inc, *FlexiForce Sensors User Manual*, Tekscan Inc., Sept. 23, 2005.

[63] Texas Instruments Incorporated, *MSP430xG461x MIXED SIGNAL MICROCONTROLLER*. Texas Instruments Incorporated, 2007.

[64] Texas Instruments Incorporated, *OPA333 OPA2333*, Burr-Brown Products from Texas Instruments, May 2007.

[65] Texas instruments Incorporated, *OPA336 OPA2336 OPA4336*, Burr Brown Products from Texas Instruments, Jan. 2005.

[66] Texas Instruments Incorporated, *TLV341, TLV342, TLV342S, TLV344 LOW-VOLTAGE RAIL-TO-RAIL OUTPUT CMOS OPERATIONAL AMPLIFIERS WITH SHUTDOWN*, Texas Instruments Incorporated, Jan. 2005.
[67] Texas Instruments Incorporated, *TLV2381 TLV2382*, Texas Instruments Incorporated, Jul. 2003.
[68] Texas Instruments Incorporated, *TLV2760, TLV2761, TLV2762, TLV2763, TLV2764, TLV2765 FAMILY OF 1.8V MICROPOWER RAIL-TO-RAIL INPUT/OUTPUT OPERATIONAL AMPLIFIERS WITH SHUTDOWN*, Texas Instruments Incorporated, Jan. 2005.
[69] Texas Instruments Incorporated, "Analog Technologies, Semiconductors, Digital Signal Processing – Texas Instruments," Sept. 30, 2008. [Online]. Available: http://www.ti.com/ . [Accessed: Sept. 2, 2008].
[70] P. Horowitz, W. Hill, "5.09 Twin-T Notch filters," in *The Art of Electronics*, 2nd ed., New York: Cambridge University Press, 2006, pp. 279 – 281.
[71] Premier Farnell plc, "Farnell IE | world-leading distributor of electronic and maintenance, repair and operations products.," Oct. 8, 2008. [Online]. Available: http://ie.farnell.com/. [Accessed: Oct. 8, 2008].
[72] Texas Instruments Incorporated, *MSP430x4xx Family User's Guide*, Texas Instruments Incorporated, 2007.
[73] Analog Devices Incorporated, "*Small, Low Power, 3-Axis ±3 g i MEMS® Accelerometer"*, pp 3-11.
[74] Sparkfun Electronics, "Triple Axis Accelerometer Breakout - ADXL330," *Sparkfun Electronics*, 2008. [Online]. Available: http://www.sparkfun.com/commerce /product_info.php?products_id=692. [Accesed: Oct. 6, 2008].
[75] Karki, J. "Analysis of the Sallen-Key Architecture," Mixed Signal Products, July 1999. [PDF]. Available**:** http://focus.ti.com/lit/an/sloa024b/sloa024b.pdf. [Accessed: Oct. 10, 2008].
[76] McNeill, J. "Filter Design in the S-Plane," *EE3204 B2007 Microelectronics II*, Worcester Polytechnic Institute course website, Nov. 2007. [PDF]. Available: http://ece.wpi.edu/~mcneill/handouts/s-planenotes.pdf. [Accessed: Oct. 10, 2008].
[77] J. S. Schultz, R. F. Taylor, *Handbook of Chemical and Biological Sensors*, Florida: CRC Press, 1996, pp 16-24.
[78] K. F. Anderson. "NASA's Anderson Loop," *Instrumentation & Measurement, IEE*, vol. 1, no. 1, pp. 5-30, March 1998.
[79] United States. National Aeronautics and Space Administration. *Spinoff:A measurable Difference: Bridge Vesus Loop.* Edwards: NASA, 1998, pp 103.
[80] R. Northrop, *Introduction to Instrumentation and Measurements*, 2nd ed. Florida: CRC Press, 2005, pp. 176-183.
[81] S. Tumanski, *Principles of Electrical Measuremen*,. Florida: CRC Press, 2006, pp. 112-114.
[82] National Semiconductor, *LM134/234/334 3-Terminal Adjustable Current Sources*. National Semiconductor, March 2005.
[83] GlobalSpec , *About Audio Transducers and Buzzers*. [Online]. Available: http://video-equipment.globalspec.com/LearnMore/Video_Imaging_Equipment/Meters_Readouts_Indicators/ Audio_Transducers_Buzzers. [Accessed: September 2, 2008].
[84] IMO, *41.T70P015H-LF Magnetic Transducer Specifications Sheet*, CQR Security.
[85] Alan Butcher Components Ltd., *ABT-410-RC Specification Sheet*, Alan Butcher Components Ltd.
[86] Star Micronics Co., Ltd., *Washable TMB Series*, Star Micronics Co. Ltd.
[87] Sedra, A. S., & Smith, K. C. (2004). Memory and Advanced Digital Circuits. In

Microelectronic Circuits (5th ed., pp. 189-190, 1021-1022). New York: Oxford University Press, Inc. (Original work published 1982)

[88] Sedra, A. S., & Smith, K. C. (2004). Memory and Advanced Digital Circuits. In *Microelectronic Circuits* (5th ed., pp. 189-190, 1021-1022). New York: Oxford University Press, Inc. (Original work published 1982)

[89] Texas Instruments Incorporated, *TLC555LinCMOS Timer*, Texas Instruments Incorporated, 2005.

[90] Sedra, A. S., & Smith, K. C. (2004). Memory and Advanced Digital Circuits. In *Microelectronic Circuits* (5th ed., pp. 211). New York: Oxford University Press, Inc. (Original work published 1982)

[91] SanDisk, *Secure Digital Card Product Manual – Revision 1.7*, September 2003.

[92] SD Association, *SD Card*. [Online]. Available: http://sdcard.org/. [Accessed Sept. 13, 2008]

[93] Texas Instruments, *MSP430x1xx Family User's Guide*. [Online]. Available: http://focus.ti.com/lit/ug/slau049d/slau049d.pdf. [Accessed Sept.20, 2008].

[94] BatteryCity.ie. [Online]. Available: http://www.batterycity.ie/. [Accessed Sept.20, 2008].

[95] Maxim Integrated Products, *MAX761/MAX762 12V/15V or Adjustable, High-Efficiency, Low I_Q, Step-Up DC-DC Converters*, Maxim Integrated Products, Nov. 1993.

[96] Panasonic, *Choke Coils*, Mar. 2005. [Online]. Available: http://docs-europe.electrocomponents.com/webdocs/06bc/0900766b806bc529.pdf. [Accessed Sept. 20, 2008].

[97] CSG Network, *555 Negative Voltage Generator*, 2008. [Online]. Available: http://www.csgnetwork.com/ne555c1.html. [Accessed Sept. 20, 2008].

[98] National Semiconductor, *LM555 Timer*, July 2006. [Online]. Available: http://www.national.com/ds/LM/LM555.pdf. [Accessed Sept. 24, 2008].

[99] Fairchild Semiconductor, *3-Terminal 1.5A Negative Adjustable Regulator*, 2001. [Online]. Available: http://www.fairchildsemi.com/ds/LM%2FLM337.pdf. [Accessed Sept. 24, 2008].

[100] Fairchild Semiconductor, *3-Terminal Positive Adjustable Regulator*, June 2005. [Online]. Available: http://www.fairchildsemi.com/ds/LM/LM317.pdf. [Accessed Sept. 24, 2008].

[101] National Semiconductor, *LP2950/LP2951 Series of Adjustable Micropower Voltage Regulators*, May 2005. [Online]. Available: http://cache.national.com/ds/LP/LP2950.pdf. [Accessed Sept. 24, 2008].

[102] H. Zheng, N. D. Black, and N. D. Harris, "Position-sending technologies for movement analysis in stroke rehabilitation", *Medical & Biological Engineering & Computing*, vol. 43, no. 4, April, 2006, pp. 413-420.

[103] Silicon Designs Inc., *Model 2440 Triaxial Analog Accelerometer Module*, Sept. 2007. [Online]. Available: http://www.silicondesigns.com/Pdf/2440.pdf. [Accessed Oct. 10, 2008].

[104] Maxim Integrated Products, *MAX860/MAX861 50mA, Frequency-Selectable, Switched-Capacitor Voltage Converters*, Maxim Integrated Products, Mar. 2003.

[105] Maxim Integrated Products, *MAX667+5V/Programmable Low-Dropout Voltage Regulator*, Maxim Integrated Products, Oct. 1994.

[106] Analog, Linear, and Mixed-Signal Devices from Maxim/Dallas Semiconductor, 2008. [Online]. Available: http://www.maxim-ic.com/. [Accessed: Oct. 10, 2008].

[107] CadSoft, *CadSoft Online: Home of the EAGLE Layout Editor*, 2008. [Online]. Available: http://www.cadsoft.de/freeware.htm. [Accessed: Aug 27, 2008].

Appendices

Appendix A: Preliminary Project Description

Wireless 'Smart Glove' Monitoring System for Personal Protective Equipment Applications

The aim of the project is to develop and apply a wireless 'smart glove' technology to monitor the critical physiological conditions to which upper limbs are exposed in the work place. A personal protective equipment (PPE) accessory will be developed in the form of a glove to intelligently assess mechanical stresses in the upper arm and hands, and accordingly indicate safe exposure time limits to the wearer in line with regulatory standards. The purpose of this technology is to prevent the onset of repetitive strain injury (RSI) by limiting exposure in terms of severity and/or duration, and ultimately provide an audit trial that can be used to determine employee work practices, and assess workplace conformance to the applicable regulations.

OBJECTIVE
The objective is to deliver a prototype 'smart glove' system with a central wireless transceiver that can identify unique users (wearers) and process their readings into audit trails. The system will also provide instant feedback to the user in the case of an alarm condition incidental to them or directly relating to a specific excessive exposure condition. The target outputs are as follows:

a) A compact wireless 'smart glove' with the following features:
- Rechargeable battery (e.g. compact mobile phone battery or similar)
- Built-in X-Y-Z accelerometers to measure vibration
- Built-in strain gauges to measure flexion and extension
- Pressure sensor array(s) to measure impacts and other forces
- Microprocessor with built-in ADCs and memory to dynamically interpret sensor signals and assess exposure
- Built-in clock for real-time data logging
- Programmable ID to identify the wearer for audit purposes
- USB socket to configure ID, upload parameter look-up tables for exposure conditions, download audit trail, and charge the battery
- Small LCD display to indicate current exposure conditions and the permissible time remaining for such conditions
- One or more sensory mechanisms to alert the user to excessive exposure
- RF transceiver

b) A software-based central RF transceiver, with the following functionality:
- USB connection to PC to communicate with multiple gloves
- PC-based software application with provision for configuring gloves via USB, monitoring readings from gloves at regular intervals, and sending alert messages to one or all gloves simultaneously
- The software should also have the capability of color-mapping the readings on a wire-frame hand diagram to indicate the distribution and relative severity of forces
.

OUTLINE OF PHASES

Possible phases may include, but are not confined to, the following:

Phase 1: Selection of sensors and design of appropriate interfacing circuitry where required. Suitable interfacing ICs may be purchased if possible.

Phase 2: Design of circuitry to digitally record and process the sensor interface signals using a low-power PIC (or similar) microprocessor. The tasks of the microprocessor will be to address all sensors, interrogate the readings and run algorithms to calculate forces. The microprocessor should also be used to drive a small commercially produced LCD module. The programmed ID should be included in data transmissions (wireless or otherwise) to identify the source of the signal (and ultimately the user).

Phase 3: Design or purchase a USB RF transceiver for connection to a PC, to allow communication with all 'smart gloves'.

Phase 4: Design a PC-based application written in C, C++, MS visual basic, or a similar higher-level language. The application should connect to the USB ports for wireless and wired communications with the glove electronics. A number of features should be provided as indicated above under objective.

GENERAL REQUIREMENTS

- Issues of noise and co-channel interference should be considered in the design of sensor interface and RF circuitry.
- Through-Hole Technology may be used to build 'breadboard' prototypes, but Surface-Mount Technology (SMT) should be used to build the final 'smart glove' circuitry, where miniaturization and low mass are important.

Appendix B: Code files

This appendix contains the code which was developed for the project. It is written to display the use of all the sensors, as well as the alarm subsystems.

```
/*******************************************************************************
**
**
**
**
**
**                      MSP430FG4618
**                 _____________________________________
**               |                                     |   _____________
**          -->|A0/P6.0                  P.4/MISO| -|   SDCARD    |
**          -->|A1/P6.1                 P4.3/SIMO| -|             |
**          -->|A2/P6.2                   P4.2/CS| -|             |
**          -->|A3/P6.3                 P4.5/UCLK| -|_____________|
**          -->|A4/P6.4                          |
**          -->|A5/P6.5                      P10.5|
**          -->|A6/P6.6                      P10.4|
**          -->|A7/P6.7                           |
**          -->|A12/P5.1                          |
**          -->|A13/P5.0                          |
**          -->|A14/P10.7                         |
**          -->|A15/P10.6                         |
**               |_____________________________________|
**
**
**
**
** SD CODE ADAPTED FROM ORIGINAL CODE WRITTEN BY ROLLF FREEITAG AND TI.COM
** CODE DEVELOPED BY THE SMART GLOVE ALLIANCE
** LAST EDIT - 9/22/2008
** REV B0.71.5
*******************************************************************************/
```

```
#include <msp430xG46x.h>
#include <float.h>
#include <stdlib.h>
#include "sd.h"
#include <string.h>


// mmc variable
extern char mmc_buffer[512];
char mmc_buffer_test_1[512];
char state_mmc = 1;
int SD_FLAG = 0;
unsigned long SD_BLOCK = 0;

//FORCE - Five Fingers and a Palm
//From thumb to smallest finger
volatile unsigned int A0_SENSOR7[8];
volatile unsigned int A1_SENSOR4[8];
volatile unsigned int A2_SENSOR5[8];
volatile unsigned int A4_SENSOR6[8];
volatile unsigned int A6_SENSOR3[8];
volatile unsigned int A7_SENSOR2[8];

//ACCELEROMETER Z AXIS
volatile unsigned int A5_SENSORZ[8];

//GONIOMETRY AXIS
volatile unsigned int A12_SENSOR[8];
volatile unsigned int A3_SENSOR[8];

//DUMMY IFG CLEARER
volatile unsigned int IFG_CLEARER[8];

int A0_watch=0;
int A1_watch=40;
int A2_watch=80;
int A3_watch=120;
int A4_watch=160;
int A5_watch=200;
int A6_watch=240;
int A7_watch=280;
```

```
int A8_watch=320;
int A9_watch=360;
int A10_watch=400;
int A11_watch=440;









//ADC
unsigned int adc_conversion_result_index=0; //ADC ARRAY index
unsigned int adc_sets_are_ready=0;          //ADC sets are ready for processing
flag
unsigned int t=0;                             //incr each sampling period
int alarm_condition=0;




//FUNCTION DECLARATIONS
void init_ADC (void);
void adc_process(void);
void alarm (int control_signal);
int alarm_status (int control_signal);
void copyover ( void);
void watch_update(void);
void InitFreq(void);
void sd_card_test (void);

void main(void)
{
  //unsigned int ok;
  unsigned int j = 0;
  volatile unsigned int i;


  WDTCTL = WDTPW + WDTHOLD;     //STOPS watchdog timer
  P10DIR = BIT5 + BIT4;         //P10.4/.5 DIRECTION iS OUTPUT
  P10OUT = 0x00;                //P10.x IS OFF
```

```
  InitFreq();                   //INIT CLOCKS AT CORRECT FREQUENCY
  sd_card_test();               //TEST SD CARD


while(1)
{
  alarm(alarm_condition);       //SET ALARM, INITIALLY OFF
  init_ADC();                   //Prepares the ADC for Capture and Conversion
  ADC12CTL0 |= ENC;             //Enables Conversion
  ADC12CTL0 |= ADC12SC;         //ENABLES CONVERSION
   //Start Conversions
__bis_SR_register(GIE);         //ENABLE INTERRUPTS


while(adc_sets_are_ready ==0);  //HOLD UNTIL READY

if (adc_sets_are_ready == 1){
//adc_process();
adc_conversion_result_index = 0;//RESET CONVERSION INDEX
}

copyover();                     //COPY OVER DATA into MMC BUFFER
watch_update();                 //UPDATES/RESETS DATA_ARRAY_WATCHERS

if(SD_FLAG == 1)                //IF THE FLAG IS SET FOR A FULL MMC BUFFER
{
  mmcWriteBlock(SD_BLOCK);      //WRITE THE BUFFER TO THE CARD
  SD_BLOCK = SD_BLOCK + 512;    //UPDATE MEM LOCATION
  SD_FLAG = 0;                  //RESET SD FLAG
}

alarm_condition = alarm_status(alarm_condition);  //PICK RANDOM ALARM_CONDITION




//SILLY ALARM CONDITION MATH
if (alarm_condition == 0)
{P10OUT = 0x00;
alarm_condition = rand() % 4;
if(alarm_condition == 0)
{alarm_condition = 2;}
```

```
for(i=0; i<60000; i++)
{for (j = 0; j < 10; j++){}}
}

adc_sets_are_ready = 0;

//The sampling frequency is so fast, that we just grab 4 of the entrys in the array
//and average them, the array that we sample from is determined by which alarm is
being
//set off



}


}

/*****************************************************************************
FUNCTIONS
*****************************************************************************/




/*****************************************************************************
VOID init_ADC (VOID)
*****************************************************************************/
//init_ADC require no input or output
//it prepares the proper ports for input AND
//sets up everything which is required to sample from the ADC

void init_ADC (void)
{
  //Prepares ADC ports for recieving Sensor Signals
  P6SEL = BIT0 + BIT1 + BIT2 + BIT3 + BIT4 + BIT5 + BIT6 + BIT7;
  P5SEL = BIT0 + BIT1;
  P10SEL = BIT6 + BIT7;



  ADC12CTL0 = SHT0_9 + SHT1_9 + ADC12ON + REFON + MSC; //Turn on ADC12, use int.
osc.



  ADC12CTL1 = SHP + CONSEQ_3; //Sampling signal is sourced from the sampling timer
```

```
                                //Sequence of Channel CONVERSION

  ADC12MCTL0 = INCH_0;   //Input Channel A0
  ADC12MCTL1 = INCH_1;   //Input Channel A1
  ADC12MCTL2 = INCH_2;   //Input Channel A2
  ADC12MCTL3 = INCH_3;   //Input Channel A3
  ADC12MCTL4 = INCH_4;   //Input Channel A4
  ADC12MCTL5 = INCH_5;   //Input Channel A5
  ADC12MCTL6 = INCH_6;   //Input Channel A6
  ADC12MCTL7 = INCH_7;   //Input Channel A7
  ADC12MCTL12 = INCH_12;  //Input Channel A12
  ADC12MCTL13 = INCH_13;  //Input Channel A13
  ADC12MCTL14 = INCH_14;  //Input Channel A14
  ADC12MCTL15 = INCH_15 + EOS;  //Input Channel A15 and End of Sequence

  ADC12IE = 0x0F;
return;
}
/*******************************************************************************
VOID alarm (INT control_signal)
*******************************************************************************/
//alarm recieves a control signal
//depending on the input
//a specific alarm is shut on or off
void alarm (int control_signal)
{
  switch (control_signal){
  case 0:
    P10OUT = 0x00;
    break;
  case 1:
    P10OUT = BIT4;
    break;
  case 2:
    P10OUT = BIT5;
    break;
  case 3:
    P10OUT = BIT4 + BIT5;
    break;
  default:
    break;
  }
```

```
  return;
}

/*****************************************************************************
INT alarm_status (INT control_signal)
*****************************************************************************/
//alarm_status averages sensing data together to determine if input has
//passed an information threshold
int alarm_status (int control_signal)
{
  int conditions_met;
  int sum;
  int average;
  conditions_met = control_signal;

  switch (control_signal){
  case 0:
    break;
  case 1:
    sum = A4_SENSOR6[0];
    sum += A4_SENSOR6[2];
    sum += A4_SENSOR6[4];
    sum += A4_SENSOR6[7];
    average = sum / 4;
    if (average > 250)
      {conditions_met = 0;}
    break;
  case 2:
    sum = A5_SENSORZ[0];
    sum += A5_SENSORZ[2];
    sum += A5_SENSORZ[4];
    sum += A5_SENSORZ[7];
    average = sum / 4;
    if (average > 2800)
      {conditions_met = 0;}
    break;
  case 3:
    sum = A12_SENSOR[0];
    sum += A12_SENSOR[2];
    sum += A12_SENSOR[4];
    sum += A12_SENSOR[7];
    average = sum / 4;
```

```
    if (average > 2600)
      {conditions_met = 0;}
    break;
  default:
    break;

  }

return conditions_met;
}
/*****************************************************************************
VOID copyover (VOID)
*****************************************************************************/
//copyover moves the raw information from the ADC arrays into the MMC BUFFER
//
void copyover ( void)
{
  int i;
  int j;

  for (i = 0; i < 12; i++)
  {switch (i){
  case 0:
    for(j = 0; j < 8; j++)
    {mmc_buffer[A0_watch + j] = A0_SENSOR7[j];}
    break;
  case 1:
    for(j = 0; j < 8; j++)
    {mmc_buffer[A1_watch + j] = A1_SENSOR4[j];}
    break;
  case 2:
    for(j = 0; j < 8; j++)
    {mmc_buffer[A2_watch + j] = A2_SENSOR5[j];}
    break;
  case 3:
    for (j = 0; j < 8; j++)
    {mmc_buffer[A3_watch + j] = A3_SENSOR[j];}
    break;
  case 4:
    for (j = 0; j < 8; j++)
    {mmc_buffer[A4_watch + j] = A4_SENSOR6[j];}
    break;
```

```
  case 5:
    for (j = 0; j < 8; j++)
    {mmc_buffer[A5_watch + j] = A5_SENSORZ[j];}
    break;
  case 6:
    for (j = 0; j < 8; j++)
    {mmc_buffer[A6_watch + j] = A6_SENSOR3[j];}
    break;
  case 7:
    for (j = 0; j < 8; j++)
    {mmc_buffer[A7_watch + j] = A7_SENSOR2[j];}
    break;
  case 8:
    for (j = 0; j < 8; j++)
    {mmc_buffer[A8_watch + j] = IFG_CLEARER[j];}
    break;
  case 9:
    for (j = 0; j < 8; j++)
    {mmc_buffer[A9_watch + j] = IFG_CLEARER[j];}
    break;
  case 10:
    for (j = 0; j < 8; j++)
    {mmc_buffer[A10_watch + j] = IFG_CLEARER[j];}
    break;
  case 11:
    for (j = 0; j < 8; j++)
    {mmc_buffer[A11_watch + j] = A12_SENSOR[j];}
    break;
  default:
    break;

  }

  }
  return;
}
/*****************************************************************************
VOID watch_update (VOID)
*****************************************************************************/
//watch_update
//the watch variables act as indices which indicate locations within the MMC array
void watch_update(void)
```

```
{
  A0_watch = A0_watch + 8;
  if (A0_watch == 40)
  {A0_watch = 0;
   SD_FLAG = 1; }
  A1_watch = A0_watch + 40;
  A2_watch = A0_watch + 80;
  A3_watch = A0_watch + 120;
  A4_watch = A0_watch + 160;
  A5_watch = A0_watch + 200;
  A6_watch = A0_watch + 240;
  A7_watch = A0_watch + 280;
  A8_watch = A0_watch + 320;
  A9_watch = A0_watch + 360;
  A10_watch = A0_watch + 400;
  A11_watch = A0_watch + 440;

  return;
}



/*****************************************************************************
VOID sd_card_test (VOID)
*****************************************************************************/
//sd_card_test
//This function tests to see if the SD CARD is initialized and if it can be read
from
//and written to.  This is for debugging the SD card if it ceases to work.


void sd_card_test (void){


if (initMMC() == MMC_SUCCESS)
    {
      //card_state |= 1;
      memset(&mmc_buffer,0,512);
      mmcReadRegister (10, 16);
      mmc_buffer[7]=0;


      // Fill first Block (0) with 'A'
      memset(&mmc_buffer,'0',512);    //set breakpoint and trace mmc_buffer
contents
      mmcWriteBlock(0);
```

```
      // Fill second Block (1)-AbsAddr 512 with 'B'
      memset(&mmc_buffer,'1',512);
      mmcWriteBlock(512);

      // Read first Block back to buffer
      //DAVID HYDE PIERCE
      memset(&mmc_buffer,0x00,512);
      mmcReadBlock(0,512);
      memset(&mmc_buffer_test_1,'0',512);
      if(strncmp(&mmc_buffer[0], &mmc_buffer_test_1[0], 512)) state_mmc=0;

      // Read first Block back to buffer
      //Mel BrOoKs
      memset(&mmc_buffer,0x00,512);
      mmcReadBlock(512,512);
      memset(&mmc_buffer_test_1,'1',512);
      if(strncmp(&mmc_buffer[0], &mmc_buffer_test_1[0], 512)) state_mmc=0;

      memset(&mmc_buffer,0x00,512);
    }



      if(state_mmc == 1)
      {}
      if(state_mmc == 0)

      {}
return;
}
/*****************************************************************************
VOID InitFreq (VOID)
*****************************************************************************/
//This function stabilizes and intializes the clocks at the correct frequency

void InitFreq(void)
{
  int i;

  WDTCTL = WDTPW+WDTHOLD;                   // Stop watchdog timer
  FLL_CTL0 |= XCAP18PF;                     // Configure load caps
```

```
  FLL_CTL1 |= FLL_DIV_2 + XT2OFF;
  // Wait for xtal to stabilize
  do
  {
  IFG1 &= ~OFIFG;                           // Clear OSCFault flag
  for (i = 0x47FF; i > 0; i--);             // Time for flag to set
  }
  while ((IFG1 & OFIFG));                   // OSCFault flag still set?

  for(i=2100;i>0;i--);                      // Now with stable ACLK, wait for

}

/*******************************************************************************
ISRs
*******************************************************************************/
//This is the necessary ADC12 INterrupt routine

#pragma vector = ADC12_VECTOR
__interrupt void ADC12_ISR(void)
{

//Data stored on the ADC Memory Registers are stored in Arrays

//FINGER AND PALM FORCE SENSORS
A0_SENSOR7[adc_conversion_result_index] = ADC12MEM0;
A1_SENSOR4[adc_conversion_result_index] = ADC12MEM1;
A2_SENSOR5[adc_conversion_result_index] = ADC12MEM2;
A4_SENSOR6[adc_conversion_result_index] = ADC12MEM4;
A6_SENSOR3[adc_conversion_result_index] = ADC12MEM6;
A7_SENSOR2[adc_conversion_result_index] = ADC12MEM7;

//ACCELEROMETER Z AXIS
A5_SENSORZ[adc_conversion_result_index] = ADC12MEM5;

//GONIOMETRY AXES

A3_SENSOR[adc_conversion_result_index] = ADC12MEM3;
A12_SENSOR[adc_conversion_result_index] = ADC12MEM12;

//IFG CLEARER
IFG_CLEARER[adc_conversion_result_index] = ADC12MEM13;
```

```
IFG_CLEARER[adc_conversion_result_index] = ADC12MEM14;
IFG_CLEARER[adc_conversion_result_index] = ADC12MEM15;


//Increments or Resets the index
adc_conversion_result_index = (adc_conversion_result_index + 1) & (0x07);

if (adc_conversion_result_index == 0)
  {
    ADC12CTL0 &= ~ENC;
    adc_sets_are_ready = 1;
  }

//If the index is reset to 0, the array should be filled
//This alerts to the fact that the Array is filled with
//NEW data.  We'll then disable the ADC!

}
// mmc.c : MultiMediaCard functions: init, read, write ...
//
// Rollf Freiitag 5/2003
// Small changes have been made from original CODE



// MMC Lib
#ifndef _MMCLIB_C
#define _MMCLIB_C
//-----------------------------------------------------------------------
#include "sd.h"
//#include "led.h"

#include <msp430xG46x.h>
#include "math.h"
#include <string.h>


char mmcGetResponse(void);
char mmcGetXXResponse(const char resp);
char mmcCheckBusy(void);

void initSPI (void);
```

```
char mmc_buffer[512] = { 0 }; // Buffer for mmc i/o for data and registers


extern char card_state;       // 0 for no card found, 1 for card found (init
successfull)



//-------------------------------------------------------------------------




// setup usart1 in spi mode
void initSPI (void)
{


  ME2 |= USPIE1;         // Enable USART1 SPI mode
  UTCTL1 =  CKPH | SSEL1 | SSEL0 | STC;   // SMCLK, 3-pin mode, clock idle low,
data valid on rising edge, UCLK delayed
  UBR01 = 0x04;               // 0x02: UCLK/2 (4 MHz), works also with 3 and 4
  UBR11 = 0x00;               // -"-
  UMCTL1 = 0x00;         // no modulation
  UCTL1 = CHAR | SYNC | MM;   // 8-bit SPI Master **SWRST**
  P4SEL |= 0x38;         // P5.1-3 SPI option select
  P4DIR |= 0x2C;         // P5.0 output direction
//  P5OUT = 0xff;
  //while (!(IFG1 & UTXIFG0));      // USART1 TX buffer ready (empty)?


}



// Initialisieren
char initMMC (void)
{


   //raise SS and MOSI for 80 clock cycles
  //SendByte(0xff) 10 times with SS high
  //RAISE SS
  int i;
  char response=0x01;
```

```
  initSPI();
  //initialization sequence on PowerUp
  CS_HIGH();
  for(i=0;i<=9;i++)
    spiSendByte(0xff);
  CS_LOW();
  //Send Command 0 to put MMC in SPI mode
  mmcSendCmd(0x00,0,0x95);
  //Now wait for READY RESPONSE
  if(mmcGetResponse()!=0x01);


  while(response==0x01)
  {

   CS_HIGH();
   spiSendByte(0xff);
   CS_LOW();
   mmcSendCmd(0x01,0x00,0xff);
   response=mmcGetResponse();
  }
  CS_HIGH();
  spiSendByte(0xff);

  return MMC_SUCCESS;
}



// Ti added mmc Get Responce
char mmcGetResponse(void)
{
  //Response comes 1-8bytes after command
  //the first bit will be a 0
  //followed by an error code
  //data will be 0xff until response
  int i=0;

  char response;

  while(i<=64)
```

```
  {
   response=spiSendByte(0xff);
   if(response==0x00)break;
   if(response==0x01)break;
   i++;
  }
  return response;
}

char mmcGetXXResponse(const char resp)
{
  //Response comes 1-8bytes after command
  //the first bit will be a 0
  //followed by an error code
  //data will be 0xff until response
  int i=0;

  char response;

  while(i<=500)
  {
   response=spiSendByte(0xff);
   if(response==resp)break;
   i++;
  }
  return response;
}
char mmcCheckBusy(void)
{
  //Response comes 1-8bytes after command
  //the first bit will be a 0
  //followed by an error code
  //data will be 0xff until response
  int i=0;

  char response;
  char rvalue;
  while(i<=64)
  {
   response=spiSendByte(0xff);
   response &= 0x1f;
   switch(response)
```

```
    {
     case 0x05: rvalue=MMC_SUCCESS;break;
     case 0x0b: return(MMC_CRC_ERROR);
     case 0x0d: return(MMC_WRITE_ERROR);
     default:
            rvalue = MMC_OTHER_ERROR;
            break;
    }
   if(rvalue==MMC_SUCCESS)break;
    i++;
  }
  i=0;
  do
  {
   response=spiSendByte(0xff);
   i++;
  }while(response==0);
  return response;
}
// The card will respond with a standard response token followed by a data
// block suffixed with a 16 bit CRC.

// Ti Modification: long int -> long ; int -> long
char mmcReadBlock(const unsigned long address, const unsigned long count)
{
  unsigned long i = 0;
  char rvalue = MMC_RESPONSE_ERROR;

  // Set the block length to read
  if (mmcSetBlockLength (count) == MMC_SUCCESS) // block length could be set
    {
      // SS = LOW (on)
      CS_LOW ();
      // send read command MMC_READ_SINGLE_BLOCK=CMD17
      mmcSendCmd (17,address, 0xFF);
      // Send 8 Clock pulses of delay, check if the MMC acknowledged the read block
command
      // it will do this by sending an affirmative response
      // in the R1 format (0x00 is no errors)
      if (mmcGetResponse() == 0x00)
      {
        // now look for the data token to signify the start of
```

```
        // the data
        if (mmcGetXXResponse(MMC_START_DATA_BLOCK_TOKEN) ==
MMC_START_DATA_BLOCK_TOKEN)
          {
            // clock the actual data transfer and receive the bytes; spi_read
automatically finds the Data Block
            for (i = 0; i < 512; i++)
            mmc_buffer[i] = spiSendByte(0xff);  // is executed with card inserted

            // get CRC bytes (not really needed by us, but required by MMC)
            spiSendByte(0xff);
            spiSendByte(0xff);
            rvalue = MMC_SUCCESS;
          }
        else
          {
            // the data token was never received
            rvalue = MMC_DATA_TOKEN_ERROR;      // 3
          }
      }
      else
      {
        // the MMC never acknowledge the read command
        rvalue = MMC_RESPONSE_ERROR;      // 2
      }
    }
  else
    {
      rvalue = MMC_BLOCK_SET_ERROR; // 1
    }
  CS_HIGH ();
  spiSendByte(0xff);
  return rvalue;
}                       // mmc_read_block



//-----------------------------------------------------------------------
// Ti Modification: long int -> long
char mmcWriteBlock (const unsigned long address)
{
  unsigned long i = 0;
  char rvalue = MMC_RESPONSE_ERROR; // MMC_SUCCESS;
```

```
  //char c = 0x00;

  // Set the block length to read
  if (mmcSetBlockLength (512) == MMC_SUCCESS)   // block length could be set
    {
      // SS = LOW (on)
      CS_LOW ();
      // send write command
      mmcSendCmd (24,address, 0xFF);

      // check if the MMC acknowledged the write block command
      // it will do this by sending an affirmative response
      // in the R1 format (0x00 is no errors)
      if (mmcGetXXResponse(MMC_R1_RESPONSE) == MMC_R1_RESPONSE)
      {
        spiSendByte(0xff);
        // send the data token to signify the start of the data
        spiSendByte(0xfe);
        // clock the actual data transfer and transmitt the bytes
        for (i = 0; i < 512; i++)
          spiSendByte(mmc_buffer[i]);     // mmc_buffer[i];       Test: i & 0xff
        // put CRC bytes (not really needed by us, but required by MMC)
        spiSendByte(0xff);
        spiSendByte(0xff);
        // read the data response xxx0<status>1 : status 010: Data accected, status
101: Data
        //   rejected due to a crc error, status 110: Data rejected due to a Write
error.
          mmcCheckBusy();
      }
      else
      {
        // the MMC never acknowledge the write command
        rvalue = MMC_RESPONSE_ERROR;      // 2
      }
    }
  else
    {
      rvalue = MMC_BLOCK_SET_ERROR; // 1
    }
  // give the MMC the required clocks to finish up what ever it needs to do
//  for (i = 0; i < 9; ++i)
//    spiSendByte(0xff);
```

```
  CS_HIGH ();
  // Send 8 Clock pulses of delay.
  spiSendByte(0xff);
  return rvalue;
}                       // mmc_write_block




//-----------------------------------------------------------------------
void mmcSendCmd (const char cmd, unsigned long data, const char crc)
{
  char frame[6];
  char temp;
  int i;

  frame[0]=(cmd|0x40);
  for(i=3;i>=0;i--){
    temp=(char)(data>>(8*i));
    frame[4-i]=(temp);
  }
  frame[5]=(crc);
  for(i=0;i<6;i++)
    spiSendByte(frame[i]);
}



//--------------- set blocklength 2^n -------------------------------------------
---------
// Ti Modification: long int-> long
char mmcSetBlockLength (const unsigned long blocklength)
{
  //char rValue = MMC_TIMEOUT_ERROR;
  //char i = 0;

  // SS = LOW (on)
  CS_LOW();

  // Set the block length to read
  //MMC_SET_BLOCKLEN =CMD16
```

```
  mmcSendCmd(16, blocklength, 0xFF);

  // get response from MMC - make sure that its 0x00 (R1 ok response format)
  if(mmcGetResponse()!=0x00);

  CS_HIGH ();

  // Send 8 Clock pulses of delay.
  spiSendByte(0xff);

  return MMC_SUCCESS;
}                       // block_length

//TI added substitution routine for spi_read and spi_write

unsigned char spiSendByte(const unsigned char data)
{
 while ((IFG2&UTXIFG1) ==0);  // wait while not ready / for RX
 TXBUF1 = data;               // write
 while ((IFG2 & URXIFG1)==0); // wait for RX buffer (full)
 return (RXBUF1);
}

unsigned char spiReadByte()
{
 while ((IFG2 & URXIFG1)==0); // wait for RX buffer (full)
 return (RXBUF1);
}

void spiWriteByte(const unsigned char data)
{
 while ((IFG2&UTXIFG1) ==0);  // wait while not ready / for RX
 TXBUF1 = data;
}

// Reading the contents of the CSD and CID registers in SPI mode is a simple
// read-block transaction.

char mmcReadRegister (const char cmd_register, const unsigned char length)
{
  char uc = 0;
  char rvalue = MMC_TIMEOUT_ERROR;
```

```
//  char i = 0;

  if (mmcSetBlockLength (length) == MMC_SUCCESS)
    {
      CS_LOW ();
      // CRC not used: 0xff as last byte
      mmcSendCmd(cmd_register, 0x000000, 0xff);

      // wait for response
      // in the R1 format (0x00 is no errors)
      if (mmcGetResponse() == 0x00)
      {
       if (mmcGetXXResponse(0xfe)== 0xfe)
          for (uc = 0; uc < length; uc++)
            mmc_buffer[uc] = spiSendByte(0xff);
        // get CRC bytes (not really needed by us, but required by MMC)
        spiSendByte(0xff);
        spiSendByte(0xff);
      }
      else
      rvalue = MMC_RESPONSE_ERROR;
      // CS = HIGH (off)
      CS_HIGH ();

      // Send 8 Clock pulses of delay.
      spiSendByte(0xff);
    }
  CS_HIGH ();
  return rvalue;
}                       // mmc_read_register

//-------------------------------------------------------------------------
#endif /* _MMCLIB_C */
/*
      mmc.h: Dekcarations for Communikation with the MMC (see mmc.c) in unprotected
spi mode.

Pin configuration at MSP430F149:
---------------------------------
  MC              MC Pin          MMC           MMC Pin
  P5.4                  48          ChipSelect  1
  P5.1 / SlaveInMasterOut 45        DataIn            2
```

```
  .                           GND         3 (0 V)
  .                           VDD         4 (3.3 V)
  P5.3 UCLK1 / SlaveCLocK 47        Clock             5
  .                           GND         6 (0 V)
  P5.2 / SlaveOutMasterIn 46        DataOut     7
-----------------------------------------------------------------------

 Revisions
 Date             Author                                Revision
 11. May 2003           Rolf Freitag                          0.02
(2004: corrected MC pin numbers (switched only 45, 46))
*/

#ifndef _MMCLIB_H
#define _MMCLIB_H

#ifndef TXEPT                 // transmitter-empty flag
#define TEXPT 0x01
#endif

// macro defines
#define HIGH(a) ((a>>8)&0xFF) // high byte from word
#define LOW(a) (a&0xFF)       // low byte from word

#define CS_LOW()  P4OUT &= ~BIT2;   // Card Select
#define CS_HIGH() P4OUT |=  BIT2;         // Card Deselect

#define SPI_RXC (IFG2 & URXIFG1)
#define SPI_TXC (IFG2 & UTXIFG1)

#define SPI_RX_COMPLETE (IFG2 & URXIFG1)
#define SPI_TX_READY (IFG2 & UTXIFG1)

#define DUMMY 0xff



// Tokens (nessisary because at nop/idle (and CS active) only 0xff is on the
data/command line)
#define MMC_START_DATA_BLOCK_TOKEN        0xfe  // Data token start byte, Start
Single Block Read
#define MMC_START_DATA_MULTIPLE_BLOCK_READ      0xfe  // Data token start byte,
Start Multiple Block Read
```

```
#define MMC_START_DATA_BLOCK_WRITE        0xfe  // Data token start byte, Start
Single Block Write
#define MMC_START_DATA_MULTIPLE_BLOCK_WRITE     0xfc  // Data token start byte,
Start Multiple Block Write
#define MMC_STOP_DATA_MULTIPLE_BLOCK_WRITE      0xfd  // Data toke stop byte, Stop
Multiple Block Write



// an affirmative R1 response (no errors)
#define MMC_R1_RESPONSE       0x00



// this variable will be used to track the current block length
// this allows the block length to be set only when needed
// unsigned long _BlockLength = 0;

// error/success codes
#define MMC_SUCCESS           0x00
#define MMC_BLOCK_SET_ERROR   0x01
#define MMC_RESPONSE_ERROR    0x02
#define MMC_DATA_TOKEN_ERROR  0x03
#define MMC_INIT_ERROR        0x04
#define MMC_CRC_ERROR         0x10
#define MMC_WRITE_ERROR       0x11
#define MMC_OTHER_ERROR       0x12
#define MMC_TIMEOUT_ERROR     0xFF



// commands: first bit 0 (start bit), second 1 (transmission bit); CMD-number +
0ffsett 0x40
#define MMC_GO_IDLE_STATE     0x40    //CMD0
#define MMC_SEND_OP_COND      0x41    //CMD1
#define MMC_READ_CSD          0x49  //CMD9
#define MMC_SEND_CID          0x4a    //CMD10
#define MMC_STOP_TRANSMISSION       0x4c    //CMD12
#define MMC_SEND_STATUS       0x4d    //CMD13
#define MMC_SET_BLOCKLEN      0x50  //CMD16 Set block length for next read/write
#define MMC_READ_SINGLE_BLOCK       0x51  //CMD17 Read block from memory
#define MMC_READ_MULTIPLE_BLOCK 0x52    //CMD18
#define MMC_CMD_WRITEBLOCK    0x54  //CMD20 Write block to memory
#define MMC_WRITE BLOCK       0x58    //CMD25
#define MMC_WRITE_MULTIPLE_BLOCK 0x59   //CMD??
#define MMC_WRITE_CSD         0x5b  //CMD27 PROGRAM_CSD
```

```
#define MMC_SET_WRITE_PROT    0x5c    //CMD28
#define MMC_CLR_WRITE_PROT    0x5d    //CMD29
#define MMC_SEND_WRITE_PROT   0x5e    //CMD30
#define MMC_TAG_SECTOR_START  0x60    //CMD32
#define MMC_TAG_SECTOR_END    0x61    //CMD33
#define MMC_UNTAG_SECTOR      0x62    //CMD34
#define MMC_TAG_EREASE_GROUP_START 0x63 //CMD35
#define MMC_TAG_EREASE_GROUP_END 0x64   //CMD36
#define MMC_UNTAG_EREASE_GROUP      0x65    //CMD37
#define MMC_EREASE            0x66    //CMD38
#define MMC_READ_OCR          0x67    //CMD39
#define MMC_CRC_ON_OFF        0x68    //CMD40



//TI added sub function for top two spi_xxx

//my
void initSPI();
unsigned char spiReadByte();
void spiWriteByte(const unsigned char data);

// mmc init
char initMMC (void);
// send command to MMC
void mmcSendCmd (const char cmd, unsigned long data, const char crc);
// set MMC block length of count=2^n Byte
char mmcSetBlockLength (const unsigned long);
// read a size Byte big block beginning at the address.
char mmcReadBlock(const unsigned long address, const unsigned long count);
// write a 512 Byte big block beginning at the (aligned) adress
char mmcWriteBlock (const unsigned long address);
// Register arg1 der Laenge arg2 auslesen (into the buffer)
char mmcReadRegister(const char, const unsigned char);

unsigned char spiSendByte(const unsigned char data);

#endif /* _MMCLIB_H */
```

Appendix C: Project Parts List

Appendix D: Tekscan A201-100 Calibration Data

Sensor	Preconditioning	Force (lbs)	Force (N)	Resistance (Ω)	Conductance (S)
1	200 lbs	0.0	0.0	> 20M	
		9.9	44.0	136.7E+3	7.3E-6
		24.9	110.8	76.6E+3	13.1E-6
		40.5	180.2	54.3E+3	18.4E-6
		50.7	225.5	46.0E+3	21.7E-6
		59.9	266.4	40.0E+3	25.0E-6
		75.6	336.3	33.8E+3	29.6E-6
		80.7	359.0	33.2E+3	30.1E-6
		90.9	404.3	29.2E+3	34.2E-6
		100.1	445.3	26.9E+3	37.2E-6
		125.4	557.8	22.2E+3	45.0E-6
		149.9	666.8	18.7E+3	53.5E-6
2	100 lbs	0.0	0.0	>20M	
		10.5	46.7	136.6E+3	7.3E-6
		20.5	91.2	90.5E+3	11.0E-6
		25.1	111.7	78.3E+3	12.8E-6
		30.4	135.2	70.0E+3	14.3E-6
		39.6	176.1	58.3E+3	17.2E-6
		50.7	225.5	38.4E+3	26.0E-6
		60.1	267.3	33.6E+3	29.8E-6
		70.3	312.7	30.1E+3	33.2E-6
		74.5	331.4	28.8E+3	34.7E-6
		80.4	357.6	27.3E+3	36.6E-6
		90.8	403.9	25.0E+3	40.0E-6
		100.9	448.8	23.0E+3	43.5E-6
3	100 lbs	0.0	0.0	>20M	
		10.3	45.8	150.5E+3	6.6E-6
		20.2	89.9	93.0E+3	10.8E-6
		25.1	111.7	76.1E+3	13.1E-6
		30.4	135.2	65.7E+3	15.2E-6
		40.5	180.2	52.2E+3	19.2E-6
		50.0	222.4	42.6E+3	23.5E-6
		60.6	269.6	35.2E+3	28.4E-6
		70.1	311.8	30.7E+3	32.6E-6
		75.4	335.4	28.8E+3	34.7E-6
		80.4	357.6	27.3E+3	36.6E-6
		90.4	402.1	24.2E+3	41.3E-6
		99.8	443.9	21.8E+3	45.9E-6

Sensor	Preconditioning	Force (lbs)	Force (N)	Resistance Ω)	Conductance (S)
4	100 lbs	0.0	0.0	>20M	
		10.3	45.8	153.0E+3	6.5E-6
		20.5	91.2	100.1E+3	10.0E-6
		25.1	111.7	86.6E+3	11.5E-6
		29.9	133.0	74.7E+3	13.4E-6
		40.5	180.2	57.8E+3	17.3E-6
		50.9	226.4	46.0E+3	21.7E-6
		60.4	268.7	37.3E+3	26.8E-6
		70.5	313.6	31.2E+3	32.1E-6
		75.6	336.3	28.6E+3	35.0E-6
		79.6	354.1	27.3E+3	36.6E-6
		90.4	402.1	24.6E+3	40.7E-6
		100.5	447.0	22.7E+3	44.1E-6
5	100 lbs	0.0	0.0	>20M	
		10.8	48.0	164.4E+3	6.1E-6
		20.5	91.2	105.6E+3	9.5E-6
		25.1	111.7	88.0E+3	11.4E-6
		29.9	133.0	77.8E+3	12.9E-6
		40.1	178.4	62.7E+3	15.9E-6
		49.8	221.5	52.8E+3	18.9E-6
		60.1	267.3	45.7E+3	21.9E-6
		69.8	310.5	42.1E+3	23.8E-6
		74.7	332.3	40.0E+3	25.0E-6
		79.8	355.0	38.3E+3	26.1E-6
		90.4	402.1	36.2E+3	27.6E-6
		99.2	441.3	33.8E+3	29.6E-6
6	100 lbs.	0.0	0.0	>20M	
		10.5	46.7	163.0E+3	6.1E-6
		20.0	89.0	102.6E+3	9.7E-6
		25.1	111.7	86.2E+3	11.6E-6
		30.4	135.2	76.5E+3	13.1E-6
		40.3	179.3	63.2E+3	15.8E-6
		50.4	224.2	53.1E+3	18.8E-6
		60.4	268.7	46.8E+3	21.4E-6
		69.6	309.6	43.0E+3	23.3E-6
		75.4	335.4	40.9E+3	24.4E-6
		80.9	359.9	38.6E+3	25.9E-6
		90.1	400.8	35.8E+3	27.9E-6
		100.9	448.8	32.7E+3	30.6E-6

Sensor	Preconditioning	Force (lbs)	Force (N)	Resistance (Ω)	Conductance (S)
7	100 lbs	0.0	0.0	>20M	
		10.5	46.7	210.0E+3	4.8E-6
		20.2	89.9	129.1E+3	7.7E-6
		25.5	113.4	113.2E+3	8.8E-6
		30.4	135.2	97.8E+3	10.2E-6
		40.3	179.3	78.8E+3	12.7E-6
		50.2	223.3	67.4E+3	14.8E-6
		60.6	269.6	58.0E+3	17.2E-6
		70.1	311.8	51.3E+3	19.5E-6
		75.1	334.1	48.1E+3	20.8E-6
		80.2	356.7	44.6E+3	22.4E-6
		90.4	402.1	39.3E+3	25.4E-6
		100.9	448.8	34.6E+3	28.9E-6

Conductance to force characteristics of Tekscan A201-100 pressure sensors

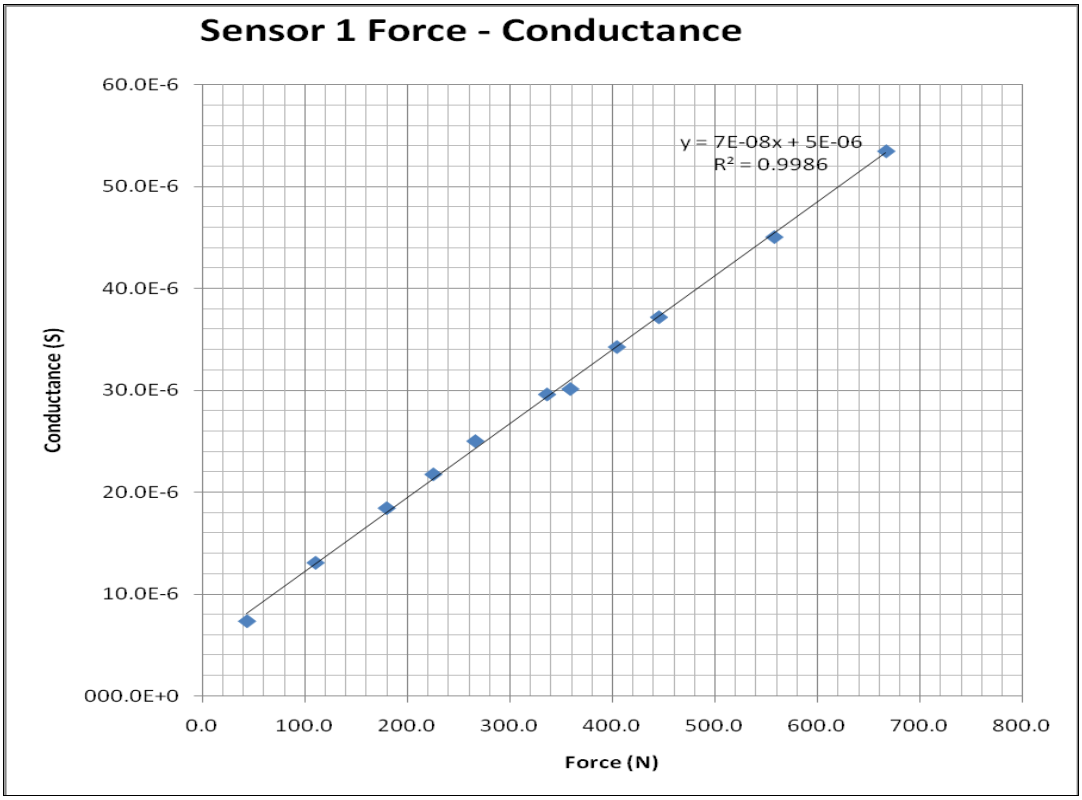

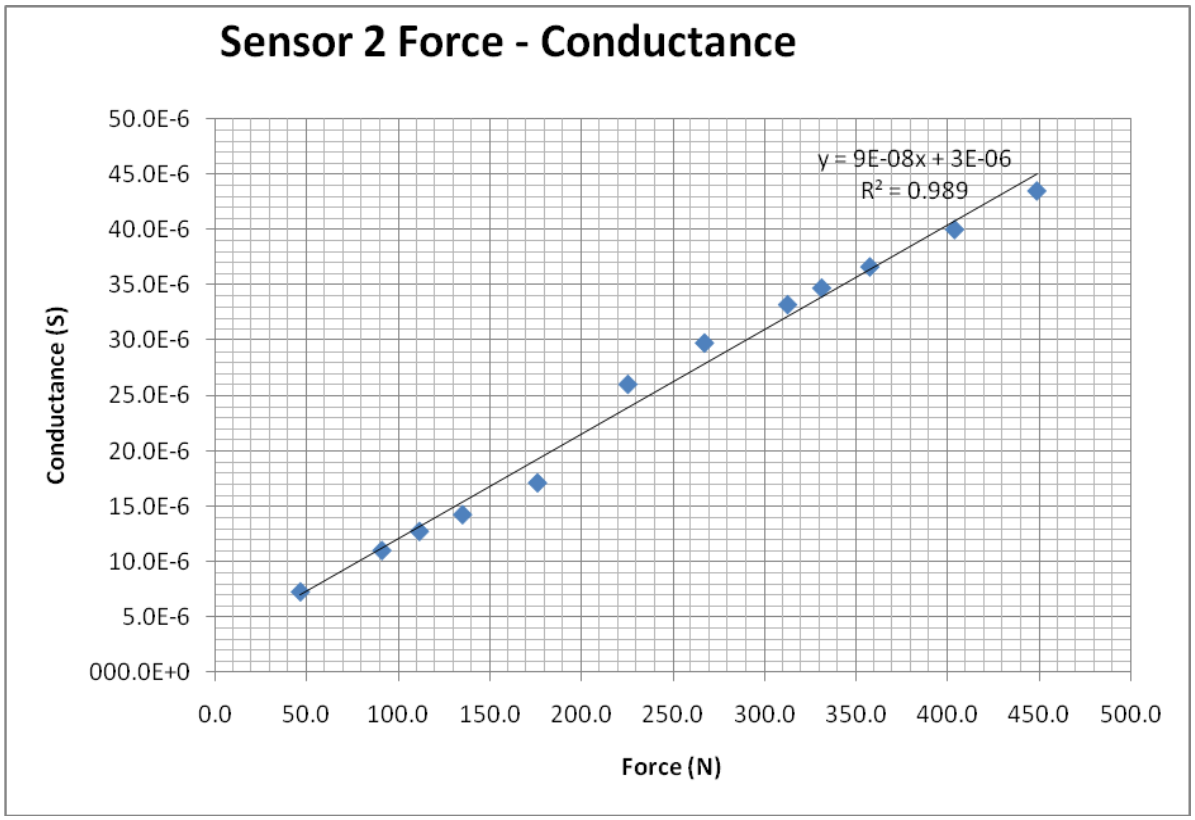
Sensor 2 Force - Conductance
y = 9E-08x + 3E-06
R² = 0.989
Conductance (S)
50.0E-6
45.0E-6
40.0E-6
35.0E-6
30.0E-6
25.0E-6
20.0E-6
15.0E-6
10.0E-6
5.0E-6
000.0E+0
0.0
50.0
100.0
150.0
200.0
250.0
300.0
350.0
400.0
450.0
500.0
Force (N)

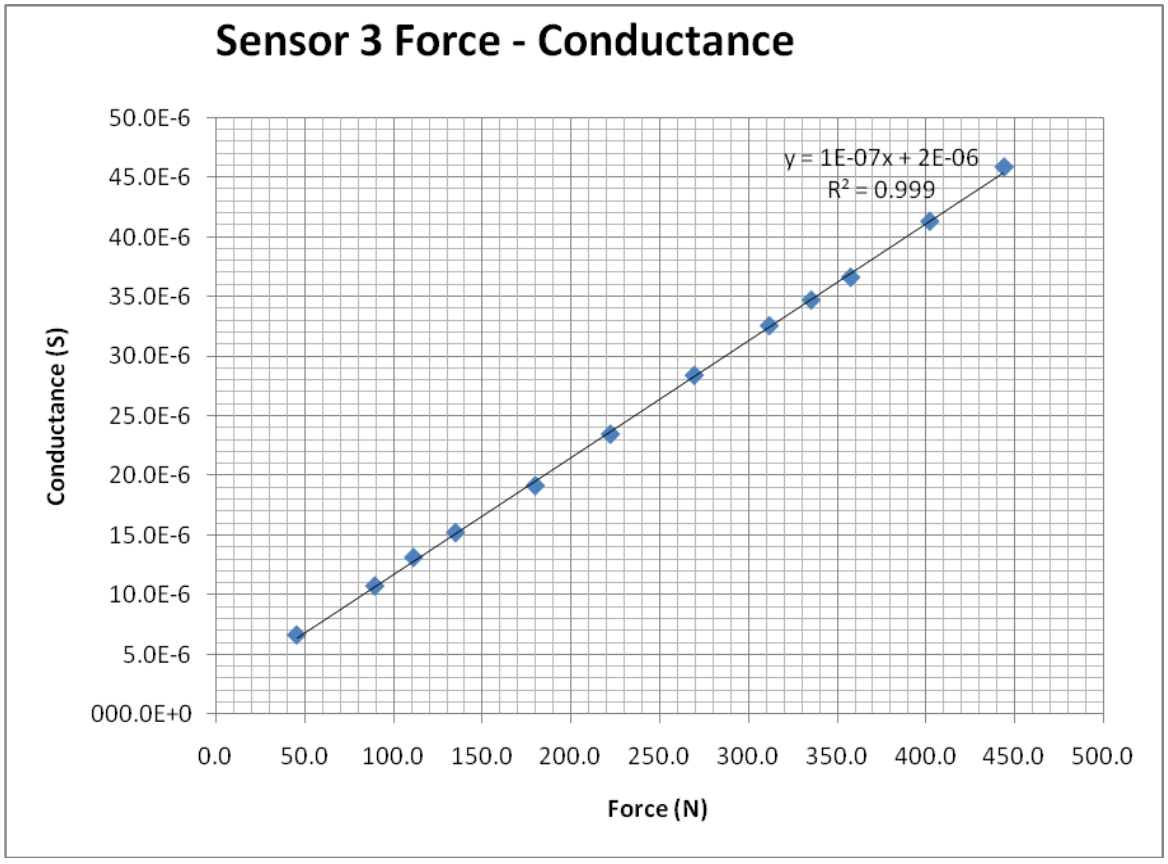
Sensor 3 Force - Conductance
y = 1E-07x + 2E-06
R² = 0.999
Conductance (S)
50.0E-6
45.0E-6
40.0E-6
35.0E-6
30.0E-6
25.0E-6
20.0E-6
15.0E-6
10.0E-6
5.0E-6
000.0E+0
0.0
50.0
100.0
150.0
200.0
250.0
300.0
350.0
400.0
450.0
500.0
Force (N)

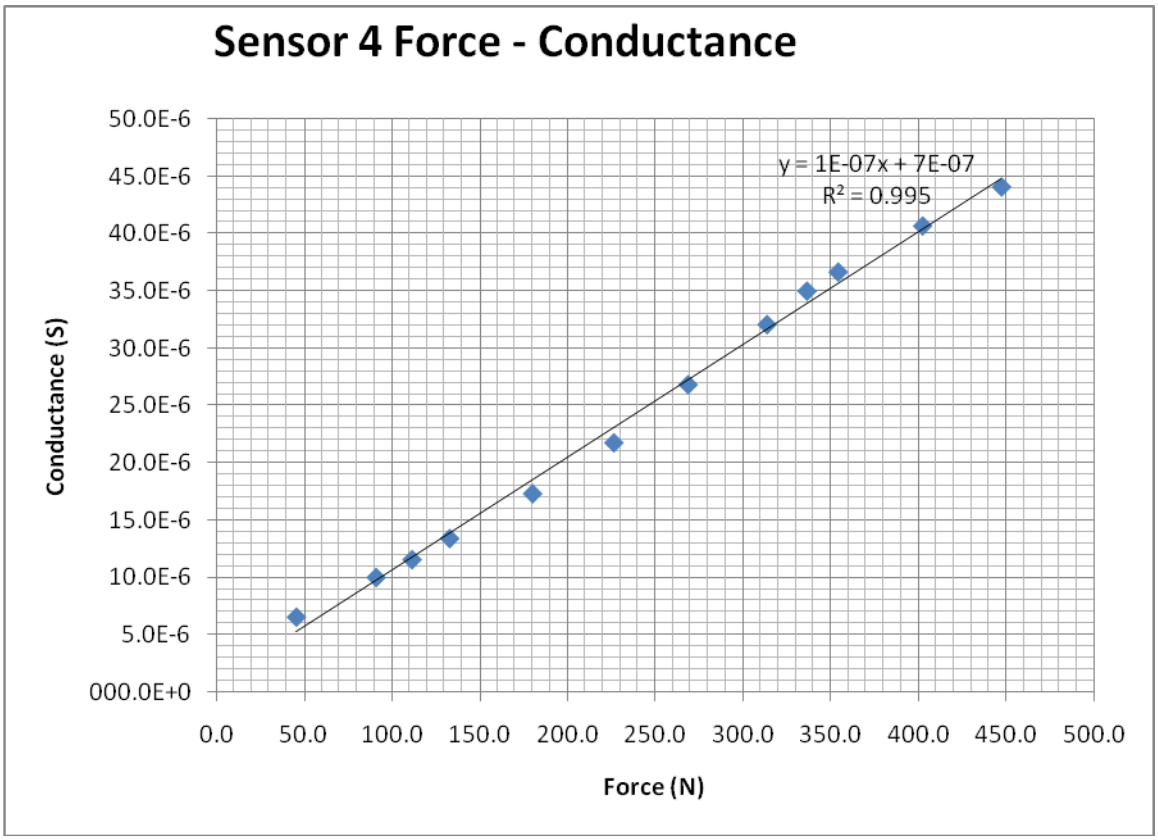
Sensor 4 Force - Conductance
y = 1E-07x + 7E-07
R² = 0.995
Conductance (S)
50.0E-6
45.0E-6
40.0E-6
35.0E-6
30.0E-6
25.0E-6
20.0E-6
15.0E-6
10.0E-6
5.0E-6
000.0E+0
0.0
50.0
100.0
150.0
200.0
250.0
300.0
350.0
400.0
450.0
500.0
Force (N)

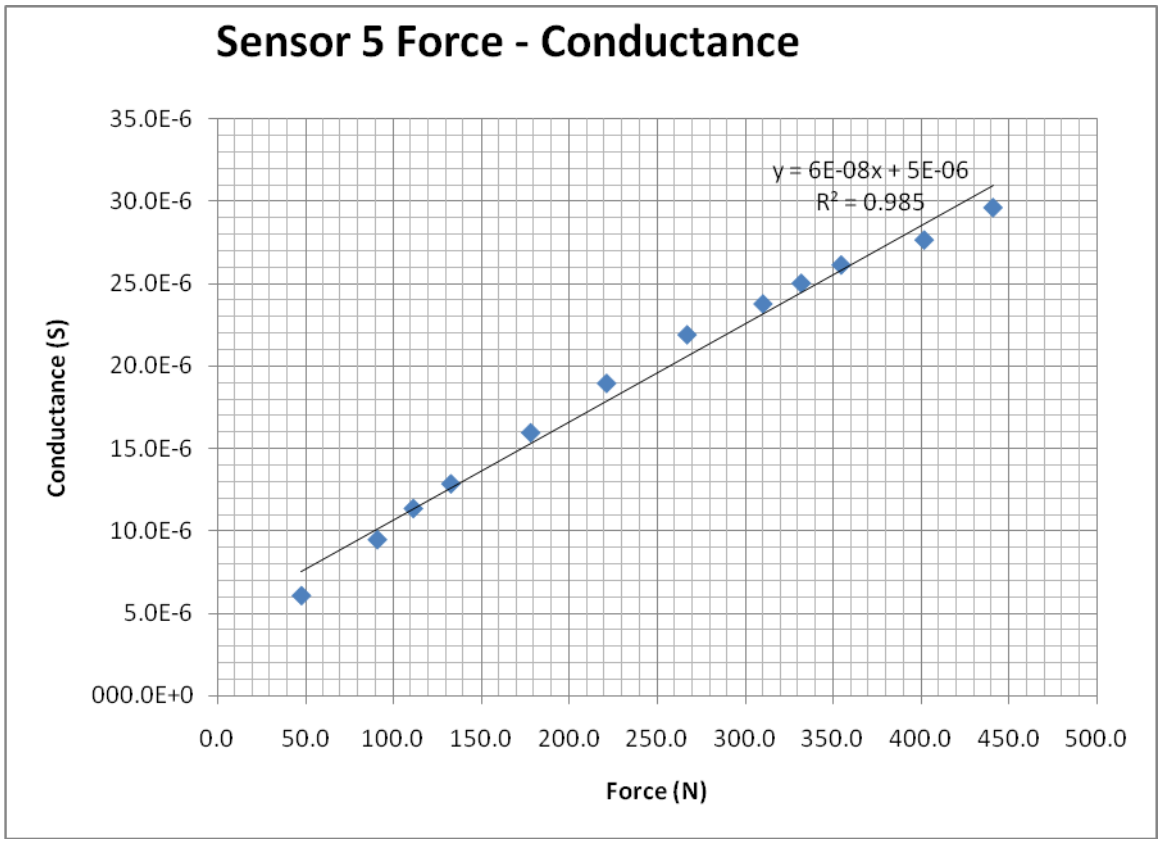
Sensor 5 Force - Conductance
y = 6E-08x + 5E-06
R² = 0.985
Conductance (S)
35.0E-6
30.0E-6
25.0E-6
20.0E-6
15.0E-6
10.0E-6
5.0E-6
000.0E+0
0.0
50.0
100.0
150.0
200.0
250.0
300.0
350.0
400.0
450.0
500.0
Force (N)

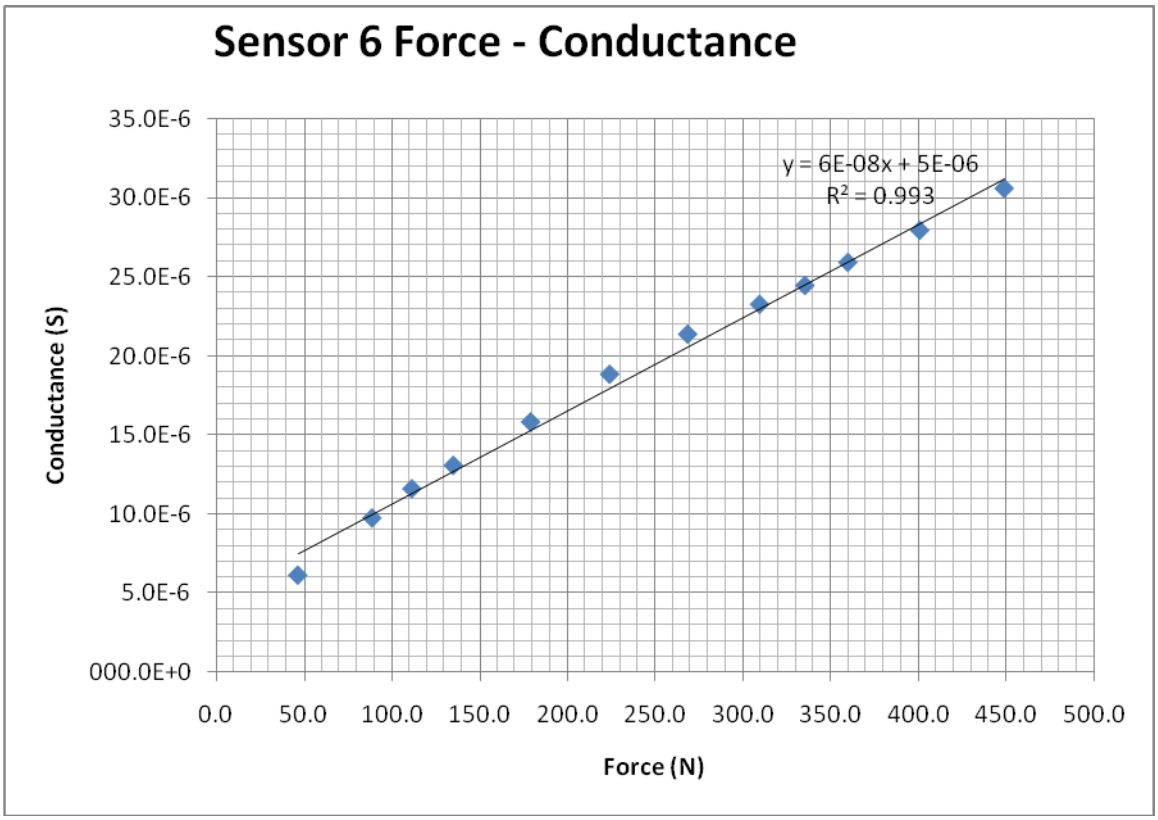
Sensor 6 Force - Conductance
y = 6E-08x + 5E-06
R² = 0.993
Conductance (S)
35.0E-6
30.0E-6
25.0E-6
20.0E-6
15.0E-6
10.0E-6
5.0E-6
000.0E+0
0.0
50.0
100.0
150.0
200.0
250.0
300.0
350.0
400.0
450.0
500.0
Force (N)

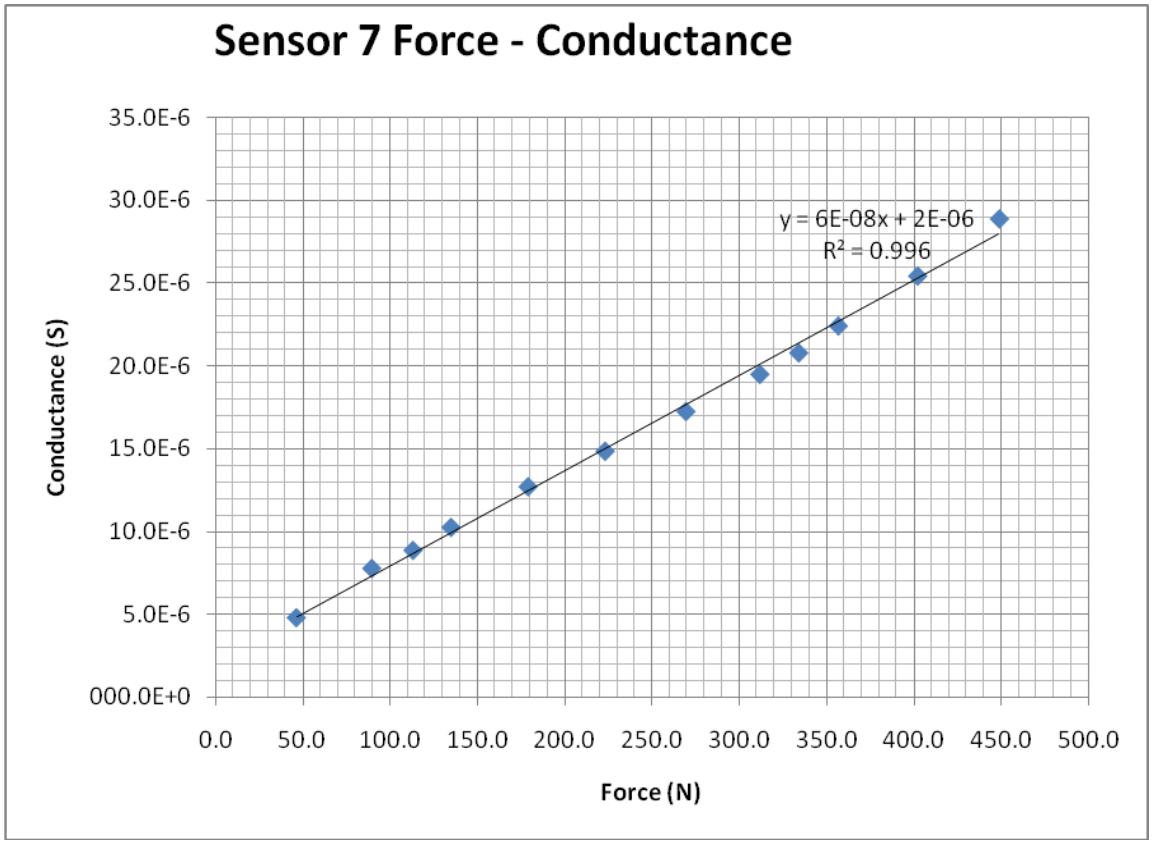
Sensor 7 Force - Conductance
y = 6E-08x + 2E-06
R² = 0.996
Conductance (S)
35.0E-6
30.0E-6
25.0E-6
20.0E-6
15.0E-6
10.0E-6
5.0E-6
000.0E+0
0.0
50.0
100.0
150.0
200.0
250.0
300.0
350.0
400.0
450.0
500.0
Force (N)

Appendix E: MATLAB Code for Error Analysis

```
%Makemyfilters, an M-File whose purpose is to make the highpass and lowpass
%filters that will make up the band limiting and frequency weighting circuits

maxfreq=1600;
f=-maxfreq:1:maxfreq;
%f=0:1:1500;
s=2*pi*f*j;
%fpos=f(1601:3201);
%HPF
F1=6.31;
FF1=F1-.12*F1;
Q1=0.71;
QQ1=Q1-.01*Q1;
HPF=s.^2./(s.^2+2*pi*F1/Q1*s+4*pi^2*(F1^2));
HHPF=s.^2./(s.^2+2*pi*FF1/QQ1*s+4*pi^2*(FF1^2));
%LPF1
F2=1258.9;
FF2=F2-.12*F2;
Q2=0.71;
QQ2=Q2-.01*Q2;
LPF1=4*pi^2*F2^2./(s.^2+2*s*pi*F2/Q2+4*pi^2*(F2^2));
LLPF1=4*pi^2*FF2^2./(s.^2+2*s*pi*FF2/QQ2+4*pi^2*(FF2^2));
%LPF2
F3=15.915;
FF3=F3-.12*F3;
Q3=0.64;
QQ3=Q3-.01*Q3;
LPF2=4*pi^2*F3^2./(s.^2+2*pi*F3/Q3*s+4*pi^2*(F3^2));
LLPF2=4*pi^2*FF3^2./(s.^2+2*pi*FF3/QQ3*s+4*pi^2*(FF3^2));
%Szero
%R7=1.111e3;
R7=20e6;
RR7=R7-.02*R7;
%R8=10e3;
R8=20e6;
RR8=R8-.01*R8;
C7=1e-9;
CC7=C7-.1*C7;
Szero=(R7+R8*(R7*s*C7+1))./R7;
SSzero=(RR7+RR8*(RR7*s*CC7+1))./RR7;
myfilt=HPF.*LPF1.*LPF2.*Szero./10; %band limited, f-weighted filter
myBADfilt=HHPF.*LLPF1.*LLPF2.*SSzero./10;
%myfiltpos=myfilt(1601:3201); %positive frequencies only
%ISO 5349-1 Band Limiting Filter BL
f1=6.31;
f2=1258.9;
q1=0.71;
BL=4*pi^2*f2^2*s.^2./((s.^2+2*pi*f1/q1*s+4*pi^2*(f1^2)).*(s.^2+2*pi*f2*s./q1+4*pi^2
*f2^2));
%ISO 5349-1 Frequequency Weighting Filter FW
f3=15.915;
q2=0.64;
```

```
FW=2*pi*f3^2*(s+2*pi*f3)./((s.^2+2*pi*f3*s./q2+4*pi^2*f3^2)*f3);
BLFW=BL.*FW; %ISO Band Limiting Frequency Weighting Filter
%BLFWpos=BLFW(1601:3201); %Positive Values Only



%Create an input waveform
fo =40;   %frequency of the sine wave
Fs = 3201; %sampling rate
Ts = 1/Fs; %sampling time interval
t = 0:Ts:1-Ts; %sampling period
n = length(t); %number of samples
y=20*sin(2*pi*fo*t);

[Y,frange]= centeredFFT(y,Fs); %convert input waveform to the frequency domain
filtered=Y.*myfilt; %perform band limiting and Frequency weighting
filteredbad=Y.*myBADfilt;
ifiltered=(2/0.0006248)*ifft(ifftshift(filtered)); %bring output back to time
domain, fix ifft scaling & shifting
ifilteredbad=(2/0.0006248)*ifft(ifftshift(filteredbad));
%figure;
% subplot(2,1,1), plot(t,y); %input of filter in time domain
% subplot(2,1,2),  plot(t,ifiltered); %output of filter in time domain
%'RMS of input:';
%RMSin=sqrt(mean(y.^2));
Tcl=0:1/30:30;
%'RMS of output:';
Ah=sqrt(3*mean(ifiltered.^2))
Ahbad=sqrt(3*mean(ifilteredbad.^2));
A8=Ahbad*((Tcl/8).^.5);
%'GOOD Time left T:';
T=8*(2.5/Ah)^2-Tcl;
%'BAD Time left T:';
Tbad=8*(2.5/Ahbad)^2-Tcl;
Terror=(Tbad-T)/T
Slope=1/(4*sqrt(2))*Ahbad./(Tcl.^.5);
Test=(2.5-A8)./Slope;
subplot(5,1,1),plot(Tcl,T),title('Correct Time Value Tr');
subplot(5,1,2),plot(Tcl,Test),title('Estimated Time value Test');
subplot(5,1,3),plot(Tcl,T-Test),title('Tr-Test');
subplot(5,1,4),plot(Tcl,Tbad),title('Bad Time Value Tbad');
subplot(5,1,5),plot(Tcl,T-Tbad),title('Tr-Tbad');



function [X,freq]=centeredFFT(x,Fs)
%this is a custom function that helps in plotting the two-sided spectrum
%x is the signal that is to be transformed
%Fs is the sampling rate
N=length(x);
%this part of the code generates that frequency axis
if mod(N,2)==0
    k=-N/2:N/2-1; % N even
else
    k=-(N-1)/2:(N-1)/2; % N odd
```

```
end
T=N/Fs;
freq=k/T;  %the frequency axis
%takes the fft of the signal, and adjusts the amplitude accordingly
X=fft(x)/N; % normalize the data
X=fftshift(X); %shifts the fft data so that it is centered
```

Appendix F: Vibration magnitudes for different tools [7]

MANUFACTURER	MODEL NO.	DESCRIPTION	Vibration Magnitude in m/s²*	Max time to reach EAV 2.5 m/s² A(8) hours/mins	Max time to reach ELV 5 m/s² A(8) hours/mins	HSE points per hour
BELLE ENGINEERING	BREAKER 2021X U/D	HYDRAULIC BREAKER GUN	8.6	0.41	2.44	147
BELLE ENGINEERING	BREAKER 2025X PAN	HYDRAULIC BREAKER GUN	8.4	0.43	2.52	140
BELLE ENGINEERING	CFS 450 YANMAR	FLOOR SAW	2.9	5.54	23.36	17
BELLE ENGINEERING	COMPACTX	FLOOR SAW	2.8	6.31	>24.00	15
BELLE ENGINEERING	PCX350	COMPACTOR PLATE	1.6	18.43	>24.00	5
BELLE ENGINEERING	PCX400	COMPACTOR PLATE	2.1	11.33	>24.00	9
BELLE ENGINEERING	PCX450	COMPACTOR PLATE	1.9	13.35	>24.00	7
BELLE ENGINEERING	PCX500	COMPACTOR PLATE	2	12.04	>24.00	8
DEWALT	D25404K	COMBINATION HAMMER	11.4	0.23	1.33	259
DEWALT	D25701K	COMBINATION HAMMER	10.1	0.29	1.58	204
DEWALT	D25730K	COMBINATION HAMMER	12.7	0.19	1.14	322
DEWALT	D25840K	DEMOLITION HAMMER	14	0.15	1.01	393
DEWALT	D25900K	DEMOLITION HAMMER	12.9	0.18	1.12	334
DEWALT	D25940K	DEMOLITION HAMMER	11.9	0.21	1.24	284
DEWALT	D28113	ANGLE GRINDER 115mm	11.2	0.24	1.36	251
DEWALT	D28117	ANGLE GRINDER 115mm	8.3	0.44	2.56	136
DEWALT	D28415	ANGLE GRINDER 230mm	6.6	1.08	4.34	88
DEWALT	DC212N	ROTARY HAMMER DRILL CORDLESS	7.9	0.48	3.12	125
DEWALT	DC224KA	ROTARY HAMMER DRILL CORDLESS	7.3	0.57	3.48	105
DEWALT	DC234KL	ROTARY HAMMER DRILL CORDLESS	8	0.47	3.08	128
DIMAS - PARTNER	K1250	PETROL POWERED RAIL SAW	9.2	0.36	2.23	168
DIMAS - PARTNER	K2500	CUT OFF SAW	4.6	2.22	9.28	42
DIMAS - PARTNER	K750	CUT OFF SAW	4.4	2.38	10.31	38
DIMAS - PARTNER	K950	CUT OFF SAW	8.9	0.38	2.32	158
HILTI	AG125-S	ANGLE GRINDER 125mm	5.4	3.08	12.34	32
HILTI	AG230-S	ANGLE GRINDER 230mm	8.7	0.40	2.39	151
HILTI	DC125-S	ANGLE GRINDER 125mm	7.1	0.59	3.57	101
HILTI	DC230	ANGLE GRINDER 230mm	6.6	1.09	4.35	87
HILTI	DD100	DIAMOND CORE DRILL (RIG HELD)	4.6	2.20	9.21	43
HILTI	DD100	DIAMOND CORE DRILL (HAND HELD)	9.4	0.34	2.17	175
HILTI	DD130	DIAMOND CORE DRILL (RIG STAND)	2.2	10.20	>24.00	10
HILTI	DD130	DIAMOND CORE DRILL (HAND HELD)	7.1	0.59	3.57	101
HILTI	DD200	DIAMOND CORE DRILL	5.8	1.30	6.00	67
HILTI	SF-151-A (NiMH)	DRILL / SCREWDRIVER	2.7	6.50	>24.00	15
HILTI	SFH-151-A (NiMH)	ROTARY HAMMER DRILL CORDLESS	12.5	0.19	1.16	315
HILTI	SF 180-A	ROTARY HAMMER DRILL CORDLESS	4.1	2.59	11.57	33
HILTI	TE104	BREAKER & SCALER	8.6	0.41	2.42	148
HILTI	TE16	ROTARY HAMMER DRILL	13.3	0.17	1.08	354
HILTI	TE16-C	ROTARY HAMMER DRILL	11.4	0.23	1.32	260
HILTI	TE2	ROTARY HAMMER DRILL	13	0.18	1.11	338
HILTI	TE2-A	ROTARY HAMMER DRILL CORDLESS	9.6	0.33	2.10	184
HILTI	TE2-M	ROTARY HAMMER DRILL	10.2	0.29	1.55	208
HILTI	TE35	COMBINATION HAMMER	10.3	0.28	1.53	212
HILTI	TE505	BREAKER	12.9	0.18	1.12	333
HILTI	TE56-ATC	COMBINATION HAMMER	10	0.30	1.59	202
HILTI	TE6-A	ROTARY HAMMER DRILL CORDLESS	8.4	0.43	2.50	141
HILTI	TE6-S	ROTARY HAMMER DRILL	11.3	0.24	1.34	255
HILTI	TE706AVR	BREAKER	6.6	1.09	4.35	87
HILTI	TE76P-ATC	COMBINATION HAMMER	11.9	0.21	1.24	285
HILTI	TE905AVR	BREAKER	9.3	0.35	2.19	173
HIRE TECHNICIANS GROUP LTD	HT7-2	FLOOR EDGING SANDER	3.1	5.12	20.49	19
HIRE TECHNICIANS GROUP LTD	HT8-1	FLOOR SANDER	1.8	15.26	>24.00	6
HIRE TECHNICIANS GROUP LTD	HTF-2	FLOOR REFINISHING SANDER	9	0.37	2.28	162
JCB	HM22	MEDIUM HYDRAULIC BREAKER GUN BEAVER	4.6	2.22	9.27	42
JCB	HM25	HEAVY DUTY HYDRAULIC BREAKER GUN BEAVER	7	1.01	4.05	98
MACDONALD AIR TOOLS	15PVR	LIGHT BREAKER 18KG	5	2.00	8.02	50
MACDONALD AIR TOOLS	17PVR	LIGHT BREAKER 21KG	3.8	3.27	13.47	29
MACDONALD AIR TOOLS	19TVR	LIGHT BREAKER 25.5KG	5.6	1.34	6.17	64
MACDONALD AIR TOOLS	1UFVR	POLE SCABBLER	7.8	0.49	3.16	122
MACDONALD AIR TOOLS	23TVR	BREAKER 26.5KG	7.2	0.58	3.51	104
MACDONALD AIR TOOLS	28S-VRT	MEDIUM WEIGHT PAVING BREAKER	4.6	2.21	9.22	43
MACDONALD AIR TOOLS	34AVRS	HEAVY WEIGHT PAVING BREAKER 36KG	6.5	1.11	4.42	85
MACDONALD AIR TOOLS	CH4VRS	LIGHT WEIGHT CHIPPING HAMMER 6.5KG	4.2	2.49	11.17	35
MACDONALD AIR TOOLS	DM11VRS	HEAVY WEIGHT DEMOLITION PICK 13.5KG	5.2	1.50	7.19	55
MACDONALD AIR TOOLS	DM12VRS	HEAVY WEIGHT DEMOLITION PICK 16.5KG	4.2	2.48	11.14	36
MACDONALD AIR TOOLS	DR4VRS	LIGHT WEIGHT ROCK DRILL 7KG	5.3	1.48	7.10	56
MACDONALD AIR TOOLS	MSG3VR	3- HEAD HAND SCABBLER	4.9	2.08	8.30	47
MACDONALD AIR TOOLS	S1VR	1- HEAD HAND SCABBLER	3.8	3.28	13.51	29
MACDONALD AIR TOOLS	MH202032	HYDRAULIC BREAKER GUN	7.9	0.48	3.11	126
MACDONALD AIR TOOLS	UV3R	3- HEAD TROLLEY SCABBLER	3.6	3.54	15.36	26
MACDONALD AIR TOOLS	UV5R	5- HEAD TROLLEY SCABBLER	3.9	3.21	13.25	30
MAKITA	4112HS	ELECTRIC STONE CUTTER	7.2	0.59	3.54	103
MAKITA	8444DWFE	ROTARY HAMMER DRILL CORDLESS	15.3	0.13	0.51	471
MAKITA	9015B	ANGLE GRINDER 125mm	7.2	0.57	3.50	105
MAKITA	9069	ANGLE GRINDER 230mm	6.1	1.21	5.25	74
MAKITA	9404	BELT SANDER 100mm	2.8	6.20	>24.00	16
MAKITA	9555NB	ANGLE GRINDER 125mm	7.4	0.54	3.37	111
MAKITA	9557NB	ANGLE GRINDER 115mm	6.4	1.14	4.57	81
MAKITA	9564CV	ANGLE GRINDER 115mm	5.5	1.31	6.03	66
MAKITA	9565CV	ANGLE GRINDER 125mm	7.7	0.51	3.22	119
MAKITA	BRH200	ROTARY HAMMER DRILL CORDLESS	10.1	0.29	1.57	205
MAKITA	DPC6410	CUT OFF SAW	7.4	0.55	3.39	110
MAKITA	GA9020	ANGLE GRINDER 230mm	9.6	0.32	2.10	185
MAKITA	GA9040	ANGLE GRINDER 230mm	9.7	0.32	2.07	190
MAKITA	HM0860C	DEMOLITION HAMMER	18.2	0.09	0.36	662
MAKITA	HM1202C	DEMOLITION HAMMER	15.7	0.12	0.49	493
MAKITA	HM1810	DEMOLITION HAMMER	10.5	0.27	1.48	222
MAKITA	HP2071F	PURCUSSION DRILL	15.3	0.13	0.51	468
MAKITA	HR1830	ROTARY HAMMER DRILL	11.1	0.24	1.37	248
MAKITA	HR2020	ROTARY HAMMER DRILL	11.2	0.24	1.37	249
MAKITA	HR2440	ROTARY HAMMER DRILL	14	0.15	1.02	389
MAKITA	HR2450T	ROTARY HAMMER DRILL	12.4	0.19	1.18	309
MAKITA	HR3000C	ROTARY HAMMER DRILL 4KG	13.1	0.18	1.10	341
MAKITA	HR4011C	ROTARY HAMMER DRILL 6KG	9.3	0.35	2.19	172
MAKITA	HR4500C	ROTARY HAMMER DRILL 8KG	15.9	0.12	0.47	508
MAKITA	HR5001C	ROTARY HAMMER DRILL 10KG	20.4	0.07	0.29	833
MAKITA	JR3070CT	RECIPROCATING SAW	12.5	0.19	1.17	313
MILWAUKEE	AGV 16-125 QXC	ANGLE GRINDER 125mm	5.4	1.42	6.48	59
MILWAUKEE	LOKTOR P 18 TXC	ROTARY HAMMER DRILL CORDLESS	5.9	1.27	5.49	69
MILWAUKEE	PHE 40 SQ	ROTARY HAMMER DRILL	17.1	0.10	0.41	584
MILWAUKEE	PSH 18	RECIPROCATING SAW CORDLESS	13.3	0.17	1.08	354
MILWAUKEE	V28 CS	CIRCULAR SAW 165mm CORDLESS	1.3	>24.00	>24.00	3
MILWAUKEE	V28 HX	ROTARY HAMMER DRILL CORDLESS	18.4	0.09	0.35	676
MILWAUKEE	V28 PD	ROTARY HAMMER DRILL CORDLESS	11.4	0.23	1.33	259
SPE	BEF 200-1	MULTIPLANE ELECTRIC	4.4	2.32	10.08	40
SPE	BEF 200-4	MULTIPLANE PETROL	8.2	0.44	2.58	135
SPE	BEF275-1	MULTIPLANE PETROL	5.3	1.46	7.02	57
SPE	DFG250-2	DIAMOND FLOOR GRINDER PETROL	4.9	2.07	8.28	47
SPE	DFG400-4	DIAMOND FLOOR GRINDER PETROL	5.6	1.36	6.25	62
SPE	DFG400-5	DIAMOND FLOOR GRINDER ELECTRIC	1.2	>24.00	>24.00	3
SPE	MS230-1	FLOOR TILE LIFTER ELECTRIC	13.5	0.16	1.05	367
SPE	MS330-1	FLOOR TILE LIFTER ELECTRIC	9.4	0.34	2.17	176
SPE	STR701-1	MULTIPURPOSE PREPARATION SYSTEM ELECTRIC	1.2	>24.00	>24.00	3
STIHL	TS400	CUT OFF SAW	5.7	1.31	6.03	66
TAYLOR CONSTRUCTION PLANT	HI-C40	ROCK CRUSHER	6.3	1.15	4.59	80
TAYLOR CONSTRUCTION PLANT	HI-T500	MINI DUMPER	3.5	3.59	15.57	25

Appendix G: Technical Email Correspondence

G-1: Corresponence with Dr. O'Sullivan

From: Leonard.O'Sullivan [leonard.osullivan@ul.ie]
Sent: Friday, August 22, 2008 6:35 AM
To: Ledoux, Nikolas
Subject: RE: QTC sensor info

Hi Nick,

One sensor on each digit will be fine for the prototype. It is desirable to have sensors that work up to the full range, but if
it adds considerably to cost then up to 100N will do for the prototype.
If you have any further questions let me know.

All the best,

Len.

From: Leonard.O'Sullivan [leonard.osullivan@ul.ie]
Sent: Friday, October 03, 2008 10:35 AM
To: Ledoux, Nikolas
Subject: RE: sensitivity adjustment

Hi Nick,

If you can measure up to about 100N reliably that would be plenty.

Len.

From: Leonard.O'Sullivan
Sent: 08 October 2008 18:15
To: 'Ledoux, Nikolas'
Subject: RE: noise question

I would have thought 50 through 60 as a precaution. Best see how it turns out. As long as you can get a reasonably clean signal it will be fine for this prototype.

Thanks

Len.

G-2: Correspondence with David Pinchefsky

From: David Pinchefsky [pinchefsky@nexgenergo.com]
Sent:Thursday, September 04, 2008 9:53 AM
To: Ledoux, Nikolas

Dear Nikolas,

For both of these you will need the Base system which includes the Interface module

and software. You will also need the high pressure cal jig for the GPMS probably. Also, the ISS (Octopus format) uses the same sensors as the glove but you have less of them?

See: http://www.nexgenergo.com/ergonomics/nexintel.html

David Pinchefsky, B.A.Sc., Eng.
NexGen Ergonomics Inc.

From: David Pinchefsky [pinchefsky@nexgenergo.com]
Sent: Wednesday, September 03, 2008 3:30 PM
To: Ledoux, Nikolas
Subject: FSA FlexForm sensor and FSA Hand Sensor

Dear Nikolas,

Thank-you for your inquiry for " pricing of the FSA FlexForm sensor and FSA Hand Sensor" which was forwarded to us by Vista/FSA as we handle the ergonomics and biomechanics markets in North America. I have attached the complete price list for your reference.
Could you please advise what you mean by a Flexform sensor? Please do not hesitate to contact us with any other questions.

David Pinchefsky, B.A.Sc., Eng.
NexGen Ergonomics Inc.

G-3: Correspondence with Peter Craik

From: Peter Craik [peter@steadlands.com]
Sent: Tuesday, August 19, 2008 9:46 AM
To: Ledoux, Nikolas
Subject: RE: Interlink FSR pricing

HI Nik

ALL FSRs exhibit hysteresis....not a lot can be done about it. No conditioning exercises are necessary.

Peter

G-4: Correspondence with Gail Shaw

From: Shaw, Gail [gshaw@interlinkelec.com]
Sent: Tuesday, August 19, 2008 12:23 PM
To: Ledoux, Nikolas
Subject: RE: FSR question

Dear Nikolas,

Thank you for your interest in our Force Sensing Resistor (FSR) products. Attached is an integration guide and order form for sample sensors. We suggest that you thoroughly evaluate and test sample FSRs themselves to determine application feasibility. Please note that while the FSR is a good "qualitative" sensing device, it generally is not well suited for "quantitative" force or pressure measurement.

Custom sensors can be manufactured, but significant engineering & tooling charges apply. Opportunities, therefore, must generally be of high volume to warrant the fees.

Best Regards,

Gail Shaw
Inside Sales Manager-Touch Technologies
Phone (805) 484-8855 Ext 155
Fax (805) 484-9457
gshaw@interlinkelec.com

G-5: Correspondence with James Seiler

RE: QTC pressure sensors
From: James Seiler [JSeiler@cui.com]
Sent:Tuesday, August 19, 2008 10:23 AM
To: Ledoux, Nikolas

Hi Nik,

Price each is $8.75 for 1~9 pcs; $8.25 for 10 and up - I only have about 18 of these left and no more available from the factory.
Terms are FOB Tualatin, OR; VISA, MasterCard or American Express.

Best regards,

James

James Seiler
Stack-Novus, LLC
Toll-free: 866-318-5499 (US Only)
Tel: 260-483-7571
Fax: 503-612-2382
jseiler@stacknovus.com

G-6: Correspondence with Sara Gott

Re: QTC pressure sensor pricing
From: Sara Gott [sara.gott@peratech.com]
Sent: Tuesday, August 19, 2008 9:25 AM
To: Ledoux, Nikolas

Dear Nik,

Thanks for your enquiry.

Our QTC sensors can be made to withstand a wide range of forces – it really depends how you are using them, what they are embedded into, how the pressure is applied and for how long.

It's probably possible to withstand forces greater than 100lbs – but it depends over what area the force is applied. We no longer make the standard force sensors you mentioned - in fact we have now removed them from our website.

The way our company works now is to make custom-made sensors to our customers designs. Typically, we work with our customers through several design phases towards using our QTC in their manufacturing process. We then allow them to manufacture and distribute their products using QTC under license.

We would be able to provide you with a quote for making up a sensor to your design, but we would have to charge for this. If this is something you would like to consider, please get in touch and I can give you further details.

Thanks,

Sara Gott
Sales & Marketing Manager
Peratech Ltd
E-mail: sara.gott@peratech.com
Tel: +44 (0)1748 813670

Appendix X